Modelling phenological development, yield and quality of lucerne (*Medicago sativa* L.) using APSIM next generation

---

A thesis

submitted in partial fulfillment

of the requirement for the Degree of

Doctor of philosophy

at

Lincoln University

by

Xiumei Yang

Lincoln University

2020

Disclaimer

The data presented and analyzed in this thesis by the author, including:

a) Experiment 1 data were collected by H E Brown as part of his PhD thesis (2004).

b) Experiment 2: data were collected by H E Brown as part of his PhD thesis (2004).

c) Experiment 3: data were collected by E I Teixeira as part of his PhD thesis (2006).

d) Experiment 4: data for growth years 1, 2 and 3 were collected by H T Ta as part of his PhD thesis (2018). Data for growth year 4 was collected by the author as part of this project. Data for growth year 5 were collected by Dr. Sarah Hoppen.

Abstract of a Thesis submitted in partial fulfillment of the requirement for the Degree of doctor of philosophy

Modelling phenological development, yield and quality of lucerne (*Medicago sativa* L.) using APSIM next generation

by

Xiumei Yang

This research integrated knowledge of lucerne crop physiology into the Agricultural Production Systems sIMulator (APSIM) next generation (APSIM NextGen) model framework to develop and verify a comprehensive lucerne simulation model (APSIM NextGen lucerne model). The model was developed to simulate the growth, development and quality of lucerne cultivars grown under different defoliation management and growth conditions. One of the major challenges for developing a lucerne crop simulation model is to capture the seasonality of perennial reserves and their effect on shoot regrowth in response to different defoliation regimes.

In this thesis, model development and testing was based on long-term field datasets with multiple defoliation regimes (28 day: S; 42 day: L; and 84 day: H) and three genotypes of fall dormancy (FD; FD2, FD5 and FD10) under irrigated conditions. The APSIM Plant Modelling Framework (PMF) was used to simulate generic organs (leaf, stem and root) and represent key crop physiological processes, including crop phenological development, canopy expansion, dry matter and N accumulation, remobilization and partitioning.

Development was parameterized based on thermal time (Tt) targets and a photoperiod (Pp) response. Seedling crops required a juvenile phase (Tt_{juv} of 215 to 547 ˚Cd). For both seedling and regrowth crops, the Tt to reach 50% buds visible ($Tt_{0\text{-}bv}$) increased as Pp shortened in autumn, a minimum of 278 ˚Cd for the basic vegetative (Tt_{BVP}) period was required at Pp >14h for regrowth crops to reach buds visible stage. After crops reached buds visible stage, another 310 ˚Cd of Tt ($Tt_{bv\text{-}fl}$) was required to reach flowering.

Lucerne biomass supply was parameterized as the product of accumulated intercepted total radiation, and radiation use efficiency (RUE_{total}, g DM MJ^{-1} total radiation). The intercepted total radiation was calculated by LAI and an extinction coefficient (k) of 0.81. LAI was parameterized as leaf area expansion rate (LAER) and Pp response. LAER declined as the Pp decrease, being 0.018 m^2 m^{-2} ˚Cd^{-1} at 16.5 h and 0.008 m^2 m^{-2} ˚Cd^{-1} at 10 h. However, a Pp response was not observed in seedling crops and regrowth crops in increasing Pp conditions. The RUE_{total} was 1.1±0.31 g DM MJ^{-1} at 18 ˚C for both seedling and regrowth crops.

Biomass supply was then allocated based on the relative demand of each organ. Leaf and stem biomass demand were parameterized as positive power functions. Root biomass showed a seasonal pattern. The APSIM NextGen lucerne model provided a mechanistic framework to model root biomass dynamics with structural and storage components. Structural root biomass was defined and estimated as the amount of root biomass (~2500 kg ha^{-1}) that had no root maintenance respiration loss in winter. The ratio of storage to structural root differed among development stages and FD classes.

In an increasing Pp, there was no storage root demand. The decrease of root biomass during this period was due to remobilization from root to shoots and root maintenance respiration. A remobilization coefficient value and a regrowth coefficient function were used to calculate root remobilization. A remobilization coefficient value was defined as the percentage of storage root biomass per day (5 for FD5, 1 for FD2 and FD10). The regrowth coefficient function includes two parameters (remobilization duration and remobilization rate). Remobilization duration was defined as Tt since harvest, whereas remobilization rate is an adjusted value for the current remobilization coefficient value (ranging from 0 to 1.5). The regrowth coefficient function represents remobilization started at the maximum remobilization rate (1.5) from the beginning of each regrowth cycle (0 ˚Cd). This remained constant until 300 ˚Cd for FD5 (250 ˚Cd for FD2 and 500 ˚Cd for FD10), and then declined to 0 at 350 ˚Cd for FD5 (300 ˚Cd for FD2 and 550 ˚Cd for FD10).

In a decreasing Pp, the increasing root biomass was caused by carbon partitioning. Thus, the model was parameterized to have a maximal root demand with no remobilization. A constant root maintenance respiration coefficient (Rm_root_day) of 0.0005 g g^{-1}.day^{-1} was applied to model root storage maintenance loss. The model had good prediction on shoot

biomass and fair prediction on root biomass for 42 and 84 day defoliation treatments. However, the model did not accurately predict root biomass under a 28 day frequent defoliation (SS) probably due to a limitation of root N reserves.

The N module was linked with DM in the PMF. The N supply was estimated as 2.5% of total biomass, whereas N demand was built as N threshold functions for each organ. Root N showed a similar seasonal pattern as root biomass. A root N remobilization coefficient value (% storage root N per day; 2 for FD5, 0.5 for FD2 and FD10) was used for remobilization calculations in an increasing Pp. Applying the N module improved biomass prediction, especially for the 28 day defoliation treatment (SS).

Simulation results showed good agreement for predicting phenological development stages (NSE of 0.77 for buds visible and 0.67 for flowering stage), good agreement for canopy expansion (overall NSE = 0.61), good agreement for shoot and root biomass (NSE of 0.68 and 0.53). However, there was fair to poor agreement for leaf N (NSE of 0.16 to -0.14), stem N (NSE of 0.51 to -4.61) and root N (NSE of 0.16 to 0.29) for all three FD classes under different defoliation regimes. This was because leaf biomass was used to parameterize leaf N thresholds which resulted in systemic bias. There was a lack of measured N concentration data for the model testing for most treatments. Thus, additional measurement and a more effective approach for parameterizing N demand are required to improve the model. Overall, these results indicate that the APSIM NextGen lucerne model was successfully created to predict growth and development of crops grown under unlimited environmental conditions. Model validation is required under different climate conditions.

Keywords: Alfalfa; Biomass and N remobilization and partitioning; Leaf and stem crude protein (CP) and metabolisable energy (ME); Leaf area index; N dynamics; Plant height; Radiation use efficiency; Root seasonal pattern; Simulation model.

ACKNOWLEDGEMENTS

This last four years of my PhD has been a challeging but great journey. I would like to thank everyone who has helped and made it possible.

Firstly, I would like to extend my deepest gratitude to my primairy supervisor Professor Derrick Moot from Lincoln University. Your extensive knowledge, passion of science, and clear guidence helped me complete this thesis. I appreaciate the time and effort that you put into my PhD project and reviewing my thesis chapters. Thank you for being a great and helpful supervisor and mentor.

I would like to thank my co-supervisors Dr Hamish Brown and Dr Edmar Teixiera from Plant and Food Research Limited. It has been great to work with you both. Thank you for making time to review my thesis chapter in your busy schdule. Your invaluable knowledge with regard to modelling and statistics were very helpful throughout my PhD. I would also like to thank my associate supervisor Dr Juliano Oliveira for his constant support and encouragement.

I am grateful for the expertise and assistance with statistical analysis provided by Dr Annamaria Mills in this project. I also extend a special thank you to Dr Hamish Brown, Dr Edmar Teixiera, Dr Hung Ta, Dr José Jáuregu, Dr Sarah Hoppen for collecting and providing high quality field measured data for this project. Dr Keith Pollock, Dan Dash, Dave Jack and Malcolm Smith provided excellent assistance with the field work that was undertaken during this project, while the casual workers helped me dig lucerne roots and with field harvests.

I would like to acknowledge Lincoln University AGLS faculty that provided a teaching opportunity and stipend during my PhD.

I am very appreciative to my colleagues for their encouragement and support including Shirin, Annette, Carmen, Breanna, Thinzar, Marcus, José, Sarah, Andrew, Arul and Tommy. Thank you to all my close friends who I have enjoyed sharing my time with during this study.

I am very thankful to my parents for their encouragement and support. Your positive attitude to life is always my biggest inspiration. I am also incredibly grateful to my sister

and her family. To my niece and nephew, it has been wonderful to see you guys growing up in the last four years. Finally, I would like to thank my partner Sean for his love and support. Connecting with you in Lincoln was something I never anticipated, but it became something I am most grateful for. I look forward to starting our new life chapter together.

TABLE OF CONTENTS

LIST OF TABLES

LIST OF FIGURES

LIST OF APPENDICES

LIST OF ABBREVIATIONS

Abbreviation	Description	Units
APSIM	Agricultural production system SIMulator	
APSIM NextGen	Agricultural production system SIMulator next generation	
BBF	Basal buds factor	%
BVP	Basic vegetative phase	˚Cd
CSM	Crop simulation model	
CP	Crude protein	%
CV	Coefficient of variation	%
DM	Dry matter	kg ha^{-2}
DM_{leaf}	Leaf dry matter	g m^{-2}
DM_{root}	Root dry matter	kg ha^{-2}
DM_{shoot}	Shoot dry matter	kg ha^{-2}
DM_{stem}	Stem dry matter	g m^{-2}
FD	Fall dormancy	
GDD	Growing degree days	˚Cd
k	Extinction coefficient	
LAER	Leaf area expansion rate	m^2 m^{-2} ˚Cd^{-1}
LAGR	Leaf area growth rate	m^2 m^{-2} d^{-1}
LAI	Leaf area index	m^2 m^{-2}
LAI_{crit}	Critical leaf area index	m^2 m^{-2}
LC	Lack of correlation	
LRF	Lag reduce factor	
ME	Metabolisable energy	MJ g^{-1}
MOP	Maximal optimal Pp	H day^{-1}
MSE	Mean squared error	
NAR	Main stem node appearance rate	Node day^{-1}
N_{crit}	Critical N concentration	%
N_{max}	Maximum N concentration	%
N_{min}	Minimum N concentration	%
NSE	Nash-Sutcliffe efficiency	
NU	Nonunity slope	
P	Probability	
PMF	Plant modelling framework	
Pp	Photoperiod	h day^{-1}

R_RMSE	Relative root mean squared error	%
R^2	Coefficient of determination	
R_i/R_O	Fractional total radiation interception	
Rm_{root}	Root maintenance respiration	g g^{-1} day^{-1}
R_O	Total radiation	MJ m^{-2}
RUE	Radiation use efficiency	g DM MJ^{-1}
RUE_{shoot}	Shoot radiation use efficiency	g DM MJ^{-1}
RUE_{total}	Total radiation use efficiency	g DM MJ^{-1}
SEM	Standard error of mean	
SB	Standard bias	
SLW	Specific leaf weight	g m^{-2} leaf
T_b	Base temperature	˚C
T_{max}	Daily maximum air temperature	˚C
T_{mean}	Daily mean air temperature	˚C
T_{min}	Daily minimum air temperature	˚C
T_{soil}	Daily mean soil temperature (100 mm)	˚C
Tt	Thermal time	˚Cd
TNC	Total nonstructural carbohydrates	
VSP	Vegetative storage proteins	

1 INTRODUCTION

1.1 Overview

Lucerne (also known as alfalfa; *Medicago sativa* L.) is the oldest and most important forage crop globally. It is used for grazing and conserved feed due to its high yield, high leaf crude protein (CP), and high metabolisable energy (ME) content (Michaud et al., 1988). It is a perennial legume adapted to continental and temperate climates and well-drained, near neutral soil pH growth environments (Van Keuren and Matches, 1988). The plant has a deep taproot which enables if to extract soil moisture from depths of 6 m or more (Hanson et al., 1988). This enables it to tolerate drought conditions (Hanson et al., 1988). Lucerne is most productive when grown in rainfed or irrigated conditions that provide fully for its soil moisture needs. However, it is also productive in non-irrigated, rainfed, and summer-dry conditions (Van Keuren and Matches, 1988), where it is most commonly used in New Zealand (Moot, 2012).

Lucerne has been considered the most suitable forage species for intensive dryland sheep production in New Zealand for more than four decades (Douglas, 1986). However, successful lucerne pasture management requires balancing plant and animal requirements to produce crops of high yield and quality at times of high animal demand (Moot et al., 2003). This is challenging because lucerne yield varies widely depending on climate, soil factors, genetic factors, and management (Fick et al., 1988). Defoliation management, whether by cutting or grazing, greatly affects biomass partitioning to underground organs during regrowth periods (Teixeira et al., 2007b). This affects yield, nutritive value, and stand persistence (Belanger et al., 1999). With low levels of root and crown reserves, the plant is unable to quickly renew the canopy at the beginning of each regrowth cycle, which reduces crop yield (Avice et al., 1997b).

An important criterion for selecting a lucerne cultivar has been its fall (or autumn) growth. This has been equated with its Fall Dormancy (FD) classification. Lucerne cultivars have been classified from FD 1 to FD 11 with FD 1 being highly dormant and FD 11 cultivars being non-dormant or “winter active”. This rating is determined by its regrowth height following fall harvest (Teuber et al., 1998). Non-dormant cultivars flower earlier, initiate shoot regrowth more quickly after autumn harvest, and produce higher forage yields than

dormant cultivars (Cunningham and Volenec, 1998). However, some researchers reported that yield advantage of non-dormant cultivars disappeared after their first two years due to a lack of lucerne persistence (Gramshaw et al., 1993; Ta et al., 2020; Ventroni et al., 2010). The FD system is more suited to predict yield than winter survival (Cunningham et al., 2001).

Understanding the growth and development of lucerne cultivars under different seasonal conditions and management strategies is essential for farmers to select appropriate cultivars, accurately predict plant growth and yield for a particular environment (Undersander et al., 2011), and manage their pastures and livestock successfully year-round (Moot et al., 2003). Cultivar selection and subsequent management decisions include developing defoliation regimes that match seasonal plant growth with livestock feed requirements while ensuring stand persistence (Summers and Putnam, 2008).

The ability to accurately estimate the amount of forage available for the short- and medium-term future is necessary to develop rational grazing plans in combination with conserving excess seasonal production in the form of hay or silage. The land manager must match forage supply with livestock demand to meet targets for economically and environmentally sustainable livestock performance.

Traditional methods for pasture management and feed assessment have been based on field trials and farmers' experience. These information source provides site-specific guidance, but are time- and cost-intensive to collect (Whisler et al., 1986). Crop simulation modelling (CSM) can be used to complement traditional approaches. However, site-specific field experimental data are important for CSM calibration and validation. Computational modelling tools are advantageous due to their capability to predict the growth and development of a biological system subjected to a variety of environments. Simulation models can help producers improve yield by modifying management and genotype (Brown et al., 2019). This allows the user to optimize management decisions without doing additional experimentation (Baruah and Baruah, 2014). There are four important applications for crop models: (i) prediction, (ii) determination of optimal management, (iii) characterization of plant cultivars and germplasm, and (iv) integration with Geographic Information System (GIS) layers for landscape-level applications (Wallach et al., 2006). A key role for a CSM is to predict crop yield and quality in different climate and soil conditions.

A set of scenarios can be simulated to evaluate a range of options to identify the optimal management practice, and define an acceptable practice in a specific location. In addition, crop models can be used for evaluating germplasm developed in plant breeding programs. At the ecoregion scale, it is impossible to conduct specific experiments due to economic and organizational reasons. Thus, combining field experiments with spatial analysis methods, that is, those which integrate GIS and mathematical models (Morari et al., 2004), can be exceptionally useful for large scale yield and quality prediction.

The APSIM model (Keating et al., 2003), developed by the Agricultural Production Systems Research Unit (APSRU) in Australia, has been used worldwide in different agricultural systems (Holzworth et al., 2018). The first APSIM lucerne model was published by Robertson et al. (2002) to simulate lucerne phenology and shoot biomass. The APSIM lucerne model has been modified and calibrated by Moot et al. (2015) using field observed lucerne data from New Zealand. Currently, the APSIM next generation model (APSIM NextGen) was released (Holzworth et al., 2014), with improved functions and facilities. It uses the APSIM Plant Modelling Framework (PMF) described by Brown et al. (2014). This allows model developers to choose from a library of commonly-used functions and algorithms for plant modelling. Thus, the rationale of this thesis include the need to 1) develop a lucerne model using PMF in APSIM NextGen, 2) use data from different FD classes under long term and multiple defoliation treatments are to create a comprehensive lucerne model capable of quantifying genotype × environment × management interaction. To do this, over 15 years detailed field experimental datasets with multiple treatments from Lincoln University have been collected over 15 years and all can be used for model calibration and verification.

1.2 Aim and Objectives

The APSIM crop model considers plants as dynamic systems and aims to quantify and parameterize the response of species, genotypes, and cultivars to environmental factors and management operations (Holzworth et al., 2018). In this project, the aim is to integrate available crop knowledge and datasets into the APSIM NextGen model, to develop and verify a comprehensive lucerne simulation model that can accurately simulate growth, development and forage quality under different defoliation regimes. It must also discriminate among genotypes by defining genetic parameters that are stable under

irrigated environmental conditions. This will lead to an APSIM NextGen lucerne model able to accurately predict phenological development, seasonal and annual yield and quality to assist best management practices.

The research question is: can a lucerne model be developed in the APSIM NextGen framework to accurately simulate development, yield and quality of different FD classes for both seedling and regrowth crops under different defoliation regimes and growth conditions?

The null hypothesis is that physiological growth and development processes of lucerne cultivars of different FD classes grown under different defoliation regimes are not different, and can be quantified by the same algorithms and functions in each growth cycle. If accurate algorithms and functions can be developed, then crop growth and development can be accurately modelled within the APSIM NextGen model.

This thesis is organized in nine chapters (Figure 1.1). Chapter 2 reviews the literature that focuses on environmental yield-determining factors and mathematical approaches for estimating physiological processes. Chapter 3 describes the data collection from previous and current field experiments, management details, the experimental design used for model parameterization and verification, and climate and soil data inputs for the model. The algorithms, parameter analysis, and model evaluation methods are also explained in this chapter.

The specific research objectives of this thesis are found within each of the five results chapters.

1. Chapter 4 (Objective 1): to quantify and parameterize lucerne crop phenological development when grown as recommended for grazing in New Zealand. Equations and parameters were then tested under different defoliation regimes and FD classes. This chapter includes simulation and verification of crop vegetative and reproductive development for seedling and regrowth crops.
2. Chapter 5 (Objective 2): to calibrate and verify lucerne crop canopy expansion and radiation interception under different defoliation regimes and FD classes. This chapter includes simulation and verification of LAI and calculation of the extinction coefficient (k).

3. Chapter 6 (Objective 3): to calibrate and verify DM demand, reallocation and respiration for each generic organ, including leaf, stem and root. This includes calculating radiation use efficiency (RUE), and simulation and verification of shoot and root biomass demand function under different defoliation regimes and FD classes.
4. Chapter 7 (Objective 4): to calibrate and verify N dynamics in lucerne crops, include N supply and N demand in each organ under different defoliation regimes and FD classes.
5. Chapter 8 (Objective 5): to estimate lucerne height, forage quality and apply the model across different grazing scenarios and environments based on parameters developed in Chapters 4-7.

Chapter 9 provides a summary of the knowledge gained through the model development process. Potential applications in different environments are also discussed along with limitations of the current model version and further research needs.

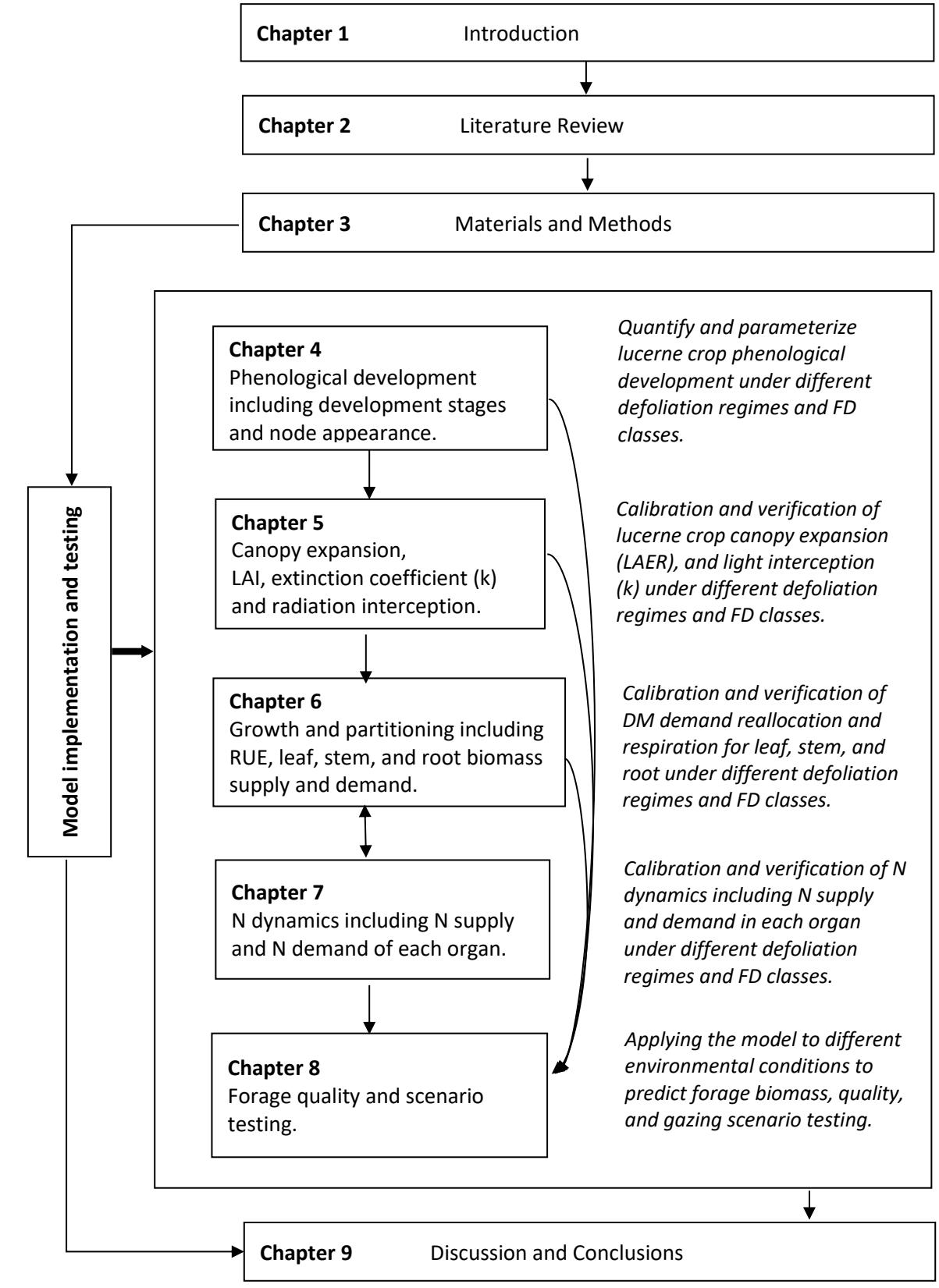

Figure 1.1. Thesis structure.

2 REVIEW OF THE LITERATURE

This chapter initially outlines the role of crop modelling in general then focuses on specific knowledge of lucerne models. This is followed by a review of the processes of phenological development, yield and quality simulation, and then reviews the present literature on lucerne physiological processes that regulate crop yield and quality. Finally, it compares and discusses the potential of integrating functions of environmental responses into lucerne model using in the APSIM next generation (APSIM NextGen).

2.1 Crop simulation modelling

A crop simulation model (CSM) predicts the growth, development and quality of a crop grown in different environments by integrating knowledge from several scientific disciplines into a coordinated whole (Hodges, 1990). Modelling the state of a plant includes both growth and development. Growth refers to the product of photosynthesis which results in an increase in weight, volume, length, or area of some parts or the whole plant. Development refers to the time of critical events in the life cycle of a plant, including leaf appearance and flowering (Ritchie and Nesmith, 1991). In a CSM, these two processes should be separated due to differential responses of growth and development to environmental variables (Ritchie and Nesmith, 1991). Plant development is driven by thermal time (Tt), and modified by photoperiod (Pp) and vernalisation (Hanson et al., 1988).

Crop yield results from biomass accumulation through photosynthesis and its partitioning into harvestable organs (leaf, stem, grain and root). Net dry matter (DM) accumulation depends on gains from photosynthesis and losses from respiration. Under resource (water, CO_2 and soil nutrition) unlimited conditions, photosynthesis depends on canopy radiation interception and temperature while respiration is a function of temperature and crop age (Marcelis et al., 1998). Leaf area expansion is an essential component that determines radiation interception by the canopy. Leaf growth is a function of the fraction of total DM partitioned to leaves and specific leaf area (Marcelis et al., 1998). Total crop yield are modulated by Pp, heat and cold stress, water, fertility stress and management (Hay and Porter, 2006). For perennial forage crops, such as lucerne, defoliation is an important management factor which affects crop regrowth. Crop yield, quality and persistence are

regulated by environmental and management factors that affect the physiological processes, as shown in Figure 2.1 (Hay and Porter, 2006), which is modified from annual crops. To predict crop yield under a range of conditions, algorithms that represent all of these interactions need to be integrated. The methods of configuration depend on the complexity of the model created.

Crop simulation models can be empirical or mechanistic (Thornley and Johnson, 1990). Empirical models are based on field data and involve statistical interpolation, but do not represent the underlying biological mechanisms (Halbleib et al., 2012). Mechanistic models attempt to simulate the important physiological processes and their interaction with the environment that affect growth, development, and yield. Most plant growth models attempt to mechanistically simulate biological process, including photosynthesis, biomass accumulation, and root/shoot partitioning (Whisler et al., 1986), but usually involve some empirical components (Keating, 2020).

Figure 2.1. Relationship between environmental and management factors and the physiological processes that regulate crop yield and quality, which is modified from annual crop (Hay and Porter, 2006).

2.2 Lucerne simulation models

Numerous empirical and mechanistic crop models have been developed or modified to simulate lucerne growth, development, yield, and quality over the last 45 years (Table 2.1).

ALSIM 1 (Fick, 1975, 1977, 1981) and SIMED (Holt et al., 1976; Holt, 1975) simulated lucerne growth and development. These two models were originally used for pest management in

lucerne weevil protection studies (Onstad and Shoemaker, 1984). The ALSIM 1 model also dealt with the remobilization of total nonstructural carbohydrates (TNC) from the taproot during lucerne regrowth. SIMFOY is a soil moisture-based empirical model that used a simple sigmoidal growth regression function to estimate daily dry matter. It assumed that potential daily growth depended directly on soil moisture, other environmental factors did not affect growth directly (Selirio and Brown, 1979). Due to the importance of dairy farms in northeastern United States and Canada, the ALSIM 1 (LEVEL 2) model was adapted and incorporated into a dairy farm simulation model, DAFOSYM (Rotz et al., 1989b). This model, derived from ALSIM 1 (LEVEL 2), was named ALF2LP (Bourgeois et al., 1990), and was described in detail by Fick (1981) and Parsch (1987). ALFAMOD (Gao and Hannaway, 1985) was designed to simulate lucerne production in Oregon. It used climatic and soil data to predict cutting dates and yield in different lucerne-producing areas. The ALFSYM lucerne growth model, developed by Rotz et al. (1986) at Michigan State University, is a dynamic computer simulation of lucerne growth and management based on the 1975 Fick model (Fick, 1975). ALFALFA (Denison and Loomis, 1989) used detailed formalization of several morphological and physiological features, including crop geometry, shoot and root structures (crown, taproot, and fibrous roots) from tissue and organ level to predict lucerne growth and development. Zhu et al. (2007) developed a lucerne model based on a two-year field experiment, to simulate photosynthesis, respiration, leaf area, dry matter production and partitioning. All of these models addressed some aspects of lucerne growth and development, but did not adequately predict the impact of perennial reserves on crop regrowth and development.

To address the weaknesses of previous modelling efforts, an integrated approach to crop modelling has become more common in recent years, with models being combined with other farming operations to simulate whole farm systems. Examples include the Agricultural Land Management Alternatives with Numerical Assessment Criteria (ALMANAC) (Kiniry et al., 1992), the cropping systems simulator (CropSyst) (Stockle and Nelson, 1998), the Agricultural Production system SIMulator (APSIM) (Keating et al., 2003), the Decision Support System for Agrotechnology Transfer (DSSAT) (Jones et al., 2003), the crop-water productivity model (AquaCrop) (Steduto et al., 2009), the multidisciplinary

simulator for standard crops (STICS) (Beaudoin et al., 2009) and the Integrated Farm System Model (IFSM) (Rotz et al., 2012).

Typically, plant modules in these models simulate physiological processes on a daily time-step in response to daily weather data, soil characteristics, and crop management practices. All plant species use the same physiological principles to capture resources (light, water and nutrients) and use these resources to grow. The main differences are the thresholds and shapes of their response functions. Thus, all crops are simulated with the same fundamental computer code, with each species being a specific instance and parameterized through its own crop parameter file, which consists of crop-specific constants (Jones et al., 2003; Keating et al., 2003).

Modelling lucerne, as a perennial forage crop, requires response functions that accurately represent seasonal carbon partitioning into above-ground and below-ground organs. This makes modelling perennial species more difficult than annual crops. Only a few crop simulations or farm system simulations have included lucerne in their initial crop module. CropSyst model (Stockle and Nelson, 1998; Stöckle et al., 2003) is a process-based generic crop simulator which uses the same approach to simulate the growth and development of a wide range of herbaceous crops. It also includes perennial crops, with processes connected with dormancy and spring growth initiation. Confalonieri and Bechini (2004) used the CropSyst model to simulate lucerne above-ground biomass accumulation and soil water content. The APSIM lucerne model (Keating et al., 2003), developed by the Agricultural Production Systems Research Unit (APSRU) in Australia, has been modified and validated by scientists from both Australia and New Zealand. The first APSIM lucerne model was published by Robertson et al. (2002) to simulate lucerne phenology and shoot biomass. The IFSM is a process-based simulation model derived from DAFOSYM. It was generated by linking lucerne and corn (*Zea mays* L.) production models with a dairy animal intake model to predict on-farm feed production and use. Validation work (Jego et al., 2015) indicated good model performance except for under extreme cold conditions. However, none of these lucerne models have included perennial organ simulation and its impact on crop regrowth.

All mechanistic models attempt to simulate the important physiological processes that affect growth, development and yield, with the primary challenge of developing a suitable

approach to parameterize this perennial effect. However, a few research groups have continued to work on lucerne modelling as part of an integrated crop model simulation system. The APSIM lucerne model has been modified and calibrated by Moot et al. (2015) using field observed lucerne data from New Zealand. The calibrated model included a perennial organ module to take account of partitioning to roots. An empirical function of root turnover rates, which increases with increasing Pp was used to represent the seasonal pattern of root biomass. However, biomass re-translocation from perennial reserves to shoots was not considered and the robustness of the empirical taproot turnover relationships need to be tested under different defoliation managements and different cultivars. Smith et al. (2017) modified GRAZPLAN to predict lucerne growth and development, and assessed growth and physiology of lucerne genotypes with different winter activity. However, validation was restricted due to limited information relating to plant roots, soil water, plant morphology and phenology.

Both the DSSAT and STICS frameworks have released lucerne models. Specifically, the CSM-CROPGRO-PFM is a software package in the DSSAT model, that has been modified to simulate perennial crops by adding perennial storage organs, setting rules for storing C and N to simulate perennial reserve impact on plant regrowth (Rymph, 2004). Malik et al. (2018) developed the lucerne model in the CSM-CROPGRO-PFM. Parameters for growth and development were based on values and relationships reported from the literature for cardinal temperatures and dry matter partitioning to root. The CROPGRO-PFM lucerne model was also used to simulate lucerne regrowth in Canada (Jing et al., 2020). The authors reported good results, although they described some limitations, including physiological mechanisms for growth responses, especially dynamics of carbon and N metabolism during regrowth. Strullu et al. (2020) adapted the STICS agro-environment model to simulate lucerne biomass production and nitrogen accumulation under common defoliation management in France. Predictions of shoot and root biomass and N concentration were promising. However, one of the assumptions of the STICS model is that there are temporary pools for N and C to balance the deficit and surplus of C and N. This approximation may be effective but not biologically reasonable in plants without showing up somewhere as biomass.

In summary, most lucerne models have focused primarily on potential production and have limitations in simulating crop physiological and morphological aspects, especially the mechanisms for perennial organ seasonal dynamics, which includes remobilization in spring and partitioning in autumn (Avice et al., 1996; Luo et al., 1995).

To our knowledge, no lucerne model has been evaluated for its ability to simulate biomass and N partitioning within leaf, stem and root of crops subjected to different defoliation treatments. Moreover, none has included the ability to simulate different lucerne FD classes. In addition, most lucerne models adapted parameters from other perennial crops, rather than generating parameters from observed data. This was due to the lack of field or lab observed data.

Therefore, this study measures and assembles more detailed field data to create and verify a lucerne model capable of accurately predicting phenological development, yield and quality of initial seedling year and subsequent year's regrowth cycles. Parameters of the lucerne environmental response for different physiological processes will then be integrated into a crop model. This model provide an important research tool for testing hypotheses and understanding biological processes which were not assessed in the field experiments, as well as provide guidance for developing best management practices on farms in different environments.

Table 2.1 Lucerne crop simulation models

Model	Author(s) and year	Processes treated	Application and Validation
ALSIM 1 (LEVEL 1)	Fick, 1975	Photosynthesis, partitioning and yield.	(Fick, 1977)
SIMED	Holt *et al*., 1975	Photosynthesis, respiration, growth.	(Holt et al., 1976; Holt, 1975)
SIMED 2	Dougherty, 1976	Photosynthesis, respiration, growth, translocation, and soil moisture up-take.	(Dougherty, 1976)
SIMFOY	Selirio & Brown, 1979	Soil moisture and yield.	(Selirio and Brown, 1979)
ALSIM 1 (LEVEL 2)	Fick, 1981	Photosynthesis, soil moisture and yield.	(Parsch, 1987)
DAFOSYM	Parsh, 1982	Photosynthesis, soil water content, forage quality and animal performance.	(Rotz et al., 1989b)
ALFAMOD	Gao & Hannaway, 1985	LAI, photosynthesis, soil water and nutrients.	(Gao and Hannaway, 1985)
AlFALFA	Denison *et al.*, 1989	Crop geometry, shoot and root biomass, root types.	(Denison and Loomis, 1989)
ALF2LP	Bourgeois *et al*., 1990	Yield of lucerne hay, growth curves for leaves, stems, basal buds, and TNC, quality (crude protein, *in vitro* dry matter digestibility, and crude fiber).	(Bourgeois et al., 1990)
CropSyst	Stockle *et al.*, 1998	Radiation interception, photosynthesis.	(Confalonieri and Bechini, 2004)
Alfalfa model	Zhu *et al.*, 2007	Radiation interception, photosynthesis, partitioning.	(Zhu et al., 2007)
IFSM	Rotz *et al.*, 2012	Leaves, stems, basal buds, and total non-structural carbohydrate reserves.	(Rotz et al., 2012)
APSIM lucerne model	Robertson *et al*. (2002)	Phenology, LAI, shoot biomass, and root biomass	(Moot et al., 2015)
GRAZPLAN	Moore *et al*. 1997	Growth rate, seasonal phenology, biomass partitioning, leaf:stem ratio and nutritive value	(Smith et al., 2017)
CSM-CROPGRO-PFM	Malik *et al*., 2018	Shoot, root biomass, LAI, and shoot crude protein content.	(Jing et al., 2020; Malik et al., 2018)
STICS	Strullu *et al.*, 2020	Stems, leaves, crown, taproot, roots, total nitrogen content, and aboveground biomass nitrogen content; water and nitrate contents of the soil during cropping and after crop destruction.	(Strullu et al., 2020)

2.3 Modelling lucerne phenological development

2.3.1 Phenological events and stages

Plant development is the maturity of the crop, including leaf, stem, root, tiller and flower, pod and seed appearance (Hodges, 1990). For annual crops, plant development stages are used to describe the dynamics of development, which are classified as sowing, germination, emergence, juvenile, floral initiation, heading, grain-fill start, grain-fill end, and physiological maturity (Hodges, 1990; Stockle and Nelson, 1998; Williams et al., 1989). Precise prediction of phenological stage is important in the APSIM model since crop development drives biomass growth and partitioning between shoot and perennial organs (Moot et al., 2015). Thus, it's important to simulate lucerne development stage in APSIM NextGen lucerne model.

Lucerne crop development is based on thermal time (Tt) with some stages being modified by photoperiod (Pp) (Hodges, 1990). Ten lucerne development stages based on visual evaluation of stems were proposed by Kalu and Fick (1983). These stages are: early vegetative, mid-vegetative, late vegetative, early bud, late bud, early flower, late flower, early seedpod, late seedpod, and ripe seedpod. They use ontogeny and phasic development of lucerne plant shoots, plant height, and initiation of reproductive structures as indicators of crop development stages. Ben-Younes (1992) quantified accumulated Tt requirements to reach each phenological development stage for nine lucerne cultivars of seedling crops from three fall dormancy (FD) groups under a constant 18 h Pp. Simulation algorithms were also tested in field experiments. Ben-Younes (1992) reported there were no differences in development stage among lucerne cultivars of three different FD classes grown under both controlled environment and field conditions. However, this author reported that Tt accumulation function showed nonsignificant year effect and would be independent of season. Major et al. (1991) investigated lucerne Pp response of 10 lucerne seedling cultivars, and divided vegetative development stages based on Pp response. This included the basic vegetative phase (BVP), which is a juvenile phase that shows no Pp response, but must be completed before the plant is responsive to Pp. The maximal optimal Pp (MOP) is beyond this Pp (~18 h), the Pp impact on lucerne flowering is constant. Lucerne is a long-day plant because the time interval from defoliation to flowering decreases as Pp increases (Major et al., 1991; Moot et al., 2001). Conversely, the time

required from defoliation to flowering increases as Pp decreases (Moot et al., 2003). Teixeira et al. (2011) quantified the Tt and Pp response for both seedling and regrowth crops. Pp_{crit} (MOP) for regrowth crops was 14 h, compared with an observed Pp_{crit} of ~18 h for the seedling phase. Most crop simulation models have integrated Tt and Pp responses to develop a system that can be used for all crops; namely sowing, germination, emergence, juvenile end, floral initiation, flowering, grain-fill start, grain-fill end, maturity, and seed harvest (Holzworth et al., 2014; Keating et al., 2003). However, several equations and base temperatures (T_b) were used to calculate Tt, thus it is difficult to compare the Tt values of each method. Therefore, Tt calculation and T_b selection for lucerne crops needs further investigation.

2.3.1.1 Thermal time calculation

Accumulated Tt or growing degree days (GDD) (Gallagher et al., 1979) is used to predict event timing when the condition in question is dependent on temperature. The use of Tt permits the description of the temperature response by linear or non-linear relationships under temperature fluctuated field conditions (Bonhomme, 2000). In its simple form, it is calculated as shown in Equation 1, wherein Tt is thermal time, T_{mean} is the average of maximum temperature and minimum temperature, and T_b is the base temperature.

Equation 1 $$\sum \boldsymbol{Tt} = \sum(\boldsymbol{Tmean} - \boldsymbol{Tb})$$

Ben-Younes (1992) used a $\log_{10}$ transformation regression function, and determined that T_b=4.6 ˚C for lucerne cultivars in three fall dormancy (FD) classes as shown in Equation 2:

Equation 2 $$\boldsymbol{log_{10}GDD} = \boldsymbol{log}_{\mathbf{10}}^{\sum[\frac{\boldsymbol{T_{max}}+\boldsymbol{T_{min}}}{\mathbf{2}}-\boldsymbol{T_b}]}$$

where GDD is growing degree days, T_{max} is the maximum air temperature, T_{min} is the minimum air temperature, and T_b is the base temperature.

Although widely used, a constant T_b value causes systematic errors in predicting lucerne development. For instance, Sharratt et al. (1989) reported that T_b is 3.5˚C in spring, 7.5˚C in early summer, and 10˚C in late summer. They proposed that accounting for this difference would lead to more accurate lucerne development simulation. However, these parameters are difficult to calibrate because the duration and the temperature threshold for each stage are correlated (Beaudoin et al., 2009). Bonhomme (2000) suggested that the

response between development and Tt is curvilinear, which would account for the systematic error reported by Sharratt et al. (1989). However, this has not been tested for lucerne Tt calculation.

Different cardinal temperatures for Tt calculation have been used widely to calculate Tt in numerous lucerne simulation models DAFOSYM (Rotz et al., 1989a), IFSM (Jego et al., 2015; Rotz, 2005), and SIMED (Holt et al., 1976; Holt, 1975). ALSIM1 Level 2 calculated daily leaf and stem dry matter accumulation based on soil-water availability and Tt, using 5˚C as the base temperature, with the growth period extending into the fall when average daily temperature dropped below -3.3˚C (Fick, 1977, 1981). Tt was linear from >5˚C to an optimum temperature (T_{opt}) of 30 ˚C, with a linear decrease to a maximum temperature (T_{max}) of 40 ˚C, T_b=5 ˚C in Figure 2.2.

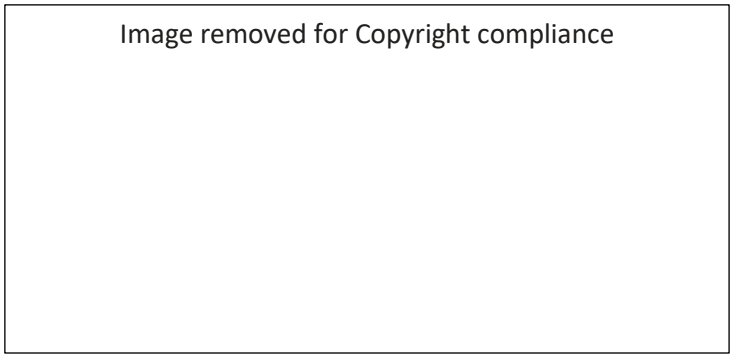

Figure 2.2 Relationship between thermal time and mean air temperature (Brown et al., 2005; Moot et al., 2001).

In the APSIM classic lucerne, Tt was initially calculated as a function of mean air temperature (Fick et al., 1988; Fick and Onstad, 1988) with a T_b of 5˚C. In the modified APSIM lucerne model, a broken-stick threshold model was used (Moot et al., 2001) (T_b=1 of Figure 2.2) in which Tt=0 for temperatures less than T_b of 1.0 °C. Tt is accumulated linearly from T_b until 15 °C at a rate of 0.7 °Cd °C^{-1}, at a rate of 1.0 °Cd °C^{-1} until 30 °C, and then decreases at a rate of 2.5 °Cd °C^{-1} until 40 °C (Brown et al., 2005). To be more accurate in cold periods of the year, each day was divided into 8 periods of 3 hours, with the mean temperature for the period n of the day ($T^n_{diurnal}$) calculated as shown in Equation 3 (Jones et al., 1986; Moot et al., 2001). Following this methodology, Teixeira et al. (2009) found that a T_b of 5°C had the lowest coefficient of variation of Tt for vegetative development stage.

Equation 3 $$T^{n}_{diurnal} = [(0.931 + 0.114n - 0.0703n^{2} + 0.0053n^{3}) \times (T_{max} - T_{min})] + T_{min}$$

In CropSyst (Confalonieri and Bechini, 2004; Stöckle et al., 2003), accumulation of Tt is accelerated by water stress (Stockle and Nelson, 1998). The model assumes that plant canopy temperature will be higher if transpiration is limited by water stress, thereby accelerating development. Thus, temperature was added to the T_{max} calculation as shown in Equation 4:

Equation 4 $$T'_{max} = [1 + (1.5 - VPD_{max})] \cdot Stressindex_{water} \cdot PSWS$$

where $StressIndex_{water}$ is the daily plant water stress index (ranging from 0 to 1), VPD_{max} is the maximum vapour pressure deficit, and PSWS is the phenological sensitivity to water stress crop input parameter. However, the relationship between lucerne's phenological stage and a water stressed Tt calculation could not be validated in field studies for accurately predicting morphological development (Confalonieri and Bechini, 2004).

The CROPGRO-PFM-Alfalfa (Malik et al., 2018) had two optimal temperature and two sets of cardinal temperatures for the vegetative and reproductive stages, with T_b of 3 ˚C and 4 ˚C, respectively. The STICS model (Beaudoin et al., 2009) combined Pp into Tt calculation to simulate the effects of Pp on crop development via a photo-thermal index (PTI) of development. The STICS lucerne model used a T_b of 3 ˚C to calculate Tt, and for a base Pp of 11.5 h and a Pp_{crit} of 18 h (Strullu et al., 2020). Those parameters were either obtained from literature or calibrated from observed data, but the calibration processes were not well documented.

The range of equations, approaches, and the lack of agreement regarding an accurate T_b and Pp response indicates that more detailed physiological understanding and model development is needed to improve the accuracy of predicting lucerne phenological development in both initial seedling crops and regrowth cycles for different lucerne FD classes grown under different defoliation regimes. This project will test different models to determine an appropriate T_b value and Pp response functions for calculating Tt values and morphological development.

2.3.2 **Node appearance**

Node appearance is often a key component when modelling the development of canopy expansion (Brown, 2004). It is a strong indicator of plant development and the number of main stem nodes data can be used to test T_b and Tt calculation for development (Teixeira, 2006). Node appearance is mainly driven by temperature and modulated by Pp (Brown et al., 2005; Moot et al., 2001). There are strong linear relationships between Tt and node appearance and the slope of these linear relationships define the phyllochron (Ta et al., 2016), or Tt requirement to develop one main stem node (Hay and Porter, 2006). A phyllochron value of 34 ˚Cd main stem node^{-1} is used in APSIM classic (Robertson et al., 2002); but 51 to 34 ˚Cd main stem node^{-1} was used in calibrated APSIM lucerne model (Moot et al., 2015). This is because phyllochron values were higher in autumn than in spring regrowth cycles (Ta, 2018; Teixeira et al., 2007b). Brown et al. (2005) proposed that phyllochron was the same in decreasing Pp and in increasing Pp, but the partitioning to roots in decreasing Pp limited the expression of node appearance. Ta et al. (2016) found that seedling crops had a consistent phyllochron (~50 ˚Cd main stem node^{-1}) across different Pp, and this was higher than in regrowth crops. For different lucerne FD genotypes, Ta (2018) reported that there was no difference of phyllochron among three FD genotypes (FD2, FD5, and FD10). Phyllochron values were ≤ 30 ˚Cd per main stem node in increasing Pp compared with ≥ 30 ˚Cd per main stem node in decreasing Pp for all genotypes

Lucerne phyllochron and its changes across a range of Pp at different development stage and under different defoliation treatments will be examined in this thesis.

2.4 Lucerne potential growth and yield

Total yield is determined by the amount of radiation intercepted by the canopy and how efficiently it is used (Teixeira et al., 2007b). The potential yield of a crop can be thought of as the product of the rate of net mass accumulation multiplied by the duration of growth (Ritchie and Nesmith, 1991). Thus, lucerne yield simulation can be organized into five major components (Marcelis et al., 1998; Teixeira et al., 2009): (i) leaf area and canopy development, (ii) radiation interception, (iii) photosynthesis and radiation use efficency (RUE), (iv) respiration, and (v) dry matter remobilization and partitioning within each organ (leaf, stem and root).

2.4.1 Modelling leaf area and canopy development

Canopy development is the primary crop factor that determines radiation interception. Leaf area index (LAI) is the critical parameter that determines radiation interception and is determined through computation of leaf area expansion rate (Brown et al., 2005). Rate and duration of leaf expansion, branching, senescence, shoot and stem population, basal buds and leaf life span are important determinants of LAI (Teixeira, 2006).

A detailed lucerne canopy model, developed by Brown et al. (2005), simulated lucerne LAI expansion from environmental responses of individual components; i.e. LAI was determined by shoot population, individual leaf area (mm^2) , and the number of primary and axillary leaves per shoot. LAI is represented by Equation (5):

Equation 5 $$\boldsymbol{LAI = Shoot/area \times Leaf/shoot \times Area/leaf}$$

However, this method requires large amounts of observed data, which normally are not available in most field measured datasets.

There are two main approaches for simulating leaf area development in lucerne simulation models. An empirical LAI model is described where leaf area is a function of accumulated Tt (Teixeira et al., 2009), with leaf area expansion rate (LAER) used as the parameter. For example, the calibrated APSIM lucerne model used a simple LAI expansion in response to Tt accumulation (Moot et al., 2015). In the STICS model, Beaudoin et al. (2009) modified this model and calculated LAER as a logistic curve based on phenological stages. This value was then multiplied by the effective crop temperature, combined with a density factor, inter-plant competition, cultivar characteristic, and the water and nitrogen stress indices. Similarly, Strullu et al. (2020) used a maximal leaf area index growth rate of 0.015 m^2 m^{-2} °Cd for lucerne LAER. However, this model did not include a Pp response.

Another approach is that leaf area is predicted from simulated leaf dry weight [simulated leaf area is obtained when leaf area is calculated on the basis of simulated leaf biomass and specific leaf area (SLA)]; e.g. CropSyst uses SLA as an input parameter, so that the LAI value changes the leaf area expansion-related biomass produced for a given day, and accumulated biomass, leaf area duration is assigned to each daily unit of LAI produced. When a given daily LAI completes its duration, it is removed from the current LAI, effectively simulating leaf senescence. Water stress affects both daily leaf area production

and leaf area duration (Stöckle et al., 2003). However, the SLA for a lucerne crop is not a constant value; it varies based on development stage, leaf age, and growth season (Moot et al., 2015).

This project modified the empirical model in APSIM classic lucerne model to include a LAER against Pp response function. This function will also include canopy senescence, basal buds and the lag phase functions of LAER to determine the most accurate simulation of lucerne leaf area expansion under different defoliation regimes and FD classes.

2.4.2 **Modelling radiation interception**

The capacity of a crop to intercept light depends on leaf area and canopy architecture. The absorption of radiation can be modeled from the principle that absorption of radiation increases with increasing leaf area, and that shading decreases radiation interception. Quantifying intercepted light uses the Lambert-Beer law (Equation 6) (Monsi and Saeki, 2005):

Equation 6 $$I/I_O = e^{-kL}$$

where *I* is intercepted radiation, I_O is irradiance above the crop canopy, L is leaf area index, and k is an extinction coefficient which combines plant and canopy characteristics to describe canopy radiation interception. The k value changes based on canopy architecture and zenith angle of incidence of light (Monteith, 1994). For crop modelling purpose, a single value is commonly used for each species to estimate radiation interception (Teixeira et al., 2007b). Critical LAI (LAI_{crit}) is defined as the LAI value when 95% of the incident light is intercepted (Hay and Porter, 2006).

However, radiation absorption is more accurately approximated by Equation 7 (Marcelis et al., 1998), where *p* is the canopy reflection coefficient.

Equation 7 $$I_{abs,L} = (1-\rho)I_O(1-e^{-kL})$$

Teixeira et al. (2007b) reported that there was no difference in the pattern of radiation interception per unit of LAI in different defoliation regimes. For each regrowth period, lucerne had a similar critical LAI (3.6) with k=0.81, resulting in Equation 8:

Equation 8 $$I_{abs,L} = I_O(1-e^{-0.81L})$$

The k value for lucerne crops has been conservative across different cultivars reported in the literature. The k values for lucerne cultivars have been reported as 0.89 for seedling, and regrowth crops (Sim, 2014), and as 0.83 for three different FD classes (Ta, 2018). In the APSIM classic lucerne model, the k values of 0.57 for seedling and 0.80 for regrowth crops are used (Robertson et al., 2002). The STICS model uses a k value of 0.88 (Strullu et al., 2020).

Thus, this project will test the relationship between radiation interception and LAI under different defoliation regimes and FD classes. The k was calculated by using datasets from long-term experiments with multiple defoliation treatments and genotypes from three FD classes.

2.4.3 Modelling radiation use efficiency

Two main approaches are used to model yield-forming processes using; 1) the photosynthesis and respiration rate to calculate total DM; 2) radation use efficency (RUE), which is the slope of a linear relationship between the accumulated above-ground biomass and the quantity of intercepted total radiation for each period of growth (Monteith, 1994).

Crop models typically estimate above-ground biomass based on the calculation of radiation intercepted by the canopy (R/R_o) and radiation use efficiency (RUE). In CropSyst, radiation-dependent growth is calculated with a simplified canopy sub-model, which is a function of intercepted total radiation efficiency and a temperature limitation factor (Confalonieri and Bechini, 2004).

However, the RUE_{shoot} approach does not accurately reflect lucerne crop physiology, because partitioning of biomass to taproots and crowns changes within regrowth cycles (Reynolds and Smith, 1962) and between seasons (Brown et al., 2006; Khaiti and Lemaire, 1992). Lucerne RUE_{shoot} was defined as the measured above-ground component of biomass in relation to radiation interception, analogous to RUE in annual crops. RUE_{total} was defined as the sum of RUE_{shoot} plus biomass in root (crowns and taproots). Khaiti and Lemaire (1992) reported RUE_{shoot} values varied from 0.40 g MJ^{-1} for the growth period after seedling to 0.9 g MJ^{-1} for summer regrowth, and 0.57 g MJ^{-1} for the autumn regrowth. However, the RUE_{total} was constant (1.2 g MJ^{-1}) for the three periods. RUE_{total} is also affected by temperature (Justes et al., 2002). Brown et al. (2006) reported that RUE_{total} increased

linearly with mean temperature at a rate of 0.18 g MJ^{-1} from 0 to 18 ˚C, until an optimum RUE_{total} of 1.6 g MJ^{-1}. This frame work was tested by Teixeira et al. (2008), who found similar results but a weaker correlation. Ta (2018) reported that the optimum RUE_{total} was 1.2 g MJ^{-1} in the same location.

Different RUE values are used in different lucerne models. For example, 1.1 g MJ^{-1} for regrowth crops and 0.6 g MJ^{-1} for seedling and winter regrowth crops in the APSIM classic model (Robertson et al., 2002). A RUE_{shoot} value of 1.5 g MJ^{-1} was used in the CropSyst model (Confalonieri and Bechini, 2004). A RUE_{shoot} value of 2 g MJ^{-1} was used in the IFSM (Jego et al., 2015). Those models only predicts shoot biomass and the perennial biomass is not included. In the STICS model, a RUE_{total} value of 0.65 g MJ^{-1} was used for the juvenile phase, and 1.45 g MJ^{-1} for the vegetative and reproductive phases (Strullu et al., 2020).

This project used the RUE_{total} temperature response frame work to determine a RUE_{total} function for both seedling and regrowth lucerne crops of several FD classes subjected to different defoliation regimes. Canopy development, radiation interception, and RUE_{total} addressed the DM supply components of the APSIM NextGen lucerne model.

2.4.4 Dry matter partitioning between shoot and perennial organs

Dry matter partitioning includes allocation, distribution and transport of assimilates (reallocation) from storage organs (sources) to structural organs (sinks) (Baysdorfer and Bassham, 1985). In lucerne, the allocation of carbon and nitrogen to storage organs is regulated by seasonal environment signals (Cunningham and Volenec, 1998). There is a preferential storage of carbon and nitrogen in perennial organs in decreasing Pp (autumn). In contrast, these reserves in perennial organs are translocated to boost new shoot growth in spring and early regrowth cycles (Khaiti and Lemaire, 1992; Ta et al., 1990). Avice et al. (1996) suggested that nonstructural carbohydrates and also hemicellulose, proteins, and organic acids were remobilized from below-ground. Brown et al. (2006) calculated the DM partitioning rate of lucerne cultivar 'Kaituna' to roots, showed it increased from ~10% in spring to 60% in autumn. To cope with this seasonal dynamic, Teixeira et al. (2008) proposed a framework to explicitly account for partitioning of biomass to below-ground organs, as represented in Equation 9:

Equation 9 $$\boldsymbol{DM_{shoot} = PAR_O \times (PAR_i/PAR_O) \times RUE_{total} \times (1 - P_{root})}$$

where DM_{shoot} is the above-ground dry matter. PARo, is the incident photosynthetically active radiation above the canopy, calculated as 0.5 × R_o (total radiation) (Szeicz, 1974). PAR_i/PAR_o is the fractional PAR interception, RUE_{total} is the conversion factor of PAR_i to total dry matter (g DM/MJ PAR_i), and 1-P_{root} is the fractional difference of the partitioning to perennial organs.

Teixeira et al. (2008) reported that defoliation regimes also affected carbon (C) and nitrogen (N) partitioning to perennial organs. Thiébeau et al. (2011) quantified partitioning to shoot (P_{shoot}) for both seedling and regrowth crops, in which P_{shoot} for regrowth crops was primarily explained by accumulated Tt and then by Pp, whereas P_{shoot} for seedling crops was constant across different accumulated Tt in spring and autumn. Ta (2018) calculated P_{root} for three different FD genotypes (FD2, FD5, and FD10), and concluded the physiological mechanisms responsible for partitioning of different genotypes, was possibly due to changes in base Pp of the genotypes. For example, among the three FD genotypes, FD2 showed the most response to Pp direction. In conclusion, DM partitioning to roots is affected by seasonal signals (Tt and Pp), defoliation management, growth stage (seedling and regrowth) and FD of genotypes.

However, P_{root} is an empirical approach to calculate DM partitioning between shoot and perennial organs. The calibrated APSIM lucerne model (Moot et al., 2015) used a similar empirical model, which is a linear function between root turnover rates and Pp to simulate root biomass dynamics. To model the seasonal changes of DM partitioning a mechanistic approach by using source and sink has been proposed to solve biomass demand for each organ. The CSM-CROPGRO-perennial forage model (Malik et al., 2018) uses different partitioning coefficients for leaf, stem, and root fraction determined by extrapolating data from the literature. The STICS model (Strullu et al., 2020) uses different DM demand functions for leaf, stem and root. The parameters of the allometric relationship were similar to the literature reported by Lemaire et al. (1992).

For leaf biomass allocation, different lucerne models use different approaches. For example, specific leaf weight (SLW) has been used to predict leaf biomass demand (Confalonieri and Bechini, 2004; Malik et al., 2018). However, SLW differs with development stage, time and growth conditions (Hanson et al., 1988; Lemaire et al., 1992;

Moot et al., 2015). Therefore, using SLW as a parameter for leaf demand is generally not a robust approach.

Considering that stem is the main component of above-ground biomass, it is important to simulate stem growth and biomass demand to predict forage quality (Lemaire et al., 1992). However, most lucerne models do not separate shoot into leaf and stem (Confalonieri and Bechini, 2004; Malik et al., 2018). The STICS model uses a stem:leaf ratio of 1.5 to predict stem biomass (Strullu et al., 2020). However, stem:leaf ratio is not a constant value, the stem proportion increases as shoot biomass increases (Lemaire et al., 1992; Ta et al., 2020).

Therefore, this thesis will quantify leaf, stem and root demand, and the biomass remobilization and partitioning process within each organ. Parameters and functions of biomass demand for each organ will be tested for different FD cultivars grown under different defoliation regimes.

2.4.5 Modelling root maintenance respiration

Modelling root maintenance respiration is important for perennial crops, such as lucerne. Avice et al. (1996) reported that ~73% of carbon (C) had been remobilized from perennial organs after 30 days of regrowth, but only 5% was recovered in the aerial biomass. The main C loss was from respiration of perennial organs (61%) and shoots (8%). Plant respiration is divided into growth and maintenance respiration (McCree, 1974). However, the RUE_{total} includes growth respiration for both shoots and roots. Thus, only maintenance respiration of root DM (Rm_{root}) needs to be calculated. A daily rate of Rm_{root} (g g.day^{-1}) can be used to adjust DM_{root} assuming a reference soil temperature (100 mm depth) of 20˚C (Equation 10) (McCree, 1974).

Equation 10 $$Rm_{root} = \left[Rm\_root\_day * Q_{10}{}^{\frac{(T_{soil}-20}{10})}\right] DM_{root}$$

where Rm_root_day is the respiration coefficient that changes with the metabolic activity of crown and taproots in different seasons (Teixeira et al., 2009). The Q_{10} value of 1.8 is a modifying factor for Rm_{root} as soil temperature fluctuates (Atkin et al., 2000), and DM_{root} is the root biomass. In most crop models, respiration is not estimated in a separate module. Teixeira et al. (2009) tested a range of Rm_root_day values to fit root biomass, values changed across the season, ranging from less than 0.005 to 0.0035 g g^{-1}.day^{-1}.

This project will quantify root maintenance respiration and verify parameters and functions under different defoliation and FD classes.

2.4.6 N dynamics and partitioning between shoot and root

2.4.6.1 Modelling N supply (N uptake and fixation)

The major difference between simulating lucerne growth and development and other non-legume crops is N_2 fixation. N assimilate through mineral uptake and N_2 fixation, is stored in perennial organs mostly in the form of soluble proteins and amino acids (Kim et al., 1991). For example, it has been estimated that N fixed through N_2 fixation in above-ground tissue in lucerne can range from 350 to 450 kg N ha^{-1} $year^{-1}$ (Carlsson and Huss-Danell, 2003; Fishbeck et al., 1987). Lucerne N_2 fixation is affected by N fertilizer and soil temperature. Ghiocel et al. (2013) reported that application of N fertilization in lucerne crops reduced plant nodule formation and N_2 fixation capacity. When 100 kg N ha^{-1} fertilizer was applied, nodule sites were decreased about 85% and nodule weight decreased significantly from 0.52 g $plant^{-1}$ in the control treatment (no fertilizer) to 0.11 g $plant^{-1}$, and the N_2 fixation rate decreased from 0.78 mg $plant^{-1}d^{-1}$ to 0.02 mg $plant^{-1}d^{-1}$. Wivstad et al. (1987) reported the impact of development stage and defoliation management on N_2 fixation rate. Specifically, lucerne crops at the bud or early flower stage had the maximum rate of N_2 fixation, followed by a rapid decline as flowering proceeded. Nitrogenase activity decreased and remained low during at least two weeks after harvest, until regrowth of new shoots started (Hannaway and Shuler, 1993).

N_2 fixation has not been included in most lucerne models. In the CSM-CROPGRO Perennial Forage Model (Malik et al., 2018), sensitivity analysis was used to set relationships to obtain a reasonable N_2 fixation rate and nodule growth. In the STICS model, N fluxes are associated with DM fluxes (Strullu et al., 2020). Daily N uptake, including absorbed N plus fixed atmospheric N_2, is calculated and defined as the minimum N between soil N availability and plant demand.

Therefore, this project will back calculate daily N uptake by using measured leaf, stem and root N concentration data. Model optimization will be used to set parameters, where no data were available.

2.4.6.2 Modelling leaf and stem N demand

A linear relationship has been found between total N and total biomass, and the average N concentration of the whole plant (shoot plus root tissues) was constant at about 2.4% regardless of plant size (Lemaire et al., 1992). Lemaire et al. (1992) also proposed that an allometric relationship between accumulated N in aerial biomass and the weight of aerial biomass. A similar relationship was also found between leaf nitrogen, and leaf biomass; and between stem nitrogen and stem biomass (Equation 11):

Equation 11 $$\boldsymbol{N = a \times W^{b}}$$

where crop N uptake is N (kg ha^{-1}) and crop accumulated mass is W(t DM ha^{-1}), and b is the allometric coefficient. To express plant N% in relation to W, Equation 11 is divided by W, known as a N dilution curve (Equation 12), which means N% decreases as biomass increases.

Equation 12 $$\boldsymbol{\%N = a/10 \times W^{b-1}}$$

Lemaire et al. (2007) proposed that W has both metabolic and structural components. The metabolic components of a plant scales with plant leaf area or the LAI, while the structural components scales with canopy height and leaf thickness. Teixeira et al. (2008) reported that leaf N concentration is between 4 and 6%. In contrast, stem N varies at wider ranges (from 5% to 2.5%), declines as internode numbers increase or stem height increase (Lemaire et al., 1992). This is because diameter, percentage of cell wall and lignin increases in response to mechanical constraints according to stem weight (Vallet et al., 1998).

However, leaf and stem N are often treated as shoot N in lucerne models (Malik et al., 2018; Strullu et al., 2020). Therefore, in the APSIM NextGen lucerne model, leaf and stem N% were simulated separately.

2.4.6.3 Modelling root N demand

Perennial roots support shoot regrowth in spring and after defoliation by remobilizing C and N (Ta et al., 1990). Some researchers have demonstrated that N reserves in perennial organs have a strong impact on lucerne shoot growth. For example, Avice et al. (1996) showed that 52 to 87% of the shoot N was derived from source tissue storage compounds. Avice et al. (1997b) and Cunningham and Volenec (1996) reported that root protein and vegetative storage protein (VSP) are the main nutrients for shoot regrowth. Noquet et al.

(2001) stated that a short Pp resulted in preferential N allocation toward taproots with an increased accumulation of VSP. Teixeira et al. (2007c) compared the impact on shoot growth rate under different levels of perennial reserves after defoliation and early spring regrowth. These authors reported that the amount of N reserves in taproots during winter had a strong positive effect on spring shoot growth rate. Liu et al. (2016) found a significant increase in the expression level of VSP in all dormant cultivar tissues in late autumn.

Therefore, root N allocation (including remobilization and partitioning) should be included in the model. However, this detailed plant physiology has not been integrated into current lucerne models. Few lucerne models include N modules to simulate and test N dynamics. In the STICS model (Strullu et al., 2020), N demand for roots is a function of daily root biomass production, the N nutrition index of the crop (NNI) and a parameter that corresponds to the C to N ratio of the organ for an NNI of 1.

This project will simulate N remobilization and partitioning within leaf, stem and root, and verify parameters and functions under different defoliation treatments and FD classes. To evaluate the potential importance of FD classification on differences in N dynamics, model optimization exercises will be performed.

2.5 Modelling forage quality

Historically, lucerne quality has been associated with phenological development stage (Kalu and Fick, 1983), cultivars (Kallenbach et al., 2002) and stubble height (Yolcu et al., 2006). Forage crude protein concentration (%CP) and digestibility (%D) decline as crops grow and develop. This results in a trade-off between forage biomass and its nutritive value (Hanson et al., 1988). Harvesting at 10% flowering stage was recommended to maximize forage yield and quality for lucerne hay production (Kalu and Fick, 1981). Therefore, farmers anticipated the decline in forage nutritive value with increasing in forage crop maturity, and decided the optimal harvest date by monitoring plant phenology (Kalu and Fick, 1983). However, Vallet et al. (1998) stated a decline in forage nutritive value occurs with advances in maturity, and is associated with increasing stem growth and decreasing stem nutritive value. Stem diameter expansion is initiated by an increase in cell wall deposition in secondary xylem and phloem with an increase in lignin deposition (Vallet et al., 1997). Stem height increases during the growth period. The whole stem digestibility

was determined by diluting the upper internodes with high digestibility progressively within an increasing mass of maturing lower internodes with low digestibility (Lemaire and Belanger, 2020). Therefore, stem height was associated with forage quality, and simulating stem height is important in lucerne modelling to predict forage quality.

There were three different equations for predicting lucerne leaf, stem and herbage quality including mean stage by weight (MSW) or count (MSC) or growing degree days (GDD) (Fick and Onstad, 1988). However, validation studies indicated that these equations were biased, calibration for specific locations and frequent recalibration is necessary (Sanderson, 1992).

Under a grazing management, animals preferentially consume the part of the lucerne sward with the highest quality of palatable fraction (leaves and soft stems) (Brown, 2004). Total crude protein (CP) and metabolisable energy (ME) in the palatable fraction of lucerne crops are important factors that determine potential livestock daily intake (Ta et al., 2020). However, the method of separating stem as palatable and unpalatable fractions are subjective. Therefore, it will not be included in the APSIM NextGen lucerne model. The APSIM NextGen lucerne model will also include simulating forage quality for different genotypes of FD classes.

2.5.1 **Modelling plant height**

Stem height is an important trait for lucerne plant breeders (Riday and Brummer, 2002). Lucerne genotypes of different FD classes are determined by fall plant height (Fairey et al., 1996). Stem height is associated with plant growth, development, and forage quality, and stem elongation rate is controlled by temperature and moisture (Hanson et al., 1988). However, to our knowledge, none of the lucerne models predict stem height and the differences among genotypes of FD classes.

2.5.2 **Modelling crude protein**

Brown and Moot (2004) reported that the CP content of the palatable fraction ranged from 29% to 27%. Similar results were reported by Ta et al. (2020), who found that the CP in whole shoots remained constant at 27% of shoot biomass. However, leaf CP accumulation was constant at 30%, soft stem at 12% and hard stem at 7%. To estimate CP, the N % was multiplied by conversion factor equal to 6.25 (Lemaire and Belanger, 2020). Therefore, the

simulation accuracy of CP depends on N simulation. This method is commonly used in crop models to simulate CP concentration. For example, Malik et al. (2018) used shoot N percentage to simulate herbage CP concentration in CROPGRO-PFM-Alfalfa model.

2.5.3 Modelling ME

Brown and Moot (2004) reported that the ME content of palatable fraction (leaf and soft stem) was 11.9 MJ kg DM^{-1} and the unpalatable fraction (hard stem) was 7.9 MJ kg DM^{-1}, remaining constant as standing herbage accumulated. Ta et al. (2020) reported the ME of whole shoots was 10.8 MJ kg DM^{-1}, leaf was 11.7 MJ kg DM^{-1}, and that soft stem (8.5 MJ kg DM^{-1}) and hard stem (5.3 MJ kg DM^{-1}) ME also remained constant.

To our knowledge, none of the lucerne models include predicting ME and plant height. Therefore, this thesis will investigate the forage quality factors of plant height, leaf and stem CP, and leaf and stem ME. Parameters and functions for forage quality will be tested under different defoliation treatments and for genotypes of different FD classes.

2.6 APSIM next generation

2.6.1 Background

The APSIM model is widely used to address long-term resource management issues in farming systems. The APSIM Next Generation model, known as APSIM NextGen (Holzworth et al., 2014), is a new version of APSIM with improved functions and facilities. It was developed to improve execution speed and cross platform development, model construction and visualization, and manager script flexibility (Holzworth et al., 2018) This allows model developers to run larger simulation faster on multiple operating systems (desktop, web, mobile), and simulate complex farming systems on temporal and spatial scales (from farm to global) (Holzworth et al., 2018). It uses the APSIM Plant Modelling Framework (PMF) described by Brown et al. (2014), which allows the model developer to choose from a library of, commonly-used functions and algorithms for plant modelling. These are subsequently configured into a model description using the eXtensible Markup Language (XML).

2.6.2 Model components

In APSIM, a crop is defined as a system with a set of components including phenology, organ genesis, and biomass production. Processes are closely related to a specific system

component and result in the change of the components' state variables. The APSIM modelling framework consists of: 1) a biophysical module which simulates biological and physical farming processes; 2) management modules which implement management practices under different scenarios; 3) input and output datasets; and 4) a simulation engine and graphic user interface (GUI) which drives the simulation process and connects all the modules (Holzworth et al., 2014; Keating et al., 2003). Plant modules simulate physiological processes and operate on a daily time-step. They require inputs of daily weather data, soil characteristics, and crop management actions.

The APSIM NextGen model retains the main concept of the PMF (Holzworth et al., 2014), it allows overwriting of any model parameter to represent cultivar specific variation (Brown et al., 2019). For simulating biomass allocation, the PMF uses a generic 'arbitration' approach to allocate C and N among plant organs. In particular, the OrganArbitrator class in PMF determines how much C and N can be allocated to each organ based on the different organ classes in relation to the total supply of biomass available to the plant and the demands from each organ in the plant model (Brown et al., 2018). Therefore, the OrganArbitrator needs to integrate all the biomass demands and supplies from each organ class. Specifically, each organ has a C and N demand for Structural, Storage and Metabolic biomass forms, whereas biomass supply has a number of potential sources for each organ, including fixation (photosynthesis supplying DM, symbiotic fixation providing N from nodules), uptake (root uptake of mineral N), re-translocation and reallocation among each organ (Brown et al., 2019).

The PMF has been used to build a range of different crop models (Holzworth et al., 2014). However, despite the importance of lucerne for livestock grazing and feeding around the world, the PMF doesn't have a lucerne model to simulate plant growth, development, yield and quality. Therefore, this thesis uses existing long term datasets from field experiments to qualify lucerne environmental response and calculate parameters for model calibration and verification. These are used to describe the process of creating lucerne PMF file in the APSIM NextGen lucerne model, and to verify the APSIM NextGen lucerne model under different defoliation regimes and for different genotype of FD classes.

2.7 Improvements and application in lucerne simulation models

The most effective way of improving lucerne simulation models is by gaining further understanding about the environmental physiology of the crop (Fick et al., 1988). However, simulation models also have known limitations in their code which allows the identification of points where knowledge needs to be gained (Hammer, 1998). Based on this review of literature, the major limitations of lucerne models are related to a lack of quantitative understanding about the changes in crop growth and development that occur seasonally and also at the onset of each regrowth cycle, particularly in remobilization and partitioning of DM and N between shoot and perennial organs. These issues are complicated by management and genetic diversity of lucerne which demands cultivar-specific parameters, for example related to FD responses.

2.8 Summary

The main conclusion from this literature review:

- There are a few lucerne models available in crop simulations or farm system simulations. None of the current lucerne models has mechanistically simulated lucerne seasonal carbon partitioning in above-ground and below-ground organs, or has been evaluated for its ability to simulate biomass production, biomass and N partitioning within leaf, stem and root of the crop subjected to different defoliation treatments and genotypes of FD classes.

- Lucerne phenological development is driven by Tt and modified by Pp. However, there are different functions and T_b that has been used to calculate Tt in different models. It is necessary to test and select the most accurate T_b and Tt function for lucerne growth and development (Objective 1).

- Lucerne canopy expansion is affected by temperature and Pp. Quantifying the canopy response to formation temperature and Pp should also include canopy senescence, basal bud appearance, and lag phase of the LAER (Objective 2).

- The key step for modelling a perennial crop is to simulate the seasonal dynamics of perennial organ biomass. This includes simulating the mechanisms for remobilization in spring and partitioning in autumn. The APSIM NextGen model

provides a feasible plant modelling framework to simulate sink and source relationships among organs (Objective 3).

- Perennial biomass remobilization and partitioning are associated with N dynamics. Therefore, simulating N concentration of each organ will help understand the impact of perennial reserves on crop regrowth (Objective 4).
- Modelling forage quality is important to estimate animal potential intake in grazing systems. Forage quality factors include stem height, leaf and stem CP and ME will included in the APSIM NextGen lucerne model (Objective 5).

3 MATERIALS AND METHODS

This chapter includes detailed descriptions of all datasets which are used for analysis and methods for field data measurements in this thesis. Model calibration, evaluation and optimization methods are also included. Additional methods specific to each individual chapter are described within the results chapter.

3.1 Field datasets

The parameters and relationships used to build the functions were derived from lucerne experiments under irrigated conditions at Lincoln University over the last 20 years (Table 3.1). Observed variables included the number of main stem nodes (node with a fully expanded leaf), days to 50% stem with a bud visible, days to 50% of stems with an open flower, soil water content, leaf area index, leaf, stem, shoot and root biomass, leaf, stem and root N (%), leaf and stem crude protein (CP) and metabolic energy (ME), and plant height. For model calibration, datasets from 42 or 84 day defoliation frequency treatments with a semi-dormant genotype (FD5) were used to generate equations and parameters. To assess how conservative the equations and parameters are, additional datasets that included different defoliation regimes and FD classes were used.

3.1.1 **Datasets description**

3.1.1.1 Experiment 1

Experiment 1 aimed to select the most appropriate species to grow in the summer dry environment. The response of lucerne was compared with red clover (*Trifolium pratense*) and chicory (*Cichorium intybus*). This experiment was conducted under dryland and irrigated conditions in Block 8 of Iversen field (I8), Lincoln University, Canterbury, New Zealand (43˚38'S and 172˚28'E). Inoculated 'Grasslands Kaituna' lucerne seeds were sown on 1 November 1996 with three replicates of 22 x 6.3 m plots. Lucerne crops grew under a 42±8 day defoliation treatment and the fully irrigated treatment was used in this thesis (E1ILL, described in Table 3.1). Data were collected from 1 November 1996 to 30 June 2002 over five growing seasons. Measurements included shoot biomass (dry matter), number of main stem nodes (node is a fully expanded leaf), soil water content, leaf area index, and plant height (Brown, 2004).

Table 3.1 Experiments and treatments for simulation and verification of an APSIM NextGen lucerne model. All experiments were conducted in Iversen field, Lincoln University, New Zealand.

Experiments	Treatments	ID	Symbols
E1(1996-2002)	Water	E1ILL	
E2(2000-2002)	Water/sowing date	E2ILLS1-S6, E2ILLS7-S9	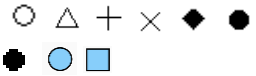
E3(2002-2004)	Defoliation	E3ILL E3ILS, E3ISL, E3ISS	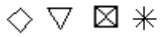
E4(2014-2019)	Defoliation/fall dormancy	E4ILLF5, E4IHHF5, E4ISSF5 E4IHHF2,E4IHHF10, E4ILLF2,E4ILLF10, E4ISSF2,E4ISSF10	

Note: Treatments are categorized according to consistent days between defoliation events; i.e. 28 day (S), 42 day (L), 84 day (H) and the combined treatments of 42 day followed by 28 day (LS) and 28 day followed by 42 day (SL) with three fall dormancy (F2, F5 and F10) under irrigated condition (I). Winter starts early May to end of August (87±19 day)

3.1.1.2 Experiment 2

Experiment 2 aimed to examine the impact of sowing date on seedling crop growth and yield. This experiment was established in Block 9 of Iversen field (I9) on 24 October 2000 at Lincoln University. Treatments included water (dryland and irrigated) and sowing date; defoliation interval was 42±5 days (E2ILLS1-S9 in Table 3.1 for full irrigated crops). Field data were collected from 2000 to 2002, for above-ground biomass (dry matter), leaf area index, and number of main stem nodes (Brown, 2004).

3.1.1.3 Experiment 3

Experiment 3 aimed to examine the seasonal changes in lucerne growth rates observed in Experiment 1 by excavating root biomass. The irrigated treatments from Experiment 2 [2000-2002 (Iversen I9)] were continued imposing four defoliation regimes, including a consistent 42±2 day cutting regime (LL), a 42±2 day and 28±4 day cutting regrowth cycle (LS and SL), and a consistent 28±4 day cutting regime (SS) to examine dry matter partitioning (E3ILL, E3ILS, E3ISL and E3ISS; Table3.1). Above-ground biomass, leaf area index, and number of main stem nodes were collected. In addition, root dry matter (crowns and taproots) and above-ground biomass (separated into shoot, leaf, and stem) were determined. Taproots were dug to a depth of 300 mm. For calculation purposes, sample tissue of crowns and the 300 mm of taproot represented 80% of total perennial biomass

(dry matter) in this experiment (Lemaire et al., 1992; Thiébeau et al., 2011). Forage quality data included total N content data of leaf, stem and taproot and crowns (Teixeira, 2006). N content was determined by the Kjeldahl method.

3.1.1.4 Experiment 4

Experiment 4 aimed to determine if the seasonal changes in partitioning observed in Experiment 3 were also apparent for genotypes of different fall dormancy (FD) and under different defoliation regimes, with an 84 day defoliation treatment (HH) to examine how lucerne responded to the environment under minimal defoliation. This experiment was established in 2014 in Block 12 of Iversen Field (I-12), at Lincoln University. Treatments were a factorial combination of three cultivars of different fall dormancy (FD): a dormant cultivar (FD2), a semi-dormant cultivar (FD5), and a non-dormant cultivar (FD10), and three defoliation frequencies: 28±3, 42±5, and 84±4 day (E4ISSF2, E4ISSF5, E4ISSF10, E4ILLF2, E4ILLF5, E4ILLF10, E4IHHF2, E4IHHF5 and E4IHHF10; Table 3.1). The experiment was established as a split-plot within a randomized complete block design with four replicates. The experiment was conducted over two growing seasons, from September 2014 to January 2017. Data collected included phenology of both seedling and regrowth crops, number of main stem nodes, shoot and root biomass (dry matter) for the seedling crop, and plant number, shoot number, and shoot biomass (separated into leaves and stems) for subsequent harvests. Root (perennial organ) biomass includes crowns and taproots. Taproots were dug to a depth of 300 mm. The same method was used as Experiment 3 to calculate total perennial dry matter, which was estimated as 80% of crowns and 300 mm of taproot. Forage nutritive values included total N content and ME of leaf, stem and taproots and crowns (Ta, 2018). N content was determined by using the Kjeldahl method and multiplied by a factor of 6.25 as for CP content of herbage (g g DM^{-1}). The ME content of herbage (MJ kg DM^{-1}) was calculated from organic matter digestibility, measured by NIR.

Field data collection at Experiment 4 was continued as part of this thesis. Collection of data began on 23 February 2017 and continued through April of 2019 as described in Table 3.2.

Table 3.2 Field measurements for Experiment 4.

Measurement	Description	Frequency
Phenology of 5 marked plants/plot		
Number of main stem nodes	5 marked stems/plot	7-10 days
Branching	5 marked stems/plot	7-10 days
Senesced leaves	Leaves >50% yellow	at harvest
Floral initiation	5 marked stems/plot	50 % of marked stems
Flowering	5 marked stems/plot	50 % of marked stems
Primary leaf appearance and senescence on 5 marked plants/plot		
Number of fully expanded primary leaves	Tall shoots	7 day intervals/cycle
Stem height (cm)	From ground to the apical bud	7 day intervals/cycle
Number of senesced leaves	50% yellow	On marked
Yield components of regrowth		
Plant/m^2	Counting number of plants/0.2 m^2 quadrat/plot	When digging /cycle
Shoot/plant	Counting number of shoots/plant/plot	When digging /cycle
DM_{leaf}	DM of all leaves/0.2 m^2 quadrat/plot	When digging /cycle
DM_{stem}	DM of all stems/0.2 m^2 quadrat/plot	When digging /cycle

3.2 The APSIM next generation model

3.2.1 **Model inputs**

3.2.1.1 Weather data

Daily meteorological data, including maximum temperature, mean temperature, minimum temperature, solar radiation, wind speed, and vapor pressure, were downloaded from the Broadfields Meteorological station (National Institute of Water and Atmospheric Research [NIWA], New Zealand https://cliflo.niwa.co.nz), located 2 km from the experimental site. The meteorological dataset is from 1990 to 2019, a period of 30 years. Rainfall (or precipitation) and air temperature were also recorded at the experiment site. All field experiments were conducted within this 30 years period (1996 to 2019).

The 30 year mean daily total solar radiation and daily air temperatures followed a seasonal pattern (Figure 3.1). Total solar radiation increased from a minimum of ~5 MJ m^{-2} day^{-1} in

July (winter) to a peak of 23 MJ m^{-2} day^{-1} in December (summer). Mean daily air temperature ranged from ~6 ˚C in July to ~17 ˚C in January and February. Average annual total precipitation was 590±143 mm and monthly average precipitation was 50±7.56 mm.

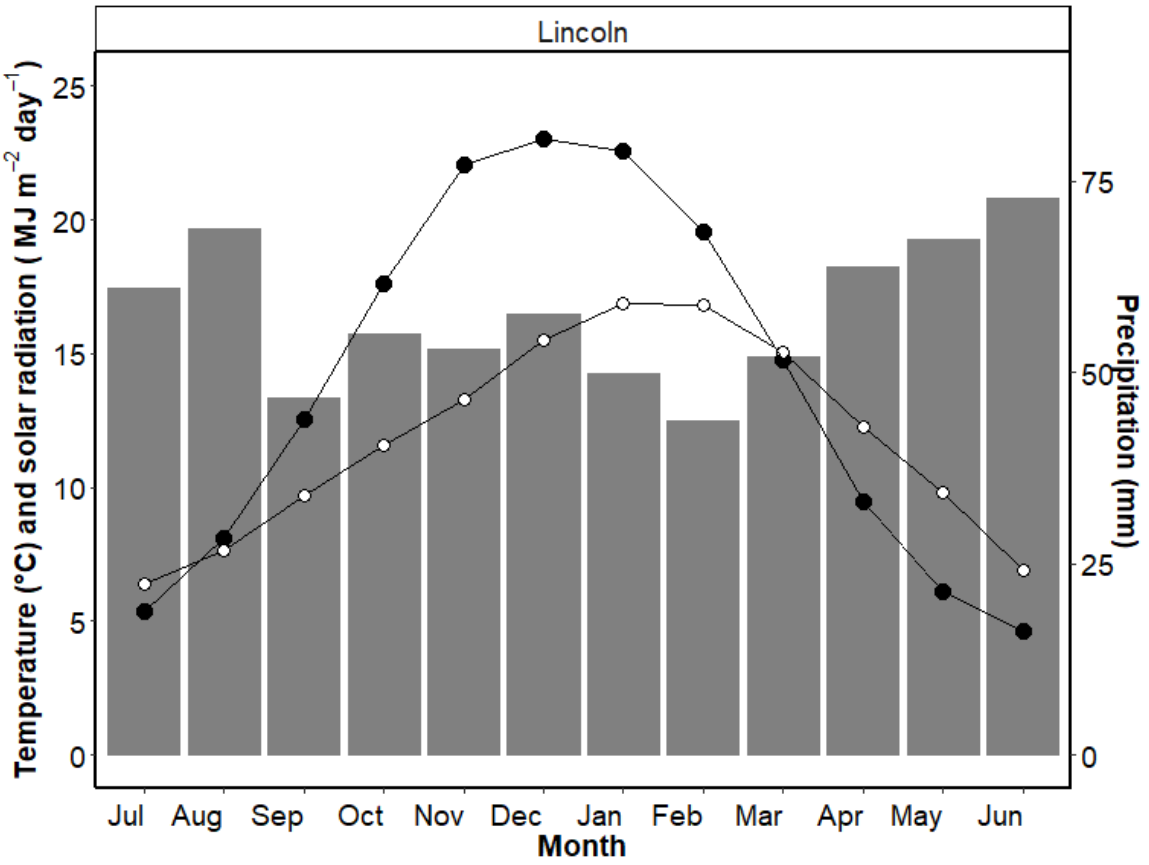

Figure 3.1. Mean solar radiation (–●–), mean air temperature (–○–) and mean precipitation (bars) for monthly periods from 1 January 1990 to 31 December 2019 at Lincoln University, Canterbury, New Zealand. Note: data were collected at the Broadfields Meteorological Station.

3.2.1.2 Soil data

The APSIM NEXTGEN model requires soil type, soil water content, and initial soil available water; soil parameters for specific plant species. The soil type at Iversen fields at Lincoln University is a 'Wakanui' deep silt loam (USDA Soil Taxonomy: Euic Ustochrept, fine silty, mixed, mesic), classified as 'Pallic' in the New Zealand Soil classification system (Hewitt, 2010; Watt and Burgham, 1992). Soil parameters was shown in Appendix 1.

3.2.2 **Model calibration**

The APSIM NextGen Plant Modelling Framework (PMF) contains three main plant class types; Top-level, Mid-level (Organ classes, Process classes, and Sub-classes), and Low-level

function classes (Brown et al., 2014). The lucerne model includes phenological development, leaf, stem, and root organs. The time-step of the lucerne model development and calibration was based on the APSIM NextGen model structure and the parameter calculation sequence, due to the interaction between each physiological process and specific plant organs. Algorithms and parameters were generated from analysis of long-term and multiple experiment datasets. Independent datasets from different treatments were used for verification and model fitting. For example, the most common (42 day) defoliation regime and irrigated treatments were used to calculate the basic algorithms and functions in the APSIM NextGen lucerne model. These were compared with specific parameterization of physiological processes previously used in APSIM and published for 'Grassland Kaituna' (Moot et al., 2015).

Long-term experimental datasets for defoliation regime and FD treatments were used to generate parameters which affect plant phenological development, yield and quality. Both calibration and verification of APSIM NextGen lucerne model were evaluated based on the agreement between observed and predicted values. Independent datasets were used to evaluate parameters and functions developed for the model (Table 1). The relationships derived from the FD5 genotype grown under a 42 day (LL) defoliation treatment were used for model development. These relationships were further tested by using datasets from two genotypes with contrasting FD (FD2 and FD10) under frequent (28 day: S) or long (84 day: H) defoliation regimes, all under irrigated conditions.

To improve model simulation accuracy, some of the parameters in the equations and relationships were adjusted to recalibrate the model to different conditions and management practises (Whisler et al., 1986). This study provided the necessary plant development and growth data for testing model assumptions and rationale for needed changes in parameters and functions.

3.2.3 **Model testing**

Crop model testing includes two main forms: 1) Evaluation in which model predictions are compared with field observed data (Whisler et al., 1986), and 2) Model optimization which estimates the most accurate values of unmeasured parameters by forcing model outputs to fit measured field data until the closest fit was obtained (Riaz et al., 2016).

3.2.3.1 Evaluation

Evaluation compares the output of the simulation with the observed data from field experiments. Statistical methods are used to assess the performance of simulated data against observed data. The relationship between the observed and actual crop yield are assessed using the method of Kobayashi and Salam (2000) and Confalonieri et al. (2010): outlined in Table 3.3. The Nash-Sutcliffe efficiency (NSE) is a normalized statistic that determines the relative magnitude of the residual variance compared with the measured data variance (Nash and Sutcliffe, 1970). The relative root mean square error (R_RMSE) is the ratio of the mean of square root of residuals squared to the mean of observed vaules (Eyduran et al., 2017). Both NSE and R_RMSE were used to determine model performance when comparing the simulated and measured values.

Table 3.3 Measures of agreement between a model predicted values and measured data. Y_i is the measured value for situation i and $\widehat{Y}_i$ is the model predicted value. $\bar{Y}$ is the average of the Y_i value and $\bar{\widehat{Y}}$ is the average of $\widehat{Y}_i$. N is the number of measurements.

Name	Equation	Meaning and range
Bias quantity	$D_i = Y_i - \widehat{Y}_i$	From -∞ to +∞
Standard bias	$SB = \frac{1}{N}\sum_{i=1}^{N} D_i$	Bias measures the average difference between measured and calculated values, a positive value means under-prediction, whereas a negative value means over-prediction.
Mean squared error	$MSE = \left(\frac{1}{N}\right)\sum_{i=1}^{N}(D_i)^2$	MSE is an average of the squared difference.
Mean squared error	$MSE^2 = (Bias)^2 + NU + LC$	MSE is an average of the squared difference calculated from the sum of its components.
Nonunity slope	$NU = (1 - b_{Y\widehat{Y}})^2 \times \left(\sum(\widehat{Y}_i - \bar{\widehat{Y}})^2/N\right)$	NU transparent relationships with regression parameters with b.

Lack of correlation	$LC = (1 - r^2) \times \left(\frac{\sum(Y_i - \bar{Y})^2}{N}\right)$	LC transparent relationships with regression parameters with r^2.
Nash-Sutcliffe efficiency	$NSE = 1 - \left[\frac{\sum_{i=1}^{n}(Y_i - \hat{Y}_i)^2}{\sum_{i=1}^{n}(Y_i - \bar{Y})^2}\right]$	Between -∞ and 1.0. Excellent: NSE = 1.0; Good: 0.50 <NSE < 1.0; Fair: 0.0 <NSE < 0.50; Poor: NSE<0.0 (He et al., 2019; Moriasi et al., 2007).
Root mean square error	$RMSE = \sqrt{MSE}$	RMSE has the same units as Y.
Relative root mean squared error	$R\_RMSE = \frac{RMSE}{\bar{Y}}$	Excellent: R_RMSE<10%; Good: 10%<R_RMSE<20%; Fair: 20%<R_RMSE < 30%; Poor: R_RMSE> 30% (Jamieson et al., 1991)
Coefficient of determination	$R^2 = \frac{\sum_{i=1}^{N}\left[(Y_i - \bar{Y})\left(\hat{Y}_i - \bar{\hat{Y}}\right)\right]}{\sqrt{\sum_{i=1}^{N}[(Y_i - \bar{Y})^2]\sum_{i=1}^{N}\left[\left(\hat{Y}_i - \bar{\hat{Y}}\right)^2\right]}}$	From 0 to 1

3.2.3.2 Model optimization

The APSIM NextGen lucerne model is also used as a hypothesis testing tool to generate parameters which were not directly assessed in the field experiments. To estimate the most accurate values of unmeasured parameters, model outputs were forced to fit measured field data until the closest fit was obtained (lowest R_RMSE and highest NSE values).

3.2.4 **Model version control**

Version control systems are software tools which help a software team to manage source code modifications over time. This project used a version control system for continual co-development of the model. The software requires systems to avoid a previous version from becoming redundant. The APSIM NextGen model uses GitHub (https://github.com/APSIMInitiative/APSIM NextGen) as the version control repository and uses an off-the-shelf product 'Jenkins' (https://jenkins-ci.org/) as the integration system. The workflow is described as follows: 1) APSIM master branch in Github is the

source of all released model components. 2) Developers are able to incorporate ‘forks’ or clones of the APSIM repository into their own GitHub account, then create a branch, name it, implement their changes, and commit as often as needed. 3) Developers can push to their repository on GitHub through pull request if they are satisfied with the results. 4) A software engineer examines minor changes. Major science changes are peer-reviewed by a lead researcher. The master branch won’t merge the new or revised branch in the APSIM repository until peer-review and the automated testing are satisfied. 5) All users can upgrade their user interface to update the continuous release system which integrates all the changes. The Jenkins testing system evaluates the validation simulations, calculates validation statistics and compares these values with expected statistics (Holzworth et al., 2014).

4 SIMULATION AND VERIFICATION OF LUCERNE PHENOLOGICAL DEVELOPMENT FOR SEEDLING AND REGROWTH CROPS

4.1 Introduction

The prediction of lucerne phenological development is important to estimate maximum herbage yield and quality, and optimize defoliation strategies. This is because crop development also affects the amount and time of biomass accumulation and partitioning between shoot and perennial organs (Moot et al., 2015). Therefore, the aim of this chapter is to determine whether lucerne crop phenological development responses to temperature and photoperiod (Pp) can be accurately simulated and predicted under different management practices for both seedling and regrowth crops. The hypothesis is that functions and algorithms (Table 4.1) used in previous versions of the APSIM classic lucerne model (Moot et al., 2015; Robertson et al., 2002) can be adapted to use in the APSIM next generation (APSIM NextGen) lucerne model to accurately quantify seasonal responses for crops of different fall dormancy (FD) classes, grown under different defoliation regimes.

This chapter therefore focus on Objective 1 of the thesis, to quantify, simulate and verify lucerne crop phenological development in seedling and regrowth crops using Plant Modelling Framework (PMF) in the APSIM NextGen. Datasets that recorded phenological development from multiple, long-term experiments (1-4) with standard management practices (irrigated with 42 day defoliation regime) were used to calculate functions and parameters. This model was then evaluated and verified with independent datasets from different defoliation treatments and FD classes (Chapter 3). The APSIM NextGen lucerne model parameters were compared with those reported in the previous literature and used in previous models (Table 4.1).

Table 4.1 Parameters used in the APSIM classic lucerne model.

Parameter name	Units	Parameter description	Lucerne (Robertson et al. 2002)	Lucerne (Moot et al. 2015)
T_b	˚C	Base temperature	5	1
Phyllochron (seedling)	˚Cd node^{-1}	Thermal time (Tt)required for node appearance on main stem	51	51
Phyllochron (regrowth)	˚Cd node^{-1}	Tt required for node appearance on main stem	34	34 to 51
$Tt_{0\text{-}fl}$	˚Cd	Tt to 50% flowering from 50% buds visible stage	*	161(seedling), 274(regrowth)
Tt_{Juv}	˚Cd	Tt from emergence to end of juvenile period	125 to 325	243 to 700

Note: * not parameterized.

4.2 Materials and Methods

The description of the experimental design, treatments and data collection were presented in Section 3.1. Statistical analyses and model evaluation were described in Section 3.2.4. Only additional measurement and calculations related to results of this chapter are reported.

4.2.1 Field experimental data

The parameters and relationships that were necessary to build the functions in the model were derived from experiments described in Section 3.1.1 and treatments listed in Table 4.2. Observed variables included the number of main stem nodes (node is a fully expanded leaf), days to 50% of buds visible, and days to 50% flowering. For model calibration, datasets from long regrowth cycle (42 and 84) defoliation treatments with a semi-dormant genotype (FD5) were used to generate equations and parameters. To determine how conservative the equations and parameters are, additional datasets that included different defoliation regimes and FD classes were used.

Table 4.2 Experiments and treatments for simulation and verification of the APSIM NextGen lucerne model. All experiments were conducted in Iversen field, Lincoln University, New Zealand.

	Experiments	Treatments	ID	Symbols
Calibration	E1(1996-2001)	Water	E1ILL	
	E2(2000-2002)	Water/sowing date	E2ILLS1-S4, E2ILLS5-S7, E2ILLS8-S9	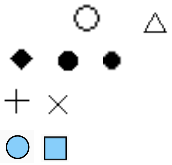
	E3(2002-2004)	Defoliation	E3ILL	
	E4(2014-2019)	Defoliation/fall dormancy	E4ILLF5, E4IHHF5	
Verification	E3(2002-2004)	Defoliation	E3ILS, E3ISL, E3ISS;	
	E4(2014-2019)	Defoliation/fall dormancy	E4ISSF5	
	E4(2014-2019)	Defoliation/fall dormancy	E4IHHF2,E4IHHF10, E4ILLF2,E4ILLF10, E4ISSF2,E4ISSF10	

Note: Treatments are categorized according to consistent days between defoliation events; i.e. 28 day (S), 42 day (L), 84 day (H) and the combined treatments of 42 day followed by 28 day (LS) and 28 day followed by 42 day (SL) with three fall dormancy (F2, F5 and F10) under irrigated condition (I). Winter starts early May to end of August (87±19 day)

4.2.2 **Model description**

Phenology is one of the classes in the PMF in the APSIM NextGen model. It represents a specific crop process and contains repeated data structures (Brown et al., 2014). Specially, phenological development is driven by thermal time (Tt). Daily Tt values are accumulated until specific targets (Tt sum thresholds) are reached and determine the duration of each phase. Lucerne phenological development is divided into phases separated by stages, the duration of each is based on accumulated Tt and maybe modified by photoperiod (Pp). Lucerne phenological development phases include: germinating (sowing to germination), emerging (germination to emergence), juvenile (emergence to end of juvenile), inductive (end of juvenile to floral initiation), induced (floral initiation to start flowering), flowering (start flowering to start podfill), podfilling (start podfill to maturity), and ripening (maturity to harvest ripe).

Sowing to germination is dependent on soil water status. If soil water at sowing depth is adequate, the minimum level controlled by the parameter pesw_germ, then germination

happens one day after sowing (Robertson et al., 2002). The accumulated Tt target from germination to emergence is affected by sowing depth and shoot elongation towards the soil surface. The initial period during which shoot elongation is slow is called the lag phase (shootlag) and was quantified as ~15 ˚Cd. Following the lag phase, the shoot elongation rate (shoot_rate) is linearly related to air temperature, equal to 10 ˚Cd mm^{-1} (Robertson et al., 2002). Any Tt and Pp responses in juvenile, inductive and induced phases were parameterized and verified as described in Section 4.2.3.2. The duration from flowering to physiological maturity was divided into three phases (flowering, podfilling and ripening), each based on fixed Tt requirements which were adapted from the APSIM classic model (Robertson et al., 2002). These phases were not included in the current model development because most of the available data focused on forage, so drops were not used for seed production.

4.2.3 Model calibration and parameterization

Node appearance, buds visible and flowering are components of phenological development. Parameters include several components of Tt: Tt to visual buds ($Tt_{0\text{-}bv}$); Tt from buds visible to flowering ($Tt_{bv\text{-}fl}$); Tt from emergence to end of juvenile (Tt_{juv}), and phyllochron (the Tt requirement of the period between the sequential emergence of main stem nodes). These are described and calculated in the following sections. The first step for phenological development parameterization was to determine the most appropriate method to calculate Tt and base temperature (T_b). The main stem node appearance rate (NAR) was used to assess this because it has been shown to be constant within regrowth cycles (Figure 4.3) and it is the observation with the most data points.

4.2.3.1 Tt calculation

To account for temperature around the cardinal points, each day was divided into 8 segments of 3 hours, with the mean temperature for each segment n of the day ($T^n_{diurnal}$) calculated as shown in Equation 3 (Jones et al., 1986; Moot et al., 2001). This approach is also more accurate than the daily mean when temperatures are above T_o. Tt calculations above T_o were included in the model for other users to test in regions where air temperature are above T_o, which does not occur in the temperate New Zealand environment.

Daily Tt, expressed as ˚Cd, may be calculated in numerous ways. In this study, three methods were evaluated: 1) the Moot model proposed by Moot et al. (2001), 2) the Fick framework (Fick et al., 1988), and 3) a beta function (referred to as the WE model) proposed by Wang and Engel (1998).

In the Moot model, Tt was calculated from daily mean air temperature using a broken stick threshold model, where T_b is 1 ˚C (Figure 4.1, solid line). Tt increases linearly at a rate of 0.7 ˚Cd˚C^{-1} up to 15˚C and then at a rate of 1.0 ˚Cd˚C^{-1} until 30 ˚C (Brown et al., 2005; Moot et al., 2001; Sim et al., 2015). This approach was developed based on the premise that the response between development and Tt is curvilinear (Bonhomme, 2000). Previously such adjustments to cardinal temperatures were required for accurately estimating maize (*Zea mays* L.) development in the cool temperate climate of Canterbury (Wilson et al., 1995).

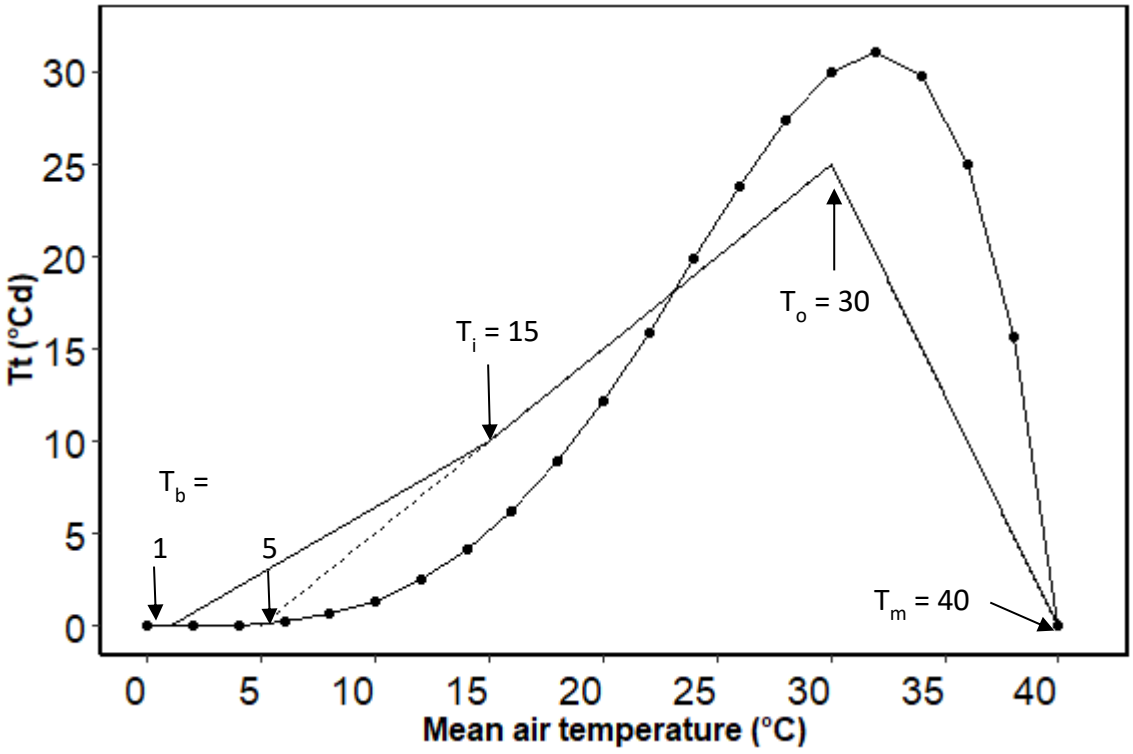

Figure 4.1. Accumulated thermal time [Tt (˚Cd)] against mean air temperature for the WE model (Beta function; dotted line), the Fick framework (dashed line) and the Moot model (broken-stick model; solid line).T_b is base temperature; T_i is the inflection point; T_o is optimum temperature; and T_m is maximum temperature.

The Fick framework (originally developed for lucerne Tt calculation) uses a broken-stick framework with a T_b of 5˚C, an optimal temperature (T_o) of 30 ˚C, and a maximum temperature (T_m) of 40 ˚C (Fick et al., 1988) (Figure 4.1, dashed line).

The WE model (dotted line) for Tt was originally developed for wheat (*Triticum aestivum* L.) crops, calculated as a beta function (Streck et al., 2007; Wang and Engel, 1998). The beta function used the same cardinal temperatures as the Fick framework proposed, attempting to represent the biological interactions between plant development and environmental factors (Streck et al., 2003). The WE model is described in Equations 13 to 16 and shown in Figure 4.1:

Equation 13 $$\boldsymbol{Tt = 0,\ T < Tb}$$

Equation 14 $$\boldsymbol{Tt = \frac{2(T-Tb)^{a}(To-Tb)^{a}-(T-Tb)^{2a}}{(To-Tb)^{2a}},\ \ Tb \leq T \leq Tm}$$

Equation 15 $$\boldsymbol{Tt = 0, T > Tm}$$

Equation 16 $$\boldsymbol{a = \frac{\ln 2}{\ln[(Tm-Tb)/(To-Tb)]}}$$

where T_b, T_o, and T_m are the cardinal temperatures (minimum, optimum, and maximum temperature) for lucerne development, T is the mean daily air temperature, T_o and T_m are 30 ˚C and 40 ˚C, respectively.

4.2.3.1 T_b evaluation

For the Moot model, T_b values were tested from T_b=0 ˚C to T_b= 4˚C at 1 ˚C intervals. For the Fick framework, T_b values were tested from T_b=5 to 10 ˚C at 1 ˚C intervals. For the WE model, T_b values were tested from T_b=0 to 5 ˚C at 1 ˚C intervals. Three statistical methods were used to determine the most appropriate T_b value: 1) x-intercept; 2) least variable; and 3) regression coefficient (Sharratt et al., 1989; Teixeira, 2006).

1) The x-intercept method plots the main stem node appearance rate (nodes day^{-1}) against the mean air temperature of the respective regrowth cycle. The main stem node appearance rate (NAR; nodes day^{-1}) was calculated as a linear slope between the number of main stem nodes and the number of days after grazing for each regrowth cycle. NAR was then plotted as a function of mean air temperature (Tmean), with the extrapolation of the linear relationship to y=0 giving the x-intercept (the T_b value±SE).

2) The least variable method determines the T_b value which results in the lowest coefficient of variation (CV%) of Tt over a specific phenological stage over different periods. The mean phyllochron (˚Cd main stem node^{-1}) was calculated for 17 different

T_b values for each regrowth cycle. The T_b value that produced the lowest CV% was identified as the most accurate T_b.

3) The regression coefficient method calculated the phyllochron for each regrowth cycle also using 17 different T_b values. Phyllochron values were then plotted against Tmean values for the respective regrowth cycle. The selected T_b value was the one that produced a slope with the highest probability (P value) of being non-zero.

4.2.3.2 Development stages

Lucerne plants have a basic vegetative phase (BVP), defined as the minimum Tt requirement for the transition from the vegetative to the reproductive phase (Tt_{BVP}, ˚Cd). The first field-observable sign of transition to the reproductive phase is the appearance of visible floral buds, defined as the "buds visible" stage (Teixeira et al., 2011). The Tt requirements for this stage were calculated from emergence (seedling crop), or after harvest (regrowth crops) to reach the 50% buds visible ($Tt_{0\text{-}bv}$) and 50% open flowers ($Tt_{0\text{-}fl}$) stages. Tt_{juv} was defined as $Tt_{0\text{-}bv}$ the difference between seedling and regrowth crops, once the Tt function had been defined.

4.2.3.3 Phyllochron

Phyllochron (˚Cd main stem node^{-1}) is the Tt interval between the appearance of successive nodes with fully expanded main stem leaves. Phyllochron was calculated as the linear slope between the number of main stem nodes and Tt accumulation from emergence date in seedling crops or from the end of grazing date in each regrowth crop. The mean Pp of each regrowth cycle was calculated as the average Pp value from the first to the last day of each regrowth cycle, tested as a phyllochron predictor.

For a 42 day defoliation treatment (LL), most regrowth cycles were in the vegetative stage at defoliation. Therefore, these observed data were used to calculate the phyllochron for the vegetative phase ($phyllochron_{veg}$), and plotted as a function of increasing or decreasing Pp. These relationships were analysed by least squares linear regression. The 84 day defoliation treatment (HH), had the longest regrowth duration, and was the only treatment that consistently gave lucerne plants adequate time to transition from vegetative to reproductive development. This treatment enabled the post-flowering phyllochron

(phyllochron$_{rep}$) to be calculated and plotted as a function of Pp and tested with linear regression, to determine whether it was different from phyllochron$_{veg}$.

4.2.4 Model verification

Independent datasets were used to evaluate parameters and functions developed for the model (Table 4.2). The first dataset was from Experiment 3 including regrowth crops only. This experiment differed in the number of days in spring and autumn defoliation regimes, with LS (42, 28 day), SL (28, 42 day), and SS (28, 28 day) treatments (Table 4.2). The second dataset was from Experiment 4 with both seedling and regrowth crops, with two FD classes (FD2 and FD10) grown under three defoliation regimes [HH (84 day), LL (42 day), and SS (28 day)], as described in Table 4.2.

4.2.5 Statistical analyses and model evaluation

Statistical analyses were performed using RStudio (R 3.4.0) (R Core Team, 2019). Several statistical indices were used to evaluate APSIM NextGen lucerne model performance: Coefficient of determination (R^2); Nash-Sutcliffe efficiency (NSE); mean square error (MSE); and relative root mean square error (R_RMSE). MSE was further segmented into components to quantify the causes of deviation: standard bias (SB), non-unit (NU) slope, or lack of correlation (LC). These are described in Chapter 3, Section 3.2.4.

4.3 Results

4.3.1 Base temperature estimation for Tt calculation

4.3.1.1 The x-intercept method

The relationship between main stem node appearance rate (NAR) and mean air temperature ranged from the highest R^2=0.80 in E3 to R^2=0.31 in E4 (Figure 4.2). Extrapolating the model to y=0 (no development), using the x-intercept method, gave estimated T_b values that ranged from -5.64 to 2.79 ˚C, with an average value of -1.12±1.67 ˚C (Table 4.3).

Table 4.3 Base temperature values (T_b) derived from four datasets using the x-intercept method.

Treatment	N	T_b (˚C)
X-intercept	E1(1997-2001)	-1.36
	E2(2000-2002)	-0.28
	E3(2002-2004)	2.79
	E4(2014-2019)	-5.64

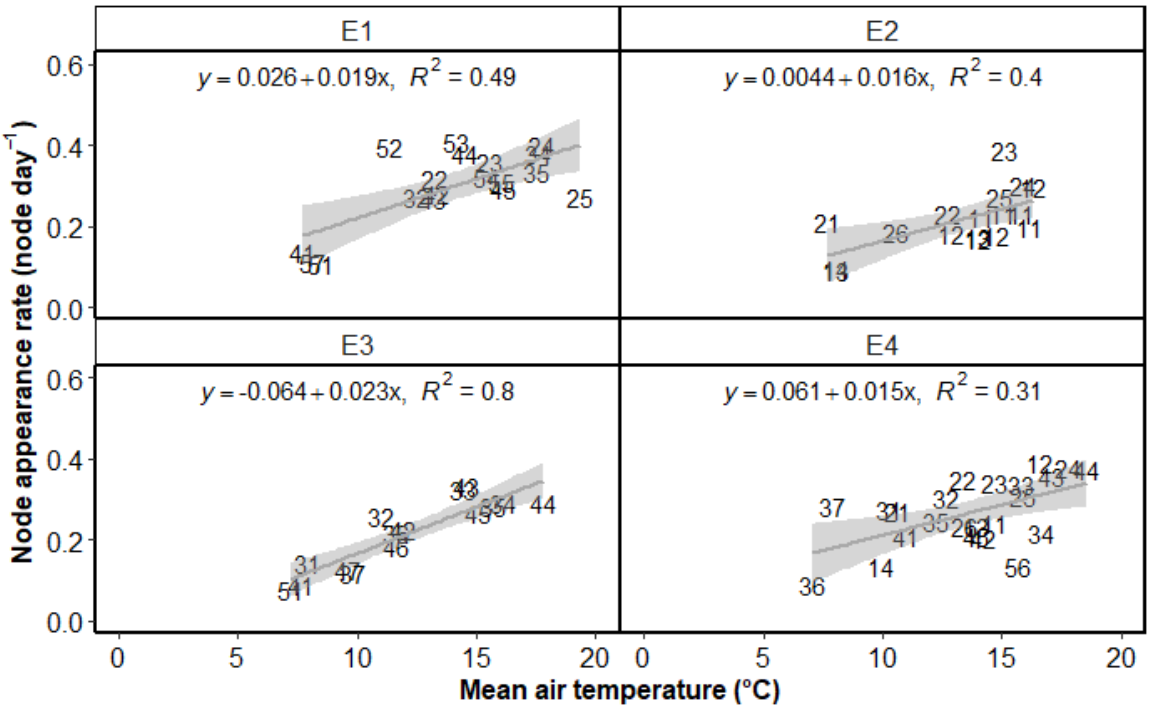

Figure 4.2. Main stem node appearance rate (nodes day^{-1}) against mean air temperature (˚C) derived from four field experiments with experiment 2 having four sowing dates between 1997 and 2019 at Iversen field, Lincoln University, Canterbury, New Zealand. Two digit code represents growth years and regrowth cycles. Details of E1-E4 are provided in Table 4.3.

4.3.1.2 Least variable and regression coefficient methods

The least variable method was used to select the least variable (CV%), whereas the regression coefficient method choose the highest probability (P) of slope being different from zero. CV% and P values were calculated for T_b values from 0 to 10 ˚C (Table 4.3). Since the Moot and Fick models are identical from T_b=5 to 10 ˚C, only T_b values from 0 to 4 ˚C are listed in Table 4.4. For the WE model only 0 to 5 ˚C are listed because the values clearly exceeded the lowest CV% values and produced the lowest P values of the three methods.

The Moot model resulted in the same CV% values (26%) for T_b from 0 to 4 ˚C, but the P value was the highest (0.82) at T_b=1 ˚C. The Fick model resulted in increased CV% and

decreased P values as T_b increased from 5 to 10 ˚C. For T_b=5 ˚C, the CV% was lowest (26%) and the P value was highest (0.009). The WE model resulted in the lowest CV% and highest P value with T_b=1 ˚C. However, these values were higher in CV% and lower in P value than the Moot model with T_b=1 ˚C. Thus, the Moot model with T_b=1 ˚C (Table 4.4) was used subsequently for Tt calculations for lucerne phenological development, throughout this thesis (Appendix 2 for model structure of Tt function).

Table 4.4 Statistical measures [percent coefficient of variation (%CV) and probability (P) value] resulting from three calculation methods (Moot model, Fick framework, and ME model) for various base temperature (T_b) values using the number of main stem nodes from four lucerne field experiments grown at Iversen field, Lincoln University, Canterbury, New Zealand.

Method	T_b (˚C)	CV (%)	P value
Moot model	0	26	0.44
	1	26	0.82
	2	26	0.71
	3	26	0.30
	4	26	0.08
Fick framework	5	26	0.009
	6	27	3.0e-4
	7	29	3.56e-6
	8	31	1.79e-8
	9	35	5.88e-11
	10	39	1.78e-13
ME model	0	36	2.46e-15
	1	37	9.42e-11
	2	38	3.34e-11
	3	40	1.09e-11
	4	41	3.31e-12
	5	44	9.31e-13

4.3.2 **Development stages**

4.3.2.1 Tt to 50% buds visible stages

The Pp at the start of each regrowth cycle was used in this analysis based on the assumption that Pp is perceived by the first leaves in each regrowth cycle. Seedling crops had a higher $Tt_{0\text{-}bv}$ value than regrowth crops at all Pp values (Figure 4.3). In seedling crops, $Tt_{0\text{-}bv}$ decreased linearly from 1191 ˚Cd to 423 ˚Cd as Pp increased from 10 to 16.5h. In

regrowth crops, a broken-stick relationship was found between $Tt_{0\text{-}bv}$ and Pp at the start of regrowth (R^2=0.66). $Tt_{0\text{-}bv}$ declined from 644 ˚Cd at 10 h of Pp to 278 ˚Cd and with 14 h Pp. $Tt_{0\text{-}bv}$ was consistent from 14 to 16.5 h of Pp, which represents the basic vegetative phase (BVP) (Major et al., 1991). Seedling crops required an additional Tt_{juv} to reach the buds visible stage, which ranged from 214 ±21 ˚Cd at Pp>14 h to 547 ±35 ˚Cd at shorter Pp (Appendices 3 and 4 for model structure for juvenile and inductive stage).

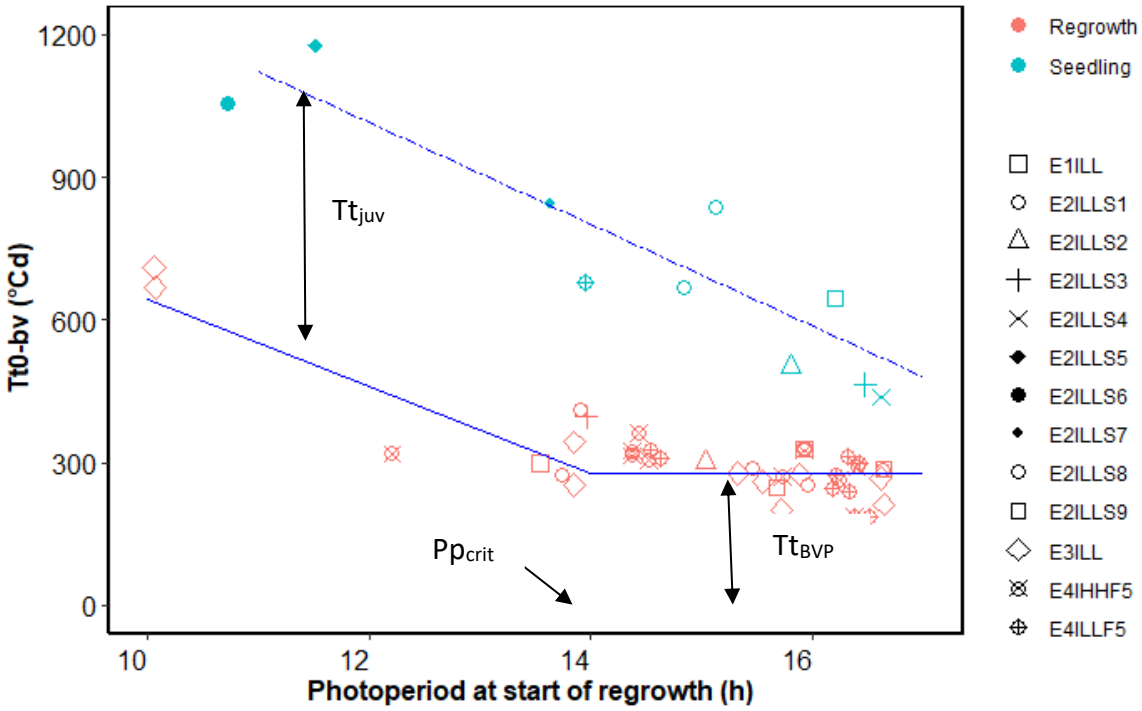

Figure 4.3. Relationship between thermal time (Tt) to the buds visual stage ($Tt_{0\text{-}bv}$) and photoperiod at the start of regrowth period (h) for four field experiments with Experiment 2 having nine sowing dates conducted from 1997 to 2019 at Iversen field, Lincoln University, Canterbury, New Zealand. The dashed line represents seedling crops and the solid line represents regrowth crops. Seedling crop: y= 2265-107.4x, R^2=0.76; Regrowth crop: y=1559-91.5x at Pp<14 h; y=278 at Pp≥14 h, R^2=0.67.

4.3.2.2 Tt to 50% flowering

After the buds visible stage, a strong linear relationship was found between $Tt_{0\text{-}bv}$ and $Tt_{0\text{-}fl}$ (Figure 4.4).This indicates that temperature was the main driver of development after buds became visible. The Tt requirement from buds visible to open flowers ($Tt_{bv\text{-}fl}$) was determined from the y-intercept, and was 310 ˚Cd for both seedling and regrowth crops (Appendix 4 for model structure for induced stage).

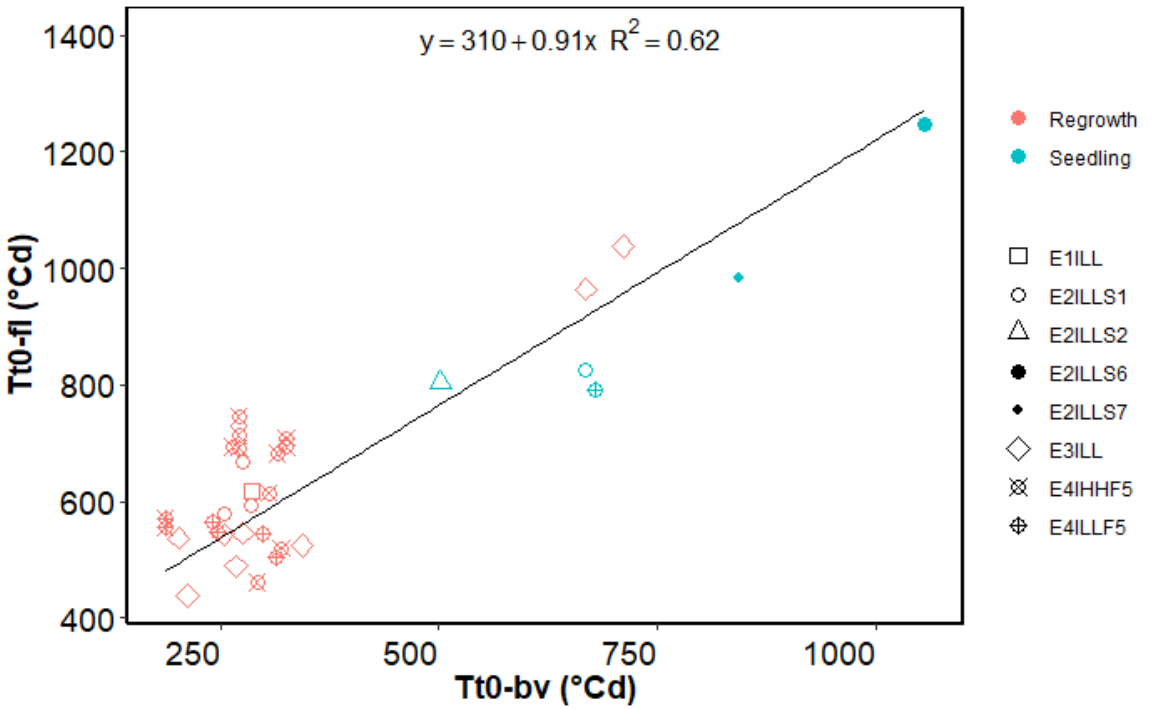

Figure 4.4. The thermal time requirement for the 50% buds visible stage ($Tt_{0\text{-}bv}$) in relation to 50% flowering ($Tt_{0\text{-}fl}$) for seedling and regrowth lucerne crops grown between 1997 and 2019 at Iversen field, Lincoln University, Canterbury, New Zealand.

4.3.2.3 Model simulation of the 50% buds visible stage

Parameters and functions for buds visible and flowering simulation were generated from previous sections (4.3.2.1 and 4.3.2.2) and were implemented into the APSIM NextGen lucerne model (Appendices 3-5 for model structure for phenology). Figure 4.5 and Table 4.5 provide statistical measures of the agreement for predicted and observed values for days to the 50% buds visible stage for the four experiments with three defoliation treatments and three FD classes. Overall, good agreement was observed between predicted and observed values (R_RMSE=22.3% and NSE=0.76). The model under-estimated the number of days to 50% bud visible for seedling crops (Figure 4.5a), but had good agreement for regrowth crops (Figure 4.5b), NSE values were -0.38 and 0.69, respectively (Table 4.5).

For the three defoliation treatments (HH, LL and SS), there was good agreement between predicted and observed values, although SS had a lower NSE value (0.29) due to fewer data points. There was no difference in the number of the days to 50% buds visible for genotypes from the three FD classes; NSE ranged from 0.68 to 0.83.

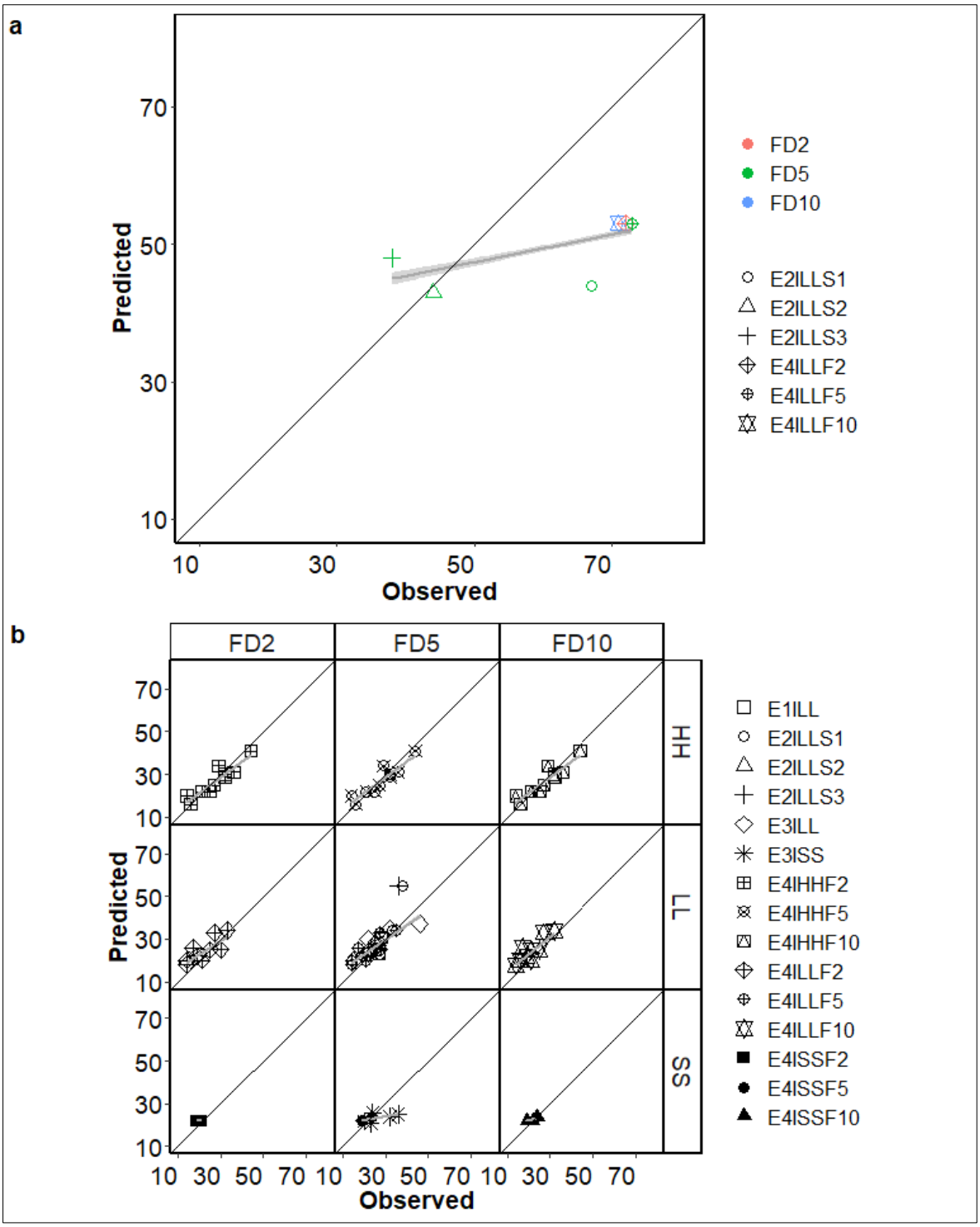

Figure 4.5. Predicted and observed values of days to 50% buds visible for a) seedling crops and b) regrowth crops from four field experiments with Experiment 2 having four sowing dates, three defoliation treatments [HH (84 day), LL (42 day), and SS (28 day)] and three fall dormancy (FD; FD2, FD5, and FD10) conducted between 1997 and 2019 at Iversen field, Lincoln University, Canterbury, New Zealand.

Table 4.5 Statistical measures of days to 50% buds visible stage for four field experiments with Experiment 2 having four sowing dates, three defoliation treatments [HH (84 day), LL (42 day), and SS (28 day)] and three fall dormancy (FD; FD2, FD5, and FD10) classes conducted between 1997 and 2019 at Iversen field, Lincoln University, Canterbury, New Zealand. N = number of simulated and observed data pairs; R^2= coefficient of determination; R_RMSE = relative root mean square error (%); NSE = Nash-Sutcliffe efficiency; SB = Standard bias; NU = Nonunity slope; LC = Lack of correlation.

Treatment	N	R^2	R_RMSE	NSE	SB	NU	LC
Total	143	0.79	22.3	0.76	0	11.3	88.7
Seedling	10	0.70	27.5	-0.38	48.0	11.9	40.1
Regrowth	133	0.45	17.5	0.69	3.9	0.6	95.5
HH	60	0.85	12.7	0.84	3.0	7.4	89.7
LL	70	0.78	28.0	0.75	0.5	14.9	84.6
SS	13	0.44	18.3	0.29	0.5	19.8	79.7
FD2	37	0.90	21.2	0.81	0.4	44.4	55.2
FD5	68	0.69	24.0	0.68	0.2	0.6	99.3
FD10	38	0.90	20.0	0.83	0.1	43.5	56.4

4.3.2.4 Model simulation of 50% flowering stage

Figure 4.6 and Table 4.6 show the statistical measures of agreement for predicted and observed values for days to the 50% flowering stage for the four experiments with two defoliation treatments and three FD classes. The model showed good agreement between predicted and observed values (R_RMSE=14.5% and NSE=0.66). The model accurately predicted the days to 50% flowering for regrowth crops: R_RMSE and NSE were 15.7% and 0.50, respectively. There was insufficient seedling crop data to test the model (n=4). For the two defoliation treatments (HH and LL), there was early prediction of flowering for the HH treatment. However, the prediction for the LL treatment was more accurate (NSE values of 0.96 for LL and 0.17 for HH). There was no difference in the number of days to 50% flowering among the three genotypes of different FD classes: R_RMSE was ~ 14 % and NSE ranged from 0.64 to 0.67.

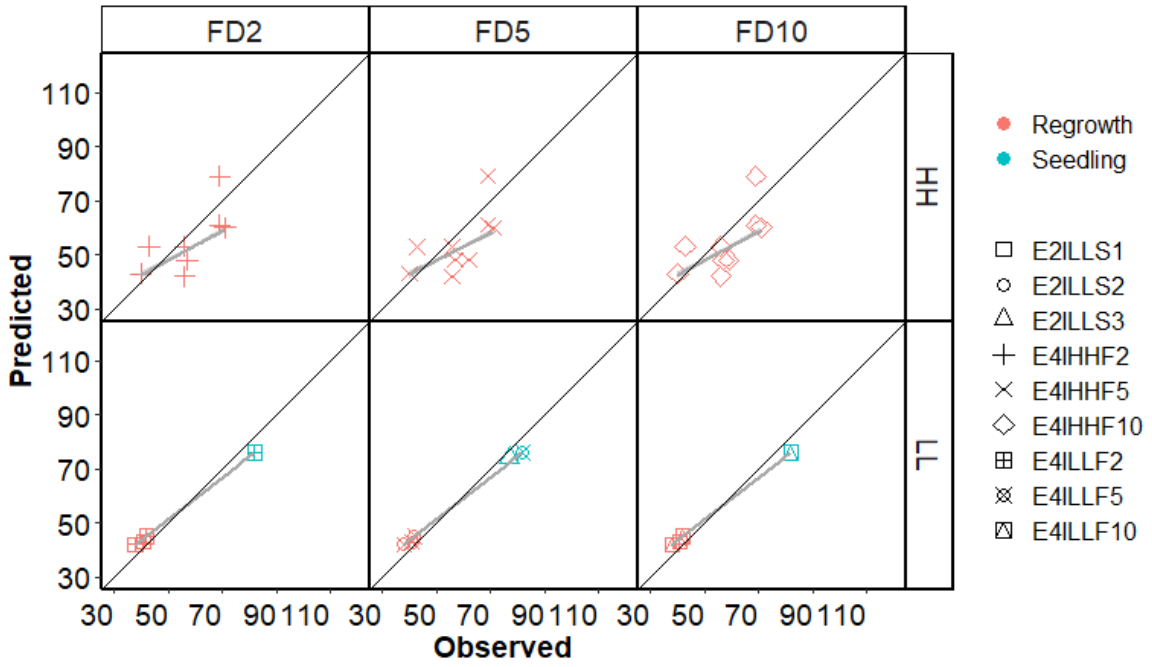

Figure 4.6. Predicted and observed values of days to the 50% flowering stage for four field experiments with Experiment 2 having four sowing dates, three defoliation treatments [HH (84 day), LL (42 day) and SS (28 day; did not reach flowering stage)] and three fall dormancy (FD; FD2, FD5, and FD10) classes conducted between 1997 and 2019 at Iversen field, Lincoln University, Canterbury, New Zealand.

Table 4.6 Statistical measures of days to the 50% flowering stage for four field experiments with Experiment 2 having four sowing dates, three defoliation treatments [HH (84 day), LL (42 day) and SS (28 day; did not reach flowering stage)] and three fall dormancy (FD; FD2, FD5, and FD10) classes conducted between 1997 and 2019 at Iversen field, Lincoln University, Canterbury, New Zealand. N = number of simulated and observed data pairs; R^2= coefficient of determination; R_RMSE = relative root mean square error (%); NSE = Nash-Sutcliffe efficiency; SB = Standard bias; NU = Nonunity slope; LC = Lack of correlation.

Treatment	N	R^2	R_RMSE	NSE	SB	NU	LC
Total	40	0.69	14.5	0.66	8.4	0.9	90.8
Seedling	4	0	6.7	-5.24	94.2	5.8	0.0
Regrowth	36	0.55	15.7	0.50	5.9	4.3	89.8
HH	27	0.44	16.4	0.17	15.2	17.1	67.7
LL	13	0.99	7.5	0.96	1.4	93.7	4.9
FD2	13	0.68	14.4	0.66	7.3	0.9	91.8
FD5	13	0.70	14.4	0.67	9.7	0.8	89.4
FD10	13	0.67	14.7	0.64	8.0	1.0	91.0

4.3.3 **Node appearance**

4.3.3.1 Node appearance and Tt

Five different sowing dates across two experiments (2 and 4) showed lucerne seedling crops required ~200 ˚Cd from sowing to emergence of the first true leaf (Figures 4.7; S_1). Figure 4.8 demonstrates that seedling crops produced a maximum of 11 main stem nodes within a 42 day regrowth cycle of 400 to 500 ˚Cd. In this duration, the number of main stem nodes had a strong linear relationship with accumulated Tt (R^2 from 0.92 to 0.99). E4ILLF5 (E4) and E2ILLS1 treatments had a similar slope (~0.02) of linear regression between the number of main stem nodes plotted against Tt in the first growth year (Appendix 6 for R^2, P, slope and intercept). Thus, data from Rt_2 to Rt_4 behaved like seedling crops and were included in subsequent analyses.

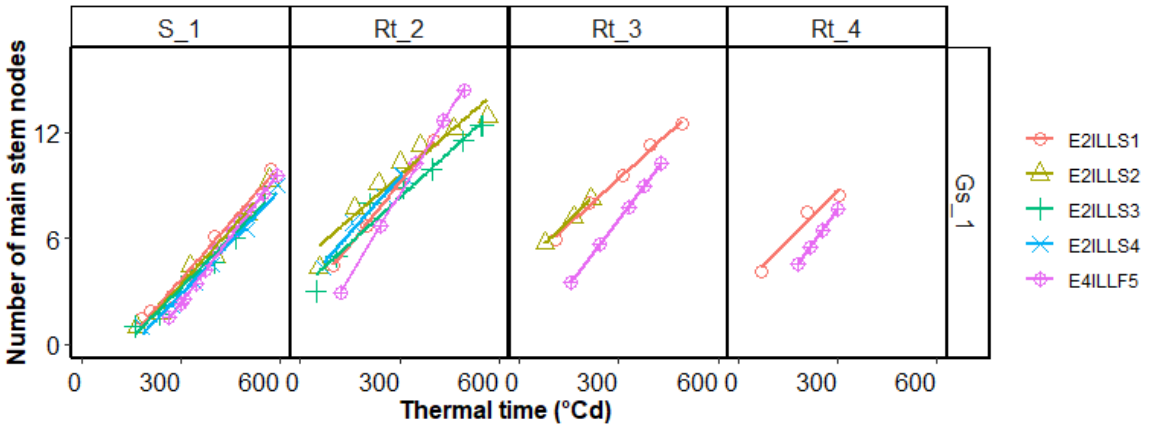

Figure 4.7. Number of main stem nodes plotted against thermal time (˚Cd) accumulated after sowing for seedling crops or after defoliation for regrowth crops from field Experiments 2 and 4 (E2 had four sowing date) conducted between 2000 and 2019 at Iversen field, Lincoln University, Canterbury, New Zealand. Row GS_1 is the first growth season (seedling crop). Column S_1 is the first growth cycle and columns Rt_2 to Rt_4 represent regrowth cycles. Lines represent linear regressions.

Figure 4.8 illustrates the number of main nodes plotted against Tt within seven regrowth cycles in five growth years for four experiments under a 42 day defoliation regime (~400 to 550 ˚Cd). There was a strong linear relationship between the number of main stem nodes and Tt in each regrowth cycle and every experiment. The linear relationship between number of main stem nodes and Tt explained 88 to 99% of the observed variation. Within a regrowth cycle (a column), the regression lines from different experiments were mostly parallel or overlapping. This indicates that the slope of each regrowth cycle was consistent

across different growth years. However, within a year (a row), a pattern of decreasing slope of linear regressions was observed in a condition of decreasing Pp (Appendix 6 for R^2, P, slope and intercept values). To explain this pattern, regression slopes were plotted against Pp in increasing and decreasing Pp separately. Seedling and regrowth crops produced the same maximum number of main stem nodes (~ 15), but seedling crops had lower slopes than regrowth crops (Figure 4.7 and Figure 4.8).

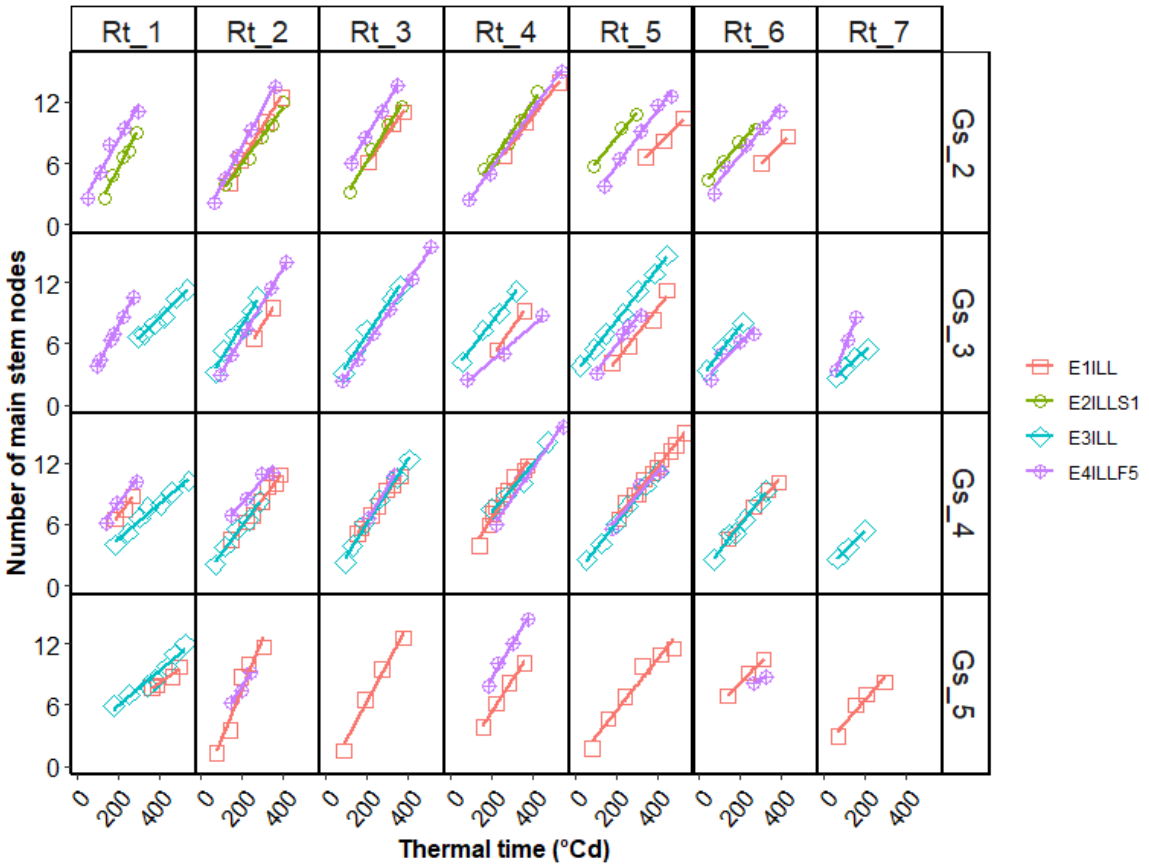

Figure 4.8. Number of main stem nodes against thermal time (˚Cd) accumulated after defoliation from four field experiments conducted from 1997 to 2019 at Iversen field, Lincoln University, Canterbury, New Zealand. Columns Rt_1 to Rt_7 represent regrowth cycles within a year, whereas rows GS_2 to GS_5 represent different growth years. Lines represent linear regressions.

4.3.3.2 Phyllochron and photoperiod

The linear regression between $phyllochron_{veg}$ and mean Pp in the vegetative stage of seedling and regrowth lucerne crops was separated into increasing and decreasing Pp conditions, due to the different development patterns (Figure 4.9). For regrowth crops, in increasing Pp conditions, the $phyllochron_{veg}$ was consistent across different day lengths, ~31 ˚Cd main stem $node^{-1}$ (Appendix 7 for model structure of $phyllochron_{veg}$ in increasing

Pp). In decreasing Pp conditions, the phyllochron$_{veg}$ increased from 35 to 49 ˚Cd main stem node^{-1} as Pp decreased from 16.5 to 10 h (Appendix 8 for model structure of phyllochron$_{veg}$ in decreasing Pp). This shows that as day lengths reduced the Tt required for each node to appear increased. Seedling crops also had a consistent phyllochron$_{veg}$ (~50 ˚Cd main stem node^{-1}), which was independent of Pp (Appendix 9 for model structure of seedling phyllochron).

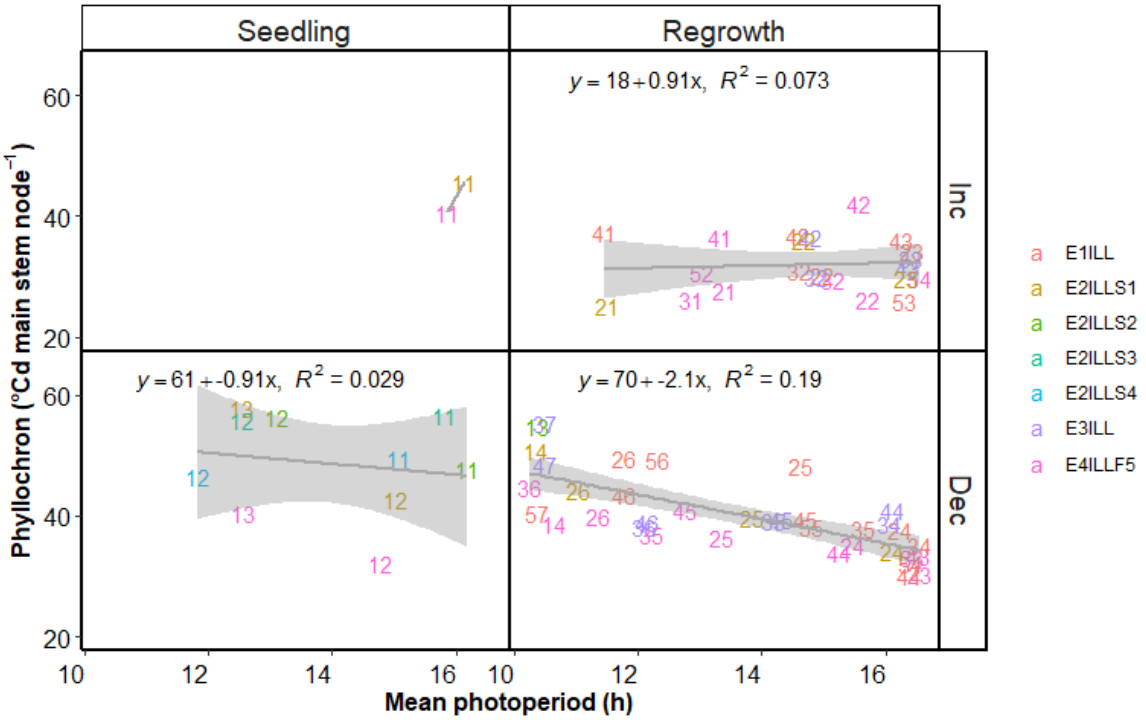

Figure 4.9. Phyllochron$_{veg}$ plotted against mean increasing (Inc) or decreasing (Dec) photoperiod for seedling and regrowth crops from four field experiments conducted from 1997 to 2019 at Iversen field, Lincoln University, Canterbury, New Zealand. The two dimension code represents growth years and regrowth cycles. The shaded areas are 95% confident interval.

4.3.3.3 Phyllochron$_{rep}$

The observed data showed two distinct phyllochron responses for the HH treatment (Figure 4.10). Node appearance rate (the slope of the number of main stem nodes plotted against Tt in linear regression models) decreased after plants had 10 to 12 nodes, typically when crops had reached the buds visible stage. Therefore, the number of main stem nodes data from the HH treatment were separated into vegetative and reproductive stages. Linear regressions between main stem node appearance and Tt improved with separate

functions (R^2=0.93 to 0.99) for the two stages (Figures 4.10; Appendix 10 for R^2, P, slope, and intercept).

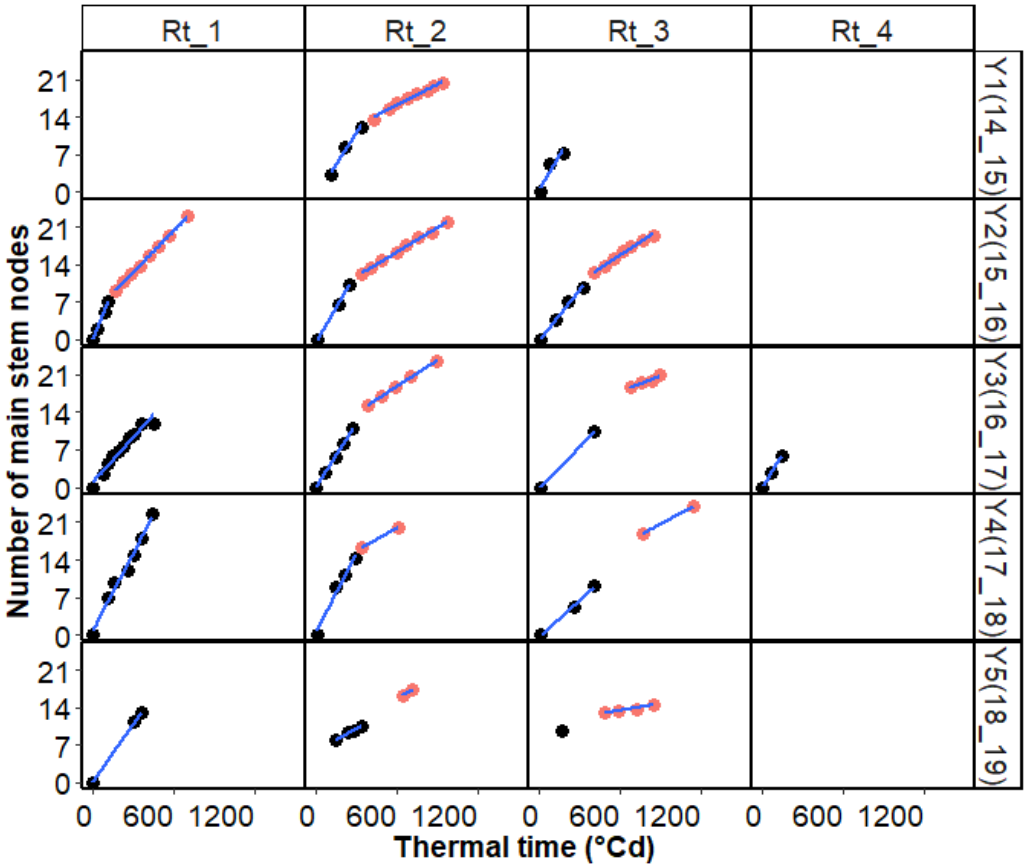

Figure 4.10. Number of main stem nodes against Tt (˚Cd) from Experiment 4 with the HH (84 day) defoliation treatments conducted from 2014 to 2019 at Iversen field Lincoln University, Canterbury, New Zealand. Columns Rt_1 to Rt_4 represent regrowth cycles and rows Y1 to Y5 represent growth years. Lines represent linear regressions.

The relationship between phyllochron and mean Pp in regrowth lucerne crops was therefore separated into vegetative ($phyllochron_{veg}$) and reproductive ($phyllochron_{rep}$) stages (Figure 4.11). In the vegetative stage, $phyllochron_{veg}$ decreased from 30 to 25 ˚Cd main stem $node^{-1}$ as Pp increased from 12.5 to 16 h. This was similar to the 31 ˚Cd main stem $node^{-1}$ in increasing Pp (Section 4.3.3.2), although the LL treatments had a bigger range of Pp. However, $phyllochron_{rep}$ was constant at ~69 ˚Cd main stem $node^{-1}$ across different Pp conditions (Appendix 11 for model structure of $phyllochron_{rep}$ in NodeNumber). Thus, more Tt was required to develop each fully expanded leaf following the 50% buds visible stage.

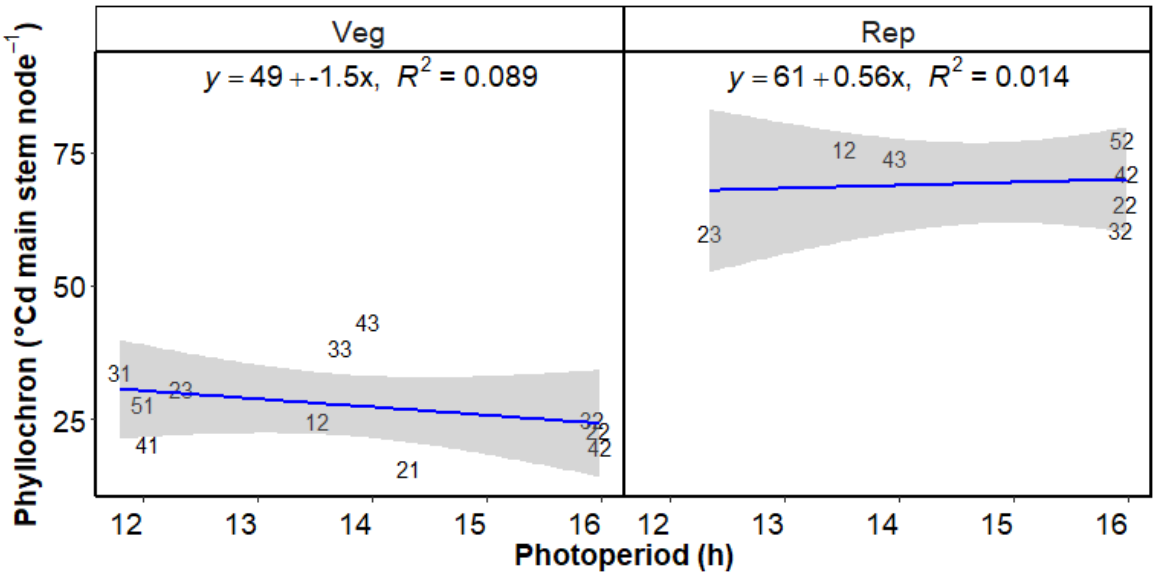

Figure 4.11. Phyllochron plotted against mean photoperiod for vegetative and reproductive crops for Experiment 4 with the HH (84 day) defoliation treatment conducted from 2014 to 2019 at Iversen field Lincoln University, Canterbury, New Zealand. The two dimension code (x, y) represents growth years and regrowth cycles. The shaded areas are 95% confident interval.

4.3.3.4 Simulation and analysis

Parameters and functions for node appearance simulations were generated from previous sections (4.3.3.2 and 4.3.3.3) and were implemented into the APSIM NextGen lucerne model (Appendices 7 to 9 and 11 for model structure for NodeNumber). Simulation results for predicting the number of main stem nodes in each regrowth cycle of four field experiments conducted from 1998 to 2019 (Figure 4.12 and Table 4.7) showed a good overall agreement (NSE = 0.74 and R_RMSE = 21.6%).

For seedling crops, there was good agreement between predicted and observed values (NSE was 0.78 and R_RMSE was 23.6%). However, under-estimation occurred in treatments E2ILLS1 and E2ILLS4 (Figure 4.12), with R_RMSE of 29.0% and 24.1%, respectively.

For regrowth crops, there was good agreement between predicted and observed values shown in Figure 4.12 and Table 4.7 (NSE = 0.71 and R_RMSE = 20.8 %). Over-predictions of node appearance were observed in the first regrowth cycle (Figure 4.13). Over-prediction also occurred at the end of the seasons (Figure.4.13).

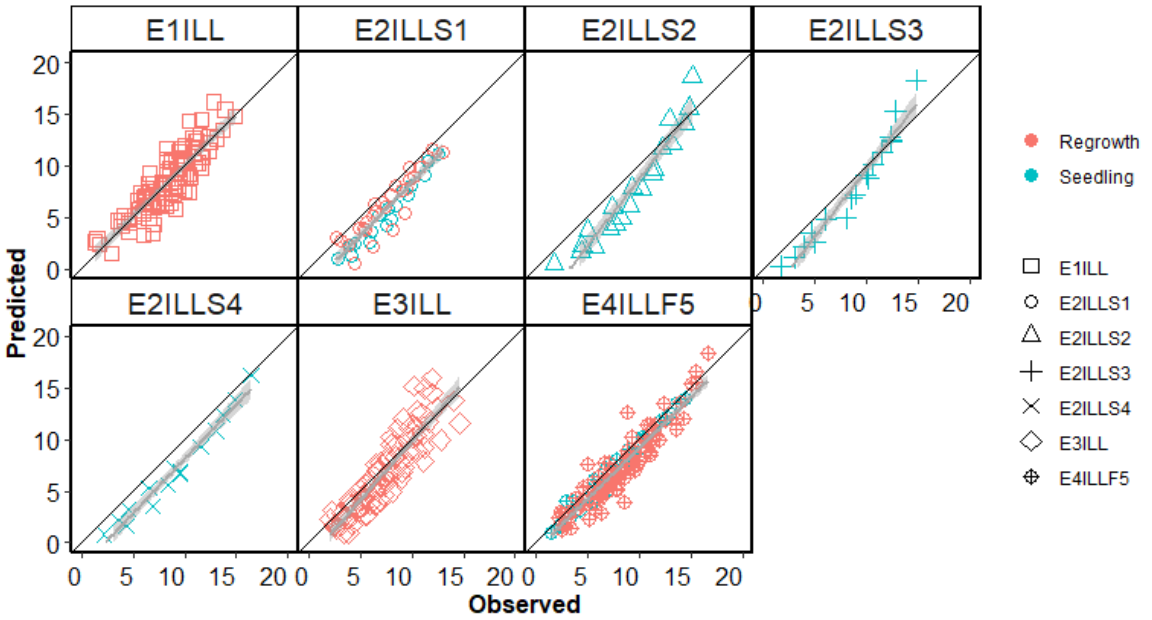

Figure 4.12. Predicted and observed values of the number of main stem nodes for calibration datasets for four field experiments with Experiment 2 having four sowing dates conducted between 1997 and 2019 at Iversen field, Lincoln University, Canterbury, New Zealand.

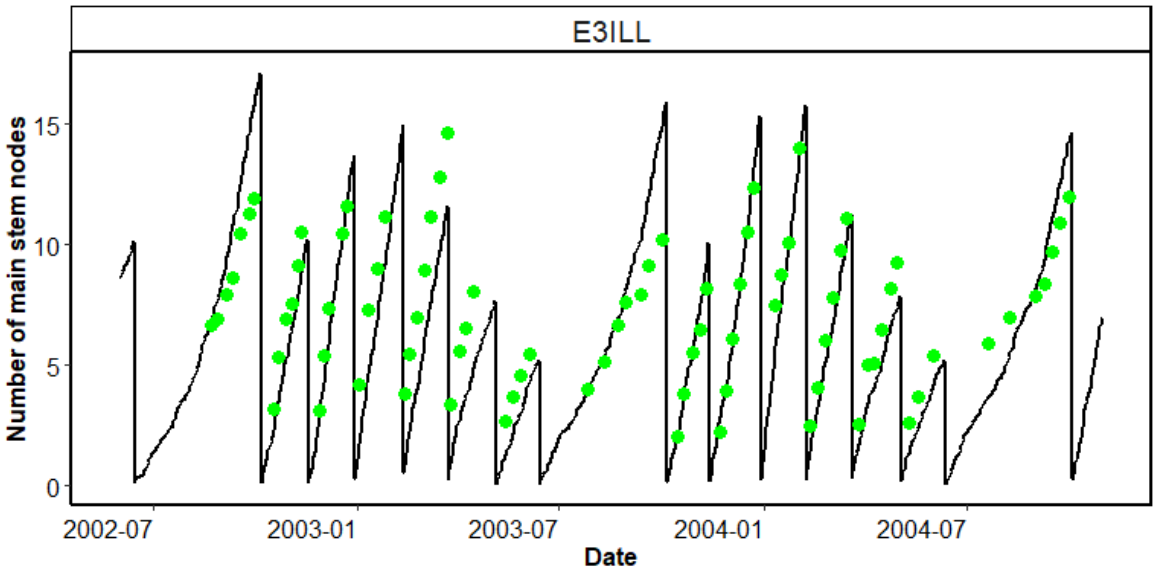

Figure 4.13. Predicted and observed values of the number of main stem nodes for Experiment 3 conducted between 2002 and 2004 at Iversen field, Lincoln University, Canterbury, New Zealand. Lines represent simulated values and points represent observed values.

Table 4.7 Statistical measures of the number of main stem nodes simulated using a calibration dataset from four field experiments conducted between 1997 and 2019 at Iversen field, Lincoln University, Canterbury, New Zealand. N = number of simulated and observed data pairs; R^2= coefficient of determination; R_RMSE = relative root mean square error (%); NSE = Nash-Sutcliffe efficiency; SB = Standard bias; NU = Nonunity slope; LC = Lack of correlation.

Treatment	N	R^2	R_RMSE	NSE	SB	NU	LC
Total	394	0.85	21.6	0.74	20.4	20.4	59.2
Seedling	104	0.92	23.6	0.78	43.4	20.6	36.0
Regrowth	290	0.81	20.8	0.71	13.6	19.1	67.3
E1ILL	97	0.78	17.9	0.72	0.9	15.1	84.0
E2ILLS1	46	0.88	27.4	0.53	72.2	3.80	24.0
E2ILLS2	21	0.92	25.2	0.70	48.6	27.5	24.0
E2ILLS3	20	0.95	22.0	0.80	10.9	64.0	25.0
E2ILLS4	16	0.97	24.1	0.80	82.0	1.6	16.4
E3ILL	81	0.80	24.8	0.63	12.3	33.6	54.1
E4ILLF5	113	0.89	18.3	0.83	40.5	1.7	57.8

4.3.3.5 Verification for defoliation treatments

The NodeNumber model was used to test lucerne crops (FD5) grown under different defoliation regimes. Overall, predicted and observed values of node appearance for two experiments (3-4) with multiple defoliation treatments (HH, LS, SL and SS) showed good agreement, with NSE of 0.86 and R_RMSE of 26.0 % (Figure 4.14 and Table 4.8). Among the three defoliation treatments, the HH treatment had the highest number of main stem nodes (~25), whereas the SS treatment had the lowest number ~10 (Figure 4.14). However, there was no difference in terms of model prediction of node appearance among HH, LL, and SS defoliation treatments. R^2 values ranged from 0.77 to 0.89, R_RMSE ranged from 22.4% to 27.3%, and NSE ranged from 0.60 to 0.84.

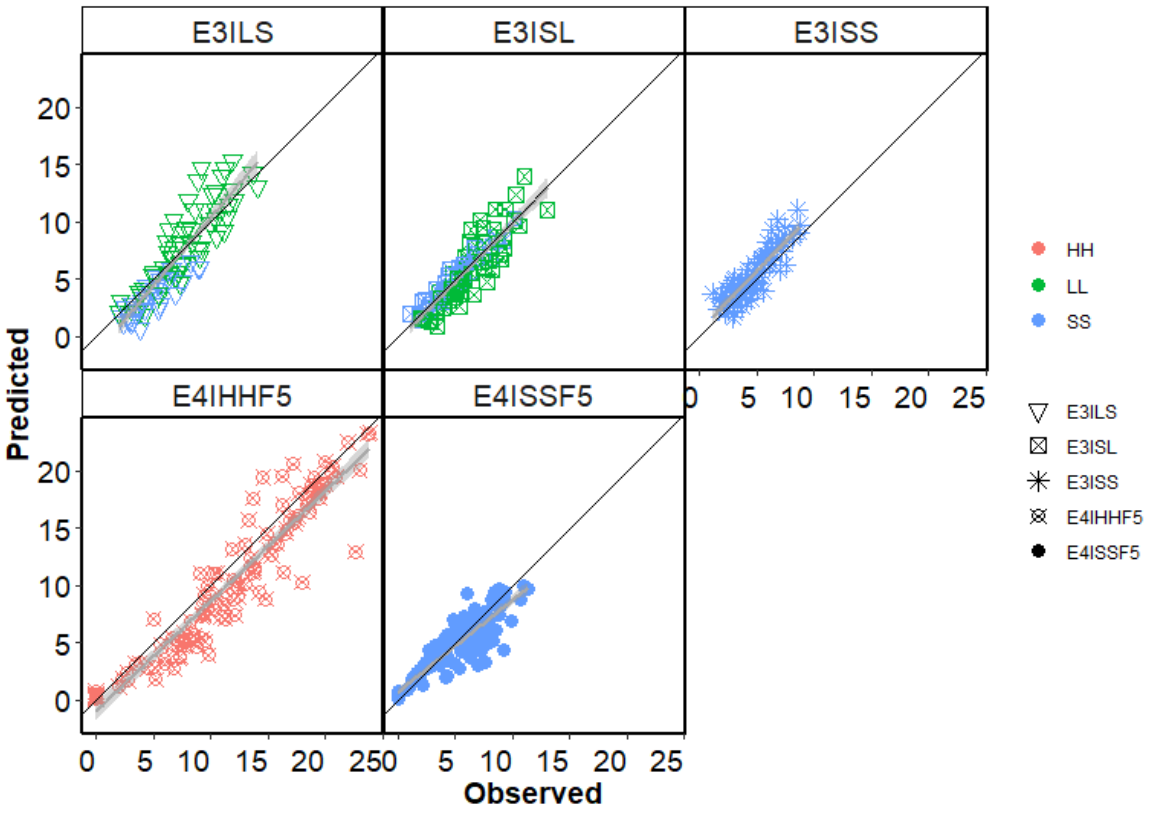

Figure 4.14. Predicted and observed values of the number of main stem nodes from field Experiments 3 and 4 with multiple defoliation treatments [HH (84 day), LS (42, 28 day), SL (28, 42 day), and SS (28 day)] conducted between 2002 and 2019 at Iversen field, Lincoln University, Canterbury, New Zealand.

Table 4.8 Statistical measures for the number of main stem nodes from two field Experiments 3 and 4 with multiple defoliation treatments [HH (84 day), LS (42, 28 day), SL (28, 42 day), and SS (28 day)] conducted between 2002 and 2019 at Iversen field, Lincoln University, Canterbury, New Zealand. N = number of simulated and observed data pairs; R^2= coefficient of determination; R_RMSE = relative root mean square error (%); NSE = Nash-Sutcliffe efficiency; SB = Standard bias; NU = Nonunity slope; LC = Lack of correlation.

Treatment	N	R^2	R_RMSE	NSE	SB	NU	LC
Total	499	0.87	26.0	0.86	2.30	2.60	95.1
HH	115	0.89	22.4	0.84	23.0	6.70	70.3
LL	107	0.79	24.5	0.60	0.10	47.1	52.3
SS	277	0.77	27.3	0.75	0.0	5.20	94.8
E3ILS	86	0.81	26.6	0.61	1.0	49.4	49.6
E3ISL	89	0.81	22.2	0.73	2.10	24.5	73.4
E3ISS	77	0.78	26.1	0.53	32.2	20.1	47.8
E4IHHF5	115	0.89	22.4	0.84	23.0	6.70	70.3
E4ISSF5	132	0.82	29.6	0.82	0.80	0.0	99.2

4.3.3.6 *Verification for fall dormancy classes*

The NodeNumber model was used to test lucerne crops FD2 and FD10 under different defoliation regimes. Overall, predicted and observed values of number of main stem nodes from Experiment 4 for two FD classes (FD2 and FD10) with multiple defoliation treatments (HH, LL and SS) had good agreement, with NSE of 0.86 and R_RMSE of 24.5% (Figure 4.15 and Table 4.9). For the three defoliation treatments, there was no difference in terms of model prediction for node appearance among HH, LL, and SS defoliation treatments; NSE ranged from 0.69 to 0.75, which were similar to Section 4.3.3.5 (Figure 4.14). For the two FD classes, predicted and observed values had good agreement: R_RMSE values were 24.4% to 24.6% and NSE values were 0.84 to 0.83. There was no difference between the two FD classes in terms of model prediction.

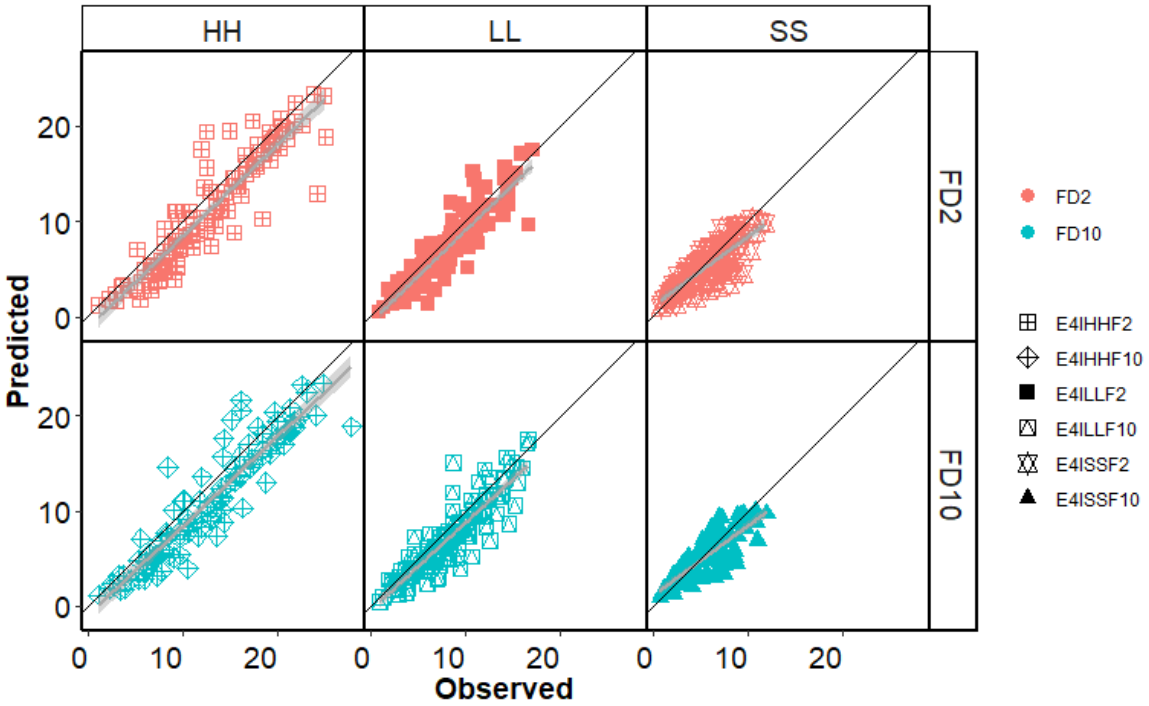

Figure 4.15. Predicted and observed values of the number of main stem nodes from field Experiment 4 with three defoliation treatments [HH (84 day), LL (42 day), and SS (28 day)] and two fall dormancy (FD; FD2 and FD10) classes conducted between 2014 and 2019 at Iversen field, Lincoln University, Canterbury, New Zealand.

Table 4.9 Statistical measures of the number of main stem nodes from field Experiment 4 with three defoliation treatments [HH (84 day), LL (42 day), and SS (28 day)] and two fall dormancy (FD; FD2 and FD10) classes, conducted between 2014 and 2019 at Iversen field, Lincoln University, Canterbury, New Zealand. N = number of simulated and observed data pairs; R^2= coefficient of determination; R_RMSE = relative root mean square error (%); NSE = Nash-Sutcliffe efficiency; SB = Standard bias; NU = Nonunity slope; LC = Lack of correlation.

Treatment	N	R^2	R_RMSE	NSE	SB	NU	LC
Total	690	0.86	24.5	0.82	20.8	0.5	78.7
HH	206	0.85	22.5	0.75	33.0	5.4	61.6
LL	265	0.82	23.0	0.73	26.1	6.8	67.2
SS	219	0.71	27.5	0.69	5.1	0.3	94.6
FD2	345	0.86	24.4	0.82	19.0	1.1	79.9
FD10	345	0.87	24.6	0.83	22.7	0.1	77.2
E4IHHF2	103	0.83	22.8	0.74	30.6	7.5	62.0
E4IHHF10	103	0.86	22.1	0.77	35.6	3.7	60.7
E4ILLF2	132	0.83	21.8	0.76	22.8	8.6	68.6
E4ILLF10	133	0.81	24.0	0.70	29.3	5.4	65.3
E4ISSF2	110	0.69	28.1	0.67	5.6	0.7	93.8
E4ISSF10	109	0.72	27.0	0.71	4.6	0.1	95.3

4.4 Discussion

Objective 1 of this thesis was to quantify and test the accuracy of phenological development in the APSIM NextGen lucerne model. The relationships derived from the FD5 genotype grown under 42 day (LL) defoliation treatment were successfully integrated into the model. This was then used to simulate development stages and main stem node appearance. Those relationships were further tested by using datasets from different FD classes grown under different defoliation treatments, to determine whether FD class or defoliation regime impacted on lucerne phenological development.

4.4.1 Tt calculations

The number of main stem nodes (leaf appearance) data were used to test thermal time (Tt) and base temperature (T_b) of phenological development in this thesis, because node appearance is conservative in response to temperature (Zaka et al., 2017) and successive data in a period of time can be easily obtained in the field. Pervious literature has also used data from germination (Andreucci et al., 2012; Black et al., 2006; Monks et al., 2009) and days to flowering (Ben-Younes, 1992) to calculate and test Tt and T_b for crop development.

However, germination rates differ from other process, specifically in natural populations where the proportion of germinating seeds is dependent on temperature (Zaka et al., 2017) and moisture, or hydrothermal time (Sharifiamina et al., 2016). Furthermore, the problem of using field measured days to flowering to estimate Tt and T_b is that the data generated may have only a narrow temperature range, which leads to inaccurate cardinal temperature (Bonhomme, 2000). In our experiments, flowering also only occurred in 39 of 410 regrowth cycles from all treatments, so leaf appearance had the most robust dataset and therefore was the most appropriate measurement to use.

The validity of the commonly used T_b ˚C (Section 4.3.1) was tested because of its significance for accurate calculation of Tt accumulation. Three different Tt functions and evaluation methods were used to test the best T_b and Tt function. The x-intercept method resulted in an important bias that affected the selection of T_b (Table 4.3 and Figure 4.2), because the average minimum air temperature ranged between 5 to 6 ˚C in Canterbury, NZ (Figure 3.1). Therefore, a large extrapolation was required to obtain x-axis intercept, which adds uncertainty in the determination of T_b values. Moreover, the coefficient of variation method showed no difference between T_b from 1 to 5˚C for the Fick and Moot models, thus it was not informative to select the most accurate T_b value. However, the regression method showed that the Moot model, with a T_b of 1˚C, was the most accurate method for determining Tt and T_b; it had the lowest CV=26% and highest P value (0.82). This was the same as previously reported for lucerne grown in Canterbury (Brown et al., 2005; Moot et al., 2001; Sim et al., 2016). Although the WE model (beta function) is claimed to be the most biological realistic method to reflect the interaction between plant development and environmental factors (Bonhomme, 2000), our results did not support its use for this cool and temperate environment. This might be related to the WE model structure and shape of the curve which gave low accumulated Tt values at the low temperature range (Figure 4.1).

Several T_b values have been reported in lucerne models. However, it is difficult to compare our T_b value with other models because different methods are used for Tt calculation. For example, the CROPGRO-PFM-Alfalfa (Malik et al., 2018) uses two sets of cardinal temperature for vegetative and reproductive stages, with T_b of 3 and 4 ˚C, respectively. The STICS model (Beaudoin et al., 2009) uses a photo-thermal index (PTI) to quantify

development. Specially, T_b of 3 ˚C is used to calculate Tt, base Pp of 11.5 h and Pp_{crit} of 18 h are used to determine Pp response (Strullu et al., 2020). However, those parameters were either from literature or calibrated from observed data, most models did not report how the parameters had been selected and tested in their publications.

4.4.2 Temperature and photoperiod response

Temperature and Pp were the main driving factors for lucerne phenological and morphological development under a 42 day (LL) defoliation treatment, including the time to each development phase (Hanson et al., 1988) and the number of main stem nodes (Hay and Walker, 1989; Teixeira, 2006).

Lucerne seedling and regrowth crops had different development patterns. Seedling crops required a higher Tt accumulation (Figure 4.3) to reach buds visible compared with regrowth crops grown in the same temperature and Pp conditions. This additional Tt requirement was due to a juvenile phase, when plants do not respond to Pp (Pearson and Hunt, 1972; Teixeira et al., 2011). Both seedling and regrowth crops required higher Tt accumulation in a short Pp to reach flowering. However, there was insufficient data to determine the Pp_{crit} for seedling crops. Major et al. (1991) observed a Pp_{crit} of ~18 h for seedling crops of different cultivars. In this study, the Pp_{crit} was 14 h for regrowth crops (Figure 4.3). However, there wasn't sufficient data points with daylengths of less than 12 hours from the datasets used in this study. Hence further data points from less than 12 h daylength are needed to fit the function. This is consistent with reports of lucerne as a long day plant from field Experiment 3 at this location (Teixeira et al., 2011). Regrowth crops required a minimum of 278 ˚Cd to reach buds visible (Figure 4.3), which was defined as the basic vegetative period (Tt_{BVP}). Reanalysis with a larger dataset showed the functions between Tt to buds visible and Pp at start of regrowth for seedling and regrowth crops were similar to those reported by Teixeira et al. (2011). Pp had no influence on the duration between the bud visible and the flowering stage. Specifically, once the reproductive organ (bud) was initiated, ~310˚Cd were required to reach flowering (Figure 4.4), and this was conservative between seedling and regrowth crops. This value was larger than that reported by Teixeira et al. (2011) at 274˚Cd for regrowth crops, which may be because this larger dataset had sufficient observations to separate the buds visible and open flowering stages.

To quantify and simulate lucerne development stages in the APSIM NextGen lucerne model, lucerne phenological stages were adapted from the classic APSIM lucerne model and the Tt for the juvenile phase (emergence to end of juvenile) and the inductive phase (end of juvenile to floral initiation) were calculated. A minimum of 278 ˚Cd was used for the basic vegetative period and Pp-induced phase (Figure 4.3). This Pp-induced phase increased as Pp decreased beyond the base Pp (14 h). The induced (floral initiation to start flowering) phase was only regulated by temperature (310 ˚Cd). However, flowering (start of flowering to start podfill), podfilling (start podfill to maturity) and ripening (maturity to harvest ripe) phases are still to be quantified, due to a lack of data for the crops after flowering.

This development stage system in APSIM NextGen lucerne model is different to the 10-stage classification developed by Kalu and Fick (1983) with the mean stage by weight (MSW) for all the shoots calculated as the average stage, weighted by the dry mass of shoots within each stage. Ben-Younes (1992) refined the 10-stage classification system by using accumulated Tt. The 10-stage classification system emphasised morphological stages and forage nutritive value, and included a stem height measurement for the first three stages [early (≤ 15 cm), mid- (15 to 30 cm), and late (≥ 30 cm) vegetative stage]. However, lucerne growth and development are driven by different environmental factors and need to be treated separately (Hodges, 1990). Thus, characterizing the vegetative stage in the APSIM NextGen lucerne model did not include stem height measurements and was not separated into three sub-stages.

In the vegetative stage, $phyllochron_{veg}$ was constant (~31.0 ˚Cd main stem $node^{-1}$) in an increasing Pp (spring) as Pp changed from 10 h to 16 h, but responsive to a decreasing Pp in autumn, from 49.0 to 35.0 ˚Cd per main stem node (Figure 4.9). These $phyllochron_{veg}$ values are similar to those used in APSIM classic lucerne model (51 to 34 ˚Cd main stem $node^{-1}$) which were derived solely from Experiment 3. It is possible that $phyllochron_{veg}$ is the same in decreasing Pp as in increasing Pp, but changes in partitioning of carbon and nitrogen to roots in decreasing Pp limited the expression of node appearance as manifest of a longer phyllochron (Brown et al., 2005). Carbon and Nitrogen dynamics are examined tested in Chapters 6 and 7. Seedling crops had a consistent phyllochron (~50.0 ˚Cd main stem $node^{-1}$) across different Pp, which was higher than in regrowth crops, but consistent

with previous values used in the APSIM classic lucerne model (51 ˚Cd main stem node^{-1}) calculated from Experiment 2 (Table 4.2). Slower leaf appearance in seedling crops could also be due to greater partitioning to roots for storage in the early growth stage (Sim, 2014; Ta et al., 2016).

After plants reached the reproductive stage (50% buds visible), phyllochron values doubled (~69.0 ˚Cd main stem node^{-1}) compared with in the vegetative stage. This field observation is consistent with previous field experiments (Ta, 2018; Teixeira, 2006). One possible explanation is that the supply of carbon is insufficient to maintain the leaf appearance rate after plants reach reproductive stage. This would occur if at the reproductive stage perennial organs have partitioning priority for carbon and nutrients (Sinclair and Muchow, 1999; Ta, 2018). For these crops, the demand from pods and seeds was minimal, so it seems likely that changes in partitioning priority are responsible.

Simulation of development stage showed good agreement between predicted and observed values for days to buds visible and days to flowering for regrowth crops. However, it was poor for seedling crops due to the limited dataset (Figure 4.5 and 4.6). Simulation of the number of main stem nodes showed good agreement between predicted and observed values for both seedling and regrowth crops. On occasion, over-predictions were observed in later stages of first regrowth cycles (data not shown). This may be because early spring frost (minimum of -5˚C was recorded on experiment site) occurred. This would restrict node appearance rate. Therefore, data for a frost response are needed for future model development to accurately predict node appearance in early spring regrowth cycles.

4.4.3 **Defoliation effect**

The hypothesis that defoliation treatments would affect development stage, node appearance rate and stem elongation was tested using data collected under different defoliation treatments (HH, LS, SL and SS). Defoliation treatments did not affect crop development rates. The parameters and equations generated from the 42 day (LL) and 84 day (HH) defoliation treatments were also appropriate for shorter defoliation intervals. The model gave fair prediction of buds visible under the 28 day (SS) defoliation (NSE=0.29 and R_RMSE=18.3%). This finding was consistent with previous reports from the same location (Ta, 2018). Furthermore, there was good agreement between predicted and observed

values for the number of main stem nodes under all defoliation treatments. This indicates that node appearance was independent of defoliation treatments. This also suggests that lucerne node appearance was not affected by the root reserve levels, created by the different defoliation treatments (Teixeira et al., 2008). A similar seasonal pattern of changes in phyllochron occurred regardless of root reserve levels. For example, partitioning to roots in the autumn resulted in a higher Tt requirement for node appearance in the same Pp irrespective of defoliation regimes (Figure 4.14).

4.4.4 **FD effect**

Development stage was also independent of FD class based on our analysis of these FD2, FD5, and FD10 genotypes. There was no difference in the number of days to 50% buds visible and 50% flowering among the three FD classes. The calibrated model from the FD5 treatments accurately predicted FD2 and FD10 days to buds visible and flowering responses, NSE ranged from 0.64 to 0.67. This finding was consistent with the previous year's observation from the Experiment 4 (Ta, 2018). Previously, Ben-Younes (1992) also reported there was no difference of development stage among lucerne cultivars of three FD classes from very dormant to non-dormant grown under both controlled environment and field conditions.

Equally, the seasonal changes in phyllochron and node appearance were not cultivar dependent for the genotypes tested. Predicted and observed values had good agreement for all three FD classes. Therefore, phyllochron functions derived from the FD5 cultivar were used to predict node appearance of FD2 and FD10 genotypes. This result is consistent with previous reports that phyllochron remains constant regardless of genotype (Fick et al., 1988), but should be tested across a wider range of genetic materials. A tradeoff between lucerne internode length and number of main stem nodes in response to FD has been reported by Liu et al. (2015). However, the difference in node appearance rate was not significant in our studies.

Node appearance is an important component of the canopy. However, defoliation regimes and FD classes are expected to influence canopy expansion and plant growth at different phenological development stages. Chapter 5 aims to quantify and model lucerne canopy expansion and radiation interception in relation to defoliation and FD treatments.

4.5 Conclusions

The results of this chapter permit the following conclusions:

- The Moot model with a T_b of 1 ˚C was the most accurate method for estimating Tt accumulation of lucerne crops development.
- Tt to buds visible ($Tt_{0\text{-}bv}$) decreased as Pp increased to 14 h for regrowth crops.
- The number of main stem nodes had a strong positive linear relationship with Tt. $Phyllochron_{veg}$ was responsive to Pp only in decreasing Pp conditions (autumn). Greater Tt was required for node appearance in the reproductive phase.
- Lucerne phenological development was not affected by defoliation regime or FD class. There was good agreement between predicted and observed values of number of main stem nodes, and days to 50% buds visible and 50% flowering.

5 MODELLING CANOPY EXPANSION AND RADIATION INTERCEPTION

5.1 Introduction

Total shoot and root yield are determined primarily by the amount of radiation intercepted by the canopy and how efficiently it is used (Brown et al., 2006). One of the major challenges for constructing a crop simulation model is to capture the seasonal changes of physiological processes in response to the environment. Specifically, this includes changes in the canopy expansion rate (Teixeira, 2006).

Therefore, the research question is can crop canopy expansion responses to seasonal changes temperature and photoperiod (Pp) be accurately simulated and predicted under different management practices for lucerne seedling and regrowth crops? The hypothesis is that functions and algorithms (Table 5.1) used in APSIM classic lucerne model (Moot et al., 2015; Robertson et al., 2002) can be adapted for use in the APSIM NextGen lucerne model to accurately quantify seasonal responses for crops of different fall dormancy (FD) classes grown under different defoliation regimes.

To test this, Objective 2 of this thesis is to quantify, simulate and verify lucerne crop canopy expansion and radiation interception in seedling and regrowth crops using the APSIM next generation (APSIM NextGen) Plant Modelling Framework (PMF).

Field measured data of LAI and radiation interception from irrigated experiments (1-4) with the LL defoliation regimes were used to calculate functions and parameters in the PMF. This model was then evaluated and verified using additional datasets from different defoliation treatments and fall dormancy (FD) classes. This procedure allows the consistency of the relationships and parameters derived in standard management conditions to be determined under different defoliation regimes and FD classes, and identify any physiological reasons for any changes. Resulting parameters were compared with those derived in previous models (Table 5.1).

Table 5.1 Parameters used in the APSIM classic lucerne model.

Parameter name	Units	Parameter description	Lucerne (Robertson et al. 2002)	Lucerne (Moot et al. 2015)
T_b	˚C	Base temperature for leaf area expansion	5	1
LAER	m^2m^{-2} ˚Cd^{-1}	Leaf area expansion rate	*	0.005-0.013
Leaves_per_node		Number of leaves per plant per main stem node	1	*
k		Extinction coefficient	0.43 (Seedling); 0.8 (Regrowth)	0.81

Note: * not parameterized.

5.2 Materials and methods

The description of the experimental design, treatments and data collection were presented in Section 3.1. Statistical analyses and model evaluation were described in Section 3.2.4. Only additional measurement and calculations related to results of this chapter are reported.

5.2.1 Field experimental data

Simulation and verification of lucerne canopy expansion and radiation interception used data from Experiments 1 to 4 as described in Section 3.1.1. The datasets for model testing and calibration for three FD classes under different defoliation regimes were described in Section 4.2.1 (Table 4.2). Observed variables include LAI and intercepted radiation.

5.2.2 Model structure

In this chapter, the PMF in APSIM NextGen was used for testing and evaluating lucerne canopy expansion and radiation interception-related parameters under different defoliation regimes and FD classes. In the PMF, LeafArea (functions for leaf area calculation) and ExtinctionCoefficient (extinction coefficient; k) functions are under leaf organ. Several of the parameters derived in Chapter 4, such as buds visible and flowering stages were used in this chapter, and new parameters were calculated and added to the model structure to simulate canopy expansion and radiation interception.

5.2.3 Model calibration and parameterization

5.2.3.1 Thermal time and leaf area expansion T_b

To determine the most accurate base temperature to calculate thermal time (Tt) for canopy expansion, which includes both growth and development components, the three methods also used to calculate Tt for development were evaluated: 1) the Moot model, 2) the Fick framework, and 3) the WE model. As in Chapter 4, for the Moot model, T_b values were tested from T_b=0 ˚C to T_b= 4˚C at 1 ˚C intervals. For the Fick framework, T_b values were tested from T_b=5 to 10 ˚C at 1 ˚C intervals. For the WE model, T_b values were tested from T_b=0 to 5 ˚C at 1 ˚C intervals. The three statistical methods were again used to determine the most accurate T_b value: 1) x-intercept, 2) least variable, and 3) regression coefficient (as described in Sections 4.2.3.1 and 4.2.3.2)

5.2.3.2 Leaf area expansion rate

The average leaf area expansion rate (LAER, m^2 m^{-2} ˚Cd^{-1}) for a given regrowth cycle was calculated as the slope of linear regression between LAI against accumulated Tt. To ensure maximum LAER was accurately estimated, senescence and flowering were excluded by using LAI values from 5% to 95% of the maximum LAI within each crop cycle.

5.2.3.3 Lag phase of canopy expansion

From the early regrowth stage, there was a lag phase before canopy expansion rate reached the maximum value of LAER for any given regrowth cycle. Therefore, a lag phase function was introduced to slow down the initial LAER. It was tested by comparing predicted and observed LAI data in the early stage to improve the model fitting. The lag phase function was parameterized as a linear relationship of Tt since defoliation date and a lag reduce factor (LRF, percentage of LAER).

5.2.3.4 Basal buds

For lucerne crops, at times (HH treatment), new basal buds may accumulate in the crown before the canopy has been removed (Moot et al., 2015). This was not considered in the APSIM classic lucerne model. In this chapter, a basal bud module was added to the PMF to estimate basal bud initiation. This module assumed that crops started to accumulate basal buds after they reached the reproductive phase (StartFlowering stage in APSIM NextGen

phenology module). These basal buds were assumed to have started to expand their leaf area before defoliation, and became the initial leaf area for the next regrowth cycle. An additional parameter (basal buds factor; BBF) was defined as the percentage of potential LAER, added to adjust initial LAI. Simulated LAI was compared with observed LAI values to determine the most accurate basal buds factor. Basal buds factor values were tested from 0 to 0.5 at 0.1 intervals.

5.2.3.5 Canopy senescence

Canopy senescence occurred mainly in the 84 day treatment (HH), shown as decreasing LAI after ~50 days in each regrowth cycle (Ta, 2018). Therefore, a senescence function from APSIM NEXTGEN was used to test and fit observed LAI data. This SenescenceRate model used a constant senescence rate (-0.2 m^2 m^{-2} day^{-1}), which was then multiplied by a StageFactor function, CoverFactor function and TemperatureFactor function. This SenescenceRate model was originally developed for red clover leaf senescence, models' complete documentation and cultivar specific parameters are referred to a webpage (https://apsimdev.apsim.info/APSIM NextGen/Releases/2020.11.27.5887/RedClover.description.pdf).

5.2.3.6 Extinction coefficient

The extinction coefficient (k) was used as an indicator of canopy architecture, with higher values indicating greater radiation interception per unit of LAI. It was calculated as the linear slope of the natural log of diffuse radiation transmission against LAI, considering values up to 95% of maximum LAI as the critical LAI (LAI_{crit}) value (Monsi and Saeki, 2005).

5.2.3.7 Radiation interception

The accumulated amount of radiation intercepted was calculated by summing daily estimates from each regrowth period. The daily amount of intercepted radiation (MJ total radiation m^{-2}) was calculated by using the daily LAI and k, which were multiplied by the daily incident radiation (R_o).

5.2.4 **Model validation and verification**

For model calibration, datasets from 42 day (LL) defoliation treatments and a semi-dormant cultivar (FD5) were used to generate equations and parameters. To determine

how conservative the equations and parameters were, additional datasets from Experiments 3 and 4 that included different defoliation regimes (HH, LS, SL and SS) and FD classes (FD2 and FD10) were used to test and verify those functions and parameters, as described in Section 4.2.4 (Table 4.2).

5.3 Results

5.3.1 Leaf area expansion base temperature

5.3.1.1 The x-intercept method

There was a poor linear relationship between leaf area growth rate (defined as the slope of LAI against days since defoliation, LAGR) and mean air temperature, R^2 ranged from 0.53 in E3 to 0.17 in E4 (Figure 4.3). Using the x-intercept method, extrapolation of the linear function to y=0 (no growth), gave estimated T_b values that ranged from -8.75 to 3.09 ˚C, with an average value of -0.56±8.2 ˚C (Table 5.2).

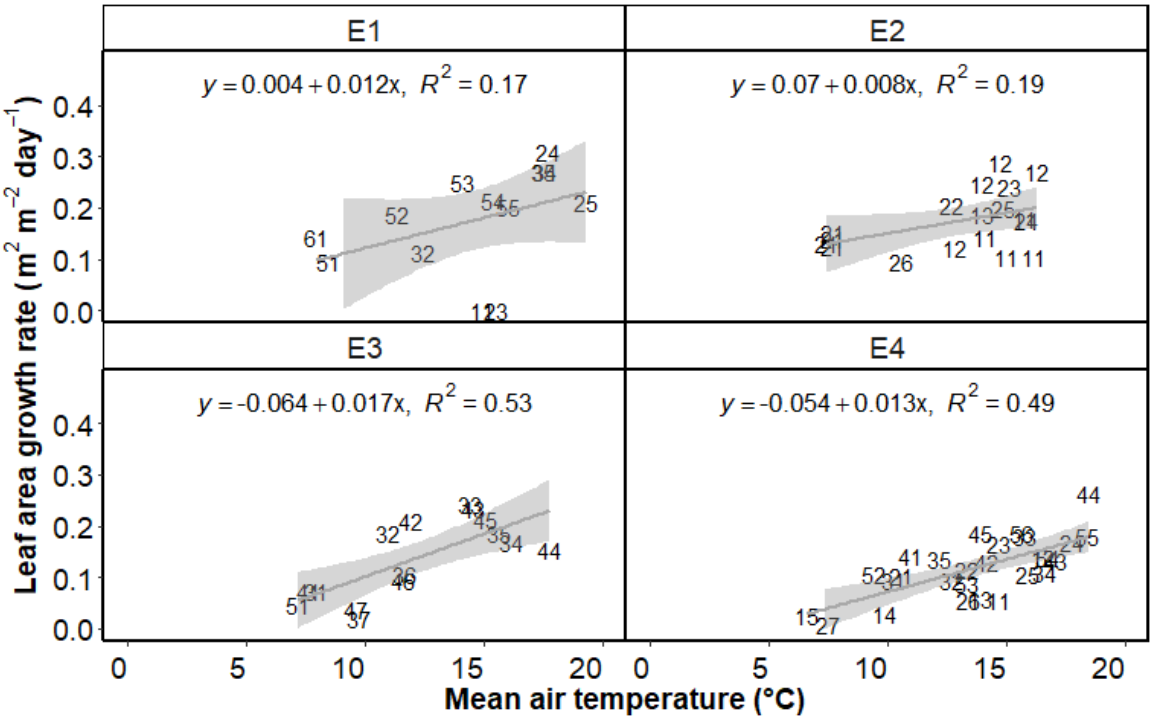

Figure 5.1. Leaf area growth rate (m^2 m^{-2} day^{-1}) against mean air temperature (˚C) derived from four field experiments with Experiment 2 having four sowing dates between 1997 and 2019 at Iversen field, Lincoln University, Canterbury, New Zealand. Details of E1-E4 are given in Table 5.2.

Table 5.2 Base temperature values (T_b) derived from four datasets using the x-intercept method.

Method	Experiments	T_b (˚C)	Mean T_b
X-intercept	E1(1997-2001)	-0.33	-0.56±8.2
	E2(2000-2002)	-8.75	
	E3(2002-2004)	3.76	
	E4(2014-2019)	3.09	

5.3.1.2 Least variable and regression coefficient methods

Least variable (CV%) and probability (P) values were calculated from T_b values from 0 to 10 ˚C (Table 5.3). Since the Moot and Fick models are identical from T_b=5 to 10 ˚C, only T_b values from 0 to 4 ˚C are listed in the Table 5.3. For the WE model, only 0 to 5 are listed because the values clearly exceeded the lowest CV% values and had the lowest P values of the three methods.

The Moot model resulted in the same CV% values (39%) for T_b from 0 to 4 ˚C, but the P value (0.94) was highest at T_b=2 ˚C. The Fick model resulted in increased CV% and decreased P values as T_b increased from 5 to 10 ˚C. For T_b=5, CV% was the lowest (40%) and P value was highest (0.27). The WE model resulted in the lowest CV% and highest P value with T_b=1 ˚C. However, these values were higher in CV% and lower in P value than the Moot model with T_b=2 ˚C. Thus, the Moot model with T_b=2 ˚C (Table 5.3) was subsequently used for Tt calculations of leaf area expansion.

Table 5.3 Statistical measures [percent coefficient of variation (%CV) and probability (P) value] resulting from three calculation methods (Moot model, Fick framework, and ME model) for various base temperature (T_b) values using LAI data from four lucerne field experimental datasets grown at Iversen field, Lincoln University, Canterbury, New Zealand.

Method	T_b	CV (%)	P value
Moot model	0	39	0.53
	1	39	0.71
	2	39	0.94
	3	39	0.78
	4	39	0.51
Fick framework	5	40	0.27
	6	41	0.08
	7	42	0.016
	8	44	0.0018
	9	47	1.2e-4
	10	51	5.6e-6
ME model	0	50	2.46e-5
	1	51	1.25e-5
	2	52	5.91e-6
	3	53	2.54e-6
	4	54	9.94e-7
	5	55	3.51e-7

5.3.2 **Canopy expansion**

5.3.2.1 LAI

Five different sowing dates across two experiments (2 and 4) showed lucerne seedling crops required ~400 ˚Cd from sowing to the start of canopy expansion (Figures 5.2; S_1). The relationship between LAI (m^2 m^{-2}) and Tt for each regrowth cycle was a positive linear relationship for all experiments, with R^2 values ranging from 0.88 to 0.99 (Figures 5.2). Maximum LAI (~5.5) was reached after 500 ˚Cd (Appendix 12 for R^2, P value, slope, and intercept values).

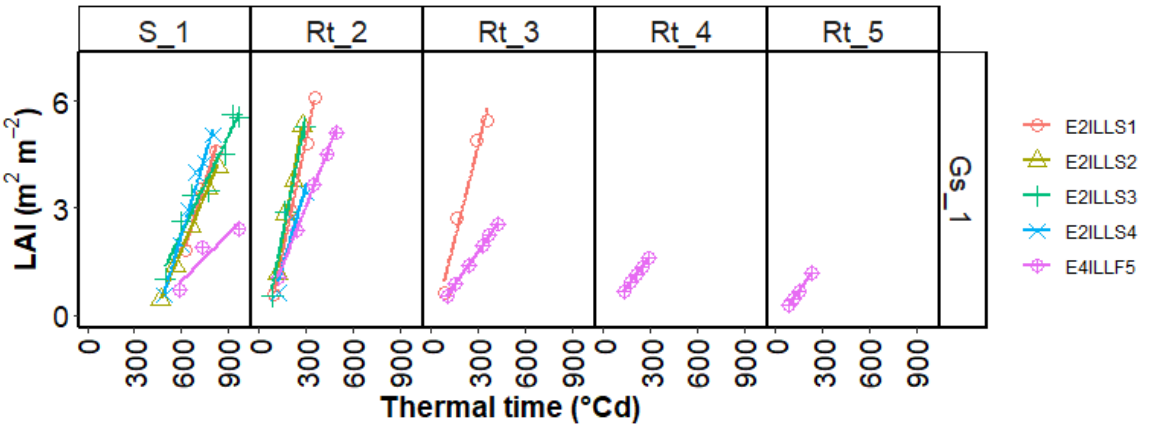

Figure 5.2. Leaf area index (LAI) against accumulated thermal time (˚Cd) from field Experiments 2 and 4 (E2 had four sowing dates) conducted between 2000 and 2019 at Iversen field, Lincoln University, Canterbury, New Zealand. Row GS_1 is the first growth season (seedling crop). Column S_1 is the first growth cycle and columns Rt_2 to Rt_5 represent regrowth cycles. Lines represent linear regressions.

Figure 5.3 shows LAI against Tt within seven regrowth cycles in five regrowth years for four experiments under the LL defoliation regime (~400 to 550 ˚Cd). There was a strong linear relationship between the LAI and Tt in each regrowth cycle and each experiment (R^2=0.82 to 0.99) (Appendix 12 for R^2, P value, slope, and intercept values).

Within a year (a row), the slope of the linear regressions (leaf area expansion rate; LAER) changed across different regrowth cycles (Appendix 12 for R^2, P value, slope, and intercept values). This suggests that other seasonal drivers beyond temperature control LAER. To illustrate this seasonality, subsequent analyses were separated into increasing and decreasing Pp conditions.

The x-intercept values from the linear regression between LAI and Tt ranged from ~-50 to ~200 ˚Cd (Appendix 13). This indicates that some regrowth cycles (-50 to 0 ˚Cd) had leaves (basal buds) present before defoliation occurred (described in below section 5.3.2.3), whereas some regrowth cycles required about 200 ˚Cd to reach the calculated LAER, described as a lag phase. Therefore, the lag phase function was parameterized as the linear relationship of Tt since defoliation date and a lag reduce factor (LRF, percentage of LAER). Tt since defoliation date increased from 0 to 200 ˚Cd as LRF increased from 0 to 1. Therefore, a lag phase function was implemented into the canopy expansion model in each regrowth cycle, as described in Appendix 14.

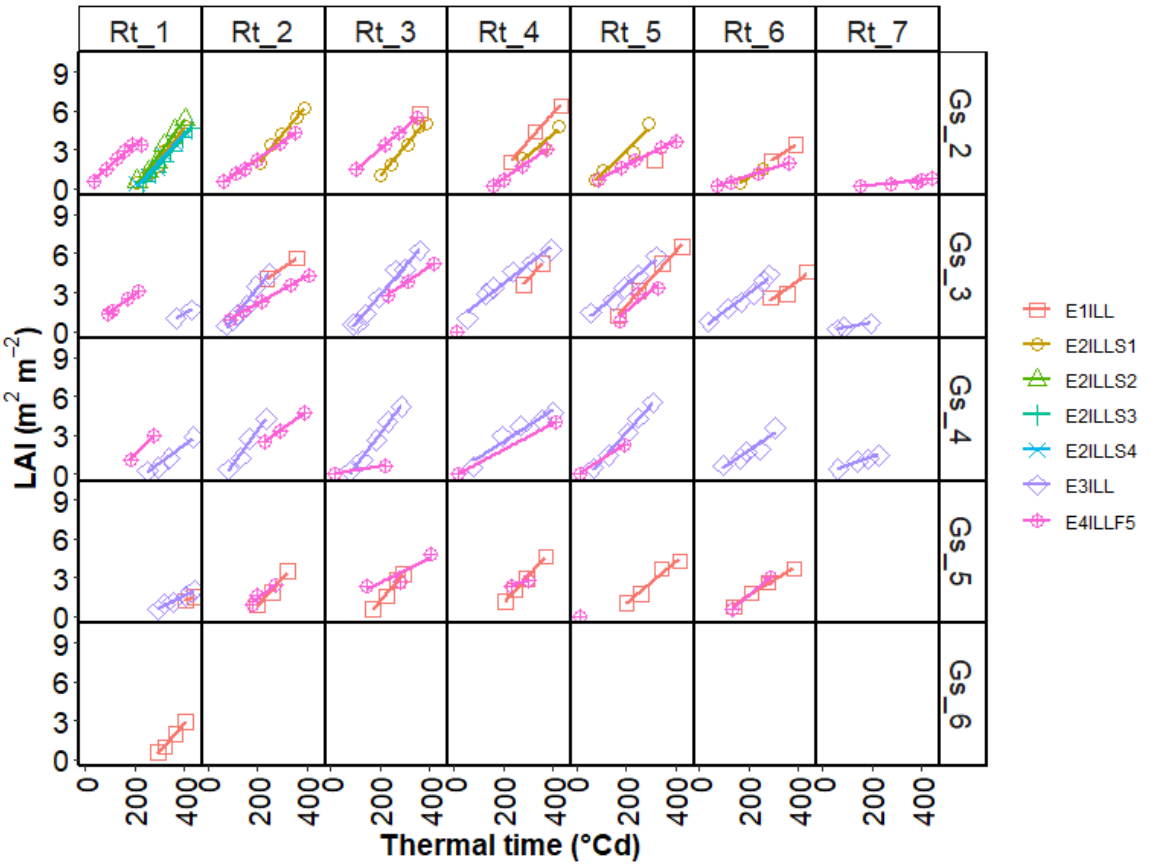

Figure 5.3. Leaf area index (LAI) against accumulated thermal time (˚Cd) for four field experiments conducted from 1997 to 2019 at Iversen field, Lincoln University, Canterbury, New Zealand. Columns Rt_1 to Rt_7 represent regrowth cycles, whereas rows GS_2 to GS_6 represent growth years. Lines represent linear regressions.

5.3.2.2 Leaf area expansion rate (LAER)

For seedling crops, LAER was consistent across Pp, at ~0.015 m^2 m^{-2} ˚Cd^{-1} (Figure 5.4). The relationship between LAER and mean Pp in regrowth lucerne crops showed a different response pattern in increasing and decreasing Pp (Figure 5.4). During a decreasing Pp, LAER slowed as Pp decreased; being 0.018 m^2 m^{-2} ˚Cd^{-1} at 16.5 h and 0.008 m^2 m^{-2} ˚Cd^{-1} at 10 h (Appendix 15 for model structure of LAER in decreasing Pp). Lucerne crops also expanded leaf area faster with increasing Pp conditions. The LAER increased from 0.018 at 12 h to 0.022 m^2 m^{-2} ˚Cd^{-1} at 16.5 h (Appendix 16 for model structure of LAER in increasing Pp). There was also a systematic error in the first growth regrowth cycle (two dimension code: 21). Specifically, in the early part of the first year following establishment, LAER is underestimated by the linear model, whereas in 3-4 growth years (two dimension code of 32 and 42), LAER values were lower than predicted values.

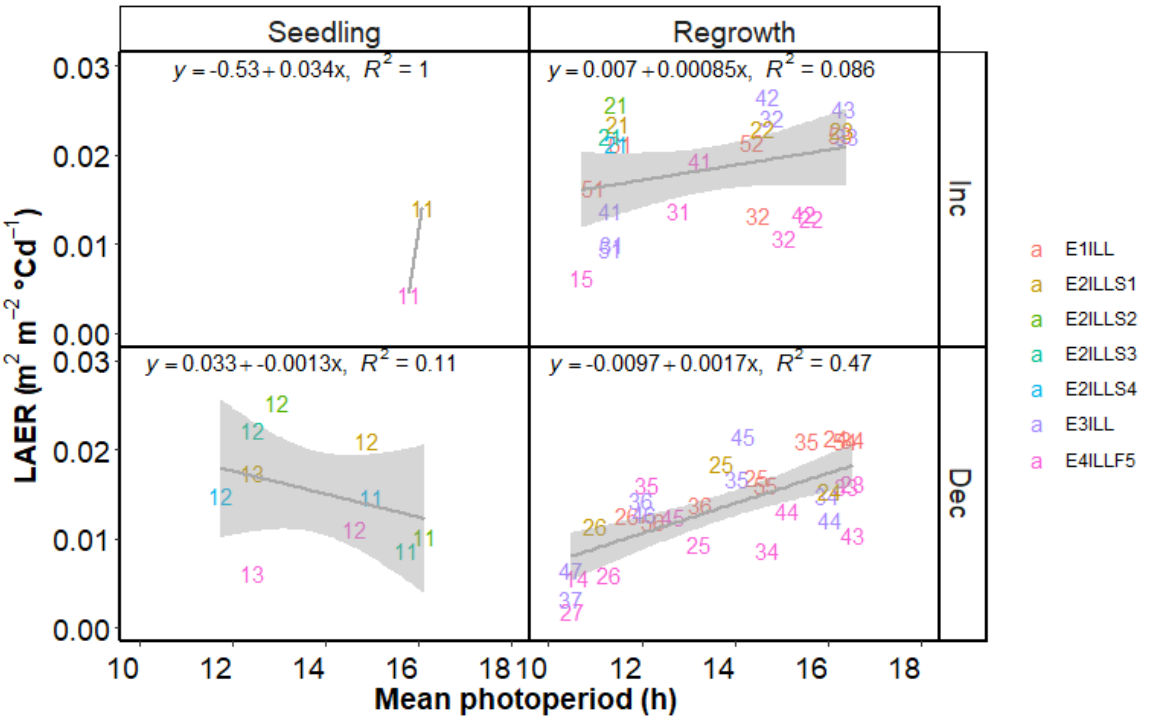

Figure 5.4. Leaf area expansion rate (LAER) against mean photoperiod (Pp) for seedling and regrowth crops from four field experiments conducted at Iversen field, Lincoln University, Canterbury, New Zealand. Two dimension code represents growth years and regrowth cycles.

5.3.2.3 Model fitting for basal buds

After applying the LeafArea functions in the model (Appendices 14-16), a range of basal bud factor (BBF) values were tested to improve prediction of LAI during early phases of crop regrowth. Statistical measures of BBF values for comparing predicted and observed values of LAI are provided in Figure 5.5 and Table 5.4. A BBF of 0.2 (20% of the potential LAER) had the lowest R_RMSE and highest NSE values, 39.3% and 0.61, respectively. By applying a small value of basal bud factor, the LAI prediction improved (R_RMSE decreased 3.9% and NSE increased 0.8). Therefore, BBF = 0.2 was used in this model (Appendix 16 for model structure of basal buds function).

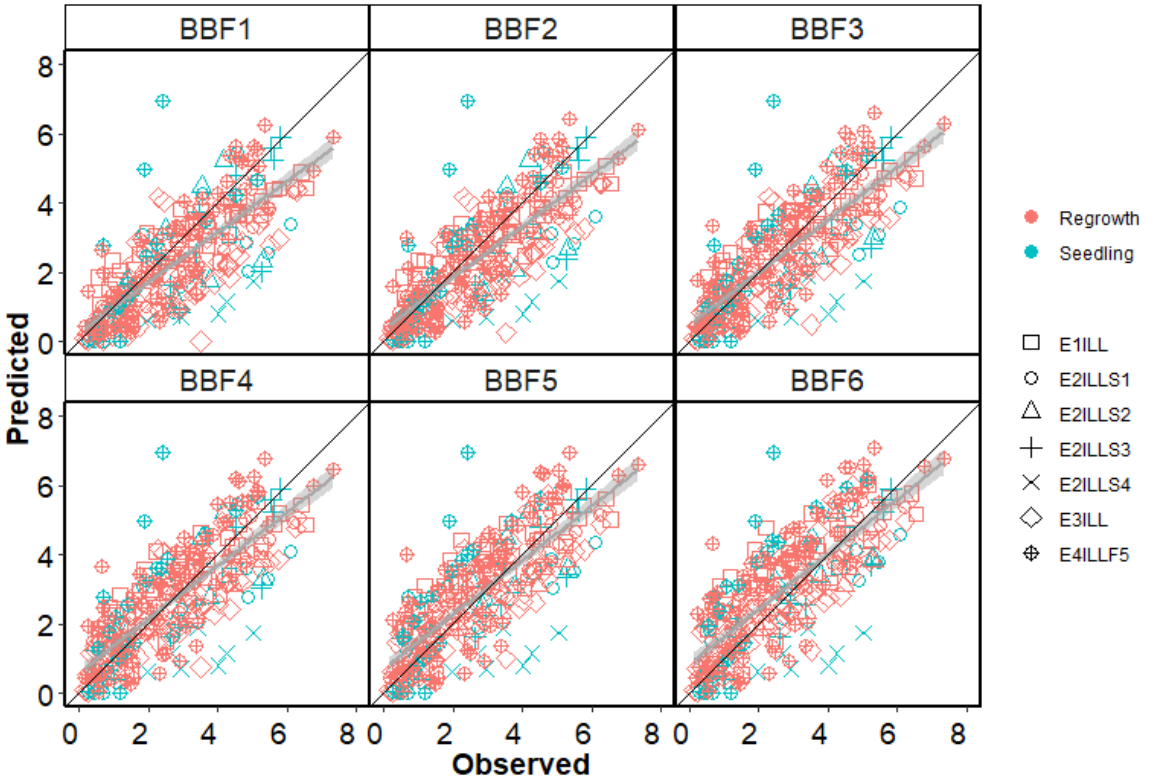

Figure 5.5. Predicted and observed LAI values on calibration datasets for four field experiments with Experiment 2 having four sowing dates conducted between 1997 and 2019 at Iversen field, Lincoln University, Canterbury, New Zealand. Basal buds factors (BBF 1-6) represent BBF values from 0 to 0.5 at 0.1 intervals.

Table 5.4 Statistical measures of LAI simulation on testing basal buds factor (BBF), calibration datasets from four field experiments conducted between 1997 and 2019 at Iversen field, Lincoln University, Canterbury, New Zealand. n = number of simulated and observed data pairs; R^2= coefficient of determination; R_RMSE = relative root mean square error (%); NSE = Nash-Sutcliffe efficiency; SB = Standard bias; NU = Nonunity slope; LC = Lack of correlation.

Basal buds factor	Value	N	R^2	R_RMSE	NSE	SB	NU	LC
BBF1	0	305	0.62	43.4	0.53	16.4	3.8	79.8
BBF2	0.1	305	0.64	40.6	0.59	8.4	4.2	87.4
BBF3	0.2	305	0.64	39.3	0.61	2.3	5.3	92.4
BBF4	0.3	305	0.64	39.4	0.61	0.0	7.1	92.9
BBF5	0.4	305	0.63	41.0	0.58	1.7	9.5	88.8
BBF6	0.5	305	0.61	43.8	0.52	6.3	12.1	81.7

5.3.2.4 Model simulation of LAI

Parameters and functions for canopy expansion were generated from pervious sections (5.3.2.2 and 5.3.2.3) and were implemented into the APSIM NextGen lucerne model (Appendices 15 to 18 for model structure of LeafArea). Simulation results for predicting LAI in each regrowth cycle of field Experiments 1 to 4 conducted from 1997 to 2019 (Figure 5.6 and Table 5.5) showed a good overall agreement (R_RMSE = 39.9 %, NSE = 0.61). However, most of the variation was from the E2ILLS4 treatment, which had the highest R_RMSE and the lowest NSE, 67.2% and -0.42, respectively. Seedling crops had fair agreement between predicted and observed LAI values (R_RMSE = 56.1%, NSE = 0.23). For regrowth crops, there was good agreement between predicted and observed values, as shown in Figure 5.6 and Table 5.5 (R_RMSE = 34.3 %, NSE = 0.71).

Data collection in the field followed the same protocol for all experiments. However, another source of variation may have resulted from different instruments for LAI measurements. Specifically, early experiments (1-3) used a canopy analyzer, whereas E4 used a Sunscan instrument for LAI and radiation interception measurements (Section 3.1.1). This may explain the over-prediction in E4ILLF5 and under-prediction in E3ILL (Figure 5.5)

Nevertheless, there was no difference in prediction of LAI across different Pp conditions, although simulation results were slightly more accurate in increasing Pp (NSE = 0.67 and R_RMSE = 36.4 %).

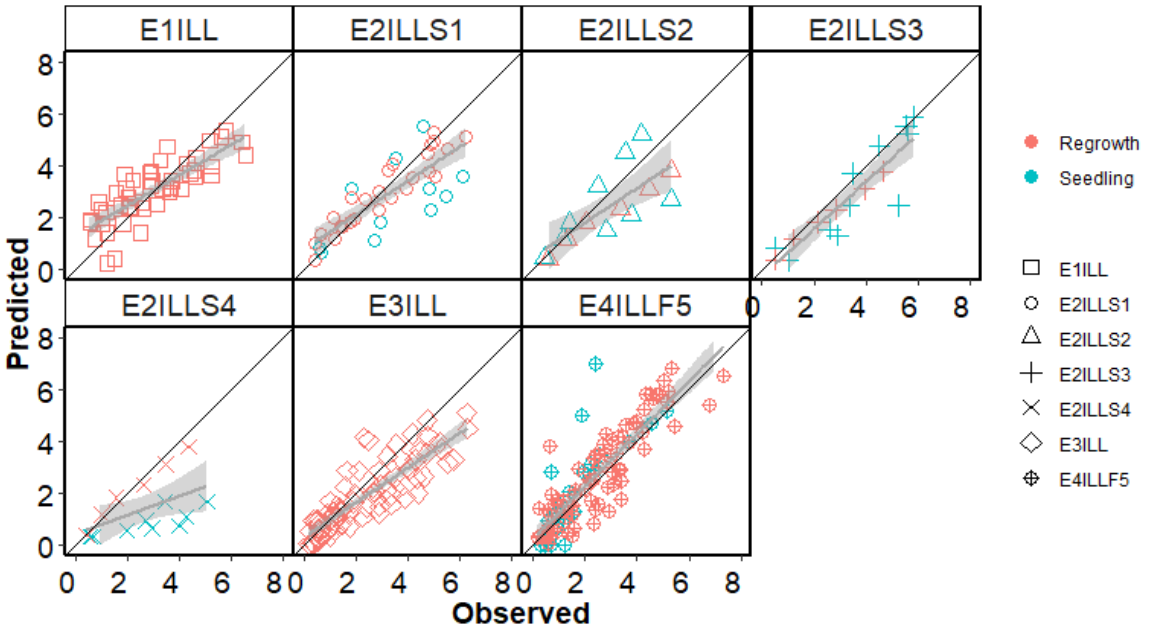

Figure 5.6. Predicted and observed LAI values on calibration datasets for four field experiments with Experiment 2 having four sowing dates conducted between 1997 and 2019 at Iversen field, Lincoln University, Canterbury, New Zealand.

Table 5.5 Statistical measures of LAI simulation on a calibration dataset from four field experiments conducted between 1997 and 2019 at Iversen field, Lincoln University, Canterbury, New Zealand. n = number of simulated and observed data pairs; R^2= coefficient of determination; R_RMSE = relative root mean square error (%); NSE = Nash-Sutcliffe efficiency; SB = Standard bias; NU = Nonunity slope; LC = Lack of correlation.

Treatments	N	R^2	R_RMSE	NSE	SB	NU	LC
Total	305	0.64	39.9	0.61	1.9	6.3	91.8
Seedling	63	0.42	56.1	0.23	5.9	18.9	75.2
Regrowth	242	0.72	34.3	0.71	1	2.5	96.5
Increasing Pp	148	0.70	36.4	0.67	0	8.4	91.6
Decreasing Pp	157	0.60	42.2	0.55	6.2	5.1	88.7
E1ILL	46	0.65	32.3	0.64	0.7	1.9	97.4
E2ILLS1	37	0.67	32.7	0.65	6.5	0.1	93.4
E2ILLS2	15	0.58	40.1	0.49	15.5	2.2	82.3
E2ILLS3	17	0.82	28.2	0.72	32.4	3.6	63.9
E2ILLS4	15	0.29	67.2	-0.42	48.2	1.6	50.2
E3ILL	77	0.73	41.8	0.65	20.6	1.5	77.9
E4ILLF5	98	0.73	43.1	0.59	8.6	25.8	65.6

5.3.2.5 Verification for defoliation treatments

The LeafArea model was used to test LAI prediction of an independent dataset (FD5) under different defoliation regimes. A preliminary simulation result is shown in Appendices 17-19. The HH treatment had poor agreement between predicted and observed LAI (NSE= -0.63 and R_RMSE =65.2%). To improve model fit for the HH treatment, the SenescenceRate function was applied to the LeafArea function.

Overall, predicted and observed LAI values for experiments (3 and 4) with multiple defoliation treatments (HH, LS, SL, and SS) had good agreement, with NSE of 0.74 and R_RMSE of 42.7% (Figure 5.7 and Table 5.6). Among the three defoliation treatments, the HH and LL treatments had a similar R_RMSE value (~35%). The SenescenceRate function improved simulation results for the 84 day defoliation treatment (E4IHHF5), with R_RMSE of 34.4% and NSE of 0.55 (Figure 5.8). In the final year (2019), over-prediction was observed in the simulation.

The SS treatment had the highest R_RMSE values (50.9%) (Table 5.6). Specifically, over-estimation occurred in E4ISSF5 (Figure 5.7 and Table 5.6; R_RMSE=50.3% and NSE=0.38), whereas over-estimation only occurred in the early spring in E3ISS (Figure 5.9 and Table 5.6; R_RMSE=44.8% and NSE=0.78).

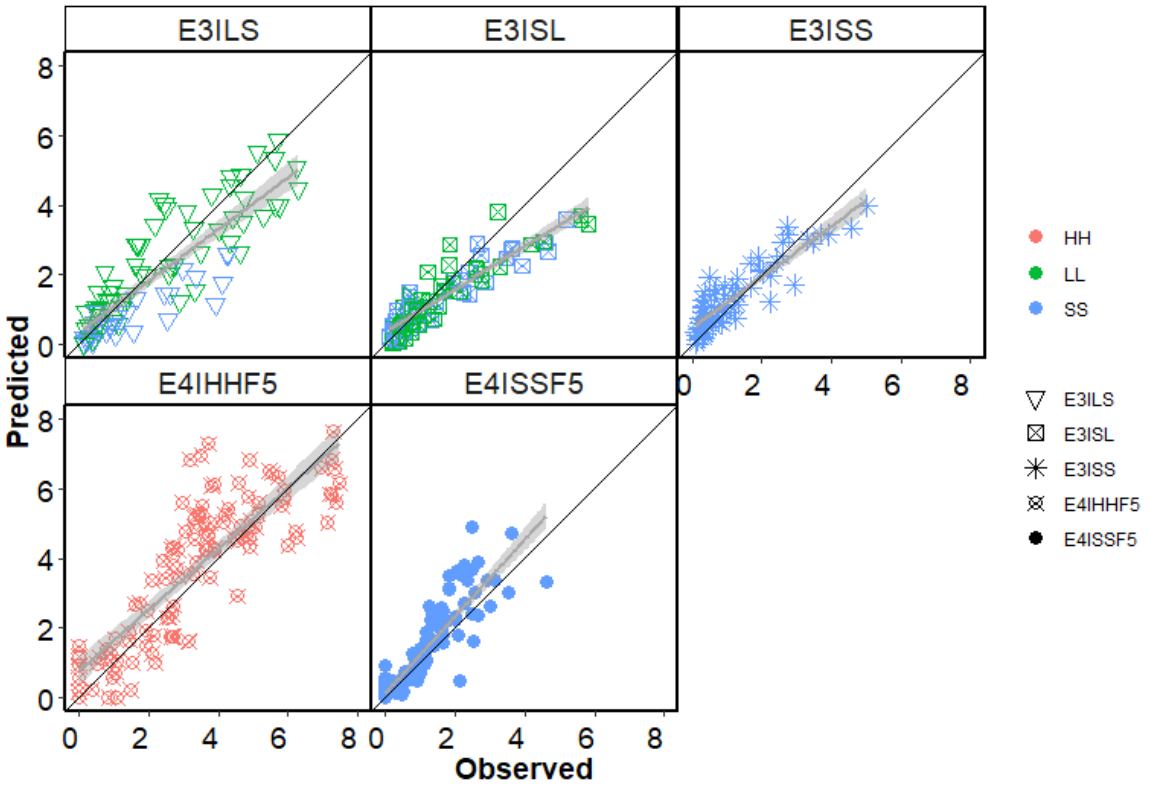

Figure 5.7. Predicted and observed LAI values from two field Experiments (3 and 4) with multiple defoliation treatments [HH (84 day), LS (42, 28 day), SL (28, 42 day), and SS (28 day)] conducted between 2002 and 2019 at Iversen field, Lincoln University, Canterbury, New Zealand.

Table 5.6 Statistical measures of LAI from two field Experiments (3 and 4) with multiple defoliation treatments [HH (84 day), LS (42, 28 day), SL (28, 42 day), and SS (28 day)] conducted between 2002 and 2019 at Iversen field, Lincoln University, Canterbury, New Zealand. N = number of simulated and observed data pairs; R^2= coefficient of determination; R_RMSE = relative root mean square error (%); NSE = Nash-Sutcliffe efficiency; SB = Standard bias; NU = Nonunity slope; LC = Lack of correlation

Treatment	N	R^2	R_RMSE	NSE	SB	NU	LC
Total	428	0.75	42.7	0.74	0.5	6.7	92.8
HH	101	0.65	34.4	0.55	7.6	15.4	76.9
LL	100	0.77	39.5	0.76	1.8	1	97.2
SS	227	0.64	50.9	0.62	0.1	3.3	96.6
E3ILS	86	0.72	43.1	0.71	5.5	0.2	94.3
E3ISL	82	0.83	45.1	0.74	13.4	21.5	65.2
E3ISS	67	0.81	44.8	0.78	8.0	3.1	88.8
E4IHHF5	101	0.65	34.4	0.55	7.6	15.4	76.9
E4ISSF5	92	0.72	50.3	0.38	15.6	39	45.4

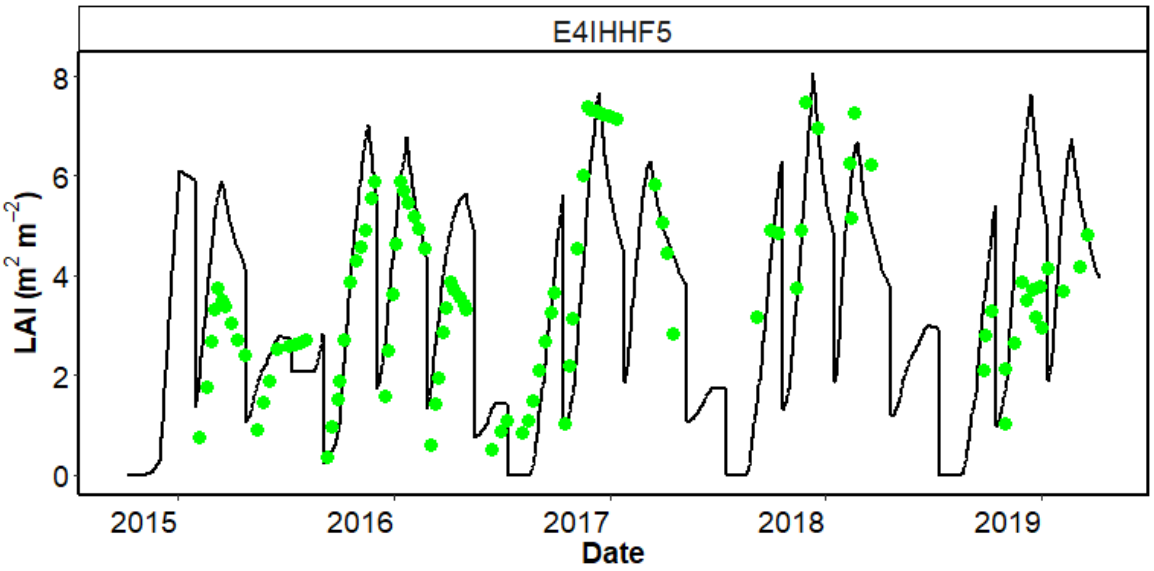

Figure 5.8. Predicted and observed LAI values for field Experiment 4 with an 84 day (HH) defoliation treatment, conducted between 2014 and 2019 at Iversen field, Lincoln University, Canterbury, New Zealand.

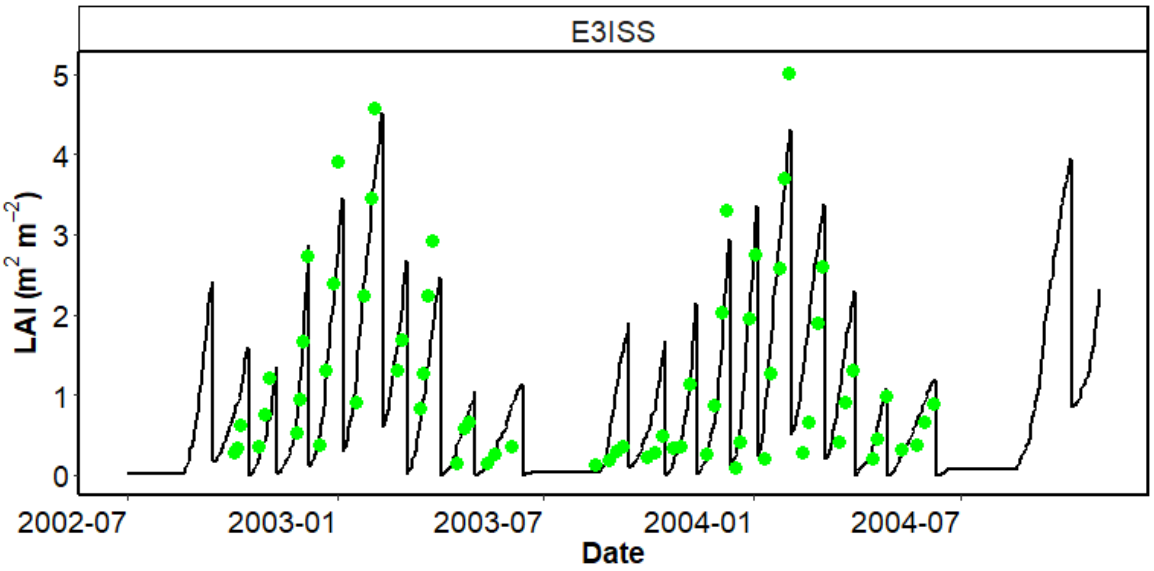

Figure 5.9. Predicted and observed LAI values for field Experiment 4 with the SS (28 day) defoliation treatment, conducted between 2002 and 2004 at Iversen field, Lincoln University, Canterbury, New Zealand.

5.3.2.6 Verification for fall dormancy classes

Different FD classes had different canopy expansion rates, therefore a separate set of parameters was needed to improve model simulation results. The relationship between LAER and mean Pp for FD2 and FD10 crops under the LL defoliation treatment showed a different response pattern in increasing and decreasing Pp (Figure 5.10). During an increasing Pp, FD2 and FD10 lucerne crops had a similar LAER, which was consistent at

~0.01m^2 m^{-2} ˚Cd^{-1} across different Pp conditions. For FD2 crops grown in a decreasing Pp, LAER decreased with decreased Pp; being 0.012 m^2 m^{-2} ˚Cd^{-1} at 16.5 h and 0.006 m^2 m^{-2} ˚Cd^{-1} at 10 h, whereas LAER of FD10 crops was constant (~0.01) in a decreasing Pp (Appendices 22 and 23 for model structure of FD 2and FD10 LAER).

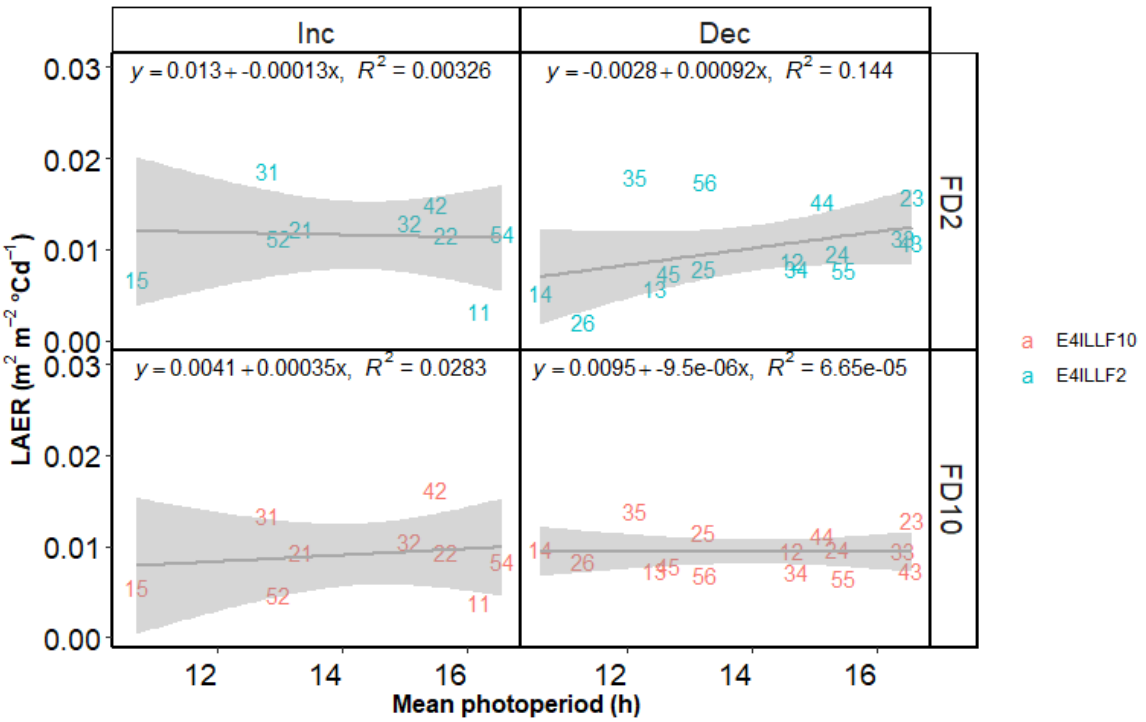

Figure 5.10. Leaf area expansion rate (LAER) against mean photoperiod (Pp) for lucerne two fall dormancy (FD; FD2 and FD10) classes regrowth crops from field Experiment 4, conducted at Iversen field, Lincoln University, Canterbury, New Zealand. The two dimension code represents growth years and regrowth cycles.

The verified LeafArea model was used to test FD2 and FD10 lucerne crops under different defoliation regimes. Overall, predicted and observed LAI values from Experiment 4 for two FD classes (FD2 and FD10) with multiple defoliation treatments (HH, LL, and SS) had good agreement, with NSE of 0.61 and R_RMSE of 49.7%. Notably, the variation was from both FD2 and FD10 treatments, with NSE of 0.63 and 0.56 (Figure 5.11 and Table 5.7). This variation may be explained by the fair agreement observed in the seedling crops (R_RMSE=65.9%, NSE=0.32).

Among the three defoliation treatments, the LL treatment had the highest agreement (R_RMSE=51.5%, NSE=0.38), whereas the SS treatment had the lowest agreement (R_RMSE=59.9%, NSE=0.30). Good agreement was found in the FD2 class under the SS

defoliation treatment. However, FD10 under the SS treatment, there was poor agreement with the highest R_RMSE value (R_RMSE=81.6%, NSE=-0.88).

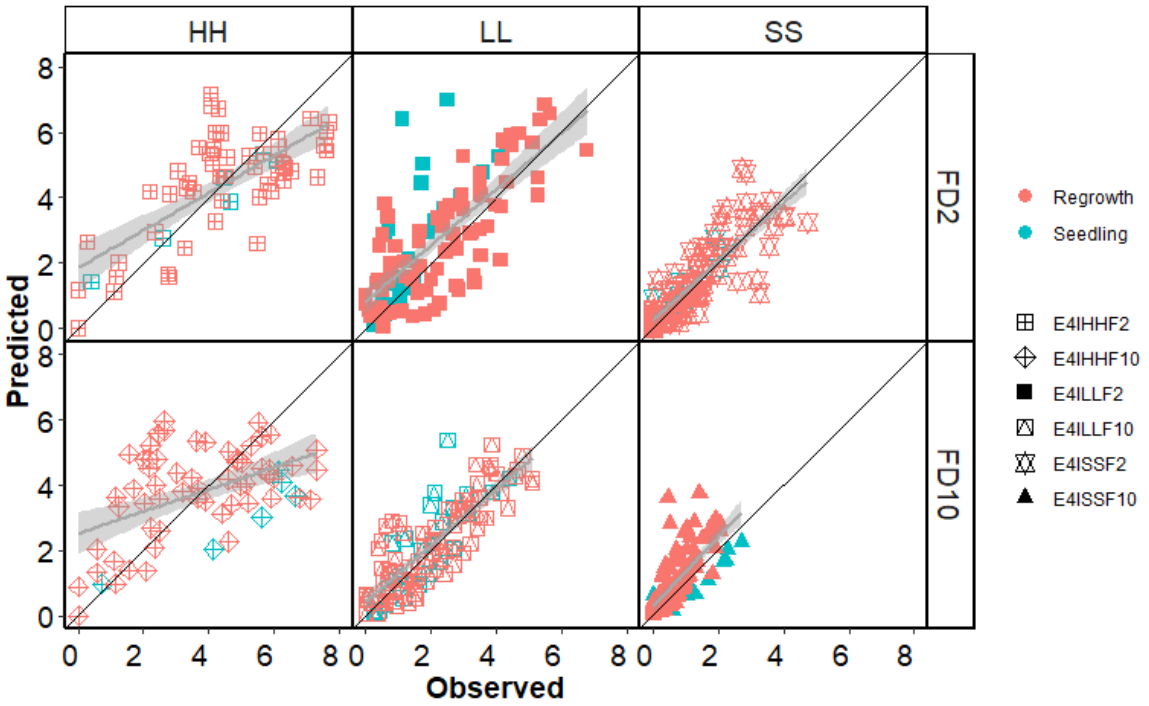

Figure 5.11. Predicted and observed LAI values from field Experiment 4 with three defoliation treatments [HH (84 day), LL (42 day), and SS (28 day)] and two fall dormancy (FD; FD2 and FD10) classes conducted between 2014 and 2019 at Iversen field, Lincoln University, Canterbury, New Zealand.

Table 5.7 Statistical measures of LAI from field Experiment 4 with three defoliation treatments [HH (84 day), LL (42 day), and SS (28 day)] and two fall dormancy (FD; FD2 and FD10) classes conducted between 2014 and 2019 at Iversen field, Lincoln University, Canterbury, New Zealand. N = number of simulated and observed data pairs; R^2= coefficient of determination; R_RMSE = relative root mean square error (%); NSE = Nash-Sutcliffe efficiency; SB = Standard bias; NU = Nonunity slope; LC = Lack of correlation.

Treatment	N	R^2	R_RMSE	NSE	SB	NU	LC
Total	506	0.63	49.7	0.61	2.4	3.9	93.7
FD2	254	0.65	46.8	0.63	1.8	4.1	94.1
FD10	252	0.59	53.2	0.56	3.2	3.9	92.9
Seedling	85	0.48	65.9	0.32	4.2	19.2	76.6
Regrowth	421	0.65	47.1	0.64	2.1	2.3	95.6
HH	126	0.33	38.9	0.32	0.5	1.6	97.8
LL	204	0.58	51.5	0.38	8.4	23.7	68
SS	176	0.55	59.9	0.30	11	25.1	63.9
E4IHHF2	63	0.43	32.5	0.40	3.3	0.3	96.4
E4IHHF10	63	0.16	46.9	0.10	0	7	92.9
E4ILLF2	103	0.53	60.2	0.22	13.5	26.2	60.2
E4ILLF10	101	0.67	38.7	0.61	3.2	14	82.8
E4ISSF2	88	0.64	46.4	0.54	2.3	20.3	77.4
E4ISSF10	88	0.40	81.6	-0.88	24.7	43.3	32.1

5.3.3 Radiation interception

5.3.3.1 Extinction coefficient (k)

Seedling and regrowth crops showed a similar asymptotic relationship between fractional radiation interception and destructively sampled LAI (R^2=0.96) (Figures 5.11). Lucerne crops reached 95% radiation interception, the critical LAI (LAI_{crit}), at LAI =3.6. There was no difference among different defoliation regimes and FD classes. The calculated extinction coefficient (k) was the same for seedling and regrowth crops (0.81) (Figure 5.12) (Appendix 24 for model structure of k).

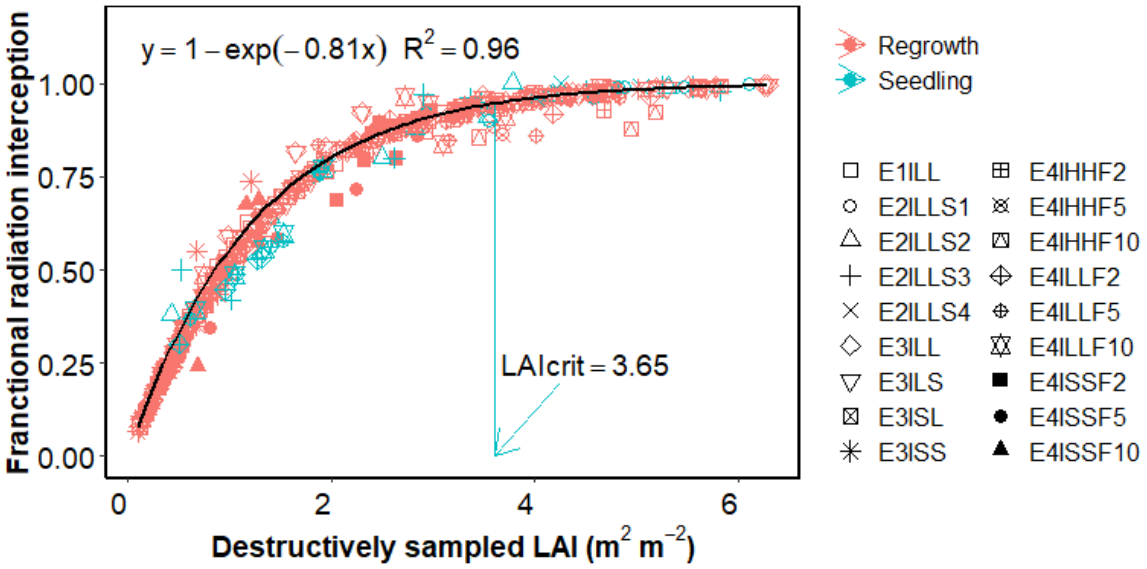

Figure 5.12. Fractional interception of total radiation against leaf area index (LAI) for regrowth crops from four field experiments with multiple defoliation treatments [HH (84 day), LL (42 day), LS (42, 28 day), SL (28, 42 day) and SS (28 day)] and three fall dormancy (FD; FD2, FD5 and FD10) classes conducted between 2000 and 2019 at Iversen field, Lincoln University, Canterbury, New Zealand.

5.4 Discussion

Objective 2 of this thesis was to quantify, test and verify the accuracy of canopy expansion and radiation interception module in the APSIM NextGen lucerne model. Parameters were derived from the FD5 genotype grown under the LL defoliation treatments and then integrated into the model. This included parameters and functions for LAER, lag phase, basal buds and canopy senescence. These parameters were further tested by using datasets from different defoliation treatments and FD classes, to determine whether FD class or defoliation regime impacted on lucerne canopy expansion and radiation interception.

5.4.1 Leaf area expansion base temperature

The first step to quantify lucerne leaf area expansion responses was the determination of an appropriate temperature threshold for thermal time (Tt) accumulation. However, growth and development are different processes (Hodges, 1990). The null hypothesis was that leaf area expansion and development base temperature (T_b) are the same. Leaf area expansion T_b was determined by using LAI data in the current study, three different Tt functions and evaluation methods were used, as described in Section 4.3.1.

The x-intercept method resulted in a large bias that affected the selection of T_b (Table 5.2 and Figure 5.1). This was due to the average minimum air temperature which ranged between 5 to 6 ˚C in Canterbury, NZ (Figure 3.1). Therefore, a large extrapolation was required to obtain the x-axis intercept value. This creates large uncertainty as the data are not close to the point of interest of T_b value. Moreover, the coefficient of variation method showed no difference between T_b from 0 to 5˚C for the Fick and Moot models, thus it was not informative to select the most accurate T_b value. The regression method showed that the Moot model, with a T_b of 2˚C, was the most accurate method for determining Tt and T_b; it had the lowest CV=39% and highest P value (0.94). This indicates that leaf area expansion T_b was similar to development T_b, with 1 ˚C. Biologically, it is possible because LAER includes both development (node appearance and branching) and growth (increase in leaf area and weight) elements, and growth is the product of photosynthesis, whereas development relies on cell division. In contrast, Thiébeau et al. (2011) investigated T_b values that ranged from 0 to 5 ˚C using LAI data for seedling and regrowth crops in France. These authors concluded T_b of 5˚C had the best fit for seedling crops, but these fits were less clear for regrowth crops because no low temperatures occurred during growth periods (Thiébeau et al., 2011). Their different temperature range and the continental versus temperate climates, could be the reason that our experimental data showed a lower T_b for canopy expansion (Wilson et al., 1995).

Another reason for this could be from the observed data used to perform this analysis. Specifically, the instrument (Sunscan canopy analyzer) used to measure LAI often overestimates when the canopy is small and stems are short in the field (Sim, 2014). This would translate into observed LAI data being inaccurate, typically in lower temperature conditions. The data were used to determine the development T_b was the number of main stem nodes. These are easily observed in the field in the lower temperature ranges. Therefore, to confirm development T_b is similar to leaf area expansion T_b, more and accurate LAI data are required at the beginning of regrowth cycles in early spring and late autumn.

The APSIM NextGen lucerne model used 2 ˚C for the leaf area expansion T_b. However, this is different compared with most lucerne models, which do not separate growth and development and only use one T_b for both growth and development processes. For

example, the APSIM classic lucerne model (Robertson et al., 2002) used T_b of 5 ˚C, STICS model (Strullu et al., 2020) used T_b of 3 ˚C, and GRAZPLAN pasture growth model (Smith et al., 2017) used T_b of 0 ˚C. However, the CROPGRO model (Jing et al., 2020; Malik et al., 2018) separated development and growth cardinal temperatures, and used development T_b of 3 ˚C and growth T_b of 0.2 ˚C.

5.4.2 Canopy expansion

LAI has been simulated in response to Tt for many crops (Ritchie and Nesmith, 1991). LAI data showed a strong positive linear relationship with Tt for seedling and regrowth crops (Figure 5.2 and 5.3). This indicated that temperature is the main factor driving lucerne leaf area expansion (Christian, 1977; Teixeira et al., 2007b). The slope of the linear regression (LAER) between LAI and Tt changed across different regrowth cycles for all experiments. To represent this seasonality, the response of LAER to Pp on LAER for seedling and regrowth crops was examined (Figure 5.4). However, these changes in LAER response to Pp was driven by a substantial proportion of total biomass and N that was translocated below ground under a decreasing Pp (Teixeira et al., 2007b). Biologically, photosynthesis should not respond to Pp changes. Therefore, a more mechanical approach is need to link C and N availability as part of further model development.

LAER is an empirical approach to simulate canopy expansion. This method integrates the crop canopy, but does not consider each component of the canopy, which includes nodes, branching, and leaf senescence (Brown et al., 2005). This is predominantly because detailed canopy component data are difficult to obtain in the field, and the challenge is to represent the complexity of different leaf and branching through the available model structure. However, the goal for canopy expansion simulation was to predict radiation interception. The critical LAI (LAI_{crit}) for lucerne was approximately 3.65 (Figure 5.12). Therefore, changes in LAI above LAI_{crit} will have little influence on radiation interception and subsequent growth simulations. Thus, a simple but robust model for canopy expansion is critical before crops reach the LAI_{crit}.

For seedling crops, the LAER values were smaller than regrowth crops, and constant in increasing Pp conditions (Figure 5.4). This confirmed previous findings reported by Thiébeau et al. (2011), that the seedling crop net leaf development is independent of Pp in spring and summer. This is expected because sufficient N and water were available for

seedling crops, and temperature and Pp were the only driving factors for canopy expansion in irrigated conditions. A longer phyllochron (Section 4.3.3.2) could be one of the reasons that seedling crops had slower LAER compared with regrowth crops (Teixeira et al., 2011). Nevertheless, there was insufficient data to inform any pattern of LAER in a decreasing Pp for seedling crops. Additional measurements for seedling crops sown in autumn, are required to accurately understand canopy expansion in decreasing Pp conditions.

For regrowth crops, the relationship between LAER and mean Pp showed a different response pattern in increasing and decreasing Pp. Specifically, LAER declined significantly in a decreasing Pp ($p<0.0001$).There was no significant change in LAER ($p=0.16$) in an increasing Pp. However, changes in Pp direction do not the cause slower LAER biologically. This response is consistent with node appearance, which may be related to the change in partitioning to below ground in decreasing Pp. This is because below-ground organs appear to have priority for biomass and N in a decreasing Pp (Teixeira et al., 2008). Thus, it is possible that LAER was limited by availability of assimilates to canopy expansion and shoot regrowth (Brown et al., 2005). Biomass and N partitioning are investigated further in Chapters 6 and 7.

The LAER function averaged the canopy response to temperature within each regrowth cycle into one value. This ignores the different growth phases within each regrowth cycle. Specifically, for regrowth crops at the beginning of each regrowth cycle, there was a slow regrowth phase before crops reach linear growth. X-intercept values from the linear regression between LAI and Tt ranged from ~-50 to ~200 ˚Cd (Appendix 12). This indicates that some regrowth cycles required about 200 ˚Cd to reach the calculated LAER, described as a lag phase. This is consistent with the literature reported by Avice et al. (1996), who suggested that root reserve shows intense N depletion in the first ~10 days of post-harvest. Furthermore, Cunningham and Volenec (1996) demonstrated cell division was highly sensitive to N supply in the early regrowth period. This might be the cause of slow LAER for some treatments with low root reserves. Therefore, a lag phase function were added to improve the accuracy of the model.

Other regrowth cycles had leaves (basal buds) present before defoliation occurred (x-intercepted values ≤ 0 ˚Cd). For example, the first expanded leaves probably occurred close to the defoliation day when root reserves reached their maximum for most LL and HH

defoliation treatments (Teixeira et al., 2007b). To test this hypothesis, a basal buds function was tested under the assumption that plants start to produce basal buds when crops reach their reproductive stage in the prior regrowth cycle. The model simulation results suggest that the basal buds factor (BBF) was 20% of the potential LAER, which indicates new formed basal buds expanded with a rate of 20% of the potential LAER after crops reached in vegetative stage (Figure 5.5). However, the basal buds link with the lag phase was not tested due to a lack of observed LAI data from the early regrowth cycles. The hypothesis assumes that having developed basal buds shortens the lag phase, but this needs further testing. To test this hypothesis, more measurements are required to accurately determine the time of first node appearance and basal buds expansion rate under different levels of canopy cover. In addition, it is important to acknowledge that basal buds depend on the defoliation methods. Gazing or cutting of these basal buds should be avoided when measurements are taken in the field.

Canopy senescence happened in the 84 day (HH) defoliation treatment, which showed a steep decline in LAI after if peaked (Figure 5.7). This highlights the importance of including a canopy senescence module in the APSIM NextGen lucerne model. Brown et al. (2005) stated that leaf senescence proceeded up to at a rate of 1.08 leaves per main stem node after the ninth node. The LAI peaked after plants reached their flowering stage (Ta et al., 2020). Therefore, a senescence function was applied after flowering. Another factor that would contribute to canopy senescence is canopy cover. This is because mutual shading of lower leaves leads to increase leaf senescence (Brouwer et al., 2012). Specifically, when the crop reaches full canopy cover, the lower layer leaves senesces because less light comes through to maintain them (Brown et al., 2005).

The implementation of the lag phase (Appendix 14), basal buds (Appendix 17) and canopy senescence (Appendix 21) functions resulted in acceptable prediction of LAI using the LAER adjusted by Pp under the LL and HH defoliation treatments for regrowth crops. However, additional data measurements for seedling crops may be required to accurately understand its canopy expansion patterns or a different modeling approach is needed.

5.4.2.1 Defoliation effect

The hypothesis that defoliation treatments would affect LAER was tested using data collected under different defoliation treatments (HH, LS, SL and SS). There was close agreement between predicted and observed values under the HH and LS defoliation treatments. However, parameters and functions generated from the LL defoliation treatment did not accurately represent the short (28 day) defoliation treatment (SS). This probably reflects the treatment effect reducing perennial organ N and C reserves which then reduce LAER (Ta et al., 2020; Teixeira et al., 2007c). There was an important difference between the two experiments with the SS treatment (E3ISS and E4ISSF5) in relation to the root biomass reserves. Specifically, for E3ISS, the SS defoliation was applied after crops had been grown under a longer defoliation regime (LL) for two years. In contrast, crops in E4ISSF5 treatment, were defoliated at short regrowth intervals (SS) after their seedling phase. This may be the reason that E3ISS treatment had good agreement for the first regrowth year, but under-prediction was found in the second regrowth year (Figure 5.9). In contrast, the E4ISSF5 treatment was under-estimated in all years. This also reflects the limitation of an empirical LAER approach in this model. Therefore, a more mechanistic model approach to deal with C and N reserves is needed for future model development.

The difference in predicted LAI among different defoliation regimes indicates that lucerne canopy expansion was one of the variables affected by defoliation treatments. Furthermore, it supports the previous conclusions that canopy expansion were more sensitive to defoliation treatment than development processes (e.g. main stem node appearance; Section 4.43) (Teixeira et al., 2007b).

5.4.2.1 FD effect

A cultivar-dependent set of parameters was implemented to improve model simulation results, because the three FD classes had different LAER (Ta, 2018). Specifically, in decreasing Pp, LAER decreased with decreased Pp for FD2, whereas LAER was constant (~0.01) for FD10 (Figure 5.9). This indicates that FD2 had the strongest response to Pp in decreasing Pp among these three FD genotypes. In contrast, the FD10 was independent of Pp. This is also consistent with the FD ranking system which is determined based on plant height in autumn/fall (Fairey et al., 1996). Therefore, greater autumn growth of FD10 appeared related to LAER and plant height. Plant height will be investigated in Chapter 8.

The comparison between predicted and observed LAI of FD10, showed a poor agreement with FD10 grown under the SS treatment. This maybe because FD10 was most sensitive to frequent defoliation. This result agrees with the literature that has demonstrated that dormant cultivars may be more suited than non-dormant for frequent harvesting (Ventroni et al., 2010), and plant population declines significantly from field observation. This might be because the FD10 genotype had faster depletion of N reserves in taproots (Ta, 2018). This is further evidence of the limitation of the empirical LAER model. Future model development could link LAER with C and N availability.

The APSIM NextGen lucerne model comprises a few aspects of canopy expansion and uses a simple but robust LeafArea model (Appendices 14 to 21). Other models used different approaches. For example, the APSIM classic lucerne model used a linear relationship between LAI and number of main stem nodes to predict lucerne LAI (Robertson et al., 2002). However, our data did not show a clear relationship between LAI and number of main stem nodes (Appendix 25), mostly because this method ignores other canopy components (e.g. branching). Confalonieri and Bechini (2004) described the increase in leaf area derived from increasing mass by means of the specific leaf area (SLA) in the CropSyst model. However, the SLA is not a constant value. It differs depending on the ratio between structural and non-structural mass according to leaf age and the environmental stresses and season (Beaudoin et al., 2009; Moot et al., 2015). Consequently, this modelling approach is generally not considered robust. The STICS model used a logistic function between Tt and LAI to simulate canopy expansion (Strullu et al., 2020), which was similar to the concept of a lag phase implemented in the APSIM NextGen lucerne model.

There are few lucerne simulation models that include different genotypes of FD classes canopy expansion in their simulations. In CSM-CROPGRO-perennial forage model (Jing et al., 2020), LAI was calculated based on SLA for different FD classes, which is interconnected to the partitioning rules of assimilates to storage organ with a shortening of the day length in autumn. However, this approach was not used in the current model development.

5.4.3 **Extinction coefficient**

The extinction coefficient (k) was used as an indicator of morphological changes in canopy architecture (Monsi and Saeki, 2005). Lucerne canopy structure was the same for seedling and regrowth crops (k=0.81). This agrees with the literature that seedling and regrowth

crops had the same k value (Teixeira et al., 2011). All crops from different treatments had a similar k value (Figure 5.12). This is consistent with previous reports that found little variation in k among different cultivars in different locations (Gosse et al., 1988; Mattera et al., 2013; Thiébeau et al., 2011).

The k value was not affected by defoliation management (Teixeira et al., 2007b). Furthermore, k was not different among the three FD genotypes for five growth years under different defoliation treatments. This agrees with the literature reported by Ta (2018) and Rimi et al. (2010) that there was no difference among different FD genotypes from field observations in relation to k value.

The differences of LAER response to different Pp conditions may be related to changes in partitioning to below ground organs which had the partitioning priority for biomass and N in decreasing Pp. Consequently, leaf and stem biomass changes may lead to change in resource capture (e.g. radiation interception), efficiency of conversion of resources in biomass (e.g. RUE) and partitioning patterns of DM among leaf, stem and root. These issues will be addressed in the following chapters.

5.5 Conclusions

The results of this chapter permit the following conclusions:

- Leaf area expansion T_b was not different to the development T_b. This is consistent with leaf area expansion including both growth and development elements.
- LAER declined significantly with decreasing Pp. However, this Pp response was not observed in increasing Pp, which indicates that there is a more universal relationship with change in partitioning than Pp, and partitioning is more likely the driver of this response. This will be considered in Chapter 6.
- Attempts to predict LAI from a function that varies LAER against Pp resulted in acceptably predictions between experiments under the LL and HH defoliation treatments. Applying lag phase, basal buds and canopy senescence functions improved prediction of canopy expansion. However, more measurements were required in the early regrowth cycle to understand the relationship between lag phase and basal bud initiation.

- Parameters and functions to estimate canopy expansion for the 42 day (LL) defoliation treatment did not give accurate LAI prediction for the extreme short defoliation treatment (SS). This reflects the limitation of the empirical LAER function which was not related to C and N availability.
- Three different FD classes had different LAER. Among these three FD classes, the FD10 was more sensitive to frequent (28 day) defoliation. The reason for this is investigated in Chapter 6.
- The extinction coefficient (k) was consistent for seedling and regrowth crops (0.81), and unaffected by defoliation management and FD classes.

6 MODELLING GROWTH AND PARTITIONING

6.1 Introduction

Accurate prediction of shoot and root biomass is one of the main objectives of crop simulation models. The major challenge for yield prediction in perennial crops is capturing the seasonal changes in DM partitioning to the perennial organs (root and crown) (Teixeira et al., 2007c). Chapter 5 quantified radiation intercepted by the canopy. This chapter focuses on how efficiently that intercepted radiation is used, and how dry matter is partitioned into each organ.

The research question to be answered is: can growth and partitioning responses to seasonal environmental changes [temperature and photoperiod (Pp)] be accurately simulated and predicted under different management practices for seedling and regrowth lucerne crops? The hypothesis is that functions and algorithms (Table 6.1) used in previous versions of the APSIM classic lucerne model (Moot et al., 2015; Robertson et al., 2002) can be adapted for use in the APSIM next generation (APSIM NextGen) lucerne model to accurately quantify seasonal responses of cultivars from different fall dormancy (FD) classes, grown under different defoliation regimes.

To test this, Objective 3 of the thesis is to quantify, simulate, and verify lucerne growth and biomass accumulation and partitioning in seedling and regrowth crops using the Plant Modelling Framework (PMF) in APSIM NextGen. Field measured data of leaf, stem, and root biomass (crown and taproot) from multiple, long-term experiments (1-4) grown under standard management practices were used to calculate functions and parameters in the PMF. The model was also used as a hypothesis testing tool to generate parameters which were not assessed in the field experiments. Once the model structure was built, it was tested with additional datasets from different defoliation treatments and FD classes (Experiments 3 and 4). This procedure was used to determine which parameters changed under different defoliation regimes and FD classes, and to explain the physiological basis for any changes. Parameters were compared with those derived in previous models (Table 6.1).

Table 6.1 Parameters for the classic APSIM lucerne model.

Parameter name	Units	Parameter description	Lucerne (Robertson et al. 2002)	Lucerne (Moot et al. 2015)
RUE_{shoot}	MJ g^{-1} DM	Radiation use efficiency for shoot biomass	0.6 (seedling) 1.0 (regrowth) 0.6 (regrowth winter)	*
RUE_{total}	MJ g^{-1} DM	Radiation use efficiency for total biomass	*	0.9 (seedling) 1.6 (regrowth)
Fraction to leaf	fraction	Partitioning fraction to leaf	0.1-0.45	0.3-0.9
Rate of dry matter partitioning to root	fraction	Root partitioning rate	*	0.1-0.4
Rm_root_day	g g^{-1} day^{-1}	Root respiration coefficient	*	0.005-0.035

Note: * not parameterized.

6.2 Materials and Methods

This chapter focuses on defoliation and genotype effects on lucerne crop growth and partitioning. Observed variables include leaf biomass, stem biomass, shoot biomass, and root biomass (crown and taproot).

The description of the experimental design, treatments and data collection were presented in Section 3.1. Statistical analyses and model evaluation were described in Section 3.2.4. Only additional measurements and calculations related to results of this chapter are reported.

6.2.1 **Field experimental data**

Lucerne field experimental data (Experiments 1-4) were used for simulation and verification (Table 4.2). Data described in Section 3.1.1 were used for leaf, stem, and root (crown and taproot) biomass. Datasets described in Section 4.2.1 were used for model testing and calibration of three FD classes grown under different defoliation regimes. Mechanisms are proposed for root maintenance respiration, remobilization in spring, and partitioning in autumn to account for changes in root biomass.

6.2.2 **Model structure**

In the PMF, dry matter is obtained from photosynthesis plus that reallocated from senesced tissues or from reserve remobilization, and allocated to each organ by the OrganArbitator (Brown et al., 2019). Allocation is based on the relative demand of each organ, which includes structure, storage, and metabolic biomass form. Demand is first controlled by phenology, with seedling crops having a bigger root demand than regrowth crops. Seasonal signals also change partitioning with remobilization to shoots during an increasing Pp and partitioning to perennial organs in a decreasing Pp. It is then maintained given ratios of partitioning among the different organs (Cichota et al., 2020). Predicting biomass supply is more complex because it includes a number of potential sources of DM for each organ. These are: 1) fixation: photosynthesis supplying DM from green organs; 2) translocation: the supply of storage DM from a 'live' organ; and 3) reallocation: the supply of storage and metabolic DM from a 'senescing' organ (Brown et al., 2019).

Datasets from crops grown under the LL (42 day) defoliation treatment (Experiments 1 to 4) were used to generate parameters for dry matter supply and demand for each organ (leaf, stem, and root). Two additional datasets (Experiments 3 and 4) were used to test and verify lucerne growth and partitioning-related parameters under shorter or longer defoliation regimes and FD classes. Several of the parameters derived in previous chapters (4 and 5) were used, and new parameters were calculated and added to the model structure to simulate shoot and root biomass.

6.2.3 **Model calibration and parameterization**

6.2.3.1 Radiation use efficiency (RUE)

Radiation use efficiency (RUE_{total}) for total DM (DM_{total}) was calculated from the linear regression of DM_{total} in response to accumulated intercepted radiation for each regrowth cycle where the slope of the linear regression represents RUE. The calculated values for RUE_{total} were then used to develop the function of RUE_{total} in response to mean air temperature. Shoot radiation use efficiency (RUE_{shoot}) was the slope of the linear regression between accumulated intercepted radiation and shoot biomass for each regrowth cycle.

6.2.3.2 Leaf dry matter supply and demand

The APSIM NextGen lucerne model used the SimpleLeaf model to estimate canopy expansion and senescence. In the SimpleLeaf model, all leaves are simulated as a whole canopy, without reference to differences in age or place (Section 5.3.2). The main function of the leaf organ for lucerne crops is to provide a value for DMFixationSupply (photosynthesis). DMFixationSupply uses an extinction coefficient (k) model to predict total radiation interception, and an RUE model to predict total radiation use efficiency, shown in Equation 17:

Equation 17 $DMFixationSupply = SolarRadiation \times (1 - e^{LAI \times -k}) \times RUE_{total}$

where leaf area index (LAI) is the sum of the canopy and RUE_{total} is total radiation use efficiency.

The daily leaf structural biomass demand was calculated based on LAI, given the demand for the leaf organ, shown in Equation 18:

Equation 18 $Leaf\ DM\ demand = a * LAI\hat{}b$

where 'a' is an adjustable constant value and 'b' is the power index.

In the APSIM NextGen lucerne model, leaf storage and metabolic demand were zero, i.e. assuming that all leaf DM demand was structural.

6.2.3.3 Stem dry matter demand

The stem parameters represent all stems and branches of the lucerne plants. Stem structural DM demand was calculated as a power function of total shoot biomass as shown in Equation 19:

Equation 19 $Stem\ DM\ demand = a * Shootwt\hat{}b$

where 'a' is an adjustable constant value and 'b' is the power index. Shootwt is equal to leaf biomass plus stem biomass.

Stem storage and metabolic demand are set to zero, based on the assumption that all stem DM demand was structural.

6.2.3.4 Structural taproot dry matter demand

The root organ provides the plant's connection with the soil, facilitating the extraction of water and nutrients, including nitrogen (N). For lucerne, its perennial root system (crown and taproot; defined as taproot in the PMF) serves as the storage organ for N and nonstructural carbohydrates in autumn (defined as storage demand or partitioning), and as a supplier of N and nonstructural carbohydrate to boost above-ground growth in early spring and after defoliation (defined as remobilization).

In winter, there is little above-ground growth and below-ground DM loss can be attributed mainly to root respiration. Therefore root biomass in this period was used to calculate the structural root biomass. Structural root biomass was calculated as the extrapolation of the linear relationship between root biomass lost during winter and initial root biomass at the beginning of winter, an x-intercept value when y=0. This assumes that structural DM does not respire, so extrapolating respiration rates to zero gave the amount of non-respiring biomass as an estimated root structural biomass.

6.2.3.5 Storage taproot demand

Storage root demand was determined by comparing RUE_{shoot} and RUE_{total}. The difference between RUE_{shoot} and RUE_{total} is the proportion partitioned to storage root, defined as storage root demand. A linear function between RUE_{shoot} and mean air temperature was plotted to compare with RUE_{total} in increasing and decreasing Pp. A model optimization exercise for optimal RUE_{shoot} at 18˚C was conducted external to APSIM NextGen. Values were tested from 0.7 to 1.25 at 0.05 intervals. Predicted shoot biomass values were compared with observed values to determine the most accurate value for RUE_{shoot} at 18˚C in increasing and decreasing Pp.

6.2.3.6 Root remobilization

Perennial roots support shoot regrowth in spring and after defoliation (Avice et al., 1997b; Ta et al., 1990). In the PMF, root C remobilization was separated from N remobilization. However, root remobilization was not measured in our experiments. Therefore, a model optimization approach was used to determine the most accurate remobilization coefficient value by comparing predicted shoot and root biomass with observed values. Biomass remobilization was parameterized based on crop development stage. Specifically, no

remobilization occurred in seedling crops, because seedling crops showed a preferential partitioning of biomass to roots until a critical level of perennial reserves was reached (Sim, 2014). In contrast, remobilization occurred for regrowth crops, especially in the early stage of each regrowth cycle and in spring. Remobilization coefficient values (percentage of storage root biomass per day) were tested from 0 to 0.175 at 0.025 intervals. Remobilization processes stopped once plants reached in flowering stage (Cunningham and Volenec, 1998).

6.2.3.7 Root respiration

Growth respiration for shoots and roots was accounted for in the value of RUE_{total}. Thus, only maintenance respiration of root DM (Rm_{root}) needed to be calculated for perennial crop. A daily rate of respiration coefficient (Rm_root_day; g g^{-1} day^{-1}) was used to adjust DM_{root} assuming a reference soil temperature (100 mm depth) of 20˚C (Equation 20).

Equation 20 $$Rm_{root} = \left[Rm\_root\_day * Q_{10}^{\frac{(T_{soil}-20)}{10}}\right] Storage\ DM_{root}$$

where Rm_root_day is the respiration coefficient that changes with the metabolic activity of crown and taproots in different seasons (Teixeira et al., 2009). The Q_{10} value of 1.8 is a modifying factor for Rm_{root} as soil temperature fluctuates (Atkin et al., 2000), and DM_{root} is the storage root biomass.

A model optimization exercise was conducted for determining the Rm_root_day value, Rm_root_day values were tested from 0 to 0.0035 at 0.0005 intervals. Predicted shoot and root biomass were compared with observed values to determine the most accurate Rm_root_day value.

6.2.3.8 Regrowth coefficient

To test the null hypothesis that remobilization remains constant throughout the regrowth period, a model optimization exercise was conducted to determine the pattern of the regrowth coefficient. The regrowth coefficient function includes two parameters (remobilization duration and remobilization rate). Remobilization duration was defined and calculated as thermal time (Tt) since harvest, whereas remobilization rate was an adjusted value for the current remobilization coefficient value (Section 6.2.3.6), which was 1.5 (1.5 multiply remobilization coefficient value) from defoliation for a period and then it

dropped to 0. Different durations of this period were tested ranging from 0 to 400 ˚Cd after defoliation at 50 ˚Cd intervals. Predicted shoot and root biomass were compared with observed values to determine the most accurate regrowth coefficient function and parameters.

6.3 Results

6.3.1 **RUE**

6.3.1.1 Total DM and accumulated total radiation

Total dry matter had a strong linear relationship with accumulated total radiation interception (R^2 from 0.53 to 0.99; Figure 6.1). Lucerne plants produced a total DM (shoot and root) of between 500 and 1300 g m^{-2} with a 45 day regrowth cycle of 300 to 600 MJ m^{-2}. The slope of regression changed across regrowth cycles (Appendix 26 for R^2, P value, slope, and intercept values). This is consistent with RUE responding to temperature. Therefore, regression analysis between the slope of the linear regression (RUE_{total}) and mean air temperature was investigated.

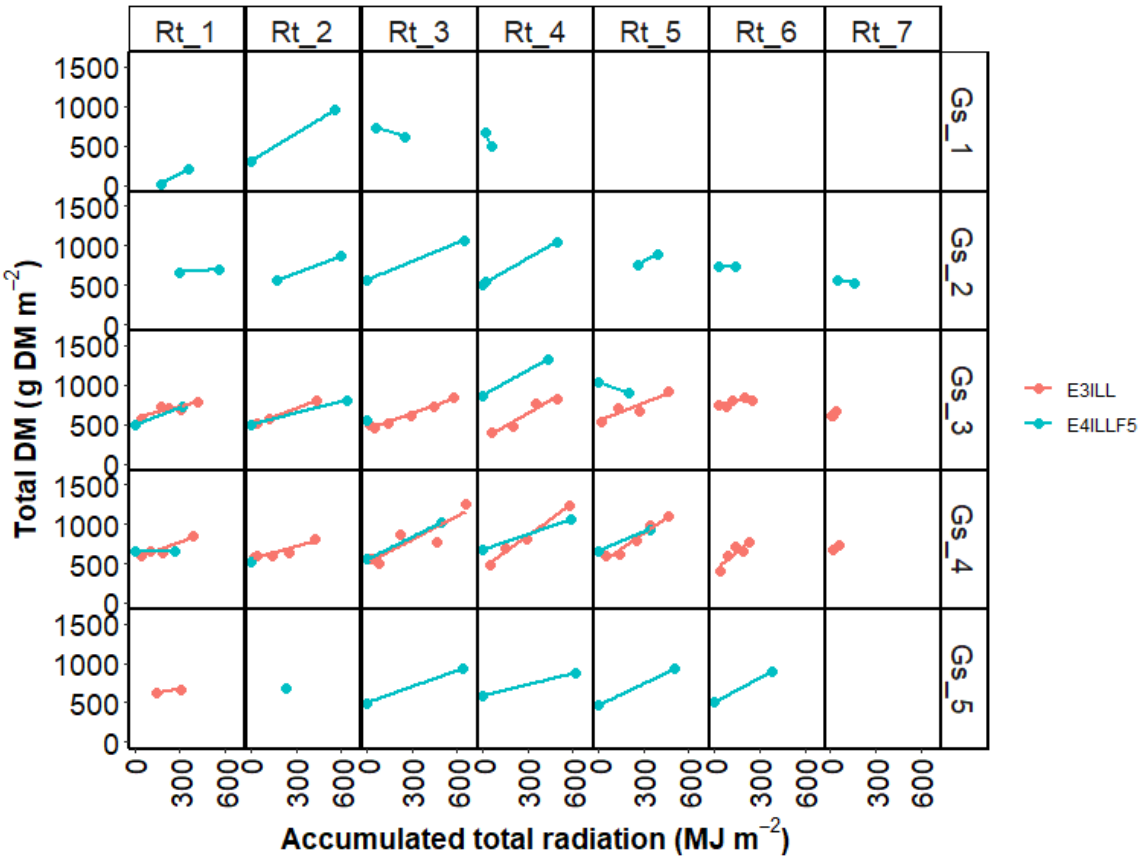

Figure 6.1. Total DM (g DM m^{-2}) against accumulated total radiation (MJ m^{-2}) from two field experiments (3 and 4) conducted from 2002-2019 at Iversen field, Lincoln University, Canterbury, New Zealand. Columns Rt_1 to Rt_7 represent regrowth cycles, and rows Gs_1 to Gs_5 represent growth years. Lines represent linear regressions.

6.3.1.2 Total RUE

A linear relationship was found between calculated RUE_{total} and mean air temperature (R^2=0.60; Figure 6.2). RUE_{total} increased from 0.52 to 1.1 g DM MJ^{-1} as mean air temperature increased from 10 to 18 ˚C (Appendix 27 for RUE_{total} model structure).

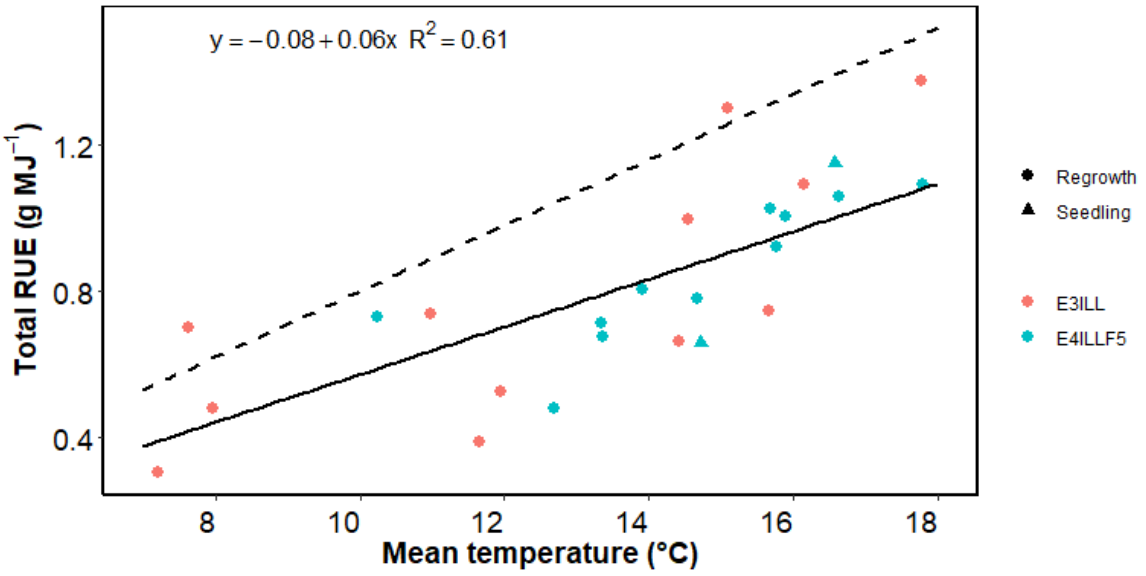

Figure 6.2. Total radiation use efficiency (RUE_{total}; g MJ^{-1} total radiation) against mean air temperature (˚C) for both seedling and regrowth crops from two field experiments (3 and 4) conducted from 2002 to 2019 at Iversen field, Lincoln University, Canterbury, New Zealand. Dashed line represents the upper bound of the regression (y = -0.1 + 0.09 x).

6.3.2 **Leaf biomass demand**

A strong power relationship was found between leaf biomass (g m^{-2}) and LAI (m^2 m^{-2}) for seedling and regrowth crops (R^2=0.88) in the four field experiments (Figure 6.3). These data illustrated that leaf biomass increased from 0 to 200 g m^{-2} as LAI increased from 0 to 6 m^2 m^{-2}. Therefore, leaf demand was parameterized as a simple power function in the APSIM NextGen lucerne model (Appendix 28 for model structure of leaf biomass demand).

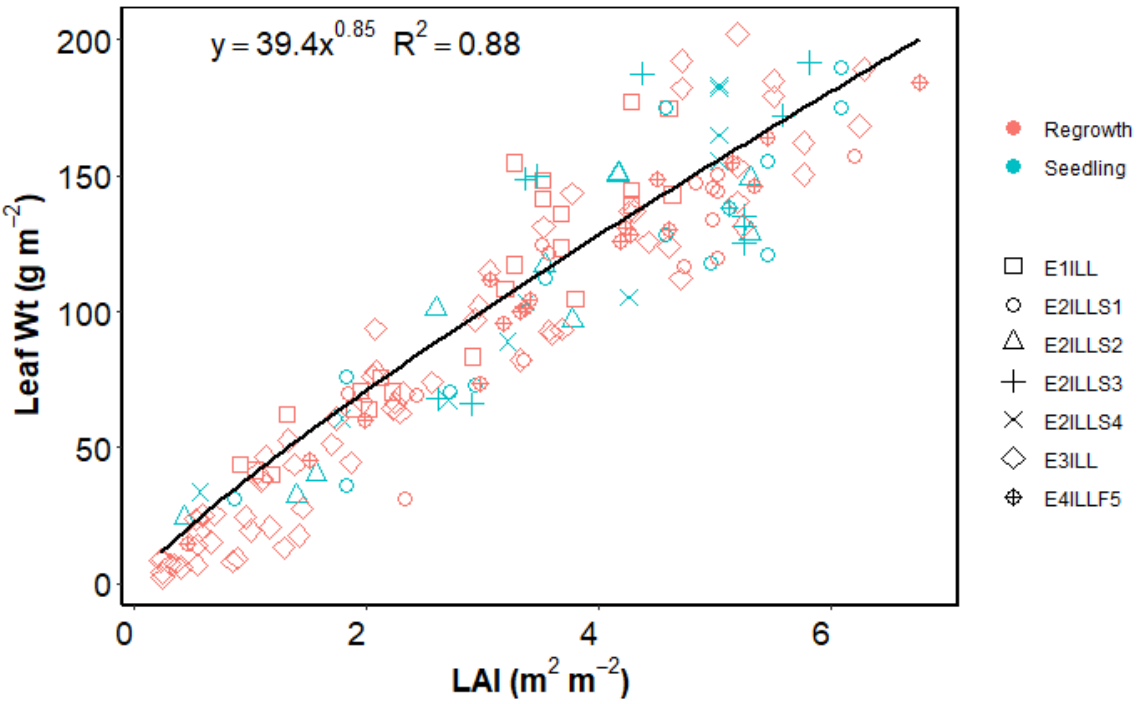

Figure 6.3. Leaf DM (g m^{-2}) against LAI (m^2 m^{-2}) for regrowth lucerne crops derived from four field experiments with the LL (42 day) defoliation treatment conducted from 2000-2019 at Iversen field, Lincoln University, Canterbury, New Zealand.

6.3.3 Stem biomass demand

A strong power relationship (R^2=0.98) was found between stem biomass and shoot biomass for regrowth crops in four field experiments (Figure 6.4). Shoot biomass increased from 0 to 500 g m^{-2} as stem biomass increased from 0 to 200 g m^{-2}. The power function was $y=0.14*x^{1.23}$. Therefore, stem demand was parameterized as a power function in the APSIM NextGen lucerne model (Appendix 29 for model structure of stem biomass demand).

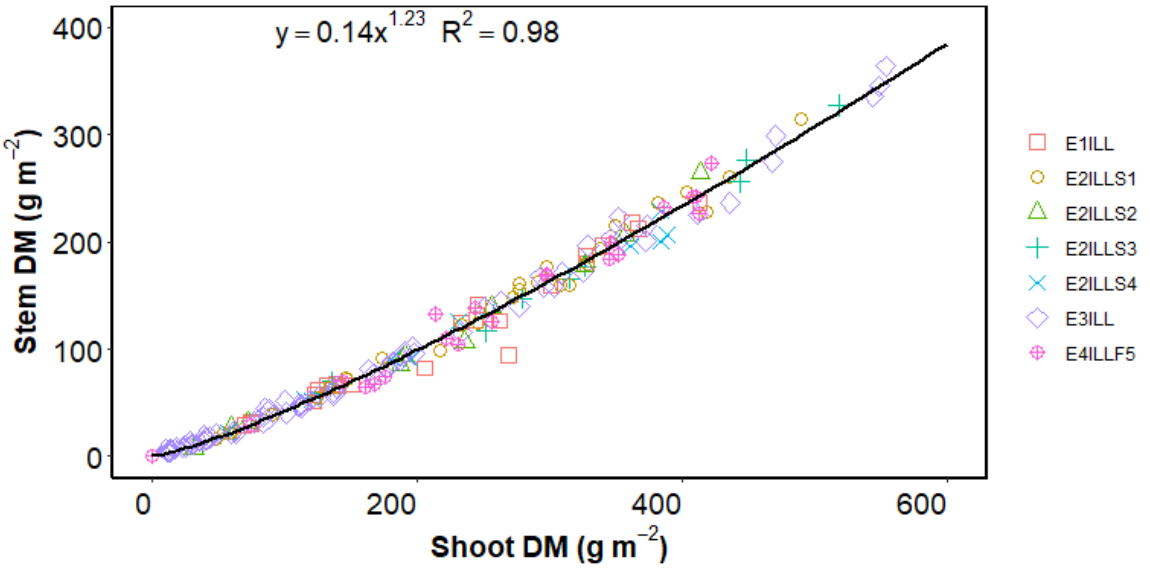

Figure 6.4. Stem DM (g m^{-2}) against shoot DM (g m^{-2}) for regrowth crops derived from four field experiments with the LL (42 day) defoliation treatment conducted from 2000 to 2019 at Iversen field, Lincoln University, Canterbury, New Zealand.

6.3.4 **Root biomass demand**

6.3.4.1 Root biomass seasonal distribution

The seasonal pattern of lucerne shoot and root biomass in different growth seasons managed with a 42 day (LL) defoliation regime are shown in Figures 6.5 and 6.6. For the experiment E3ILL, the LL defoliation treatments were applied to a two-year-old lucerne crop sown in 2000, with approximately 5000 kg ha^{-1} of root biomass (Teixeira et al., 2008). For the experiment E4ILLF5 (Ta et al., 2020), the LL defoliation treatment was applied after the seedling crop. Shoot biomass was highly dependent on the defoliation treatment. Average of annual shoot biomass for E3ILL and E4ILLF5 was ~23000 and 18000 kg ha^{-1}, respectively. However, root biomass from both treatments showed a similar seasonal pattern. It decreased from spring to mid-summer; the lowest values were found in mid-January. Root biomass increased to late autumn due to changes in partitioning to roots that occurred in the decreasing Pp. Root biomass declined gradually in winter.

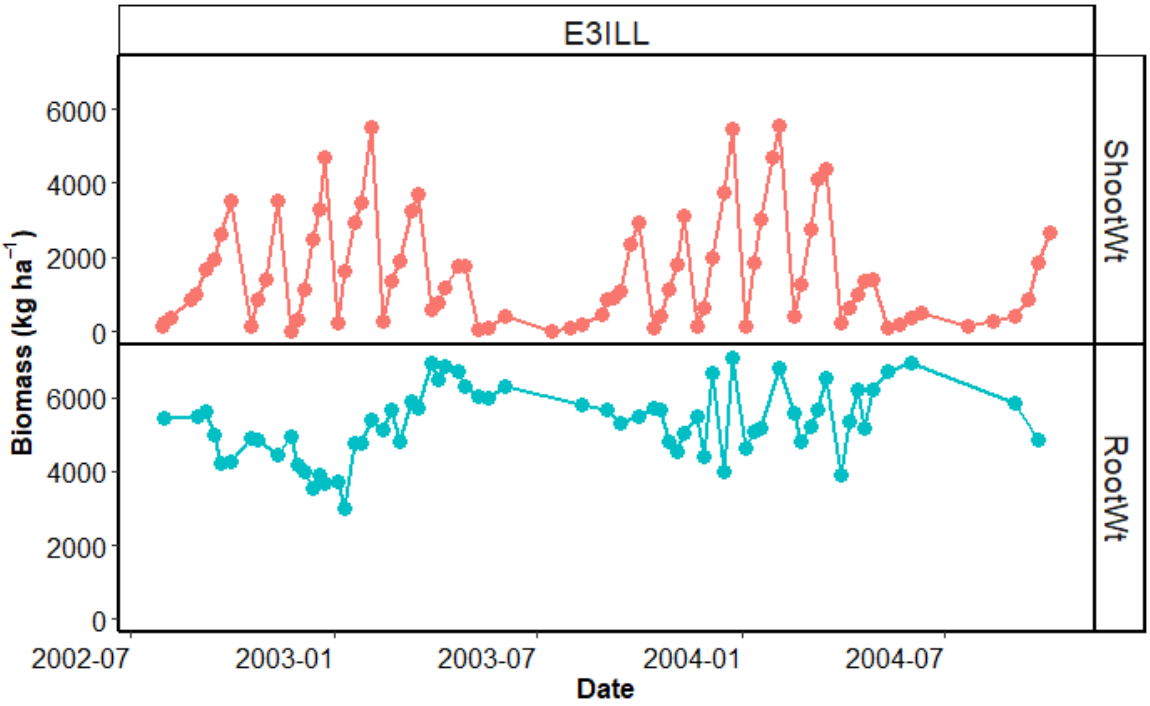

Figure 6.5. Observed seasonal shoot and root biomass for field Experiment 3 with the LL (42 day) defoliation treatment conducted in 2002-2004 at Iversen field, Lincoln University, Canterbury, New Zealand.

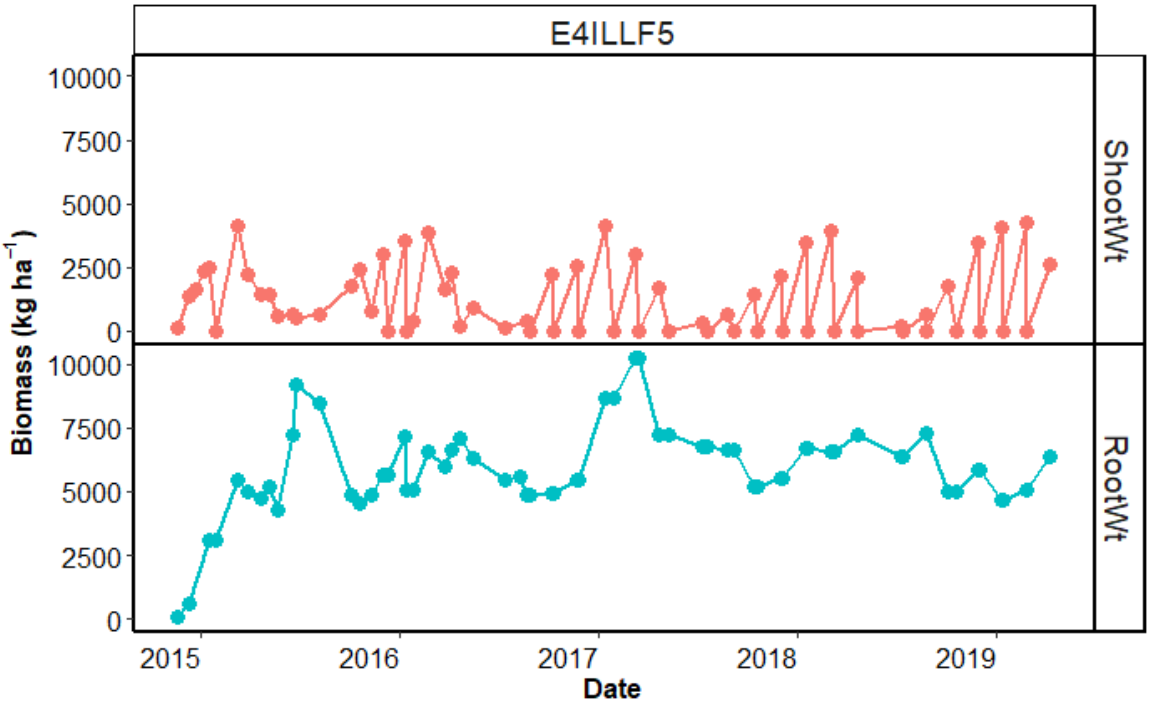

Figure 6.6. Shoot and root biomass seasonal distribution from field Experiment 4 with the LL (42 day) defoliation treatment conducted in 2014-2019 at Iversen field, Lincoln University, Canterbury, New Zealand.

6.3.4.2 *Root structural demand*

Root biomass data in the winter were used to calculate the structural root biomass under the observation that there was little above-ground growth and below-ground DM loss would mainly be due to root maintenance respiration, and not from defoliation. A strong linear relationship was found between the amount of root biomass lost in the winter and initial root biomass at the beginning of winter (R^2=0.65 in Figure 6.7). Root respiration increased from 570 to 1600 kg ha^{-1} as initial root biomass increased from 2500 to 9300 kg ha^{-1}. The extrapolation of the linear relation to y=0 gave an x-intercept value of non-respiring biomass was used to defined the structural root biomass at 2500±500 kg ha^{-1}, which assumes that structural biomass does not respire (Appendix 30 for model structure of root structural demand).

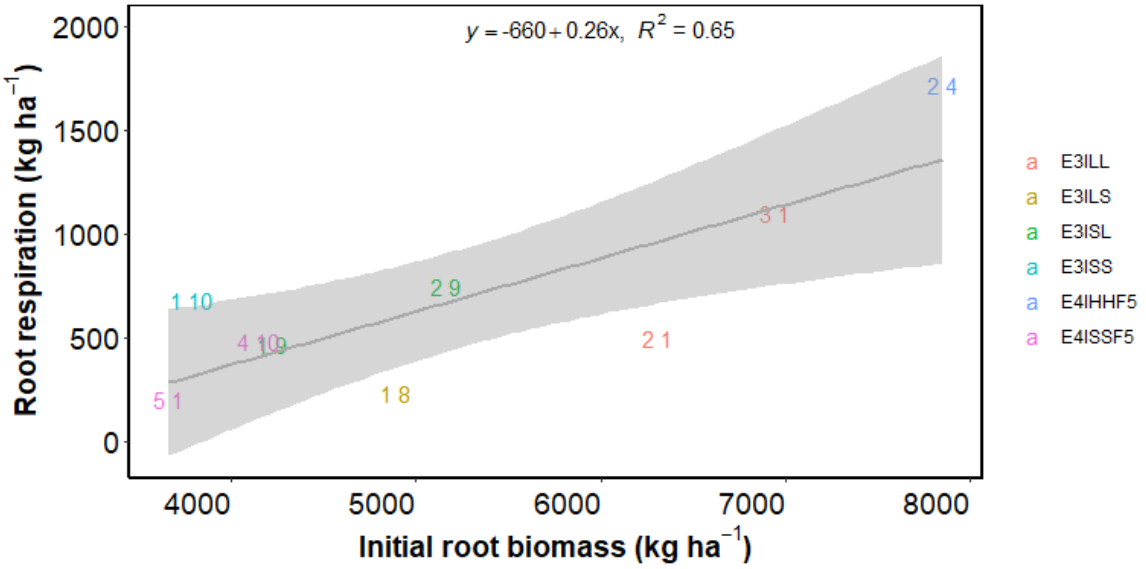

Figure 6.7. Calculated root respiration against initial root biomass in winter from two field Experiments 3 and 4 with multiple defoliation treatments [HH (84 day), LL (42 day), LS (42, 28 day), SL (28, 42 day) and SS (28 day)] conducted in 2002-2019 at Iversen field, Lincoln University, Canterbury, New Zealand.

6.3.4.3 *Storage root demand*

A model optimization exercise for optimal RUE_{shoot} at 18˚C was conducted external of APSIM NextGen to compare RUE_{shoot} and RUE_{total} (Section 6.3.1.2) in increasing and decreasing Pp. Values were tested from 0.7 to 1.25 at 0.05 intervals. Statistical measures for comparing predicted and observed values for shoot biomass in increasing and decreasing Pp were calculated and are provided in Figures 6.8 and 6.9 and Table 6.2. In an

increasing Pp, the most accurate optimum RUE_{shoot} was 1.05 at 18˚C, which was within the range of RUE_{total} at 1.1±0.31 (Section 6.3.1.2). This indicates little root biomass demand in increasing Pp conditions. However, in a decreasing Pp, the most accurate optimum RUE_{shoot} was 0.65 at 18˚C. This suggests a substantial proportion of total biomass was being moved below ground under a decreasing Pp.

The maximum storage root demand was calculated based on structure: storage root ratio. The values of structure: storage root ratio were calculated by the maximum root biomass of seedling, vegetative and reproductive stages from the E4ILL treatment divided by structural root biomass (~2500 kg ha^{-1}) for each stage. Therefore, storage root biomass demand was parametrized as the structure: storage root ratio. It was defined as a function of phenology, with a target set to 3 in the juvenile stage, decreasing to 1.6 in the vegetative stage then increasing to 2.3 after buds visible (Section 4.3.2).

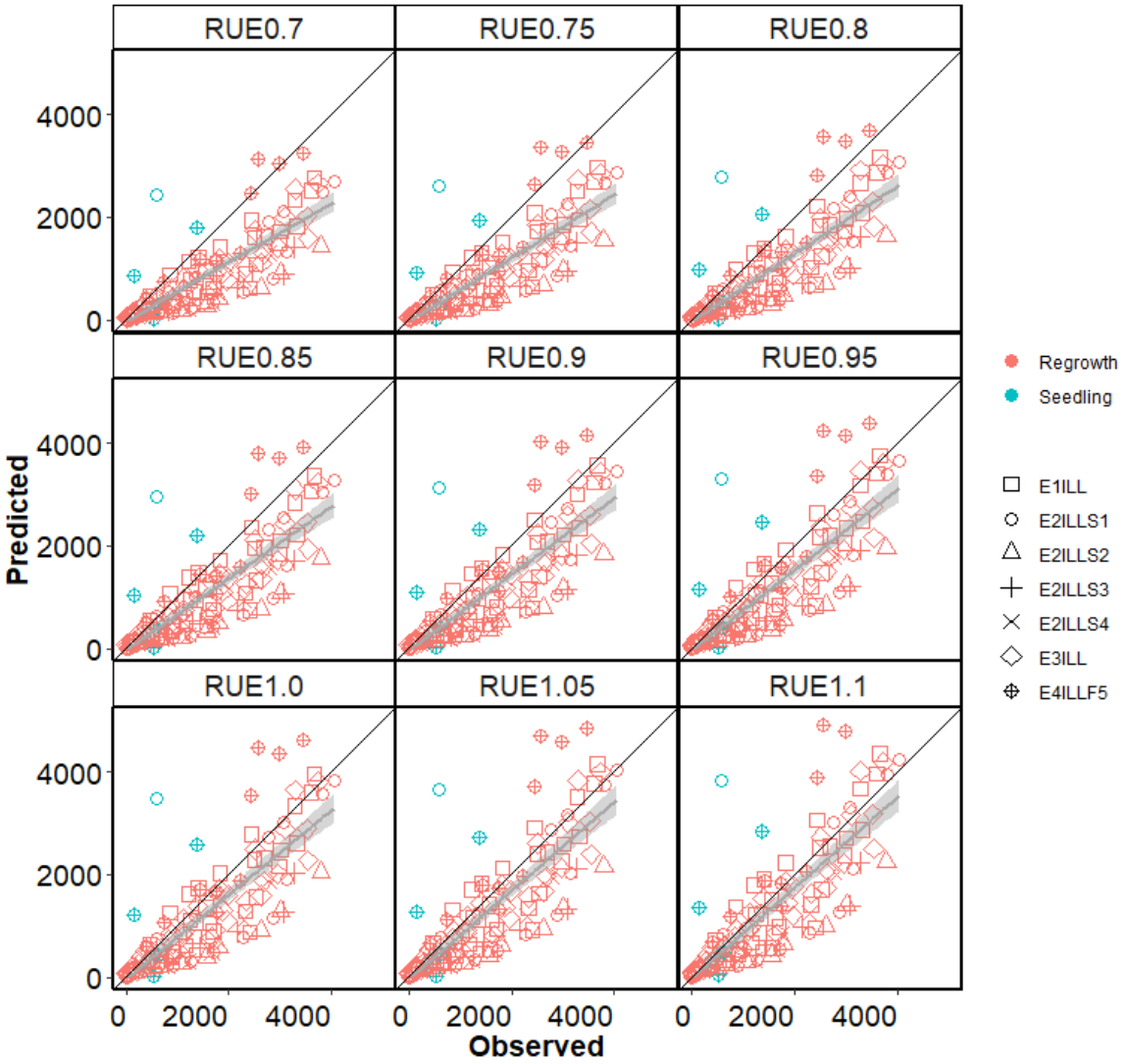

Figure 6.8. Predicted and observed shoot biomass to test RUE_{shoot} in increasing photoperiod (Pp) conditions from four field experiments with the LL (42 day) defoliation treatment conducted in 1997-2019 at Iversen field, Lincoln University, Canterbury, New Zealand.

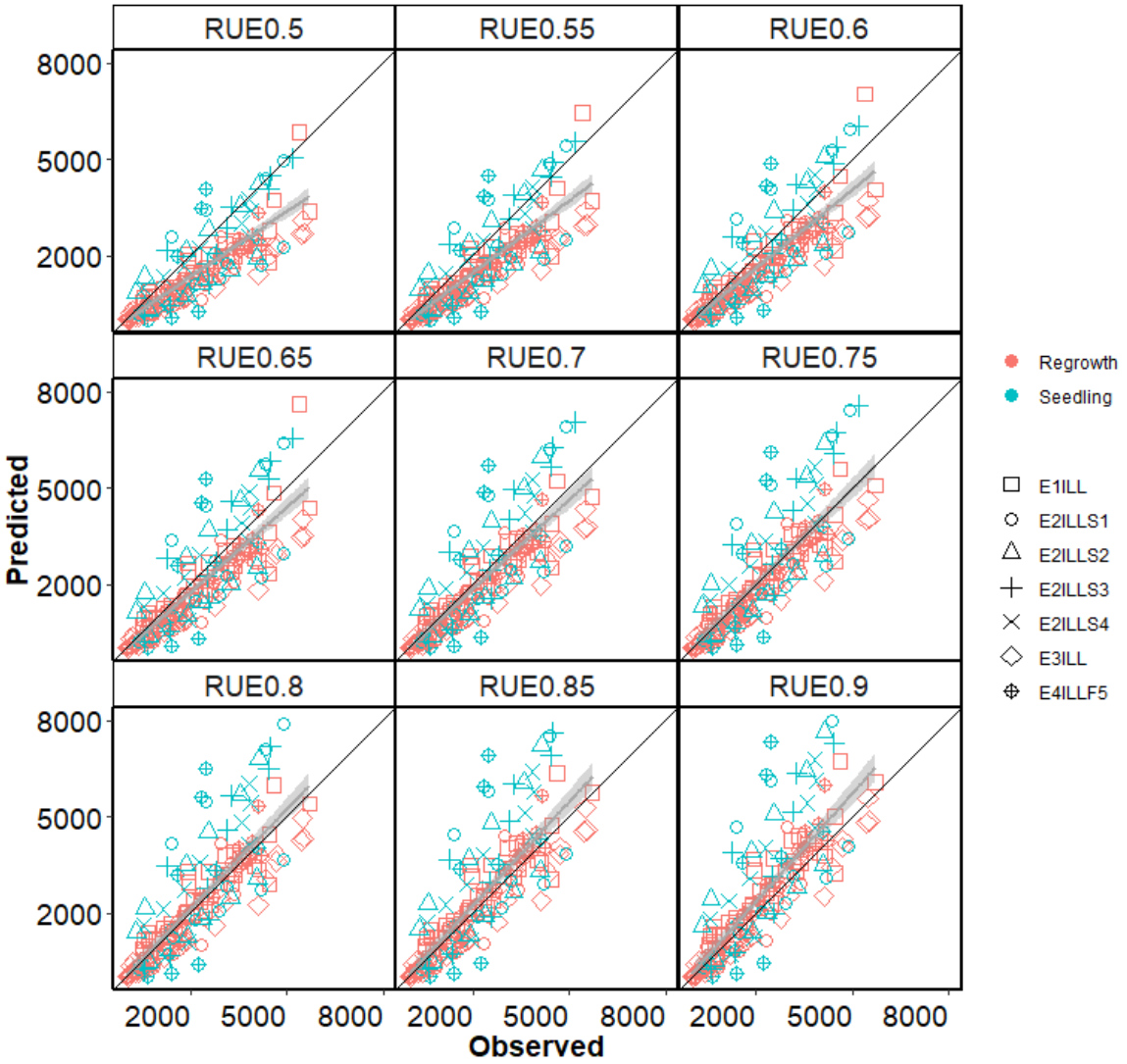

Figure 6.9. Predicted and observed shoot biomass to test RUE_{shoot} in decreasing photoperiod (Pp) conditions from four field experiments with the LL (42 day) defoliation treatment conducted in 1997-2019 at Iversen field, Lincoln University, Canterbury, New Zealand.

Table 6.2 Statistical measures of optimum RUE_{shoot} value in increasing and decreasing photoperiod (Pp) simulation on a calibration dataset from four field experiments with the LL (42 day) defoliation treatment conducted between 1997 and 2019 at Iversen field, Lincoln University, Canterbury, New Zealand. N = number of simulated and observed data pairs; R^2= coefficient of determination; R_RMSE = relative root mean square error (%); NSE = Nash-Sutcliffe efficiency; SB = Standard bias; NU = Nonunity slope; LC = Lack of correlation.

Pp	RUE_{shoot}	N	R^2	R_RMSE	NSE	SB	NU	LC
Increasing	0.7	130	0.66	62.1	0.30	50.4	1.6	48.0
	0.75	130	0.66	59.0	0.37	46.3	0.5	53.2
	0.8	130	0.66	56.2	0.42	41.4	0.0	58.6
	0.85	130	0.66	53.8	0.47	35.7	0.4	63.9
	0.9	130	0.66	51.9	0.51	29.4	1.9	68.7
	0.95	130	0.66	50.5	0.54	22.9	4.6	72.5
	1.0	130	0.66	49.7	0.55	16.5	8.6	74.9
	1.05	130	0.66	49.5	0.55	10.7	13.7	75.6
	1.1	130	0.66	49.9	0.55	6.0	19.5	74.5
Decreasing	0.5	174	0.71	49.9	0.49	42.4	0.2	57.3
	0.55	174	0.71	45.9	0.57	31.6	0.5	68.0
	0.6	174	0.71	43.2	0.62	19.3	4.2	76.5
	0.65	174	0.71	42.3	0.64	8.4	11.8	79.8
	0.7	174	0.71	43.2	0.62	1.6	21.8	76.6
	0.75	174	0.71	45.8	0.57	0.1	31.8	68.1
	0.8	174	0.71	49.8	0.49	2.6	39.9	57.5
	0.85	174	0.71	55.0	0.38	7.2	45.6	47.2
	0.9	174	0.71	61.0	0.24	12.4	49.2	38.4

6.3.4.4 Remobilization coefficient

A range of remobilization coefficient values were tested to fit with observed shoot and root biomass from two Experiments (3 and 4) conducted from 2002 to 2019. Statistical measures of remobilization coefficient values for comparing predicted and observed values of root and shoot biomass were calculated and are provided in Figures 6.10 and 6.11. A remobilization coefficient value of 0.05 had the lowest R_RMSE value and the highest NSE value for root biomass prediction, 21.6% and 0.30, respectively (Table 6.3). However, remobilization coefficient values from 0.025 to 0.175 gave the same shoot prediction with R_RMSE of 43.3% and NSE of 0.66 (Table 6.3). Thus, a remobilization coefficient value = 0.05 (5% of storage root biomass per day) was subsequently used for remobilization

calculations in the period of increasing Pp (Appendix 32 for model structure of root remobilization).

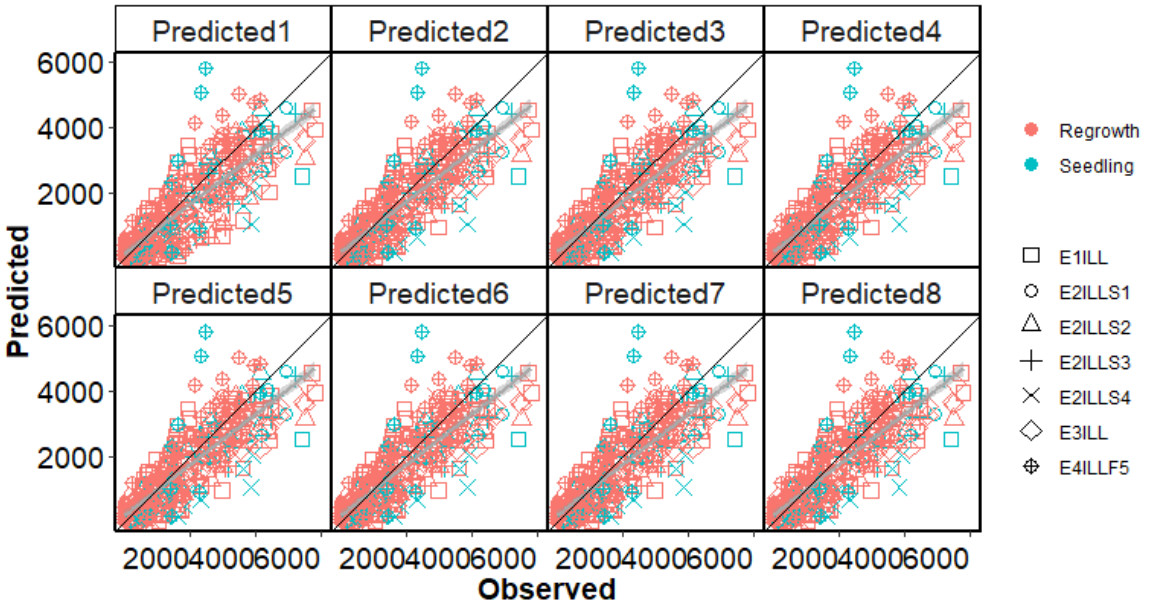

Figure 6.10. Predicted and observed shoot biomass in winter from four field experiments with the LL (42 day) treatment conducted in 1997-2019 at Iversen field, Lincoln University, Canterbury, New Zealand. Predicted1-8 represent remobilization coefficient values from 0 to 0.175 at 0.025 intervals.

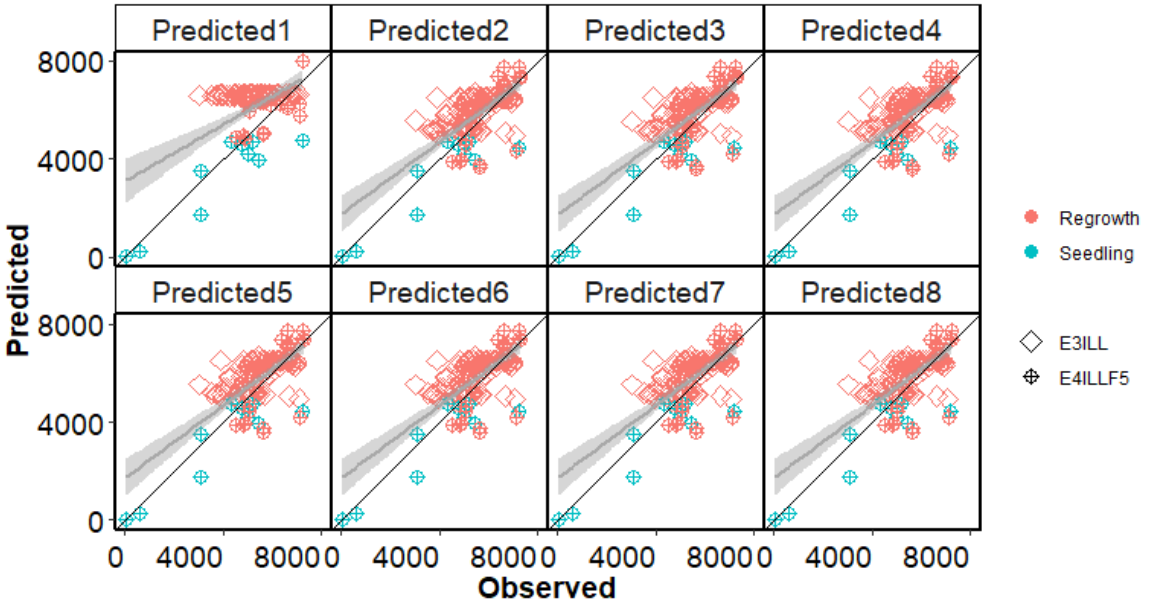

Figure 6.11. Predicted and observed root biomass in winter from two field experiments with the LL (42 day) defoliation treatment conducted in 2002-2019 at Iversen field, Lincoln University, Canterbury, New Zealand. Predicted1-8 represent remobilization coefficient values from 0 to 0.175 at 0.025 intervals.

Table 6.3 Statistical measures of remobilization coefficient value four field experiments (1-4) with the LL (42 day) defoliation treatment conducted between 1997 and 2019 at Iversen field, Lincoln University, Canterbury, New Zealand. N = number of simulated and observed data pairs; R^2= coefficient of determination; R_RMSE = relative root mean square error (%); NSE = Nash-Sutcliffe efficiency; SB = Standard bias; NU = Nonunity slope; LC = Lack of correlation.

Prediction	Remobilization coefficient	Biomass	N	R^2	R_RMSE	NSE	SB	NU	LC
Predicted1	0	shoot	360	0.65	47.75	0.58	12.4	2.6	84.9
		root	122	0.30	27.93	-0.16	28	11.5	60.5
Predicted2	0.025	shoot	360	0.69	43.28	0.66	8.6	1.2	90.2
		root	122	0.37	21.7	0.30	1.4	9.1	89.5
Predicted3	0.05	shoot	360	0.69	43.26	0.66	8.5	1.2	90.3
		root	122	0.40	21.64	0.30	1.3	9.5	89.2
Predicted4	0.075	shoot	360	0.69	43.26	0.66	8.5	1.2	90.3
		root	122	0.38	21.66	0.30	1.2	9.5	89.2
Predicted5	0.1	shoot	360	0.69	43.26	0.66	8.5	1.2	90.3
		root	122	0.38	21.67	0.30	1.3	9.6	89.2
Predicted6	0.125	shoot	360	0.69	43.26	0.66	8.5	1.2	90.3
		root	122	0.38	21.67	0.30	1.3	9.6	89.2
Predicted7	0.15	shoot	360	0.69	43.26	0.66	8.5	1.2	90.3
		root	122	0.38	21.67	0.30	1.3	9.6	89.2
Predicted8	0.175	shoot	360	0.69	43.26	0.66	8.5	1.2	90.3
		root	122	0.38	21.67	0.30	1.3	9.6	89.2

6.3.4.5 Root maintenance respiration

After applying the remobilization coefficient value in the model, a range of Rm_root_day values were tested to improve root biomass prediction from Experiments 3 and 4 conducted from 2002 to 2019. Statistical measures of Rm_root_day values for comparing predicted and observed values of root biomass are provided in Figure 6.15 and Table 6.4. A Rm_root_day value of 0.0005 had the lowest R_RMSE and highest NSE values, 21.6% and 0.31, respectively. By applying a small value of Rm_root_day, the root biomass prediction improved (R_RMSE decreased 0.04% and NSE increased 0.01) and shoot biomass predictions were the same (data not shown), with R_RMSE of 43.3% and NSE of 0.66. Therefore, a Rm_root_day value of 0.0005 was selected (Appendix 33 for model structure of root maintenance respiration).

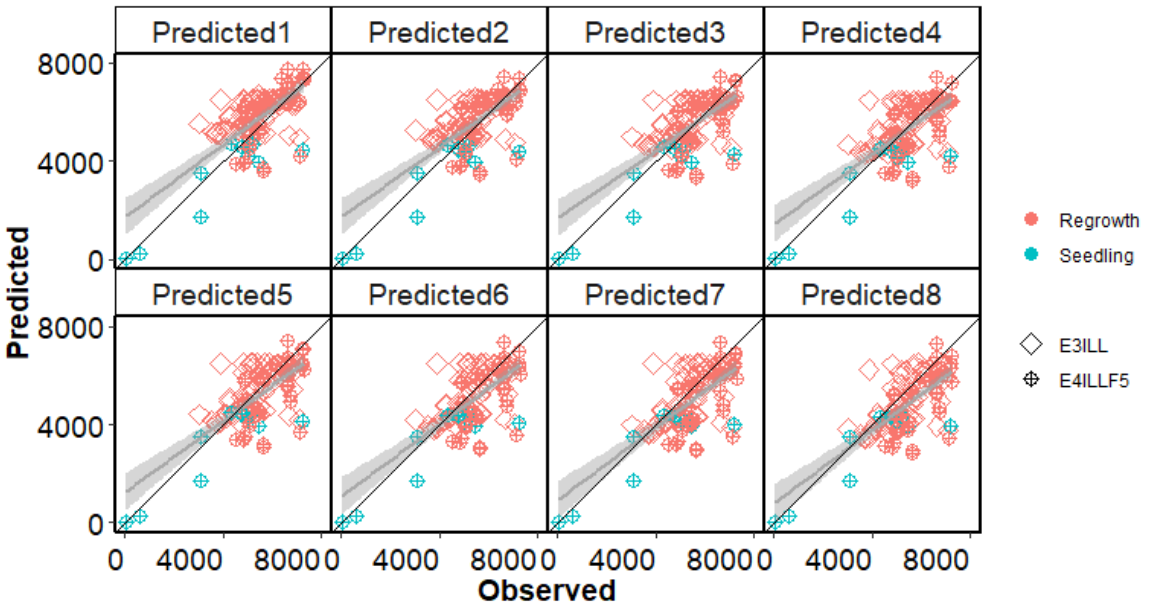

Figure 6.12. Predicted and observed root biomass from Experiments 3 and 4 with the LL (42 day) defoliation treatment conducted in 2002-2019 at Iversen field, Lincoln University, Canterbury, New Zealand. Predicted 1-8 represent Rm_root_day values from 0 to 0.035 at 0.0005 intervals.

Table 6.4 Statistical measures of Rm_root_day value for Experiments 3 and 4 with the LL (42 day) defoliation treatment conducted between 2002 and 2019 at Iversen field, Lincoln University, Canterbury, New Zealand. N = number of simulated and observed data pairs; R^2= coefficient of determination; R_RMSE = relative root mean square error (%); NSE = Nash-Sutcliffe efficiency; SB = Standard bias; NU = Nonunity slope; LC = Lack of correlation.

Prediction	Rm_root_day	N	R^2	R_RMSE	NSE	SB	NU	LC
Predicted1	0	122	0.38	21.64	0.30	1.3	9.5	89.2
Predicted2	0.0005	122	0.36	21.60	0.31	0.1	8.1	91.8
Predicted3	0.001	122	0.34	22.35	0.26	2.3	8.7	89
Predicted4	0.0015	122	0.35	22.75	0.23	6.2	8.7	85.1
Predicted5	0.002	122	0.35	23.28	0.19	10.7	8.7	80.5
Predicted6	0.0025	122	0.36	23.91	0.15	16.2	8.5	75.4
Predicted7	0.003	122	0.36	24.81	0.08	22.1	8.2	69.7
Predicted8	0.0035	122	0.37	25.75	0.01	29.8	6.7	63.5

6.3.5 **Shoot and root biomass simulation**

6.3.5.1 Model simulation of shoot and root biomass

Parameters and functions for leaf, stem, and root were implemented into the APSIM NextGen lucerne model (Appendices 28 to 33 for model structure for leaf, stem and root

biomass demand). Simulation and model evaluation results for predicting shoot biomass in each regrowth cycle of the four field experiments (Figure 6.13 and Table 6.5) showed good overall agreement (NSE = 0.66 and R_RMSE = 43.3%). However, prediction of root biomass had fair overall agreement (Figure 6.14 and Table 6.6), with an NSE of 0.31 and R_RMSE of 21.6%.

For shoot biomass simulation, regrowth crops had a closer agreement between predicted and observed values compared with seedling crops; NSE was 0.70 and 0.46, respectively. This was due to the under-estimation that occurred in treatment E2ILLS4 (autumn sowing experiment) (Figure 6.13), with R_RMSE of 56.6% and NSE of -0.21 (Table 6.5).

For root biomass simulation, there was a closer agreement between predicted and observed values for seedling crops than regrowth crops (NSE = 0.37 and 0.22). However, there was no difference between increasing and decreasing Pp in terms of prediction agreement (NSE = 0.28 and 0.21). Most of the variation was from the E3ILL treatment (NSE= -0.05).

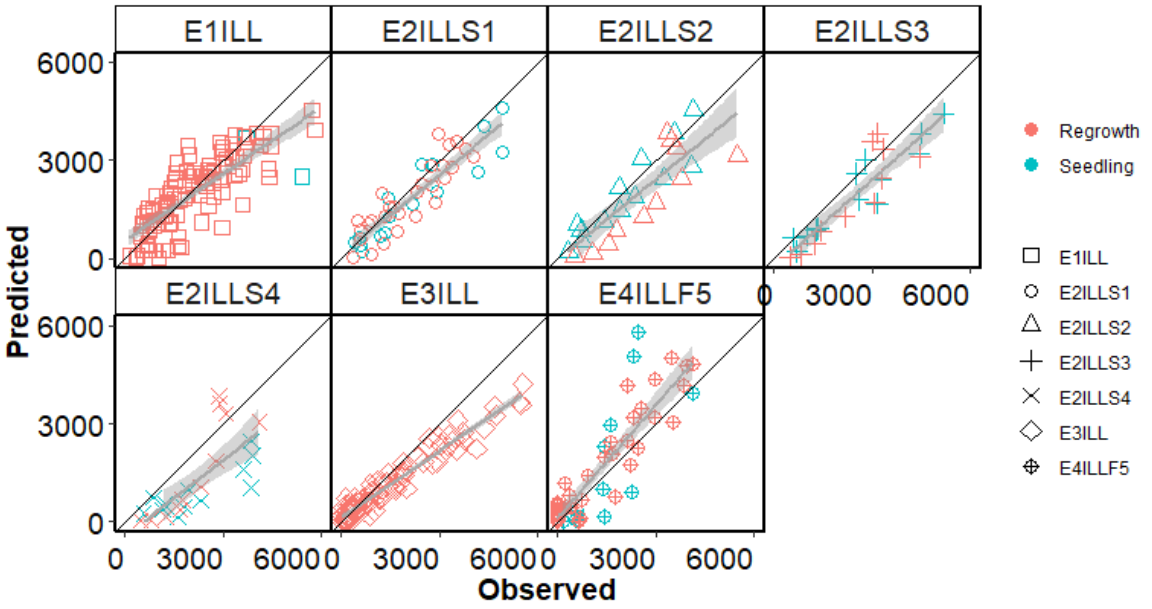

Figure 6.13. Predicted and observed values of lucerne shoot biomass (kg ha^{-1}) for four field experiments with the LL (42 day) defoliation treatment conducted between 1997 and 2019 at Iversen field, Lincoln University, Canterbury, New Zealand.

Table 6.5 Statistical measures of shoot biomass for four field experiments with the LL (42 day) defoliation treatment conducted within 1997 to 2019 at Lincoln University, Canterbury, New Zealand. N = number of simulated and observed data pairs; R^2= coefficient of determination; R_RMSE = relative root mean square error (%); NSE = Nash-Sutcliffe efficiency; SB = Standard bias; NU = Nonunity slope; LC = Lack of correlation.

Treatments	N	R^2	R_RMSE	NSE	SB	NU	LC
Total	360	0.69	43.3	0.66	0.4	3.5	96.1
Seedling	71	0.59	48.1	0.46	15.5	9.0	75.5
Regrowth	289	0.73	41.4	0.7	6.8	0.2	93
Increasing Pp	166	0.71	42.1	0.68	4.7	4.9	90.3
Decreasing Pp	194	0.69	44	0.64	12.1	0.1	87.8
E1ILL	105	0.59	41.3	0.57	3.8	0.1	96.1
E2ILLS1	45	0.82	28.4	0.77	19.5	0.0	80.5
E2ILLS2	24	0.72	35.9	0.6	28.1	3.0	68.9
E2ILLS3	24	0.83	31.1	0.67	46.7	1.5	51.8
E2ILLS4	23	0.55	56.6	-0.21	55.1	7.7	37.1
E3ILL	81	0.94	41.4	0.81	31.4	38.4	30.2
E4ILLF5	58	0.78	73	0.54	12.5	39.1	48.4

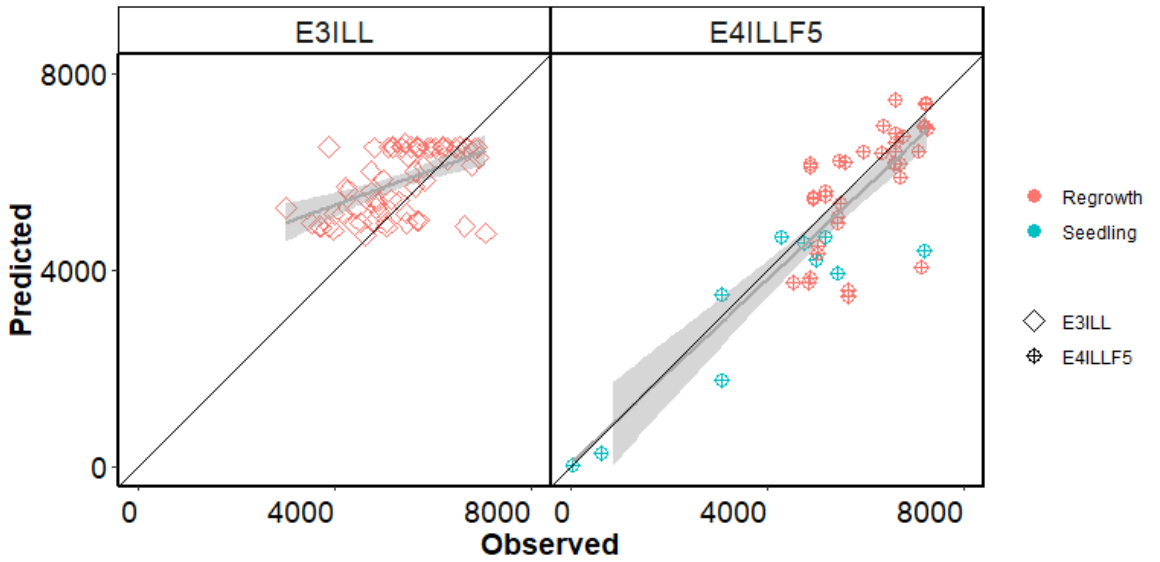

Figure 6.14. Predicted and observed values of lucerne root biomass (kg ha^{-1}) for Experiments 3 and 4 with the LL (42 day) defoliation treatment conducted between 2002 and 2019 at Iversen field, Lincoln University, Canterbury, New Zealand.

Table 6.6 Statistical measures of root biomass for Experiments 3 and 4 with the LL (42 day) defoliation treatment conducted within 2002 to 2019 at Iversen field, Lincoln University, Canterbury, New Zealand. N = number of simulated and observed data pairs; R^2= coefficient of determination; R_RMSE = relative root mean square error (%); NSE = Nash-Sutcliffe efficiency; SB = Standard bias; NU = Nonunity slope; LC = Lack of correlation.

Treatments	N	R^2	R_RMSE	NSE	SB	NU	LC
Total	122	0.36	21.6	0.31	0.1	8.1	91.8
Seedling	12	0.65	45	0.37	38.2	6	55.9
Regrowth	110	0.27	18.7	0.22	0.9	5.5	93.5
Increasing Pp	57	0.36	24.1	0.28	0.3	11.6	88.1
Decreasing Pp	65	0.26	19.7	0.21	0	6	94
E3ILL	65	0.26	18.2	-0.05	25	4.1	70.9
E4ILLF5	57	0.51	24.2	0.36	18.7	4.8	76.5

6.3.5.2 Verification of defoliation treatment

To test the null hypothesis that remobilization remained constant throughout the regrowth period, a regrowth coefficient function that includes two parameters (remobilization duration and remobilization rate) was used in the PMF. Remobilization duration was defined and calculated as Tt since harvest, whereas remobilization rate (ranging from 0 to 1.5) was an adjusted value for the current remobilization coefficient value (which equal to 5%*1.5=7.5%). Remobilization duration values were tested from 0 to 400 ˚Cd at 50 ˚Cd intervals (Figure 6.15, mod 1 to mod 8). The lines represent the remobilization pattern within each regrowth cycle, and illustrate that remobilization rates were the highest (1.5) at the beginning of each regrowth cycle, then slowed to zero. For example, mod2 represents that remobilization starts at the maximum remobilization rate (1.5) from the beginning of each regrowth cycle (0 ˚Cd), which remains constant until 50 ˚Cd, and then declines to 0 at 100 ˚Cd. (Appendix 34 for model structure for root regrowth coefficient function).

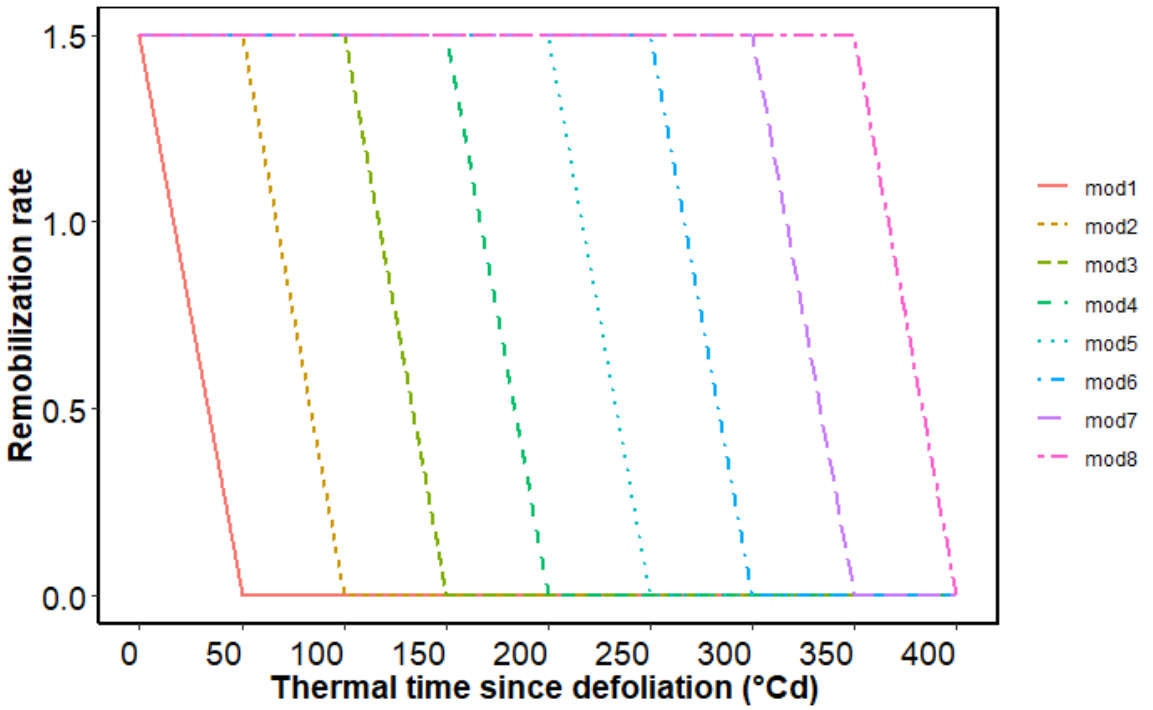

Figure 6.15. Remobilization rate against thermal time since defoliation in the regrowth coefficient function. Lines represent remobilization pattern within each regrowth cycle.

A range of regrowth coefficient functions were tested to fit observed shoot and root biomass values from the four field experiments. Statistical measures of regrowth coefficient functions (Predicted 0 to 8) were calculated and are provided in Table 6.7. A remobilization duration value (300-350 ˚Cd) had the lowest R_RMSE value and the highest NSE value for root biomass prediction, 27.5% and 0.48, respectively (Table 6.7). The remobilization duration value of 300-350 ˚Cd gave shoot prediction with R_RMSE of 53.5% and NSE of 0.71 (Table 6.7). This indicates that remobilization occurred within the first 300-350 ˚Cd in each regrowth cycle (remobilization rate being 1.5 from 0 to 300 ˚Cd; decreasing to 0 at 350 ˚Cd), which represents the biological processes of remobilization in the early regrowth cycles. Thus, a remobilization duration value of 300-350 ˚Cd was selected.

Table 6.7 Statistical measures of shoot and root biomass for four field experiments with multiple defoliation treatments [HH (84 day), LL (42 day), LS (42, 28 day), SL (28, 42 day), and SS (28 day)] conducted within 1997 to 2019 at Iversen field, Lincoln University, Canterbury, New Zealand. N = number of simulated and observed data pairs; R^2= coefficient of determination; R_RMSE = relative root mean square error (%); NSE = Nash-Sutcliffe efficiency; SB = Standard bias; NU = Nonunity slope; LC = Lack of correlation.

Regrowth coefficient	Biomass	N	R^2	R_RMSE	NSE	SB	NU	LC
Predicted0	shoot	728	0.73	52.4	0.72	1.2	1.1	97.7
(0)	root	386	0.30	36.1	0.1	21	0.9	78.2
Predicted1	shoot	728	0.69	56.4	0.67	3.8	1.8	94.4
(0-50)	root	386	0.25	44.1	-0.34	42.5	1.2	56.3
Predicted2	shoot	728	0.69	56.3	0.68	3.7	1.8	94.5
(50-100)	root	386	0.25	43.6	-0.31	41.5	1.2	57.3
Predicted3	shoot	728	0.69	56.3	0.68	3.7	1.8	94.5
(100-150)	root	386	0.27	42.8	-0.26	40.7	1.1	58.2
Prediction4	shoot	728	0.69	56.1	0.68	3.5	1.7	94.9
(150-200)	root	386	0.29	40.8	-0.15	37	0.8	62.2
Predicted5	shoot	728	0.70	55.2	0.69	3	1.4	95.6
(200-250)	root	386	0.33	38.4	-0.01	33	0.5	66.4
Predicted6	shoot	728	0.71	54.3	0.7	2.6	1.3	96.1
(250-300)	root	386	0.36	34.8	0.17	22.7	0.6	76.7
Predicted7	shoot	728	0.72	53.5	0.71	1.9	1.1	97
(300-350)	root	386	0.50	27.5	0.48	2.7	0	97.3
Predicted8	shoot	728	0.72	53	0.71	1.7	1.1	97.2
(350-400)	root	386	0.61	28.4	0.44	30	0.2	69.8

After applying a regrowth coefficient function in APSIM NextGen lucerne model (Appendix 34), there was good and fair agreement of shoot biomass prediction for regrowth crops compared with seedling crops (NSE of 0.75 and 0.38, respectively). In contrast, root biomass prediction was the same in seedling crops and in regrowth crops (NSE of 0.48) (Table 6.8).

Among the three defoliation treatments, the HH and LL treatments had good agreement of predicting shoot biomass, with similar NSE values (0.67 and 0.69) (Figure 6.16 and Table 6.8). However, the SS treatment had fair agreement between observed and predicted shoot biomass (R_RMSE=91% and NSE=0.35). For root biomass prediction, the HH and LL

treatment had fair agreement (NSE of 0.23 and 0.29). However, the SS treatment had poor agreement between observed and predicted root biomass; NSE was -0.19 and R_RMSE was 29%.

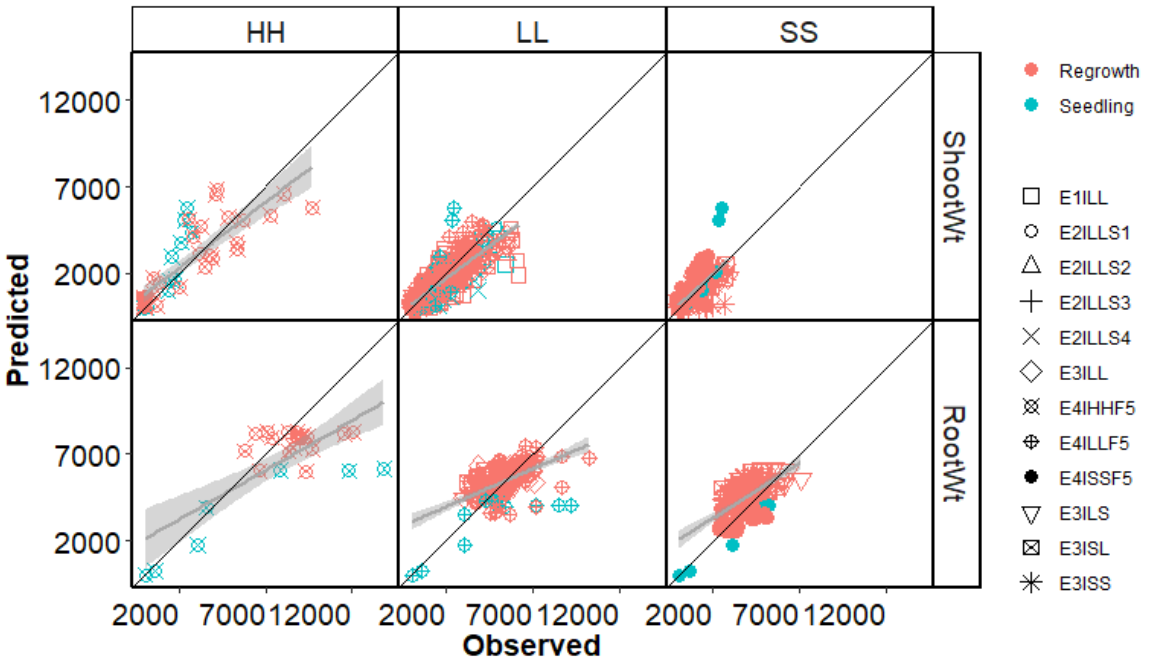

Figure 6.16. Predicted and observed shoot and root biomass from four field experiments with multiple defoliation treatments [HH (84 day), LL (42 day), LS (42, 28 day), SL (28, 42 day), and SS (28 day)] conducted in 1997-2019 at Iversen field, Lincoln University, Canterbury, New Zealand.

Table 6.8 Statistical measures of shoot and root biomass for four field experiments with multiple defoliation treatments [HH (84 day), LL (42 day), LS (42, 28 day), SL (28, 42 day), and SS (28 day)] conducted within 1997 to 2019 at Lincoln University, Canterbury, New Zealand. N = number of simulated and observed data pairs; R^2= coefficient of determination; R_RMSE = relative root mean square error (%); NSE = Nash-Sutcliffe efficiency; SB = Standard bias; NU = Nonunity slope; LC = Lack of correlation.

	Biomass	N	R^2	R_RMSE	NSE	SB	NU	LC
Total	shoot	728	0.72	53.5	0.71	1.9	1.1	97
	root	386	0.50	27.5	0.48	2.7	0	97.3
HH	shoot	45	0.69	63.1	0.67	4	2.1	93.9
	root	28	0.45	36.3	0.23	29	0	71
LL	shoot	468	0.73	44.3	0.69	9.7	0.2	90.1
	root	203	0.34	21.3	0.29	1.9	4.3	93.9
SS	shoot	215	0.56	91	0.35	3.2	29.1	67.7
	root	155	0.38	29	-0.19	32.7	15	52.3
Seedling	shoot	100	0.53	61	0.38	0.8	23.3	75.8
	root	28	0.71	54.3	0.48	28.3	15.5	56.3
Regrowth	shoot	628	0.76	51	0.75	2.4	0	97.6
	root	358	0.52	24.7	0.48	7.7	0.7	91.6
E1ILL	shoot	111	0.55	43.9	0.53	5.1	0.7	94.1
E2ILLS1	shoot	45	0.81	28.7	0.77	19.8	0	80.2
E2ILLS2	shoot	24	0.72	36.4	0.59	28.1	3	68.8
E2ILLS3	shoot	24	0.83	31.5	0.66	46.8	1.5	51.7
E2ILLS4	shoot	23	0.55	57	-0.23	55.5	7.8	36.7
E3ILL	shoot	81	0.96	43.3	0.79	37.1	42.1	20.8
	root	65	0.50	13.7	0.41	16.3	0.2	83.5
E4IHHF5	shoot	45	0.69	63.1	0.67	4	2.1	93.9
	root	28	0.45	36.3	0.23	29	0	71
E4ILLF5	shoot	67	0.81	64.4	0.64	13.4	32.3	54.4
	root	66	0.40	25.7	0.22	14.3	8.6	77.1
E4ISSF5	shoot	84	0.76	132.1	-0.24	22.4	58.4	19.2
	root	47	0.41	24.3	0.37	0.6	6.5	92.9
E3ILS	shoot	79	0.94	44.2	0.84	22.1	42.4	35.4
	root	63	0.25	18.8	-0.18	35.7	1	63.3
E3ISL	shoot	72	0.90	34	0.87	6.9	10.7	82.4
	root	58	0.21	28.9	-1.42	66.9	0.5	32.6
E3ISS	shoot	73	0.45	83.6	0.41	0	6.1	93.9

root	59	0.11	32.9	-2.2	67.2	5.1	27.7

6.3.5.3 Verification of fall dormancy treatment

Lucerne root partitioning rate has a strong FD effect. FD2 had a higher partitioning rate than FD5 and FD10 (Ta et al., 2020). Therefore, a different series of ratios was needed to define storage root biomass demand in decreasing Pp conditions for FD2 and FD10. Storage root demand were parametrized as the structure: storage root ratio within a function of phenology, which was the same for FD5 but with different target ratio values. The values of structure: storage root ratio were calculated by the maximum root biomass divided by structure root biomass (~2500 kg ha^{-1}) in each stage. For the FD2 genotype, target ratio values were set to 3 in the juvenile stage, 2.5 in the vegetative stage and 3 in the reproductive stage. For the FD10 genotype, target ratio values were set to 3 in the juvenile stage, 2.5 in the vegetative stage and 2.5 in the reproductive stage.

Ten remobilization coefficients were tested to fit with observed shoot and root biomass from Experiment 4. Values ranged from 0 to 0.045 at 0.005 intervals. The regrowth coefficient function includes two parameters (remobilization duration and remobilization rate, shown in Figure 6.15) was used to test the hypothesis that the remobilization coefficient value remains constant throughout each regrowth cycle. Twelve remobilization durations (ranging from 0-50 ˚Cd to 550-600 ˚Cd at 50 ˚Cd intervals) were tested to fit with observed shoot and root biomass from Experiment 4 conducted from 2014 to 2019. Statistical measures of remobilization coefficient values and remobilization duration values for FD2 and FD10 were calculated and are provided in Appendices 36 to 39.

For FD2, the most accurate combination was a remobilization coefficient value of 0.01 and remobilization duration value of 250-300 ˚Cd. This indicates that remobilization occurred within the first 250-300 ˚Cd in each regrowth cycle. The remobilization rate was estimated as 1.5 from 0 to 250 ˚Cd; decreasing to 0 at 300 ˚Cd in the regrowth coefficient function. For FD10, a remobilization coefficient value of 0.01 and remobilization duration values of 500-550 ˚Cd gave the most accurate prediction. This indicates that remobilization occurred for longer at 500-550 ˚Cd in each regrowth cycle, with the remobilization rate being 1.5 from 0 to 500 ˚Cd and decreasing to 0 at 550 ˚Cd in the regrowth coefficient function. Statistical measures of shoot and root biomass for FD2 and FD10 were calculated and are provided in Figures 6.17 and 6.18, and Tables 6.9 and 6.10.

Overall, predicted and observed shoot biomass values from Experiment 4 for two FD classes (FD2 and FD10) with multiple defoliation treatments (HH, LL, and SS) had good agreement, with NSE of 0.63 and R_RMSE of 58.1%. Notably, most of the variation was from seedling crops (NSE=0.15 and R_RMSE=64.5%) (Figure 6.17 and Table 6.9). However, there was no difference between FD2 and FD10 (NSE was 0.66 and 0.60).

Among the three defoliation treatments, the LL treatment had good agreement (R_RMSE=58%, NSE=0.54), whereas the SS treatment had poor agreement (R_RMSE=77.2%, NSE=-0.4). For example, both FD2 and FD10 under the SS defoliation treatment had poor agreement (NSE of -0.23 and -0.91).

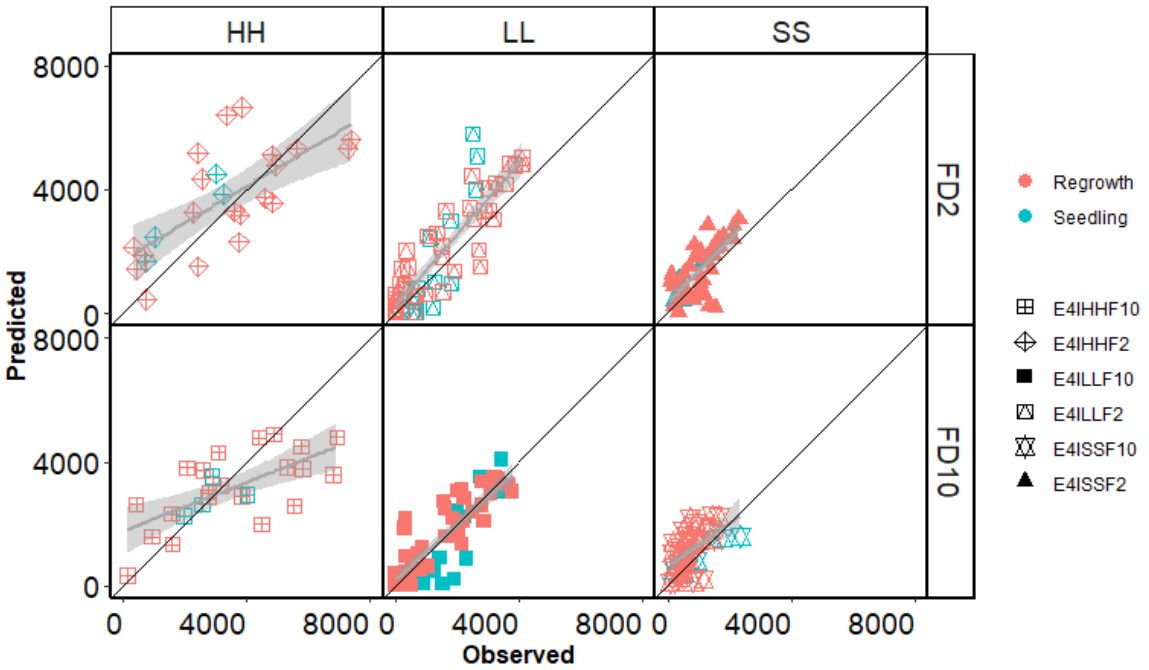

Figure 6.17. Predicted and observed shoot biomass from field Experiment 4 with three defoliation treatments [HH (84 day), LL (42 day) and SS (28 day)] and two fall dormancy treatments (FD; FD2 and FD10) classes conducted in 2014-2019 at Iversen field, Lincoln University, Canterbury, New Zealand.

Table 6.9 Statistical measures of shoot biomass for field Experiment 4 with three defoliation treatments [HH (84 day), LL (42 day) and SS (28 day)] and two fall dormancy treatments (FD; FD2 and FD10) classes conducted within 2014 to 2019 at Iversen field, Lincoln University, Canterbury, New Zealand. n = number of simulated and observed data pairs; R^2= coefficient of determination; R_RMSE = relative root mean square error (%); NSE = Nash-Sutcliffe efficiency; SB = Standard bias; NU = Nonunity slope; LC = Lack of correlation.

Treatments	N	R^2	R_RMSE	NSE	SB	NU	LC
Total	249	0.68	58.1	0.63	6.7	5	88.2
Seedling	48	0.60	64.5	0.15	2.8	50.2	47
Regrowth	201	0.71	56.8	0.68	7.9	1.1	90.9
FD2	125	0.71	61.3	0.60	15.4	10.9	73.6
FD10	124	0.68	54.5	0.67	1.1	0	98.9
HH	50	0.47	43	0.47	0	0.3	99.7
LL	112	0.72	58	0.54	9.8	29	61.2
SS	87	0.46	77.2	-0.40	30.2	31.1	38.7
E4IHHF2	25	0.54	44.1	0.52	4.7	0.4	94.9
E4IHHF10	25	0.43	41.9	0.4	4.8	0.5	94.6
E4ILLF2	56	0.76	69.1	0.42	23.6	35	41.4
E4ILLF10	56	0.72	45.4	0.68	0.6	12.3	87.1
E4ISSF2	44	0.54	68.1	-0.23	27	35.6	37.5
E4ISSF10	43	0.30	89.8	-0.91	33.8	29.4	36.8

Overall, predicted and observed root biomass values from the same treatment had good agreement, with an NSE of 0.6 and R_RMSE of 32.3%. However, the FD2 class had a closer overall prediction compared with FD10 (NSE was 0.22 and 0.10). Seedling crops had closer agreement than regrowth crops, with NSE values of 0.61 and 0.54 (Figure 6.18 and Table 6.10).

All three defoliation treatments (HH, LL, and SS) had fair to good agreement between observed and predicted root biomass. R_RMSE values ranged from 25.4 to 34.5%, NSE values ranged from 0.03 to 0.59.

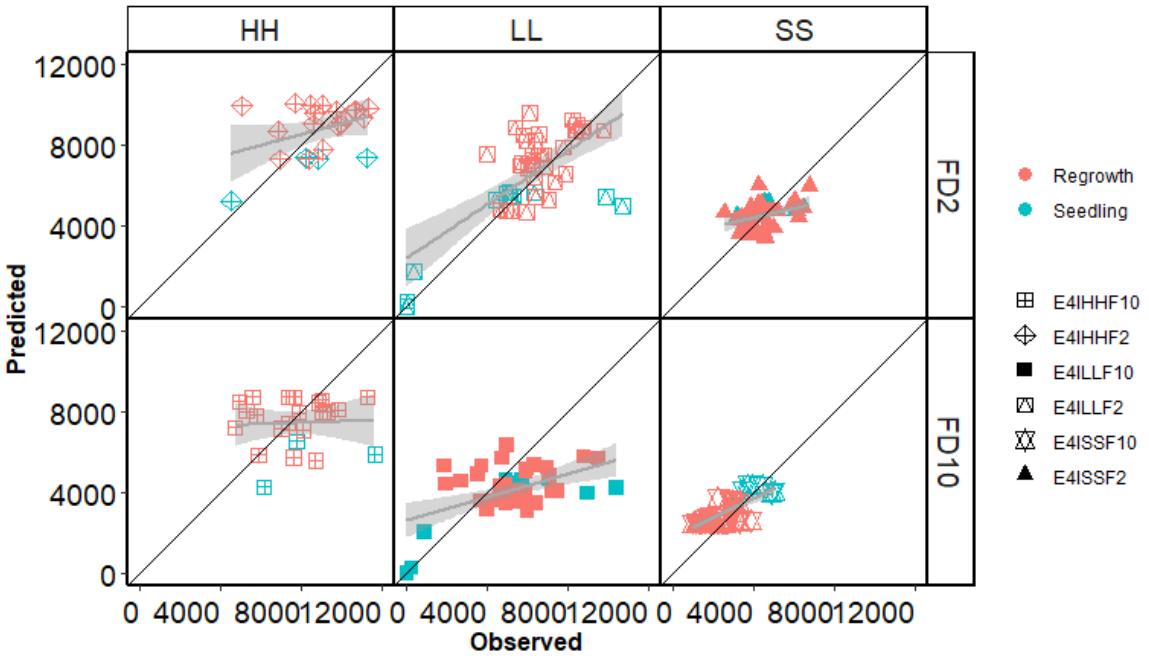

Figure 6.18. Predicted and observed root biomass from field Experiment 4 with three defoliation treatments [HH (84 day), LL (42 day) and SS (28 day)] and two fall dormancy (FD; FD2 and FD10) classes conducted in 2014-2019 at Iversen field, Lincoln University, Canterbury, New Zealand.

Table 6.10 Statistical measures of root biomass for field Experiment 4 with three defoliation treatments [HH (84 day), LL (42 day) and SS (28 day)] and two fall dormancy (FD; FD2 and FD10) classes conducted within 2014 to 2019 at Iversen field, Lincoln University, Canterbury, New Zealand. n = number of simulated and observed data pairs; R^2= coefficient of determination; R_RMSE = relative root mean square error (%); NSE = Nash-Sutcliffe efficiency; SB = Standard bias; NU = Nonunity slope; LC = Lack of correlation.

Treatments	N	R^2	R_RMSE	NSE	SB	NU	LC
Total	225	0.61	32.3	0.6	1.2	0.2	98.6
Seedling	42	0.58	42.9	0.43	19.6	6.4	74
Regrowth	183	0.65	29.4	0.65	0	0.4	99.6
FD2	113	0.61	27.3	0.61	0	0.2	99.7
FD10	112	0.56	38.8	0.54	4.2	0.2	95.6
HH	50	0.13	28.4	0.03	7	4.1	88.9
LL	88	0.36	34.5	0.22	3.5	14.8	81.7
SS	87	0.63	25.4	0.59	7.4	2.1	90.5
E4IHHF2	25	0.20	26.1	0.12	8.5	0	91.5
E4IHHF10	25	0.00	31.3	-0.39	5.7	22.5	71.8
E4ILLF2	44	0.47	28.4	0.36	4.2	12.7	83
E4ILLF10	44	0.27	41.3	0.01	25.9	0.2	73.9
E4ISSF2	44	0.14	21.2	0.08	0	6.1	93.9
E4ISSF10	43	0.53	32.8	0.29	32.9	0.9	66.2

6.4 Discussion

Objective 3 of this thesis was to quantify and test the accuracy of RUE_{total} and DM partitioning (DM demand from each organ) modules in the APSIM NextGen lucerne model. The idea of modelling shoot (leaf and stem) and root was to simulate the remobilization and partitioning of carbon among all organs in response to environmental signals and defoliation frequencies (Teixeira et al., 2008). The relationships derived from the FD5 genotype grown under the LL defoliation treatment were successfully integrated into the model. This included simulation of shoot (leaf and stem) and root biomass. Those relationships were further tested by using datasets from FD2 and FD10 classes grown under different defoliation treatments, to determine whether either FD class or defoliation regime impacted on lucerne shoot and root yield.

6.4.1 **RUE**

There were strong linear relationships between total dry matter and accumulated total radiation interception in each regrowth cycle (Figure 6.1). The slope of these linear regressions is the RUE_{total}. Similar findings were reported in previous experiments for both seedling (Brown et al., 2006; Jáuregui et al., 2019) and regrowth (Teixeira et al., 2008) crops in Canterbury, New Zealand. In contrast, Thiébeau et al. (2011) fitted a Gompertz function between total dry matter and accumulated total radiation due to leaf clumping at the early stages. However, radiation interception was not measured in the early regrowth stage in our experiments, therefore, a linear regression function was used, and this may lead to overestimation of radiation interception in early regrowth stage. This remains an area for further field measurements to clarify.

A linear relationship was found between calculated RUE_{total} and mean air temperature (R^2=0.60; Figure 6.2). This result was consistent with Brown et al. (2006), who reported a significant linear relationship between RUE_{total} and temperature, with the maximum RUE_{total} of 1.60 g DM MJ^{-1} total radiation at 18 ˚C. This value was also tested by Teixeira et al. (2008), with a weaker relationship, and Ta (2018) under a LL defoliation treatment in Canterbury, NZ. Furthermore, field studies have demonstrated temperate lucerne cultivars have an assimilation rate of 19 µmol CO_2 m^{-2} s^{-1} at 15 ˚C and 21 µmol CO_2 m^{-2} s^{-1} 30 ˚C (Zaka et al., 2016). In contrast, Thiébeau et al. (2011) reported a constant RUE_{total} value of 1.14 and 1.42 g DM MJ^{-1} from spring and autumn sowing, which had no clear relationship with mean air temperature. Authors attributed that to remobilization in early regrowth and leaf senescence in autumn.

In this study, the RUE_{total} value was 1.1 g DM MJ^{-1} total radiation at 18 ˚C, lower than that previously reported (Brown et al., 2006; Teixeira et al., 2008; Thiébeau et al., 2011). Figure 6.2 shows variation around the regression line which suggests RUE_{total} was not constant across experiments (R^2=0.61). This indicates some of the experiments were operating at suboptimal conditions. Indeed Experiment 4 experienced summer water stress, despite efforts to fully irrigated the crops (Ta, 2018). Lower RUE_{total} value used in the current model might result in underestimation of total biomass for non-water stress conditions. An estimate of the maximum RUE_{total} value can be gain by fitting the regression through the

upper bound in Figure 6.2 which would suggest a RUE_{total} of 1.52 at 18 ˚C is possible in this environment.

For perennial crops such as lucerne, the concept of RUE_{total} (Brown et al., 2006) was developed due to changes in the proportion of total biomass that partitions to shoot and roots (taproot and crown). Specifically, seasonal variations in potential shoot production of lucerne were not determined by changes in RUE_{total}, but by the annual pattern of assimilate partitioning between roots and shoots (Khaiti and Lemaire, 1992). Therefore, the APSIM NextGen lucerne model used RUE_{total} to calculate biomass supply from the photosynthesis process and total biomass was then allocated to each organ based on its demands.

The seedling crops had the same values of RUE_{total}. This suggests that seedling crops had the same total radiation use efficiency as regrowth crops. Sim (2014) and Jáuregui et al. (2019) reported similar RUE_{total} values of seedling crops. In contrast, Thiébeau et al. (2011) indicated that seedling crops had different RUE_{total} values dependent on sowing dates (early spring and summer compared with autumn). This suggests that the seasonal difference in RUE_{total} of seedling crop could be due to a temperature effect.

The APSIM NextGen lucerne model parameterized RUE_{total} as a linear regression between RUE_{total} and mean air temperature. However, there are two different modelling approaches used in other lucerne models. The first method uses RUE_{shoot} values to calculate shoot biomass supply but excludes root biomass. For example, the APSIM classic model (Robertson et al., 2002) uses two different RUE_{shoot} values, 1.1 g DM MJ^{-1} for regrowth crops and 0.60 g DM MJ^{-1} for seedling and winter regrowth crops (Table 6.1). A RUE_{shoot} value of 1.5 g DM MJ^{-1} was reported in the CropSyst model (Confalonieri and Bechini, 2004). However, the Integrated Farm System Model (IFSM) (Jego et al., 2015) uses a RUE_{shoot} value of 2 g DM MJ^{-1}. This modelling method ignores the impact of the perennial organ on regrowth, which is the biggest difference between annual and perennial crops. The second approach uses RUE_{total} to calculate the total biomass supply. For example, different RUE_{total} values for different development phases are used in the STICS model (Strullu et al., 2020), 0.65 g DM MJ^{-1} for the juvenile phase, 1.45 g DM MJ^{-1} for the vegetative and reproductive phases. This approach takes account of perennial organ effects on shoot regrowth, but

ignores RUE_{total} as net assimilation which reduces at lower temperature in perennial crops (Brown et al., 2006).

6.4.2 Leaf biomass demand

A strong power relationship was found between leaf biomass (g m^{-2}) and LAI (m^2 m^{-2}) for seedling and regrowth crops (Figure 6.3). This means that leaf biomass increases as leaf area expands. The parameters of the allometric relationship were similar to the literature reported by Lemaire et al. (1992). Therefore, leaf biomass demand was parameterized as an allometric relationship with LAI in the APSIM NextGen lucerne model. Other lucerne models use different approaches. For example, specific leaf weight (SLW) has been used to predict leaf biomass demand (Confalonieri and Bechini, 2004; Malik et al., 2018). However, SLW differs with development stage, season and growth conditions (Hanson et al., 1988; Lemaire et al., 1992; Moot et al., 2015). This is consistent with the variation of the relationship between LAI and leaf biomass, which is the variation in SLW (Figure 6.3). The allometric approach of leaf biomass demand was parameterized as leaf biomass requirement for a given LAI. It may take several days for leaf biomass to reach the value demanded by the LAI. In contrast, the SLW approach uses a daily SLW value to calculate leaf biomass demand, therefore errors can accumulate in this process.

6.4.3 Stem biomass demand

Stem biomass demand were parameterized as a positive power relationship between shoot and stem biomass (Figure 6.4). This implies that lucerne crops invest a greater proportion of structural tissues as plants grow taller to maintain an erect stature (Ta et al., 2020). Considering that stem is the main component of above-ground biomass, it is important to simulate stem growth to maximize forage quality (Lemaire et al., 1992). However, some lucerne models do not separate shoots into stems and leaves (Confalonieri and Bechini, 2004; Malik et al., 2018). The STICS model uses a stem:leaf ratio of 1.5 to predict stem biomass (Strullu et al., 2020). However, stem: leaf ratio was not a constant value, the stem proportion increases as shoot biomass increases (Lemaire et al., 1992; Ta et al., 2020). Thus, the APSIM NextGen lucerne model separates leaf and stem biomass which enables it to simulate forage quality and this is discussed in Chapter 8.

6.4.4 **Root biomass demand**

Root biomass showed a clear seasonal pattern (Figure 6.5 and 6.6) (Ta et al., 2020; Teixeira et al., 2007c). It decreased from spring to mid- summer and then increased to late autumn due to changes in partitioning to roots that occurred in the decreasing Pp. This phenomenon was also found in different FD genotypes grown independently of defoliation regimes (Ta, 2018). Luo et al. (1995) reported a seasonal pattern of root biomass, with peaks in spring and autumn separated by the summer period of low root biomass. In Spain, Malik et al. (2018) reported a similar seasonal pattern for lucerne perennial biomass. This is consistent with the previous literature (Brown et al., 2006; Teixeira et al., 2008; Thiébeau et al., 2011), that found the partitioning percentage to roots was higher in a decreasing Pp. Moreover, Cunningham and Volenec (1998) investigated that sugar, protein, low molecular weight-N, and vegetative storage protein (VSP) levels of roots all declined in spring due to remobilization from root to shoots, but increased in roots in autumn regardless of cultivar. This change in partitioning priority is consistent with the observed longer phyllochron (Section 4.3.3.2) and slower LAER (Section 5.3.2.2) in a decreasing Pp. At this stage, it is apparent that the processes are linked but difficult to determine which is the cause and which is the effect.

A strong linear relationship was found between the amount of root biomass lost in the winter and initial root biomass at the beginning of winter. This indicates that there was a large amount of root maintenance respiration loss in the winter and that larger root biomass has a higher maintenance respiration cost. The decrease in root biomass confirmed the idea that root biomass was respired throughout winter (Teixeira et al., 2007c) and partially remobilized to shoots in early-spring (Avice et al., 1996). The x-intercept value of the linear regression between calculated root respiration and initial root biomass (Figure 6.7) indicates the root biomass at which there is zero respiration loss. This was defined as structural root biomass (~2500 kg ha^{-1}). Lucerne roots can be conceptually divided into structural (e.g. cellulose and protein associated with cell walls) and storage (e.g. starch, sugar, and soluble proteins) components (Teixeira et al., 2009). The separation of perennial organs into structural and storage components provides a more mechanistic framework for modelling root biomass dynamics where the storage component represents the dynamic fraction. This is because structural and storage components can more realistically

represent source and sink relationships and mobilization among organs (Cannell and Thornley, 2000). This aspect is more important for analysing perennial than annual crops which, by definition, do not exhibit this strong seasonality in root dynamics.

To explain root biomass decreases in increasing Pp (spring) and increases in decreasing Pp (autumn), different RUE_{shoot} values were tested external of APSIM NextGen by comparing predicted and observed values for shoot biomass. In increasing Pp, the best fit for the RUE_{shoot} function was similar to RUE_{total} (Figure 6.8). This suggests that little carbon assimilate was transported from above-ground to below-ground during this period. The decrease of root biomass during this period was due to remobilization and respiration. This confirms that shoot growth and leaf expansion were the priority for lucerne crop growth in spring (Teixeira et al., 2008). To simulate this in the APSIM NextGen lucerne model, a remobilization coefficient value of 0.05 (5% of storage root biomass per day) was selected for calculations in increasing Pp, with no storage root demand in increasing Pp conditions.

However, the RUE_{shoot} value in decreasing Pp differed to the RUE_{total} function (Figure 6.9). RUE_{shoot} values were lower than RUE_{total} at the same temperature. This indicates that the increasing root biomass in a decreasing Pp was caused by carbon partitioning in autumn (Brown et al., 2006; Khaiti and Lemaire, 1992; Teixeira et al., 2008), which explains difference in growth rates observed (Moot et al., 2003). To accommodate this, the model was parameterized to have a maximal root demand in a decreasing Pp.

Root maintenance respiration, also needed to be considered as a cause of a decrease in root biomass in increasing Pp and winter loss. A root maintenance respiration coefficient (Rm_root_day) was determined by a model optimization exercise and was set as a constant value of 0.0005 g g^{-1}.day^{-1}. This value is in the range of the plant maintenance respiration values reported by Cannell and Thornley (2000). They reported that plant maintenance respiration ranged from 10^{-6} to 0.05 g g^{-1}.day^{-1} based on the plant tissues age and growth conditions. In contrast, Teixeira et al. (2009) tested a range of Rm_root_day values to fit root biomass. Values changed across the season, ranging from less than 0.005 to 0.035 g g^{-1}.day^{-1}. In that case, both root biomass remobilization and root respiration losses were aggregated into a root respiration coefficient, which explains the higher values of Rm_root_day. Their assumption was that decreasing root biomass was due to increasing respiration to remobilize N in spring (Avice et al., 1997a). However, it is difficult to translate

this seasonal variable as a parameter or to develop model algorithms within PMF from this approach.

6.4.5 Model simulation

Parameters and functions for leaf, stem, and root were implemented into the APSIM NextGen lucerne model. Predictions of shoot biomass in each regrowth cycle showed good overall agreement. Under-estimation occurred in treatment E2ILLS4 (Figure 6.13). This was because the model under-estimated LAI and canopy expansion (Section 5.3.2.3), and those biases affected the shoot biomass prediction.

For root biomass simulation, the model captured root remobilization in spring and partitioning in autumn. However, there was fair agreement between predicted and observed root biomass. This may be because root biomass decreases resulted from N remobilization in the early regrowth (Teixeira et al., 2009). This hypothesis is further investigated in Chapter 7. High variation in measured root data from Experiments 3 and 4 might be another reason for the fair prediction of root biomass.

The APSIM NextGen lucerne model implements perennial crop physiology, and models leaf, stem and perennial organs (root in APSIM NextGen model) separately. To our knowledge, this is the first attempt to simulate lucerne perennial biomass remobilization and partitioning with seasonal signal changes. This contrasts most lucerne models that only simulate leaf and stem biomass, and use different approaches to deal with biomass remobilization and partitioning. For example, the APSIM classic lucerne model only simulates leaf and stem biomass (Robertson et al., 2002). Equally, the calibrated APSIM lucerne model (Moot et al., 2015) used an empirical function of root turnover rates, which increased with increasing Pp to represent the seasonal pattern of root biomass. However, biomass remobilized from perennial reserves to shoots was not considered, and the robustness of the empirical taproot turnover relationships needs to be tested in different environments. The CropSyst model (Confalonieri and Bechini, 2004) uses SLA to calculate leaf biomass, and a constant leaf: stem ratio to calculate stem biomass. Furthermore, accumulation of carbohydrates in perennial organs (taproot and crown) is not included in CropSyst, and therefore remobilization and partitioning cannot affect crop growth rates after defoliation. The CSM-CROPGRO perennial forage model (Jing et al., 2020; Malik et al., 2018) simulates leaf, stem and root, with different partitioning fraction values to each

organ based on development stages. However, these partitioning fraction values were adopted from the partitioning of brachiaria (*Urochloa brizantha*), due to the lack of observed leaf, stem, and root fraction experimental data from lucerne. The STICS model (Strullu et al., 2020) simulates leaf, stem, and root. However, a temporary pool is used to balance the deficit and surplus of C and N. This system resulted in promising predictions of shoot and root biomass and N concentration. However, a temporary pool is not biologically reasonable in plants without showing where that biomass is. Our approach of modelling organ demand and biomass mobilization among each organ with a seasonal response, offers a more biologically realistic method to quantify lucerne root dynamics.

6.4.6 Defoliation effect

To test the null hypothesis that remobilization remains constant throughout the regrowth period. A regrowth coefficient function included two parameters (remobilization duration and remobilization rate) to compare observed and predicted shoot and root biomass. A remobilization duration value of 300-350 ˚Cd resulted in the best fit for root biomass under all defoliation treatments (Figure 6.15). This indicates that remobilization occurred within the first 300-350 ˚Cd in each regrowth cycle (remobilization rate being 1.5 from 0 to 300 ˚Cd; decreasing to 0 at 350 ˚Cd), and realistically represents the biological processes of remobilization in the regrowth cycle (Avice et al., 1996).

In a decreasing Pp, storage roots had little remobilization (value of 0 was used), but maximal demand (value of 1 was used). This is consistent with the literature reported by Ta et al. (1990), who found 12% of root C and 25% of root N were remobilized to support shoot regrowth in the first two weeks. Similar results were reported by Avice et al. (1996), who found root C lost in early regrowth periods was mainly due to root and stubble respiration, and 66% of shoot N was derived from root storage compounds after 10 days of regrowth. Luo et al. (1995) reported a general pattern of root biomass dynamic within a regrowth cycle. Root biomass decreases after defoliation and increaseS later in the cycle. Teixeira et al. (2009) proposed an explanation that the remobilization process involves degradation of soluble proteins and transport of amino acids to shoots, which may require an increase in respiration to provide energy. Therefore, the remobilization function in this study represents both C relocation from root to shoot and respiration cost of this process. The N component of remobilization is further investigated in Chapter 7.

There was good agreement between predicted and observed values under the HH and LL defoliation treatments. However, parameters and functions generated from the LL defoliation treatment did not adequately predict results of the 28 day defoliation treatment (SS). This is because frequent defoliation treatment (28 day) depleted perennial organ reserve of C and N (Teixeira et al., 2008; Teixeira et al., 2007c). Lucerne shoot production was mainly affected by the initial taproot C/N reserve levels (Meuriot et al., 2005). The difference of predicting shoot and root biomass among different defoliation regimes indicates that lucerne shoot and root growth rates were affected by defoliation treatments. Causes of this are further investigated in Chapter 7.

6.4.7 **FD effect**

Different FD classes had different growth potentials. Non-dormant cultivars have a higher growth rate in the autumn, earlier regrowth in spring, and more rapid regrowth after defoliation (Brummer et al., 2002; Rimi et al., 2014). Thus, a separate set of parameters for FD classes was needed to improve model simulation results.

As expected, a model optimization exercise showed that the FD2 had the shortest remobilization duration (250-300 ˚Cd) within each regrowth cycle, whereas FD10 had the longest remobilization duration (500-550 ˚Cd). This is consistent with understanding that dormant (FD2) cultivars have a higher partitioning of biomass to roots than non-dormant (FD10) cultivars (Cunningham et al., 1998).

Both genotypes of FD2 and FD10 under the SS defoliation treatment had poor agreement between observed and predicted shoot biomass (NSE of -0.23 and -0.91). This could be explained by severe plant population decline under the SS treatment for the FD10 class (Ta, 2018), which is currently not accounted for in the model. The current model did not capture root biomass dynamics under the SS defoliation treatment within each regrowth cycle. This is further investigated in Chapter 7.

Overall, the APSIM NextGen lucerne model uses radiation interception and RUE_{total} to calculate total dry matter supply. The biomass is then allocated based on leaf, stem and root demand. Remobilization and partitioning processes occur within each organ regulated by seasonal signals. Nevertheless, the reason for poor agreement between observed and predicted root biomass under the SS defoliation treatment deserves further investigation.

The hypothesis is that the decrease of root biomass resulted from N remobilization during the early regrowth. The seasonal pattern of N concentration in leaf, stem and root and N remobilization and partitioning are assessed in Chapter 7.

6.5 Conclusions

The results of this chapter lead to the following conclusions:

- RUE_{total} was used to calculate total biomass supply in the APSIM NextGen lucerne model. Total biomass was then allocated to leaf, stem and root organs based on their dry matter demand.

- Leaf demand was parameterized as an allometric relationship with LAI, whereas stem demand was parameterized as an allometric relationship with shoot biomass.

- Root biomass showed a seasonal pattern: it decreased in spring due to remobilization, and increased in autumn due to partitioning. Structural root biomass was about 2500 kg ha^{-1}. The root respiration coefficient (Rm_root_day) was set to a constant value of 0.0005 g $g^{-1}.day^{-1}$.

- For the FD5, in increasing Pp, there was little storage root demand but 5% of storage root biomass was remobilized from root to shoot per day (a remobilization coefficient of 0.05). Within each regrowth cycle, remobilization occurred within the first 300-350 ˚Cd in each regrowth cycle (remobilization rate being 1.5 from 0 to 300 ˚Cd; decreasing to 0 at 350 ˚Cd). In decreasing Pp, storage roots exhibited little remobilization but maximal demand.

- FD2 and FD10 had the same biomass remobilization coefficient value (1.5% of storage root biomass per day). However, FD2 had a shorter remobilization duration (250-300 ˚Cd), and FD10 had a longer remobilization duration (500-550 ˚Cd).

- Parameters and functions generated from the LL defoliation treatment for FD2, FD5 and FD10 did not cope with the extreme short defoliation treatment (SS). This was possibly due to lower perennial organ reserve levels from the SS defoliation treatment. This will be further investigated in Chapter7.

7 MODELLING NITROGEN DYNAMICS

7.1 Introduction

The Plant Modelling Framework (PMF) contains two main components, dry matter (DM) and nitrogen (N) mass. These two components are not independent because DM includes N mass, and it is common to treat all mass as a single component (Brown et al., 2014). However, in this research, Chapter 6 quantified DM supply and demand for each organ under different defoliation treatments. The assumption was that all crops in each treatment had sufficient N supply. This resulted in an overestimation of canopy expansion (Chapter 5) and biomass accumulation in the SS (28 day) defoliation treatment (Chapter 6). The hypothesis is that frequent defoliations limited root biomass accumulation and the availability of N for remobilization to shoots during early regrowth, which lead to slower canopy expansion (Teixeira et al., 2007c). This chapter focuses on N dynamics within each organ to improve the prediction of canopy expansion and biomass accumulation in the SS defoliation treatment.

There are two research questions to be answered: 1) can the N dynamics of each organ be accurately simulated and predicted for crops grown under different defoliation and fall dormancy (FD) classes? and 2) can the simulation of N dynamics of each organ improve biomass prediction in the SS treatment? To answer these questions, it is necessary to assess whether the functions and algorithms of N dynamics generated from different defoliation treatments can be adapted to accurately quantify seasonal responses for crops of different FD classes grown under different defoliation regimes. The underlying assumption is that the N limitation explains why biomass of crops grown under the SS treatment was overestimated by using parameters and functions generated from the LL treatment (42 day) in the APSIM NextGen lucerne model.

This chapter addresses Objective 4 of this thesis: to quantify and simulate N concentration and dynamics in seedling and regrowth crops using the PMF in APSIM NextGen lucerne model. Field measured data of leaf, stem, and root (crown and taproot) N concentration from multiple, long-term experiments (1, 3 and 4) conducted under different defoliation treatments were used to calculate functions and parameters in the PMF. The model was also used as a hypothesis testing tool to generate parameters which were not assessed in

the field experiments. These included: 1) N remobilization in early spring and after each defoliation; 2) partitioning in the autumn; and 3) total N supply (N fixation and N uptake from soil). After the model structure was built, it was tested with additional datasets (Experiments 3 and 4) from different defoliation treatments and FD classes. This chapter also includes fitting dry matter data from the all treatments after the N module was tested and verified.

7.2 Materials and Methods

This chapter focuses on defoliation and genotype effects on lucerne total N concentration in each organ. Observed variables include leaf, stem, and root (crown and taproot) total N concentration. The description of the experimental design, treatments and data collection were presented in Section 3.1. Statistical analyses and model evaluation were described in Section 3.2.4. Only additional measurement and calculation related to results of this chapter are reported.

7.2.1 Field experimental data

Simulation of lucerne leaf, stem, and root N concentration was based on Experiments 1, 3 and 4 described in Section 3.1.1. This includes datasets for model calibration and testing for three FD classes under different defoliation regimes described in Section 4.2.1 (Table 4.2). These data were also used to develop N dynamic mechanisms for each organ and to determine how N concentration affected the SS treatment in terms of canopy expansion and biomass accumulation.

7.2.2 Model structure

In the PMF, N supply is obtained from N fixation and N uptake of mineral N plus that reallocated from senesced tissues or from reserve remobilization, and allocated to each organ by the OrganArbitator (Brown et al., 2019). Allocation is based on the relative N demand of each organ, which includes structure, storage, and metabolic N form.

N concentration for each organ in the PMF is defined by three thresholds which simulate how N is partitioned in the plant: (1) the minimum N concentration (N_{min}) is N in structural tissues, thus the concentration of dead material; (2) the critical N concentration (N_{crit}) is the amount of N needed for plant functioning that does not limit growth; and (3) the maximum N concentration (N_{max}) is the upper limit for N storage. The N amount above N_{crit}

that represents “luxury uptake” and can be remobilized for plant growth. The N above N_{min} and below N_{crit} is made available only upon organ senescence. One of the key procedures in this chapter is to define N_{max}, N_{min}, and N_{crit} for leaf, stem and root, and simulate N concentration among each organ.

7.2.3 Model calibration and parameterization

7.2.3.1 Nitrogen supply

Nitrogen supply includes N uptake (Equation 21) from soil mineral N (NO_3^- and NH_4^+) through fine roots and biological N_2 fixation from nodules (Equation 22). However, detailed N_2 fixation was not measured in any of these experiments. Therefore, N_2 fixation was parameterized as a percentage of the photosynthesis rate to ensure sufficient N supply for lucerne growth.

Equation 21 $$NuptakeSupply = NO_3^- Supply + NH_4^+ Supply$$

Equation 22 $$FixationRate = MaxFixationRate \times [Leaf].Photosynthesis.Value$$

7.2.3.2 Leaf, stem and taproot N demand

The N demand of each organ (leaf, stem, and root N; g N g^{-1} DM^{-1} day^{-1}) was calculated based on DM demand of each organ and the N concentration of each biomass pool (structural, metabolic, and storage; as defined in Equations 23-25):

Equation 23 $$Structural = N_{min} \times PotentialStructuralDM$$

Equation 24 $$Metabolic = MetabolicNConc \times PotentialStructuralDM$$

Equation 25 $$MetabolicNConc = N_{crit} - N_{min}$$

where N_{min} is the minimum N concentration (%; g N g^{-1} DM^{-1}); PotentialStructuralDM is the potential structural dry matter (kg ha^{-1} day^{-1}), MetabolicNConc is the metabolic N concentration (%; g N g^{-1} DM^{-1}), and N_{crit} is the critical N concentration for growth (%; g N g^{-1} DM^{-1}).

The partitioning of daily growth to storage biomass brings the N content of each organ to the maximum concentration (Equations 26 and 27). The demand for storage N is further reduced by a factor specified by the [Leaf].NitrogenDemandSwitch (Brown et al., 2019).

Equation 26 $$StorageNDemand = PotentialStorageN - StorageN$$

Equation 27 $$PotentialStorageN = N_{max} \times (NonStorageDM + PotentialNonStorageDM)$$

where PotentialStorageN is the potential storage N and StorageN is the storage N.

7.2.3.3 Root nitrogen remobilization

Perennial N root reserves support shoot regrowth in spring and after defoliation (Avice et al., 1997b; Ta et al., 1990). Avice et al. (1996) reported that 52 to 87% of the shoot N was derived from source tissue storage compounds. This assumes that N is the driving factor for carbon (C) remobilization in early spring and each regrowth cycle. Therefore, regrowth coefficient values and functions for N are the same as for C remobilization (Sections 6.3.5.2 and 6.3.5.3), and data from different defoliation treatments (Experiments 3 and 4) were used for model fitting. However, root N remobilization was not measured in our experiments, thus a model optimization was used to determine the most accurate remobilization coefficient value (percentage of storage root N per day; % day^{-1}) by comparing predicted root N with observed values. Root N remobilization coefficient values (% day^{-1}) were tested from 0.01 to 0.05 at 0.005 intervals.

The N regrowth coefficient functions (N remobilization duration and N remobilization rate) were the same as those for biomass remobilization for two genotypes of FD classes. This indicates that N remobilization occurred within the first 250-300 ˚Cd for FD2 and 500-550 ˚Cd for FD10 in each regrowth cycle, N remobilization rate was 1.5 from 0 to 250 ˚Cd for FD2 and 0 to 500 ˚Cd for FD10; decreased to 0 at 300 ˚Cd for FD2 and 550 ˚Cd for FD10.

7.3 Results

7.3.1 **N supply**

Total N had a strong positive linear relationship with total (shoot and root) biomass (R^2=0.91) across all defoliation and FD treatments (Figure 7.1). Total N increased from 100 kg ha^{-1} at 5000 kg ha^{-1} of total biomass to 400 kg ha^{-1} at 20000 kg ha^{-1}. The slope of the linear regression shows that every kg of total lucerne biomass contained approximately 2.0% N. Therefore, to ensure there was sufficient N for lucerne growth, the N supply (including N uptake and N_2 fixation) in the PMF was parameterized as 2.5% of the photosynthesis rate, which is the slope of the upper threshold of the linear regression (Figure 7.1; black line) (Appendix 39 for model structure of N supply).

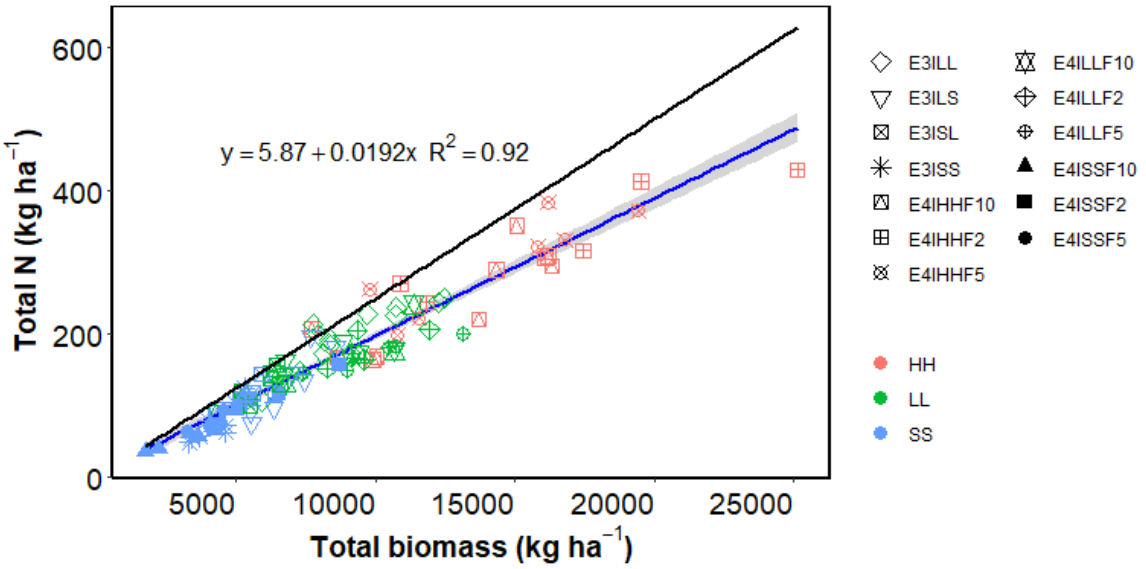

Figure 7.1. Total N (kg N ha^{-1}) against total DM (kg DM ha^{-1}) from Experiments 3 and 4 with multiple defoliation treatments [HH (84 day), LL (42 day), LS (42, 28 day), SL (28, 42 day), and SS (28 day)] and three fall dormancy (FD, FD2, FD5 and FD10) classes conducted from 2002-2019 at Iversen field, Lincoln University, Canterbury, New Zealand. Symbols represent experiment ID, and colors represent defoliation treatments. The line represent the upper threshold of the linear regression: y = 0.025x.

7.3.2 **Leaf N thresholds**

Leaf N concentration ranged from 3.6% to 6.8% (Figure 7.2). N concentration decreased as leaf biomass increased in both increasing and decreasing Pp conditions. In increasing Pp, the maximum leaf N concentration (N_{max}) was lower than in decreasing Pp, whereas the minimum leaf N (N_{min}) concentration was higher than in decreasing Pp. Therefore, the model used two separate functions for Leaf N concentration thresholds (Appendices 40 and 41 for model structure of leaf N). In increasing Pp, the N_{max} was defined as a negative linear function which decreased from 6.0% to 4% as leaf biomass increased from 10 to 3000 kg ha^{-1}. N_{min} decreased from 5.2% at 10 kg ha^{-1} of leaf biomass to 4% at 3000 kg ha^{-1}. In decreasing Pp, N_{max} was defined as a negative linear function which decreased from 6.8% to 4% as leaf biomass increased from 10 to 3000 kg ha^{-1}. N_{min} decreased from 6% at 10 kg ha^{-1} of leaf biomass to 4% at 3000 kg ha^{-1}. The critical N concentration (N_{crit}) defined the minimum N content for optimal photosynthesis.

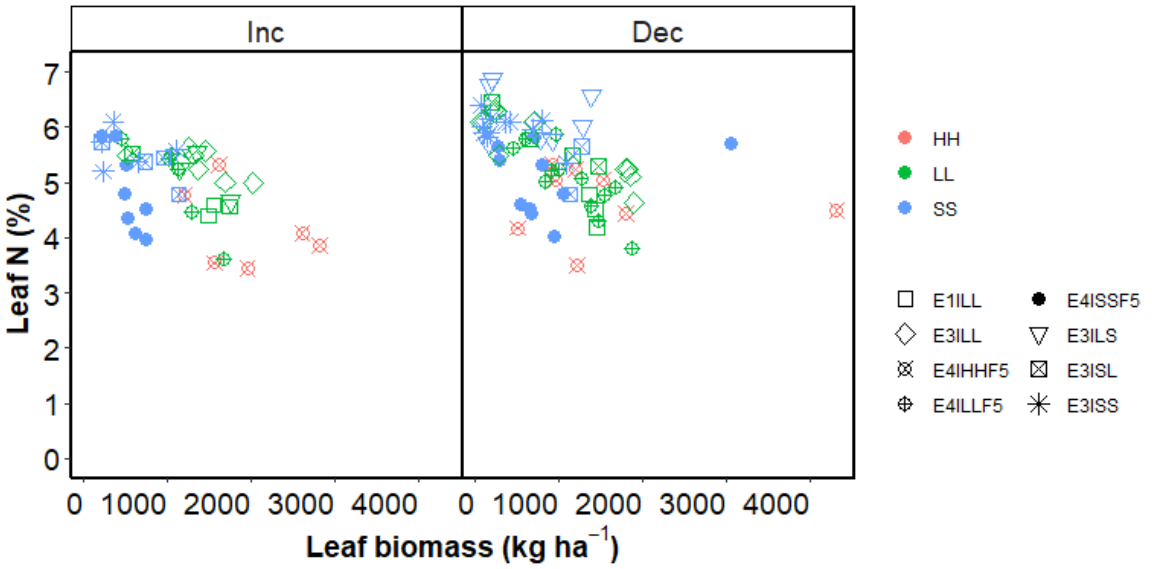

Figure 7.2. Leaf N (%) against leaf biomass (kg ha^{-1}) of Experiments 1, 3 and 4 with multiple defoliation treatments [HH (84 day), LL (42 day), LS (42, 28 day), SL (28, 42 day), and SS (28 day)] conducted from 1997 to 2019 at Iversen field, Lincoln University, Canterbury, New Zealand.

7.3.3 **Stem N thresholds**

The N thresholds for stem tissue ranged from 1.0% to 5.5% (Figure.7.3). Stem N concentration was associated with stem biomass. For example, stem N_{max} decreased from ~5.5% to 1.5% as stem biomass increased from 10 to 6000 kg ha^{-1}. N_{min} concentration had the same pattern as N_{max}, which was about 55% less than the N_{max} concentration at the same stem biomass. Thus, the APSIM NextGen lucerne model used two decreasing power functions to define N_{max} and N_{min} changes with biomass (Figure 7.3) (Appendices 42 and 43 for model structure of stem N). The N_{crit} value was assumed to be equal to the minimum value.

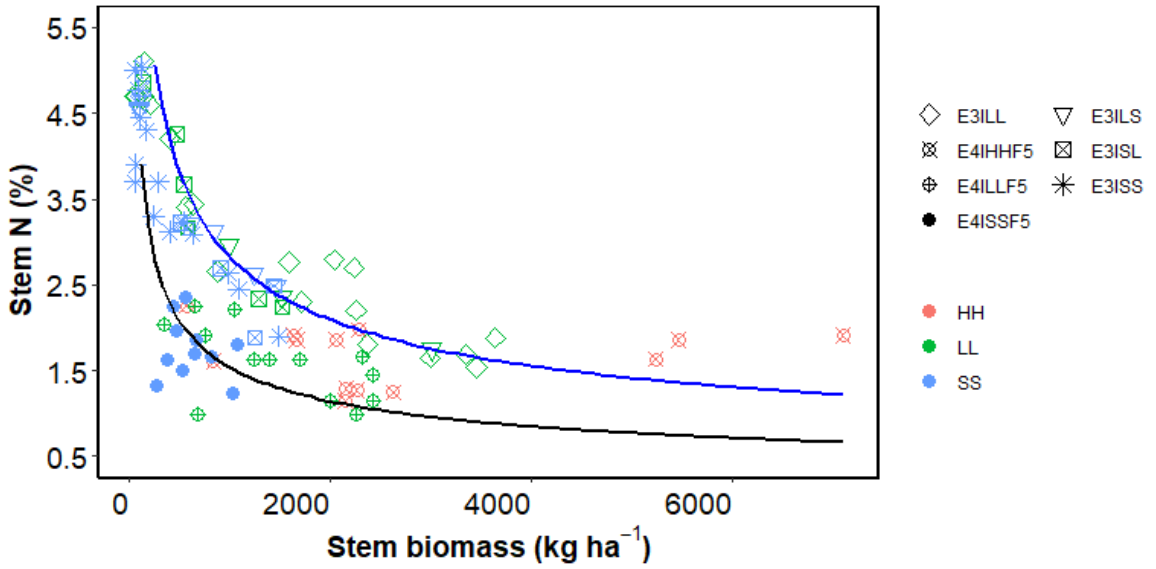

Figure 7.3. Stem N (%) against stem biomass from two Experiments 3 and 4 with multiple defoliation treatments [HH (84 day), LL (42 day), LS (42, 28 day), SL (28, 42 day), and SS (28 day)] conducted from 1997-2019 at Iversen field, Lincoln University, Canterbury, New Zealand. Maximum function (blue line): $y = 55x^{-0.43}$; and minimum function (black line): $y = 30x^{-0.43}$.

7.3.4 Root N thresholds and seasonal patterns

Root N concentration increased as root biomass increased (Figure 7.4). However, root N concentration was variable from different defoliation treatments. For example, the HH (84 day) treatments had the highest root N concentration (from 1.7% to 2.5%), whereas the SS (28 day) treatment had the lowest values (from 1.0% to 1.75%). Root N_{max} concentration ranged from 1.5% at 3000 kg ha^{-1} to 2.5% at 12000 kg ha^{-1}. Root N_{min} concentration was constant ~1.1% (Figure.7.4). N_{crit} value was assumed to be equal to the minimum value (Appendices 44 and 45 for model structure of root N).

There was a consistent seasonal pattern among the three defoliation treatments (Figure 7.5). Root N content decreased in increasing Pp (spring) and increased in decreasing Pp (autumn). For example, root N concentrations decreased from 2.5% (HH treatment) in early spring to 1.7% in early summer, then increased to 2.2% in late autumn. This annual pattern occurred in all four regrowth years across the three defoliation treatments.

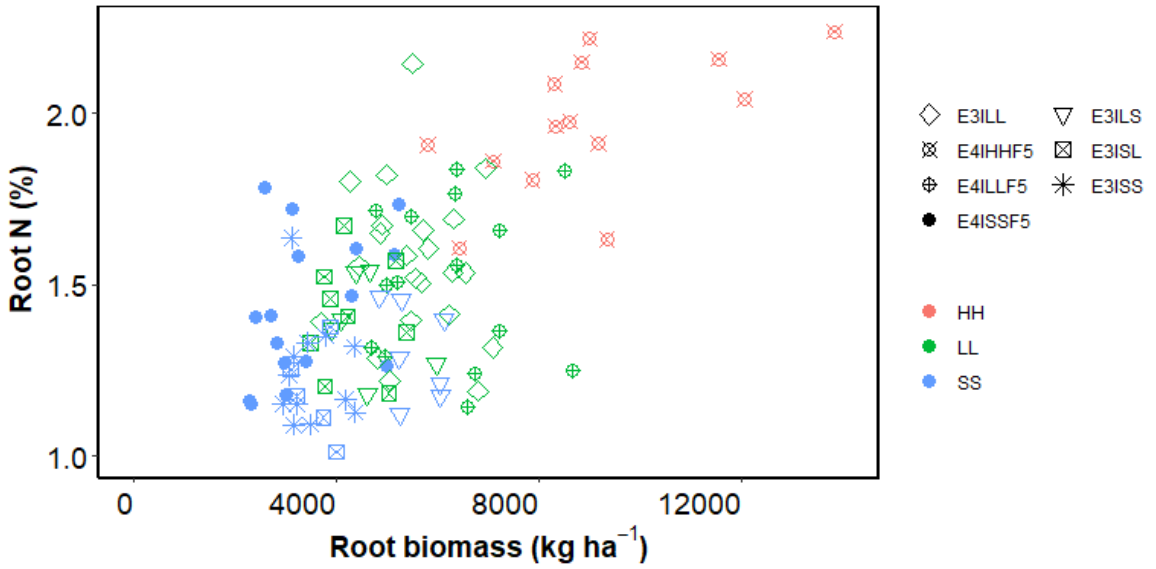

Figure 7.4. Root N (%) against root biomass (kg ha^{-1}) from Experiments 3 and 4 with multiple defoliation treatments [HH (84 day), LL (42 day), LS (42, 28 day), SL (28, 42 day), and SS (28 day)] conducted from 1997-2019 at Iversen field, Lincoln University, Canterbury, New Zealand.

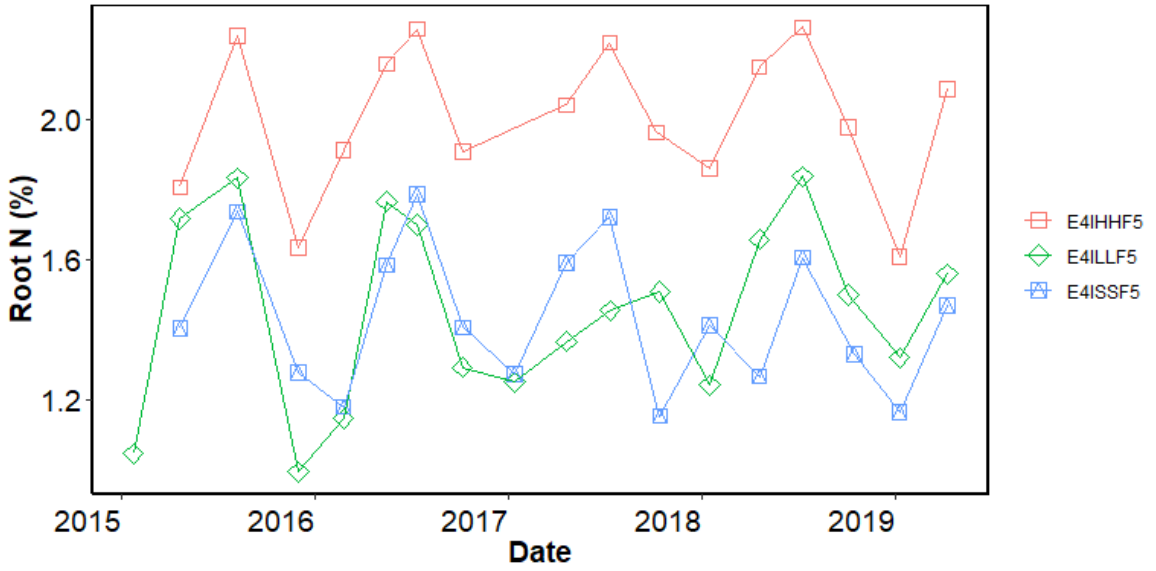

Figure 7.5. Root N (%) seasonal distribution from field experiment 4 with multiple defoliation treatments [HH (84 day), LL (42 day), and SS (28 day)] conducted from 2014-2019 at Iversen field, Lincoln University, Canterbury, New Zealand.

7.3.5 **Root N remobilization**

A range of N remobilization coefficient values were tested to fit observed root N concentration values from Experiments 3 and 4 conducted between 2002 and 2019. Statistical measures of N remobilization coefficient values for comparing predicted and observed values of root N concentration were calculated and are provided in Figure 7.6 and Table 7.1. N remobilization coefficient value = 0.02 (% of storage root N per day per

day) had the lowest R_RMSE value and the highest NSE value for root biomass prediction, 17.8% and 0.16, respectively (Table 7.1). Thus, an N remobilization coefficient value of 0.02 % day^{-1} was subsequently used for N remobilization calculations for periods of increasing Pp in the model.

The N regrowth coefficient function (N remobilization duration and N remobilization rate) was assumed to be the same as that found for biomass remobilization for FD5. This indicates that N remobilization occurred within the first 300-350 ˚Cd in each regrowth cycle (N remobilization rate being 1.5 from 0 to 300 ˚Cd; decreasing to 0 at 350 ˚Cd), (Appendix 46 for model structure of root N remobilization).

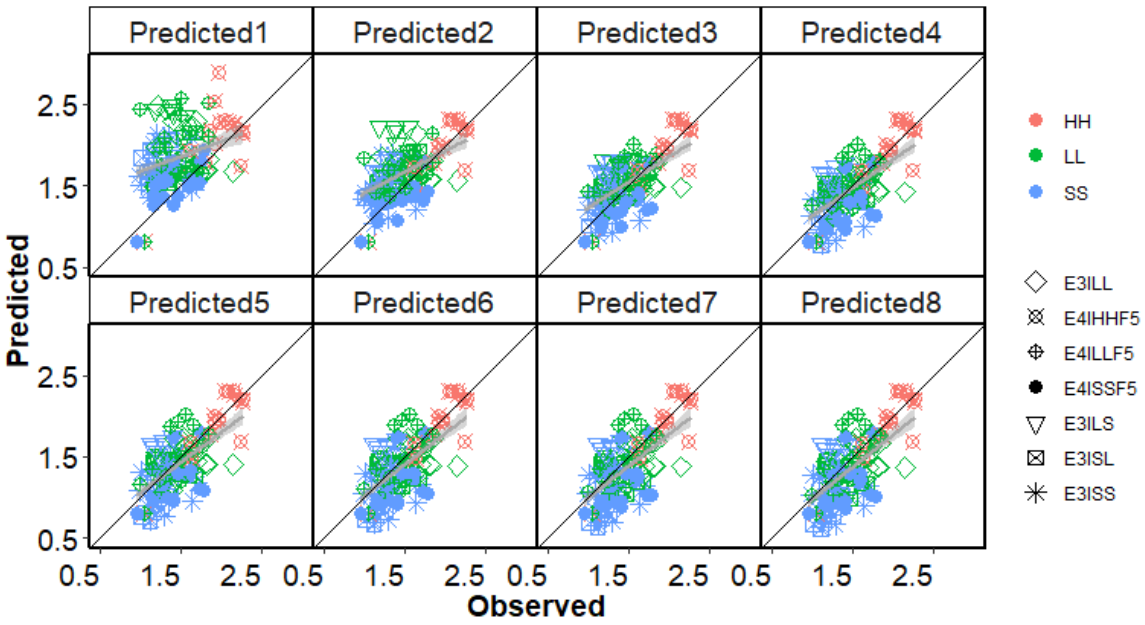

Figure 7.6. Predicted and observed root N concentration values (%) from Experiments 3 and 4 with multiple defoliation treatments [HH (84 day), LL (42 day), LS (42, 28 day), SL (28, 42 day), and SS (28 day)] conducted in 2002-2019 at Iversen field, Lincoln University, Canterbury, New Zealand. Predicted 1 to 8 represent root N remobilization coefficient values (% day^{-1}) from 0.01 to 0.05 at 0.005 intervals.

Table 7.1 Statistical measures of N remobilization coefficient values (%) for Experiments 3 and 4 with multiple defoliation treatments [HH (84 day), LL (42 day), LS (42, 28 day), SL (28, 42 day), and SS (28 day)] conducted between 2002 and 2019 at Iversen field, Lincoln University, Canterbury, New Zealand. N = number of simulated and observed data pairs; R^2= coefficient of determination; R_RMSE = relative root mean square error (%); NSE = Nash-Sutcliffe efficiency; SB = Standard bias; NU = Nonunity slope; LC = Lack of correlation. Predicted 1 to 8 represent root N remobilization coefficient values (% day^{-1}) from 0.01 to 0.05 at 0.005 intervals.

Prediction	N remobilization coefficient	N	R^2	R_RMSE	NSE	SB	NU	LC
Predicted1	0.005	209	0.10	37.1	-2.65	54.7	20.7	24.6
Predicted2	0.01	209	0.26	23.7	-0.49	32.6	17.6	49.8
Predicted3	0.015	209	0.38	17.9	0.15	6.4	20	73.6
Predicted4	0.02	209	0.40	17.8	0.16	0.2	27.6	72.2
Predicted5	0.025	209	0.40	18.8	0.06	4.2	31.6	64.2
Predicted6	0.03	209	0.39	20	-0.06	8.5	34.2	57.3
Predicted7	0.035	209	0.39	20.9	-0.16	11.7	35.5	52.8
Predicted8	0.04	209	0.38	21.6	-0.24	14.2	36.1	49.7

7.3.6 Nitrogen concentration simulation

Parameters and functions for leaf, stem, and root N were generated from previous results (Sections 7.3.1-7.3.5) and were implemented into the APSIM NextGen lucerne model. Overall, simulation results for predicting leaf and stem N in each regrowth cycle of Experiments 1, 3 and 4 (Figure 7.7 and Table 7.2) showed fair to good overall agreement; NSE values were 0.16 and 0.51, respectively. Prediction of root biomass had an NSE of 0.16 and R_RMSE value of 17.8%.

For leaf N simulation, regrowth crops grown under the LL treatments had fair agreement, with NSE of 0.16. However, poor agreement was found between predicted and observed values for crops grown under the HH (84 day) and SS (28 day) treatments; NSE values were -0.26 and -0.28, respectively.

For stem N simulation, there was good agreement between predicted and observed values for regrowth crops grown under the LL (42 day) treatment (R_RMSE = 22.4% and NSE=0.73). However, for the HH and SS treatments, simulation agreement were poor to fair between predicted and observed values, R_RMSE values were 35% to 30% and NSE values were -1.83 and 0.12.

For root N simulation, good agreement was found between predicted and observed values for crops in the HH treatment (R_RMSE = 9.5% and NSE=0.61). However, the LL and SS treatments showed poor agreement, R_RMSE values were 15.6% and 22.5% and NSE values were -0.14 and -1.32.

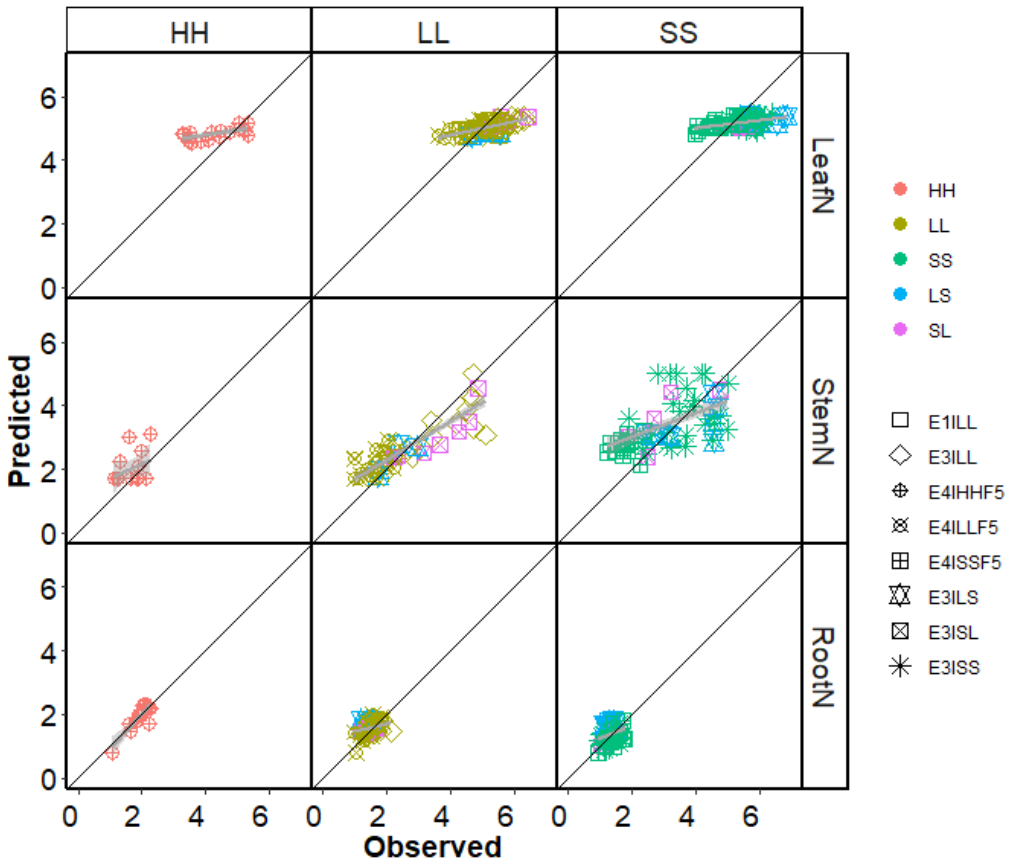

Figure 7.7. Predicted and observed leaf, stem and root N (%) from Experiments 1, 3 and 4 with multiple defoliation treatments [HH (84 day), LL (42 day), LS (42, 28 day), SL (28, 42 day), and SS (28 day)] conducted in 1997-2019 at Iversen field, Lincoln University, Canterbury, New Zealand.

Table 7.2 Statistical measures of leaf, stem, and root N values (%) for Experiment 1, 3 and 4 with multiple defoliation treatments [HH (84 day), LL (42 day), LS (42, 28 day), SL (28, 42 day), and SS (28 day)] conducted from 1997 to 2019 at Iversen field, Lincoln University, Canterbury, New Zealand. N = number of simulated and observed data pairs; R^2= coefficient of determination; R_RMSE = relative root mean square error (%); NSE = Nash-Sutcliffe efficiency; SB = Standard bias; NU = Nonunity slope; LC = Lack of correlation.

ID	Variable	N	R^2	R_RMSE	NSE	SB	NU	LC
Total	LeafN	224	0.43	11.5	0.16	16.8	15.2	68
	StemN	189	0.52	27.8	0.51	1.4	1	97.6
	RootN	209	0.40	17.8	0.16	0.2	27.6	72.2
HH	LeafN	16	0.39	19.1	-0.26	40.3	11.2	48.6
HH	StemN	15	0.11	35	-1.83	29.7	38.9	31.4
HH	RootN	17	0.76	9.5	0.61	0.9	38.2	61
LL	LeafN	101	0.41	10	0.16	18.8	10.8	70.4
LL	StemN	80	0.75	22.4	0.73	0.3	7.1	92.7
LL	RootN	102	0.13	15.6	-0.14	0	23.4	76.5
SS	LeafN	107	0.21	11.7	-0.28	35.4	3	61.6
SS	StemN	94	0.23	30	0.12	3.1	9.4	87.5
SS	RootN	90	0.09	22.5	-1.32	0.4	60.1	39.4

7.3.7 **Verification under FD treatments**

A range of N remobilization coefficient values were tested to fit with observed root N for FD2 and FD10 from Experiment 4 conducted from 2014 to 2019. Statistical measures of N remobilization coefficient values were tested and are provided in Appendices 47 (FD2) and 48 (FD10). Simulation results showed the most accurate N remobilization coefficient value for FD2 and FD10 was 0.005 (0.5% of storage root N per day).

Statistical measures of leaf N, stem N and root N for FD2 and FD10 were calculated and are provided in Figures 7.8 and 7.9 and in Tables 7.3 and 7.4. Overall, predicted and observed Leaf N values from Experiment 4 for two FD classes (FD2 and FD10) with multiple defoliation treatments (HH, LL, and SS) had fair to poor agreement, with NSE values ranged from 0.16 to -0.74, with most of the variation from the FD10 genotype under the HH and SS treatments (NSE=-0.74 and -0.09), (Figure 7.9 and Table 7.4).

Stem N treatment had poor agreement between predicted and observed values in both FD2 and FD10 (NSE=-0.91 and -4.61). Most of the variation was from the HH and SS treatments; NSE ranged from -1.31 to-20.51 (Figure 7.9 and Table 7.4).

For root N simulation in FD2 and FD10 genotypes, there was a fair overall agreement between predicted and observed values (NSE=0.16 and 0.29). This indicated that the model accurately estimated root N remobilization in spring and partitioning in autumn. Crops grown under the HH and LL treatments had closer prediction than crops grown under the SS treatment; NSE values ranged from -0.47 to -0.03.

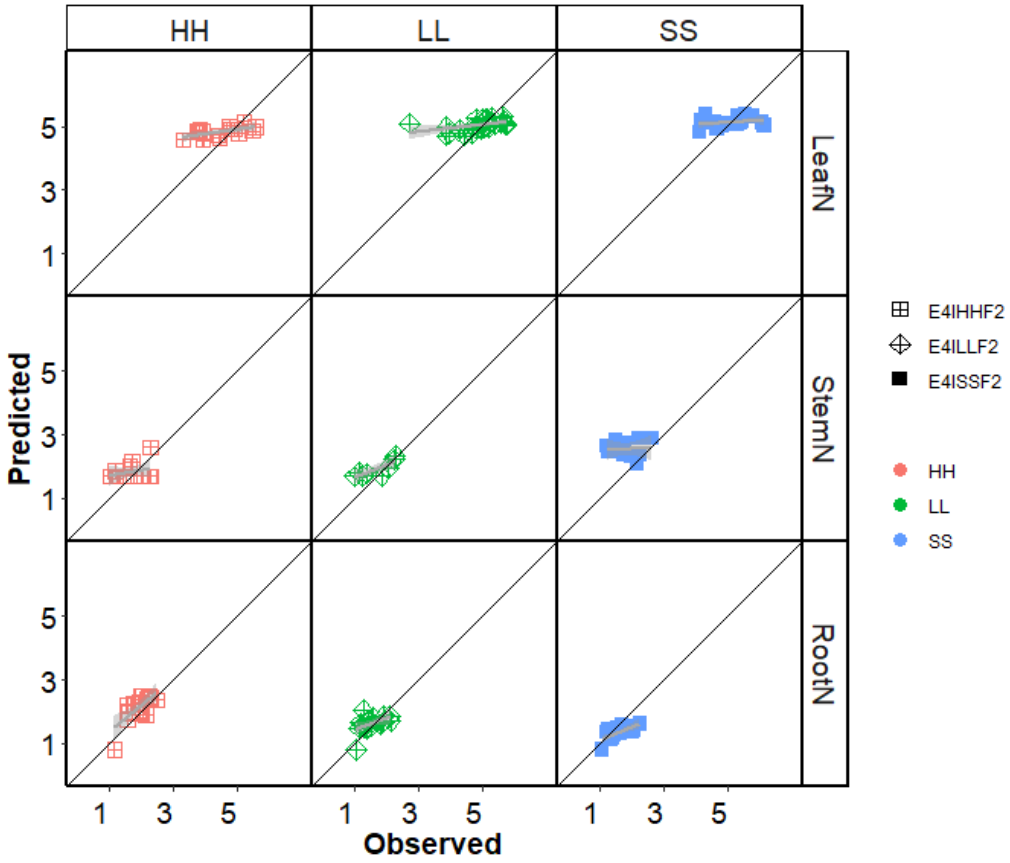

Figure 7.8. Predicted and observed values of leaf N, stem N and root N (%) from field Experiment 4 with a fall dormancy 2 (FD2) grown under three defoliation treatments [HH (84 day), LL (42 day), and SS (28 day)] conducted in 2014-2019 at Iversen field, Lincoln University, Canterbury, New Zealand.

Table 7.3 Statistical measures of leaf N, stem N and root N (%) for field Experiment 4 with a fall dormancy 2 (FD2) treatment grown under three defoliation treatments [HH (84 day), LL (42 day), and SS (28 day)] conducted from 2014 to 2019 at Iversen field, Lincoln University, Canterbury, New Zealand. N = number of simulated and observed data pairs; R^2= coefficient of determination; R_RMSE = relative root mean square error (%); NSE = Nash-Sutcliffe efficiency; SB = Standard bias; NU = Nonunity slope; LC = Lack of correlation.

ID	Variable	N	R^2	R_RMSE	NSE	SB	NU	LC
Total	LeafN	64	0.29	13.1	0.16	7.4	7.6	85
	StemN	33	0.11	35.1	-0.91	34.3	19	46.7
	RootN	54	0.44	20.3	0.16	0.6	33	66.5
E4IHHF2	LeafN	16	0.36	15.7	-0.07	28.4	12	59.5
	StemN	14	0.08	25.5	-0.14	8.5	10.5	81
	RootN	18	0.47	19	-0.27	37.2	21	41.8
E4ILLF2	LeafN	26	0.22	13.4	0.13	3.8	5.8	90.4
	StemN	8	0.65	25.7	0.23	41.2	13.4	45.4
	RootN	18	0.23	20.7	0.09	8.1	7.4	84.4
E4ISSF2	LeafN	22	0.06	10.8	0.04	2	0	98
	StemN	11	0.00	46.9	-3.02	68.3	6.9	24.8
	RootN	18	0.51	21.3	-0.03	50.7	1.6	47.7

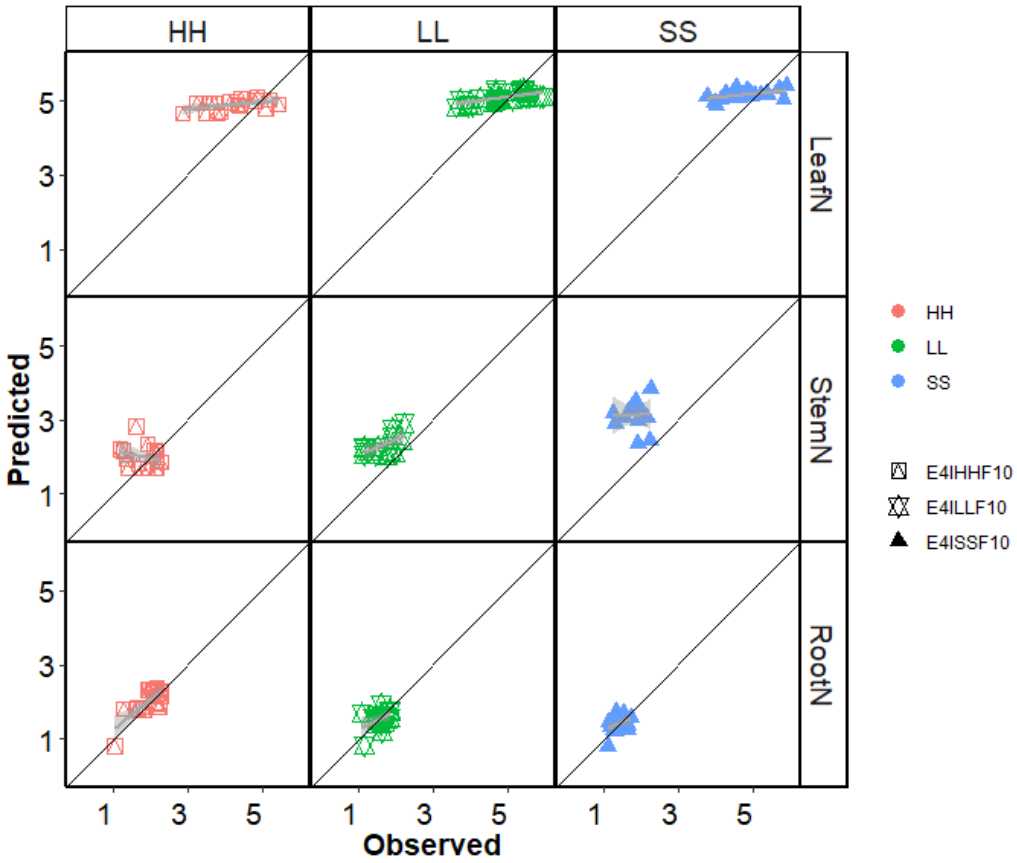

Figure 7.9. Predicted and observed values for leaf N, stem N and root N (%) from field Experiment 4 with fall dormancy 10 (FD10) grown under three defoliation treatments [HH (84 day), LL (42 day), and SS (28 day)] conducted in 2014-2019 at Iversen field, Lincoln University, Canterbury, New Zealand.

Table 7.4 Statistical measures of leaf N, stem N and root N (%) for field Experiment 4 with fall dormancy 10 (FD10) grown under three defoliation treatments [HH (84 day), LL (42 day), and SS (28 day)] conducted from 2014 to 2019 at Iversen field, Lincoln University, Canterbury, New Zealand. N = number of simulated and observed data pairs; R^2= coefficient of determination; R_RMSE = relative root mean square error (%); NSE = Nash-Sutcliffe efficiency; SB = Standard bias; NU = Nonunity slope; LC = Lack of correlation.

ID	Variable	N	R^2	R_RMSE	NSE	SB	NU	LC
Total	LeafN	66	0.40	16.8	-0.14	29.5	17.8	52.7
	StemN	47	0.04	46	-4.61	6.3	76.6	17.1
	RootN	54	0.33	17.7	0.29	1.5	4.2	94.4
E4IHHF10	LeafN	16	0.26	22.8	-0.74	51.5	5.7	42.8
	StemN	16	0.06	30.4	-1.31	9.5	49.8	40.7
	RootN	18	0.60	13.3	0.46	11.9	14.3	73.9
E4ILLF10	LeafN	26	0.36	13.1	0.15	5.6	19.4	74.9
	StemN	14	0.34	43.6	-2.9	82.6	0.5	16.8
	RootN	18	0.18	15.3	-0.37	1.9	38.3	59.7
E4ISSF10	LeafN	24	0.31	13.5	-0.09	24.1	12.5	63.5
	StemN	14	0.00	75.9	-20.51	88.3	7.1	4.6
	RootN	18	0.15	15.8	-0.47	0.6	41.3	58

7.3.8 **Shoot and root biomass**

Predicted and observed shoot and root biomass data were used to test how N parameters and functions affected dry matter simulation in the APSIM NextGen lucerne model. Simulation results for predicting shoot and root biomass in each regrowth cycle of the four field experiments (Figure 7.10, Table 7.5 and Appendix 49) showed good overall agreement (NSE = 0.68 and R_RMSE = 55.8%). Prediction of root biomass also had good overall agreement, with an NSE of 0.53 and R_RMSE of 30.7%. This was an improvement over the predicted results provided in Section 6.3.5.2.

For the FD5 genotype, lucerne crops grown under the HH and LL treatments had a similar agreement between predicted and observed shoot and root biomass compared with before the N parameters were applied (Section 6.3.5.2; Table 6.8); NSE was 0.67 and 0.49 for shoot biomass, and 0.22 and 0.24 for root biomass. However, for the SS treatment, the statistical values for predicted and observed root biomass increased; NSE value increased from -0.19 to 0.21. Shoot biomass simulation results did not change.

For the FD2 genotype, shoot and root biomass simulation results did not change after the N model was applied for the HH and LL treatments (Table 6.9 and 6.10). However, there was an improvement in shoot biomass simulation for the SS treatment, but a small reduction in accuracy of simulation for root biomass, NSE decreased from 0.08 to -1.52.

For the FD10 genotype, there was an improvement of shoot and root biomass prediction after the N model was applied for crops grown under the SS treatments (Table 6.9 and 6.10). Simulation results for the HH treatment did not change after the N model was applied. However, there was also a slight reduction in accuracy of simulation for root biomass under the LL treatment occurred, NSE decreased from 0.01 to -0.24.

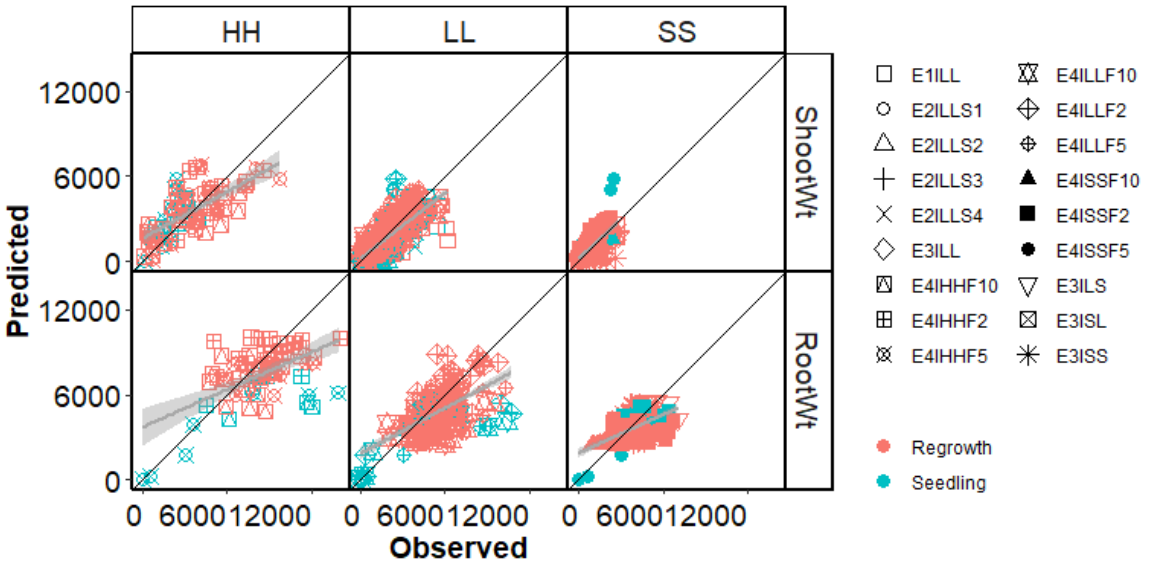

Figure 7.10. Predicted and observed shoot and root biomass data from four field experiments with multiple defoliation treatments [HH (84 day), LL (42 day), LS (42, 28 day), SL (28, 42 day), and SS (28 day)] and three fall dormancy (FD; FD2, FD5 and FD10) classes conducted in 1997-2019 at Iversen field, Lincoln University, Canterbury, New Zealand.

Table 7.5 Statistical measures of shoot and root biomass for four field experiments with multiple defoliation treatments [HH (84 day), LL (42 day), LS (42, 28 day), SL (28, 42 day), and SS (28 day)] and three fall dormancy (FD; FD2, FD5 and FD10) classes conducted within 1997 to 2019 at Iversen field, Lincoln University, Canterbury, New Zealand. N = number of simulated and observed data pairs; R^2= coefficient of determination; R_RMSE = relative root mean square error (%); NSE = Nash-Sutcliffe efficiency; SB = Standard bias; NU = Nonunity slope; LC = Lack of correlation.

Treatments	Variable	N	R^2	R_RMSE	NSE	SB	NU	LC
Total	shoot	977	0.69	55.8	0.68	0.8	3.6	95.7
	root	611	0.59	30.7	0.53	11.3	0.2	88.5
HH	shoot	95	0.62	50.3	0.61	0.7	0.7	98.7
	root	78	0.29	31.9	0.1	18.4	2.4	79.2
LL	shoot	580	0.68	48.5	0.65	5.7	3.7	90.6
	root	291	0.39	28.1	0.18	18.2	7	74.8
SS	shoot	302	0.55	82.2	0.29	3.3	33.5	63.2
	root	242	0.31	27.9	0.22	3.1	8.6	88.2
FD2	shoot	125	0.71	60	0.62	10.2	13.9	75.9
	root	113	0.61	30.2	0.52	15.4	3.4	81.2
FD5	shoot	728	0.70	55.4	0.69	3.7	1.5	94.8
	root	386	0.56	26.6	0.51	8.9	0	91
FD10	shoot	124	0.69	52.9	0.69	0.1	0.1	99.8
	root	112	0.55	41.8	0.47	15.8	0.6	83.7
FD2HH	shoot	25	0.54	44	0.52	4.1	0.6	95.4
	root	25	0.20	26.3	0.11	10.1	0	89.8
FD2LL	shoot	56	0.76	68.2	0.43	19.3	38.3	42.5
	root	44	0.44	28.7	0.35	4.8	9.2	86
FD2SS	shoot	44	0.58	61.1	0.01	10.5	47.2	42.3
	root	44	0.02	35.1	-1.52	45.8	15.2	39
FD5HH	shoot	45	0.69	63.1	0.67	3.7	2.3	94.1
	root	28	0.45	36.6	0.22	29.3	0	70.7
FD5LL	shoot	468	0.70	46.8	0.66	12.5	0.5	87
	root	203	0.41	22	0.24	16.1	6.1	77.8
FD5SS	shoot	215	0.56	89.5	0.37	0.9	28.6	70.5
	root	155	0.36	23.6	0.21	0.6	18.2	81.2
FD10HH	shoot	25	0.43	41.9	0.40	5.3	0.4	94.3
	root	25	0.01	32.8	-0.54	15.5	20	64.5

FD10LL	shoot	56	0.74	44.5	0.70	0.1	13.2	86.7
	root	44	0.44	46	-0.24	52.3	2.4	45.3
FD10SS	shoot	43	0.39	78.8	-0.47	22.6	35.9	41.5
	root	43	0.51	30.4	0.39	15.5	3.2	81.3

7.4 Discussion

Objective 4 of this thesis was to quantify and test the accuracy of N supply and allocation to each organ in the APSIM NextGen lucerne model. The relationships derived from the FD5 genotype grown under different defoliation treatmentS were successfully integrated into the model. This included simulating leaf, stem and root N concentration and remobilization and partitioning of N among all organs in response to environmental signals. Those relationships were further tested by using datasets from FD2 and FD10 classes grown under different defoliation treatments, to determine whether FD class or defoliation regime impacted on lucerne leaf, stem and root N concentration. Finally, N impact on biomass prediction was tested by fitting shoot and root biomass data to determine whether plant N status affected shoot and root growth and regrowth.

7.4.1 **N supply**

Total N mass had a strong positive linear relationship with total biomass, irrespective of defoliation and FD treatments (Figure 7.1). The N supply (N uptake and N_2 fixation) was parameterized as 2.5% of the photosynthesis rate to ensure there was sufficient N for lucerne growth. This means that every kilogram of DM contains ~2.5% N. This is consistent with the literature reported by Lemaire et al. (1992), who found that the average N concentration of a whole lucerne plant (including shoot and root) was constant at about 2.4% regardless of plant size.

Other lucerne models use different approaches to simulate N supply. For example, the CSM-CROPGRO perennial forage model (Malik et al., 2018) simulates nodule growth and N_2 fixation to calculate N supply. This module was adopted from soybean N_2 fixation by changing cardinal temperatures for nodule growth and N_2 fixation due to a lack of observed data for lucerne N_2 fixation. In the STICS model, N fluxes are associated with biomass fluxes. Daily N uptake and N_2 fixation are calculated as the minimum between N availability in the soil and plant N demand (Strullu et al., 2020). The concept of N supply (N uptake and N_2 fixation) is linked to total biomass supply, similar to the APSIM NextGen lucerne model.

However, detailed parameterization for N uptake and N_2 fixation were not included in our modelling process due to a lack of measured field or lab data. This empirical model provides an approach to parameterize N supply for other legume crops which were lack of measured N_2 fixation data. However, this approach ignored the physiological process of N_2 fixation and the defoliation treatment affects on these processes. This issue should be addressed by measuring N_2 fixation in the future for the APSIM NextGen lucerne model development.

7.4.2 **N concentration of each organ**

Leaf N concentration (%; g N g $^{-1}$DM^{-1}) ranged from 3.6% to 6.8% (Figure 7.2), and was not affected by defoliation or FD treatments. This is similar to results reported by Teixeira et al. (2008) in which leaf N concentration ranged from 4 to 6% in Experiment 3. Lemaire et al. (1992) calculated the average leaf N concentration of lucerne to be approximately 5.3%. Our data shows that N concentration decreased as leaf biomass increased in both increasing and decreasing Pp conditions, although this change was minor. This could be explained by lucerne leaves maintaining a constant N concentration to maximize photosynthesis rate through changes in specific leaf weight (SLW), which is highly variable (Lemaire et al., 1992; Teixeira et al., 2008)

The N thresholds for stem tissue ranged from 1.0% to 5.5% (Figure.7.3), which had an allometric relationship with stem biomass. This reflects the role of the stem as a support organ followed by the accumulation of structural, lignified tissue as it increases in height. As plants become bigger, structural tissues of stems become a higher proportion of the shoot biomass and they contain little N (Lemaire et al., 1992). This was found in experiment 4 by Ta (2018) who reported that the unpalatable component increased under long regrowth cycles compared with short regrowth cycles.

Root N thresholds ranged from 1.0 to 2.5% depending on defoliation treatment. Frequent defoliation (SS treatment) reduced N concentration in roots to 60-70% of the levels observed in the HH treatment. In addition, root N concentration showed a strong seasonal pattern. It decreased in an increasing Pp (spring) and increased in a decreasing Pp (autumn) (Figure 7.5). This seasonal pattern occurred in all four regrowth years across the three defoliation treatments. This is consistent with root biomass seasonal patterns (Section 6.3.4.1), and reflects the N remobilization in spring and partitioning to roots in autumn (Teixeira et al., 2007c). This agrees with the earlier research reported by Avice et al. (1996)

and Ta et al. (1990), who showed that N remobilization occurred in regrowth crops. Furthermore, Avice et al. (1997b) and Cunningham and Volenec (1996) found that root protein, especially vegetative soluble protein (VSP), are key organic components for lucerne regrowth after defoliation. Noquet et al. (2001) reported that short Pp resulted in preferential N allocation toward taproots with an increased accumulation of VSP. Liu et al. (2016) found a significant increase in the expression level of VSP in all dormant cultivar tissues in late autumn. Therefore, seasonal root N allocation (including remobilization and partitioning) should be included in the APSIM NextGen lucerne model.

7.4.3 Root N remobilization and partitioning

A N remobilization coefficient value of 2% of storage root N was used for remobilization calculations in an increasing Pp. The N remobilization coefficient value was tested using different defoliation treatments. The APSIM NextGen lucerne model uses the same regrowth coefficient function as for biomass remobilization duration (300 to 350 ˚Cd) for FD5 cultivars (Appendix 50 for model structure of N regrowth coefficient). Therefore, remobilization of N and C was found to occur in the first 300 to 350 ˚Cd in each regrowth cycle (Section 6.3.5.2). This agrees with the notion that root N is the driving factor for C remobilization in early spring and in each regrowth cycle (Avice et al., 1997b; Ta et al., 1990; Teixeira et al., 2007c). Root N demand in autumn, which drives N partitioning to roots, was parameterized as the maximum demand value, as with root biomass demand.

Few lucerne models have simulated N remobilization within plant organs. In the STICS model (Strullu et al., 2020), N remobilization is linked to biomass remobilization and used preferentially over N absorption from the soil. However, there is no clear description of how long root remobilization might last within each regrowth cycle. This may be because their defoliation treatments were not sufficiently different to detect any differences.

7.4.4 N dynamic simulation

Parameters and functions for leaf, stem, and root N were implemented into the APSIM NextGen lucerne model. Overall, simulation results for predicting leaf, stem and root N of FD5 in each regrowth cycle showed fair agreement (Figure 7.7 and Table 7.2).

For leaf N simulation, the HH and SS treatments had poor agreement between predicted and observed values. The reason for this might be that leaf N values varied across different

leaf biomass (3.6 to 6.8%), and there was no clear pattern within those data (Figure 7.8). Consequently, using leaf biomass to parameterize leaf N thresholds resulted in systemic bias for leaf N demand. Another reason was that fewer observed points being measured in the HH treatment to test the model. Therefore, this is an area that needs a more effective parameterization approach in the PMF and additional measurement to improve leaf N prediction. Lemaire et al. (1992) stated that a decline in leaf %N was due to increasing proportion of leaves that became shaded as the canopy expands. Therefore, another possible approach for parameterizing leaf N demand would be quantifying leaf N by using LAI of the canopy. However, this may not be appropriate for the HH treatment when LAI decreases in the later stage of growth cycles (Figure 5.8).

For stem N simulation, the LL treatment showed good agreement between predicted and observed values for regrowth crops. Lack of observed data did not provide a sufficient test for the HH treatment. For the SS treatment, poor prediction of stem N resulted from poor prediction of stem biomass. It is possible that the model over-estimated stem biomass in this treatment which leads to overestimates of stem N.

For root N simulation, the HH treatment showed good agreement between predicted and observed values. This indicates that the N module in the PMF was able to capture the seasonal pattern of N allocation in roots. However, for the LL and SS treatments, prediction of root biomass had poor agreement. This could be because crops grown under the LL and SS treatments did not partition sufficient dry matter to nodules which may down regulate N_2 fixation (Carlsson and Huss-Danell, 2003).

The APSIM NextGen lucerne model simulates leaf, stem and root N concentration and N remobilization and partitioning among each organ. However, most lucerne models do not include N allocation within the crop. In the STICS model, a nitrogen nutrition index (NNI) is used to simulate above-ground N concentration. This is because there is a strong allometric relationship between above-ground biomass and its N concentration (Lemaire et al., 1992; Strullu et al., 2020). This approach does not account for the N concentration difference between leaf and stem, which is an important forage quality indicator in grazing crops. Leaf and stem quality are further investigated in Chapter 8.

In addition, the main difference between the STICS and APSIM NextGen lucerne model is how DM and N allocation are simulated within organs. Specifically, the STICS model uses a

hierarchical system for N and DM allocation, which gives priority to the perennial organs, then to the fine roots, and finally to non-perennial organs. Among non-perennial organs, priority is given to the leaf, then to the stem, with the remaining N and DM being allocated to temporary reserves (Strullu et al., 2020). Temporary reserves provide a buffer between surplus and deficit of DM and N during growth period, but no indication of the location of that storage in physiological processes occurring in plants. In contrast, the APSIM NextGen lucerne model uses RelativeAllocation and Organ-Arbitrator interface to allocate DM and N among organs (Brown et al., 2019). The OrganArbitrator calculates the total available biomass which can be allocated, and then calculates and partitions based on relative demands of each biomass component for each organ. Biomass components include structural, metabolic and storage biomass. Priority is given to structural and metabolic DM, then to storage biomass. Partitioning rules based on relationships of biomass allometry in the APSIM NextGen lucerne model provide a more stable and robust method for modelling DM and N demand (Brown et al., 2018).

7.4.5 **FD effect**

A separate set of parameters for FD classes was needed to improve model simulation results. As expected, the FD2 had the lowest remobilization coefficient value (0.5% of storage root N per day) and shortest remobilization duration (250-300 ˚Cd) within each regrowth cycle. The FD10 genotype, had the same remobilization rate value (0.5% of storage root N per day), but longer remobilization duration (500-550 ˚Cd). This suggests that the FD2 remobilized less N within a shorter period after defoliation compared with FD10. This mechanism explains that the non-dormant lucerne cultivars had more vigorous shoot regrowth when compared with dormant or semi-dormant cultivars in a short-term regrowth cycle system (Lu et al., 2018; Ta, 2018). However, long term and frequent N remobilization leads to root N reserve depletion, which caused the FD10 genotype plant population to decrease over time (Ta, 2018).

Overall, leaf N values of the FD2 and FD10 genotypes under multiple defoliation treatments (HH, LL, and SS) had fair to poor agreement between observed and predicted values. This also highlighted the bias in the leaf N prediction in the PMF. Stem N simulation had poor agreement because there was insufficient measured stem N data in each defoliation treatment for both FD2 and FD10 genotype under each defoliation treatment. For root N

simulation in FD2 and FD10 genotypes, there was fair overall agreement between predicted and observed values. However, poor agreement was found in the HH and SS treatments for FD2, LL and SS treatments for FD10. One of the reasons for the poor prediction of root N concentration was that there were limited data (18 points) for each treatment to test the model. Future root N measurements for FD2 and FD10 is needed to improve model prediction.

To our knowledge, no other lucerne model simulates N allocation for different lucerne FD genotypes.

7.4.6 N impact on biomass prediction

Including the N model improved both shoot and root biomass prediction for most defoliation and FD treatments, especially the prediction of shoot and root biomass under the SS treatment. This supports the idea of N limited crop growth under the SS treatment in Experiments 3 and 4 (Teixeira et al., 2007c). However, the SS treatment had poor agreement between observed and predicted values of root biomass for the both FD2 and FD10 genotype. This could be because of a declining plant and stem population in FD10 (Ta, 2018), which the model did not account for over the five growth years. This is an area for future research. For the FD2 genotype, this could be because crops grown under the SS treatments did not partition sufficient N to roots, which could down regulate root biomass partitioning.

In this chapter, the APSIM NextGen lucerne model simulated total N supply (N from N_2 fixation and N uptake from soil mineral N). The N mass was then allocated to leaf, stem and root organs based on their N demand. N demand of each organ was calculated as three N concentration threshold functions. N remobilization and partitioning processes occur within each organ regulated by seasonal signals, the same way as for biomass. Fitting N for each organ improved both shoot and root biomass predictions, especially for the SS treatment. With the addition of the N module, the APSIM NextGen lucerne model is now capable of predicting lucerne phenological development, canopy expansion, biomass and N assimilation and allocation within plants.

To make the model more informative for animal nutrition and production on grazing farming systems, it is necessary to model and predict forage quality, which includes leaf

and stem crude protein (CP) and metabolisable energy (ME). In addition, plant height which is used as an indicator for defoliation management (Moot et al., 2016) should also be included in the model. Thus, plant height, leaf and stem quality and model application are assessed in Chapter 8.

7.5 Conclusions

The results of this chapter permit the following conclusions:

- Average lucerne crop dry matter had approximately 2.5% N. Leaf N concentration ranged from 4.5% to 6.5%, and was not affected by defoliation or FD treatments, but was affected by leaf mass. Stem N concentration ranged from 1% to 5.5%, in an allometric relationship with stem biomass.

- Root as a reserve organ, showed a strong seasonal pattern and its N concentration differed with defoliation and FD treatments.

- FD2 had a lower N root remobilization coefficient value (0.5% of storage root N day^{-1}) and the shortest remobilization duration; FD10 had the same remobilization coefficient but longer remobilization duration; FD5 had the highest remobilization coefficient value (2% of storage root N day^{-1}) and a medium remobilization duration.

- The APSIM NextGen lucerne model had a fair to poor prediction of leaf N, stem and root N. More effective parameterization approach in the PMF and additional measurement of leaf, stem and root N concentration under different defoliation treatments are needed for model future improvement.

- Fitting N improved dry matter prediction for most of the defoliation and FD treatments, with the SS treatment most effectively predicted.

8 MODELLING FORAGE QUALITY AND SCENARIOS TESTING

8.1 Introduction

A goal for building the APSIM NextGen lucerne model has been to predict lucerne forage yield and quality. This will assist recommendations for best management practices on farms in different locations where lucerne is predominantly grazed.

In previous Chapters 4-7, the responses of lucerne cultivars to environmental factors were quantified and integrated into the APSIM NextGen lucerne model. These quantitative responses were then used to simulate and verify the response of different cultivars under different defoliation regimes. The simulation of physiological processes included phenological development, canopy expansion and radiation interception, dry matter remobilization and partitioning, and N dynamics in each organ. This chapter focuses on modelling forage quality, including plant height, crude protein (CP) and metabolisable energy (ME) of leaf and stem. The model was then used for scenario testing, comparing forage yield and quality under two defoliation managements in three different regions (Canterbury, Central Otago and Hawkes bay) assuming irrigated conditions.

There are two research questions to be answered: 1) can forage quality of leaf and stem be accurately simulated for crops grown under different defoliation regimes and FD classes? and 2) can the APSIM NextGen lucerne model accurately simulate lucerne production and quality in three different locations? The corresponding hypotheses are: 1) that functions and algorithms of plant height, leaf CP and ME, and stem CP and ME generated from different defoliation treatments could be adapted to accurately quantify seasonal responses for different genotypes of FD classes grown under different defoliation regimes, and 2) that the APSIM NextGen lucerne model could sensibly predict yield and quality of crops grown in different regions.

This chapter deals with Objective 5 of the thesis; to quantify and simulate lucerne quality in regrowth crops using the Plant Modelling Framework (PMF) in the APSIM NextGen lucerne model. The model was subsequently used to predict forage yield and quality in three locations. Field-measured data of plant height, leaf and stem CP and ME from long-term experiments (1, 3 and 4) conducted under different defoliation treatments were used to calculate functions and parameters (Ta et al., 2020) in the PMF. Once the model

structure was built, it was tested with additional datasets (experiments 3 and 4) from different defoliation treatments and fall dormancy (FD) classes.

Traditional defoliation rules for lucerne are based on plant phenology, including 10% flowering (Kalu and Fick, 1981). However, Moot et al. (2003) suggested that these defoliation rules should be modified to maximize animal and plant production in grazing management systems. Plant height is a strong indicator of shoot biomass (Moot et al., 2016). For scenario testing, two defoliation rules were used based on different plant height to compare yield and quality, and number of regrowth cycles in the three locations (Moot et al., 2003). A 300 mm defoliation target represents an ideal gazing system (Moot et al., 2016) and the 450 mm defoliation target represents a cut-and-carry system. The input data included climate and soil data from the three locations where lucerne is grown and grazed in New Zealand.

8.2 Forage quality calibration and parameterization

This chapter focuses on forage quality simulation of three genotypes of different FD classes grown under different defoliation regimes and FD treatments (Experiment 4). Observed variables included plant height, CP and ME of leaves and stems.

8.2.1 Model structure

The PMF in APSIM NextGen was used for testing and evaluating lucerne plant height, CP and ME of leaf and stem-related parameters under different defoliation regimes and FD classes. Plant height, leaf CP, and ME were organized under the leaf organ portion of the model, whereas stem CP and ME were placed under the stem organ portion of the PMF. All previously derived parameters from Chapters 4 to 7 were used, and new parameters were calculated and added to the model structure to simulate plant height, and CP and ME of leaves and stems.

8.2.2 Field experimental data

Simulation and verification of lucerne plant height, CP and ME of leaf and stem used field experimental data described in Section 3.1.1. The datasets for model testing and calibration for three FD classes under different defoliation regimes were described in Section 4.2.1 (Table 4.2; Experiment 4).

8.2.3 Model calibration and parameterization

8.2.3.1 "Heightchron"

"Heightchron" (˚Cd mm^{-1}) was defined as the thermal time (Tt) requirement for an increase of one mm stem height, and calculated as the slope of height against Tt. Tt accumulation began at emergence date in seedling crops and from each grazing or cutting date in the regrowth crops. "Heightchron" was plotted as a function of photoperiod (Pp) and was tested with both linear and non-linear regression models.

For the constant 42 day defoliation treatment (LL), most regrowth cycles were only in the vegetative stage. Therefore, these observed data were used to calculate heightchron for the vegetative phase ($heightchron_{veg}$) and plotted as a function of Pp. The relationship was analysed by least squares linear regression.

The 84 day defoliation treatment (HH) has the longest regrowth duration, and was the only treatment that consistently gave lucerne plants adequate time to transition from vegetative to reproductive development. Therefore, heightchron ($heightchron_{rep}$) post-flowering was derived from these data, and calculated and plotted as a function of Pp and tested with non-linear regression.

8.2.3.2 CP and ME contents of leaf and stem

Leaf and stem N% were measured from NIR analysis and multiplied by 6.25 (Equation 28) to estimate crude protein (CP %).

Equation 28 $CP(\%) = N\% \times 6.25$

Observed leaf and stem ME were measured by NIR and estimates from the slope of leaf and stem ME against leaf and stem dry matter (Equation 29).

Equation 29 $ME(\%) = a \times dry\ matter^{b}$

8.3 Model scenario testing

For scenario testing in the three locations, daily meteorological data (maximum temperature, mean temperature, minimum temperature, solar radiation, wind speed, precipitation and vapor pressure), were downloaded from the Broadfields (described in Section 3.2.1.1), Napier Aero Aws, and Lauder Ews meteorological stations (National Institute of Water and Atmospheric Research [NIWA], New Zealand.

https://cliflo.niwa.co.nz). The meteorological datasets are for the 31-year period of 1989 to 2019, allowed for simulation of 31 years of establishment crops and 30 years of regrowth crops. Predicted variables included shoot yield, leaf biomass, stem biomass, number of growth cycles, leaf CP and ME, and stem CP and ME.

The 31 years mean daily total solar radiation and daily air temperature for both Alexandra and Napier followed a seasonal pattern (Figure 8.1). Total solar radiation for both locations were similar: it increased from a minimum of ~6 MJ m^{-2} day^{-1} in July (winter) to a peak of about 23 MJ m^{-2} day^{-1} in December (summer). However, Napier had higher mean air temperature than Alexandra. The minimum mean daily air temperature was ~3 ˚C in Alexandra and 10 ˚C in Napier in July; and the maximum mean daily air temperature was 12 ˚C in Alexandra and 18 ˚C in Napier in January and February. Average yearly total precipitation was about 438±95.5 mm in Alexandra and 798±153.9 mm in Napier.

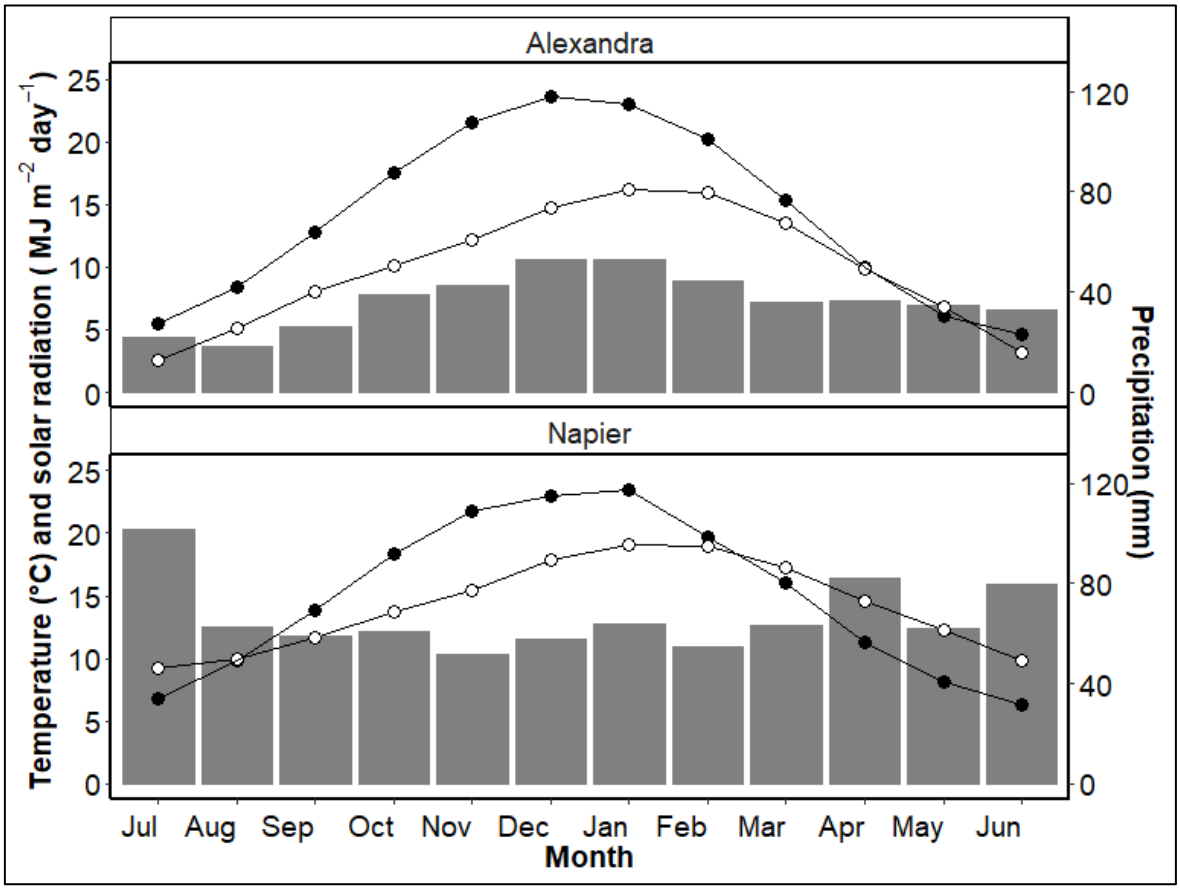

Figure 8.1 Mean solar radiation (–●–), mean air temperature (–○–) and mean precipitation (bars) for monthly periods from 1 January 1989 to 31 December 2019 at Alexandra and Napier in New Zealand. Note: data were collected at the Lauder Ews and Napier Aero Aws meteorological stations.

For scenario testing, the input data included climate and soil data from the three locations. The model sets the defoliation rule in the management script of 300 mm for grazing or 450 mm for mechanical harvest. Crops were sown on Oct 4th in each year, although this would be considered early for Alexandra. All simulations were run for two growth years and finished on Jun 10th. This allowed a comparison of average shoot yield and quality across the 30 years among three locations. Simulation results also include number of growth cycles in each year for the three locations.

8.4 Results

8.4.1 Plant height simulation

8.4.1.1 Plant height and thermal time

Five different sowing dates across Experiments 2 and 4 showed lucerne seedling crops required ~300 ˚Cd from sowing to begin stem elongation (Figures 8.2; S_1). There was a strong linear relationship between accumulated Tt (˚Cd) and plant height in each growth duration for seedling crops (R^2 from 0.92 to 0.99) (Figure 8.1). With a 42 day regrowth cycle of 400 to 550 ˚Cd, growth cycle data showed that lucerne plants grew to a height of 100 mm in the late autumn and early winter and to 600 mm in summer. The slope of the linear regressions changed across regrowth cycles (Appendix 51 for R^2, P, slope and intercept).

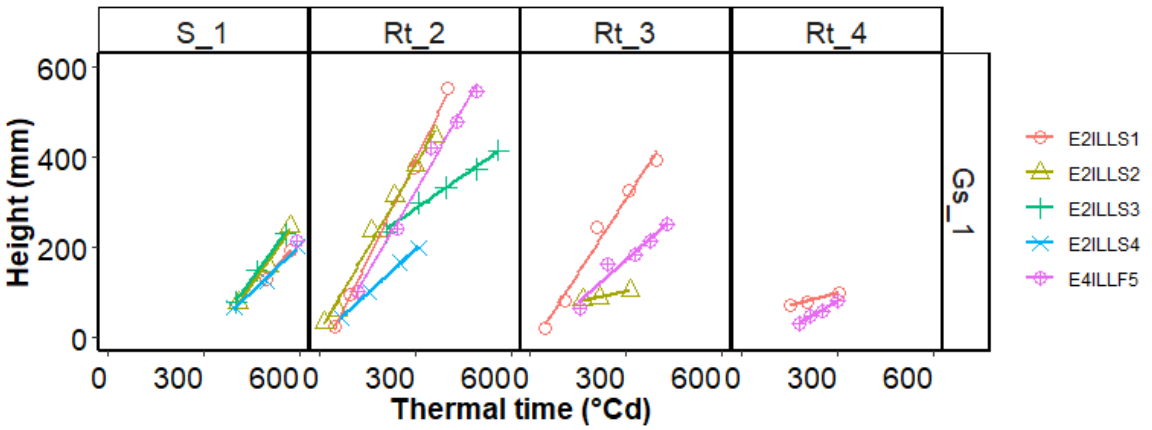

Figure 8.2. Plant height against accumulated thermal time (˚Cd) from Experiments 2 and 4; (E2 had four sowing dates) conducted between 2000 and 2019 at Lincoln University, Canterbury, New Zealand. Row GS_1 is the first growth season (seedling crop). Column S_1 is the seedling growth cycle and columns Rt_2 to Rt_4 represent regrowth cycles. Lines represent linear regressions.

Figure 8.3 illustrates height against Tt within seven regrowth cycles in five growth years for the four experiments under a 42 day defoliation regime (~400 to 550 ˚Cd). There was a

strong linear relationship between stem height and Tt in each regrowth cycle and every experiment (R^2=0.91 to 0.99). Within a regrowth cycle (a column), the regression lines from different experiments were either parallel or overlapping. This indicates that the slope of each regrowth cycle was consistent across different growth years. However, within a year (a row), the slope of the linear regressions changed across different regrowth cycles (Appendix 51 for R^2, P, slope and intercept values). This suggests a seasonal effect, and therefore the slopes of linear regressions were plotted against Pp in subsequent analyses. Seedling and regrowth crops had the same maximum height (~ 600 mm), but seedling crops had lower slopes than regrowth crops (Figure 8.3 and Figure 8.4).

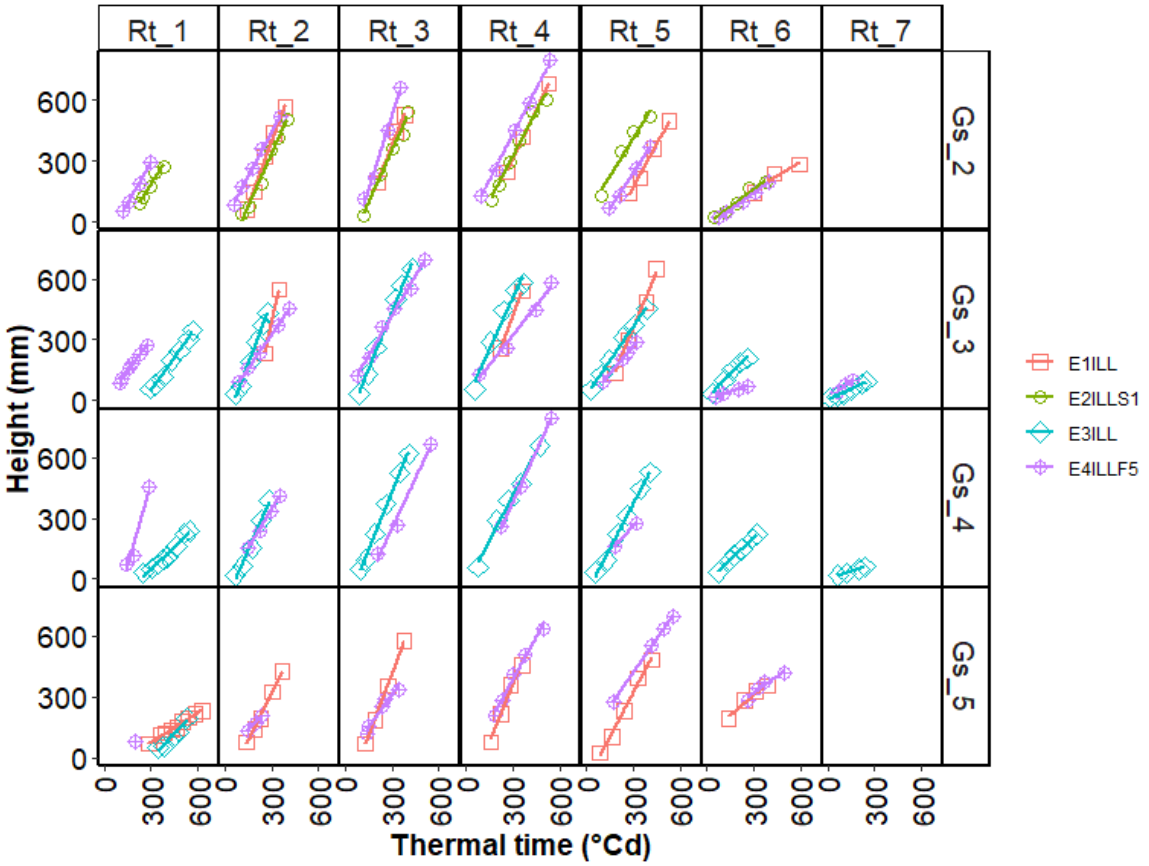

Figure 8.3. Plant height against accumulated thermal time (˚Cd) from four field experiments conducted from 1997 to 2019 at Lincoln University, Canterbury, New Zealand. Columns Rt_1 to Rt_7 represent regrowth cycles, whereas rows GS_2 to GS_5 represent growth years. Lines represent linear regressions.

8.4.1.2 Heightchron and Pp

The slope of linear regression between Tt and plant height, defined as Tt requirement to expand one mm stem height (heightchron; ˚Cd mm^{-1}), was then analysed in relation to mean Pp for regrowth and seedling crops due to their different development patterns

(Figure 8.4). For regrowth crops, a strong exponential decay response was found between heightchron and mean Pp (R^2=0.83). Heightchron decreased as photoperiod increased from 4.2 ˚Cd mm^{-1} at 10 h to 0.6 ˚Cd mm^{-1} at 16.5 h of Pp. This means that less accumulated Tt was required for the stem to increase in length in long Pp conditions. For seedling crops, heightchron was consistent across day lengths, ~1.5˚Cd mm^{-1}. Critical Pp for lucerne stem elongation was estimated as 11.1 h from inverse regression for regrowth crops, whereas seedling crops did not respond to Pp (Figure 8.5) The exponential decay function for regrowth crops of FD5 had three parameters: a= 0.62, b=97660 and c=-1 (Appendix 52 for model structure of $heightchron_{veg}$ function).

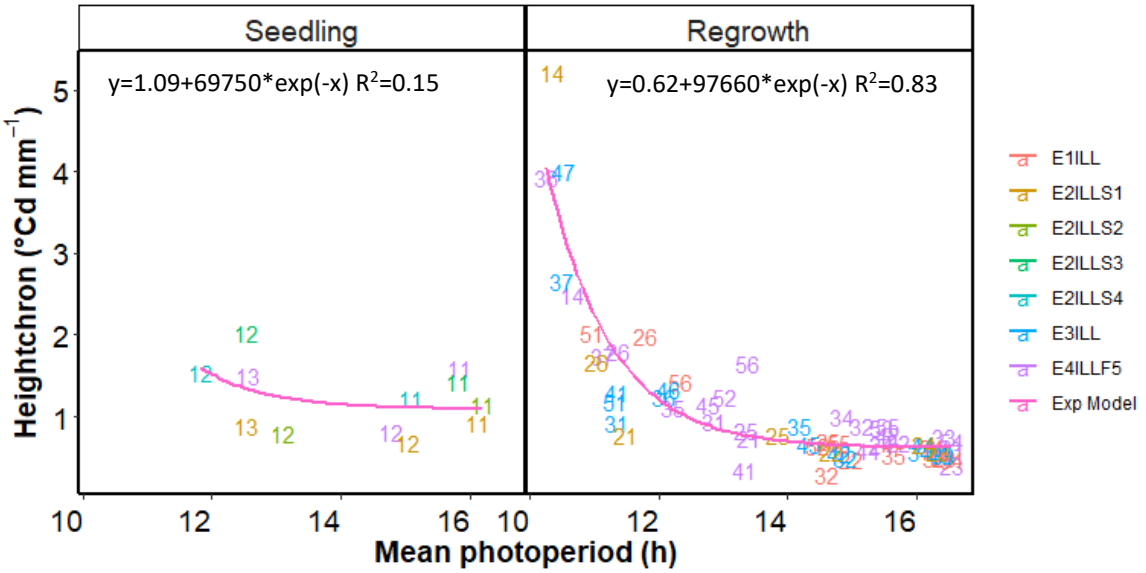

Figure 8.4. $Heightchron_{veg}$ against mean photoperiod for seedling and regrowth crops from four field experiments conducted at Lincoln University, Canterbury, New Zealand. The two dimension code represents growth years and regrowth cycles. The exponential decay function for regrowth crops of FD5 with three parameters: a=0.62, b=97660 and c=-1.

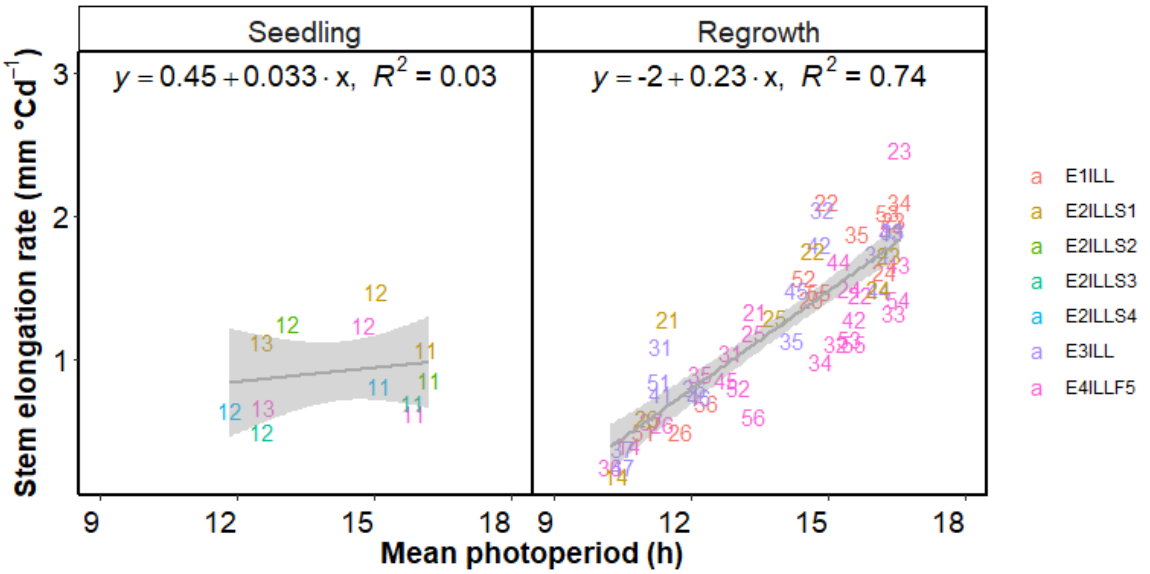

Figure 8.5. Stem elongation rate against mean photoperiod for seedling and regrowth crops from four field experiments conducted at Lincoln University, Canterbury, New Zealand. The two dimension code represents growth years and regrowth cycles.

8.4.1.3 Heightchron$_{rep}$

For the HH treatment, the relationship between accumulated Tt (˚Cd) and plant height (Figure 8.6) illustrates that the slope of the regression models changed after reaching 400 to 500 ˚Cd, due to the switch to reproductive development. Therefore, plant height data for the HH treatment were segmented into vegetative and reproductive stages (Figures 8.6 and Appendix 53 for R^2, P, slope and intercept).

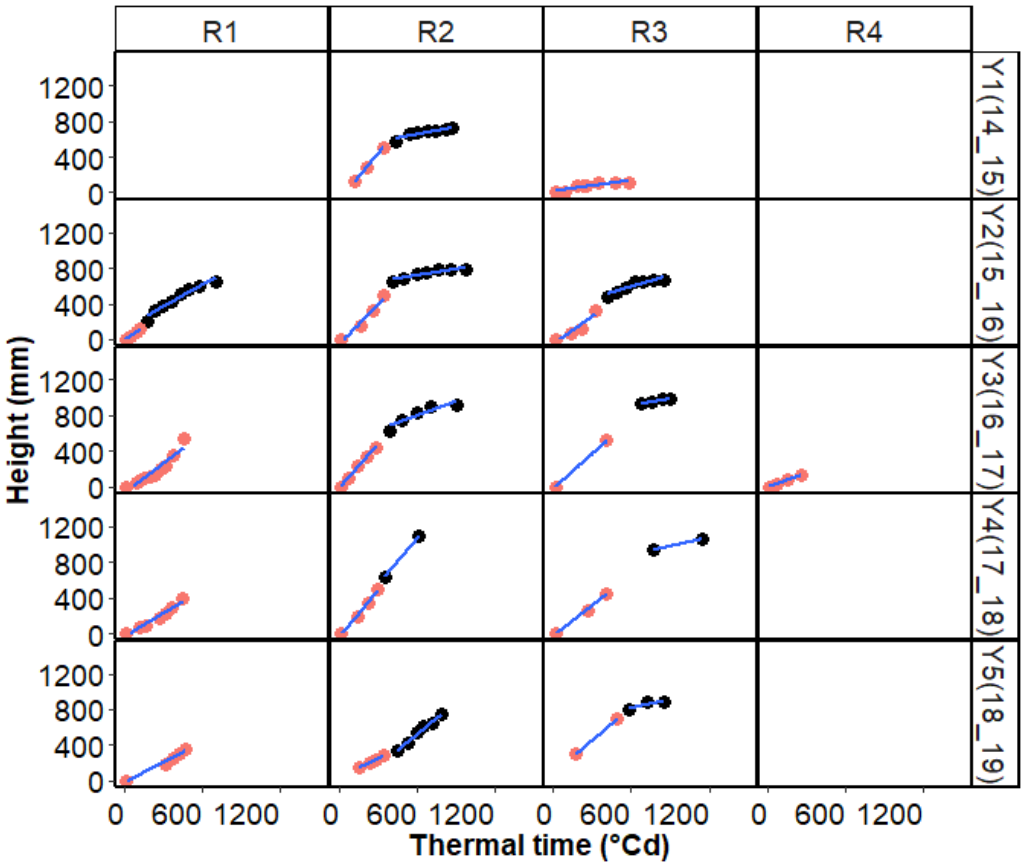

Figure 8.6. Plant height against Tt (˚Cd) from Experiment 4 with 84 day (HH) defoliation treatment conducted from 2014 to 2019 at Lincoln University, Canterbury, New Zealand. Columns R1 to R4 represent regrowth cycles and rows Y1 to Y5 represent growth years. Lines represent linear regressions.

As a consequence of the changes in plant height with Pp and development stages, the heightchron in regrowth lucerne crops was separated into vegetative heightchron$_{veg}$ and reproductive heightchron$_{rep}$ phases (Figure 8.7). In the vegetative stage, heightchron$_{veg}$ decreased from 3 to 0.92 ˚Cd mm^{-1} as photoperiod increased from 10.5 to 16 h, higher than the 2.2 to 0.6 ˚Cd mm^{-1} values reported in Section 8.3.1.2. In contrast, the heightchron$_{rep}$ was constant (~2.5˚Cd mm^{-1}) and independent of Pp.

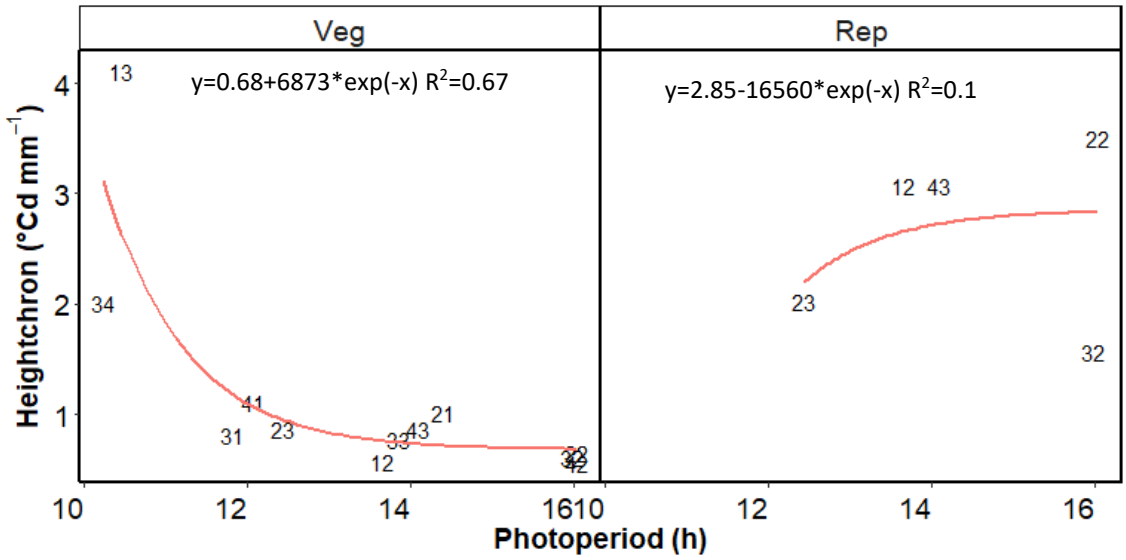

Figure 8.7. Heightchron against mean photoperiod for vegetative and reproductive crops for Experiment 4 with 84 day (HH) defoliation treatment conducted from 2014 to 2019 at Lincoln University, Canterbury, New Zealand. The two dimension code represents growth years and regrowth cycles.

After applying heightchron$_{rep}$ when plants reached flowering (Appendix 54 for model structure of heightchron$_{rep}$), simulation results for the HH treatment in each regrowth cycle (Figure 8.8 and Table 8.1) showed close agreement (NSE value of 0.83 and R_RSME of 31.7%) between predicted and observed values. However, over-predictions were observed in mid-summer growth periods.

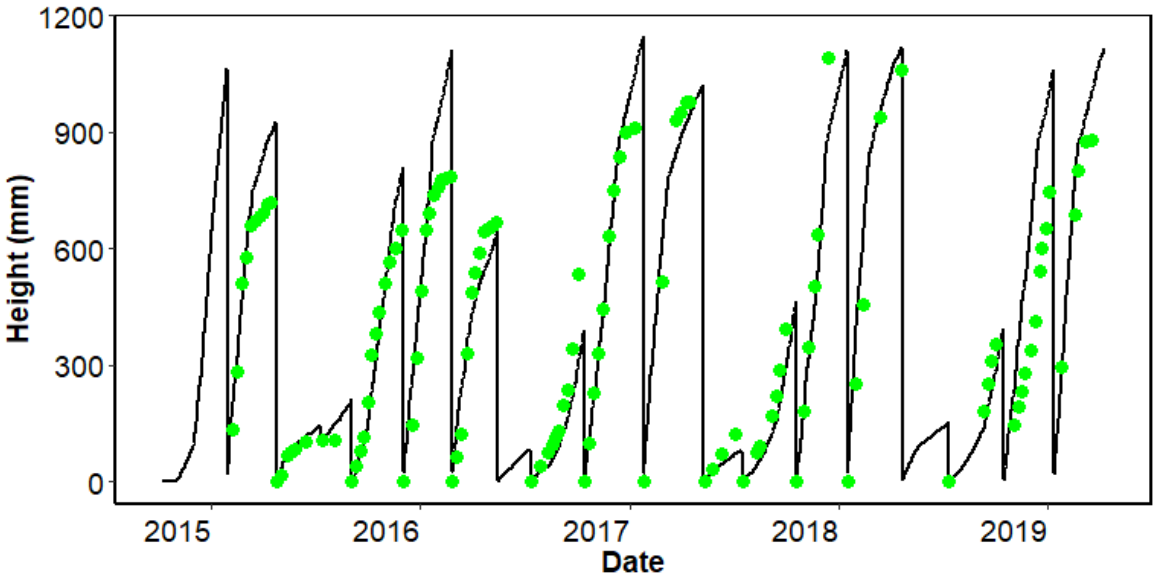

Figure 8.8. Predicted (line) and observed (green dots) values of plant height for Experiment 4 with the 84 day (HH) defoliation treatment conducted in 2014-2019 at Lincoln University, Canterbury, New Zealand.

8.4.1.4 Simulation and verification of height

Parameters and functions for heightchron (Sections 8.3.1.2 and 8.3.1.3) were incorporated into the APSIM NextGen lucerne model (Appendices 52 and 54 for model structure for plant height). Simulation results for predicting plant height in each regrowth cycle of the four field experiments conducted from 1997 to 2019 (Figure 8.9 and Table 8.1) showed good overall agreement (R_RMSE = 39.3% and NSE = 0.66).

For seedling crops, there was fair agreement between predicted and observed values (R_RMSE was 40.6% and NSE was 0.34). For example, under-estimation was observed in treatments E2ILLS3 (sown in a decreasing Pp condition; Figure 8.9), with NSE of -0.32.

For regrowth crops, there was good agreement between predicted and observed values shown in Figure 8.8 and Table 8.1 (R_RMSE = 38.0% and NSE = 0.71). Height predictions for the first regrowth cycle showed good agreement even in the early spring.

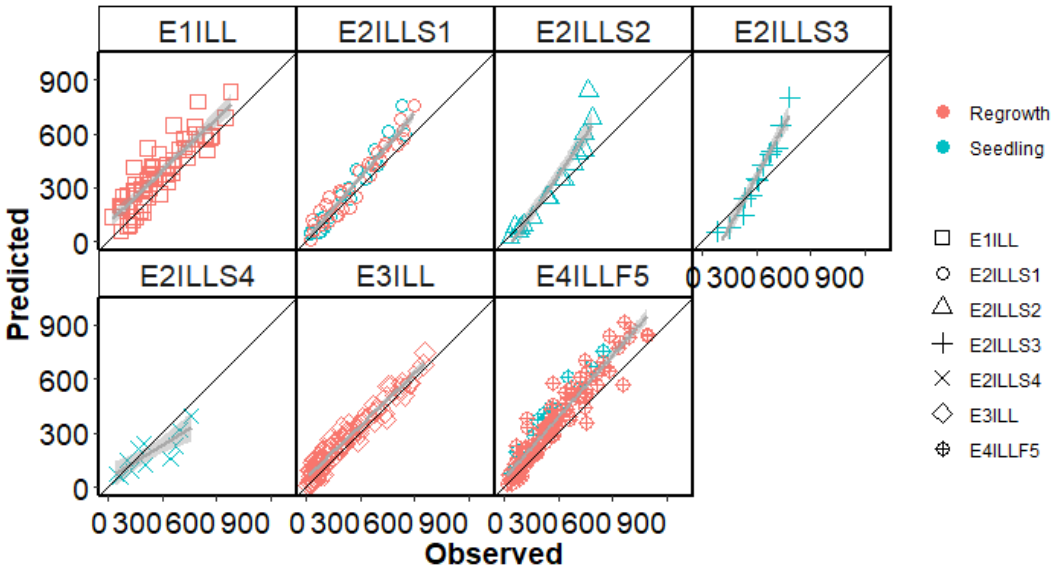

Figure 8.9. Predicted and observed values of plant height (mm) for calibration datasets for four field experiments with Experiment 2 having four sowing dates conducted between 1997 and 2019 at Lincoln University, Canterbury, New Zealand.

Table 8.1 Statistical measures of plant height (mm) simulation on a calibration dataset from four field experiments conducted between 1997 and 2019 at Lincoln University, Canterbury, New Zealand. n = number of simulated and observed data pairs; R^2= coefficient of determination; R_RMSE = relative root mean square error (%); NSE = Nash-Sutcliffe efficiency; SB = Standard bias; NU = Nonunity slope; LC = Lack of correlation.

Treatment	N	R^2	R_RMSE	NSE	SB	NU	LC
Total	348	0.87	39.3	0.66	43.8	17.7	38.6
Seedling	78	0.83	46.0	0.43	27.9	42.5	29.6
Regrowth	270	0.89	38.0	0.71	50.3	11.4	38.3
E1ILL	57	0.79	44.5	0.40	57.7	6.7	35.6
E2ILLS1	50	0.94	31.2	0.78	46.4	24.6	29.1
E2ILLS2	17	0.92	44.5	0.48	22.9	61.3	15.8
E2ILLS3	13	0.94	41.5	-0.32	28.1	67.2	4.8
E2ILLS4	11	0.71	38.1	0.61	21.3	3.3	75.4
E3ILL	86	0.95	29.3	0.88	54.7	0.2	45.0
E4ILLF5	114	0.90	42.8	0.62	56.6	16.1	27.2

8.4.1.5 Verification of defoliation treatment

The height model was used to test the prediction of lucerne crop height (FD5) under different defoliation regimes. Overall, predicted and observed height values for Experiments 3 and 4 with multiple defoliation treatments (HH, LS, SL, and SS) had good agreement, with NSE of 0.76 and R_RMSE of 60.3% (Figure 8.9 and Table 8.2).

Among the three defoliation treatments, the HH and LL treatments had good agreement between predicted and observed values, with similar R_RMSE value (~37%) and NSE values (~0.82). However, the SS treatment had the highest R_RMSE values (110.7%) and the lowest NSE value (-0.09) (Table 8.2). Over-estimation occurred in both E3ISS and E4ISSF5 treatments (Figure 8.9); NSE values were -0.86 and 0.23, respectively (Table 8.2).

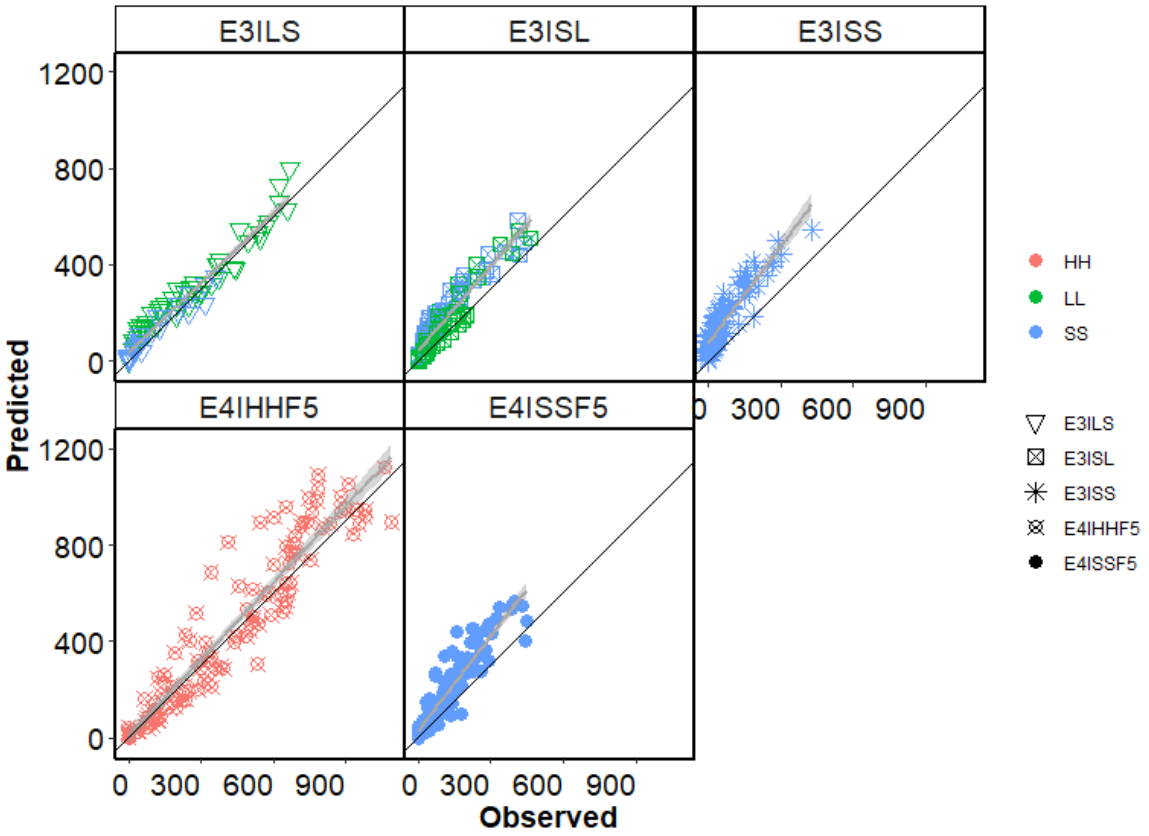

Figure 8.10. Predicted and observed values of plant height from Experiments 3 and 4 with multiple defoliation treatments [HH (84 day), LS (42, 28 day), SL (28, 42 day), and SS (28 day)] conducted between 2002 and 2019 at Lincoln University, Canterbury, New Zealand.

Table 8.2 Statistical measures of plant height from Experiments 3 and 4 with multiple defoliation treatments [HH (84 day), LS (42, 28 day), SL (28, 42 day), and SS (28 day)] conducted between 2002 and 2019 at Lincoln University, Canterbury, New Zealand. N = number of simulated and observed data pairs; R^2= coefficient of determination; R_RMSE = relative root mean square error (%); NSE = Nash-Sutcliffe efficiency; SB = Standard bias; NU = Nonunity slope; LC = Lack of correlation.

Treatment	N	R^2	R_RMSE	NSE	SB	NU	LC
Total	552	0.90	61	0.75	50	11.2	38.8
HH	120	0.91	31.7	0.83	26	23.9	50
LL	123	0.91	52.9	0.77	54.1	6.7	39.3
SS	309	0.83	110.1	-0.08	64	20.1	16
E3ILS	102	0.94	39.8	0.88	51.9	2	46.1
E3ISL	107	0.90	93.4	0.27	65.9	20.7	13.5
E3ISS	88	0.82	184.8	-1.32	74.9	17.1	8
E4IHHF5	120	0.91	31.7	0.83	26	23.9	50
E4ISSF5	135	0.85	92.4	-0.07	59.9	26.2	14

The difference in the SS defoliation regimes indicates that lucerne stem elongation was affected by perennial reserves reduced by frequent defoliations. This is consistent with previous results that showed the SS treatments had lower root biomass and leaf area expansion rate (LAER) over time due to the impact of lower N reserves on shoot elongation (Chapters 6 and 7). Therefore, height model was investigated further by associating root storage N to improve height prediction. A model optimization exercise was conducted for N limitation factor (NLF; percentage of heightchron) by comparing predicted and observed height data, as described in Appendix 55 and 56. The N limitation function parameterized as a linear relationship between storage root N concentration and NLF. Storage root N concentration decreased from 1.5 (the lowest storage root N concentration of the LL treatment) to 0 as NLF decreased from 1 to 0.7 (1.7 used in a divided function in the model). The N limitation function model was tested by comparing predicted and observed height data (Figure 8.11 and Table 8.3).

Overall, the model improved height prediction results for both seedling and regrowth crops (NSE =0.87 and R_RMSE= 35.4%). For the SS treatment, the agreement between predicted and observed values was improved, NSE values increased from -0.09 to 0.48. The majority of variation was from treatment E3ISS, with an R_RMSE value of 129.4% and NSE values of -0.13. This treatment involved two years under the LL defoliation and two years under the SS treatment.

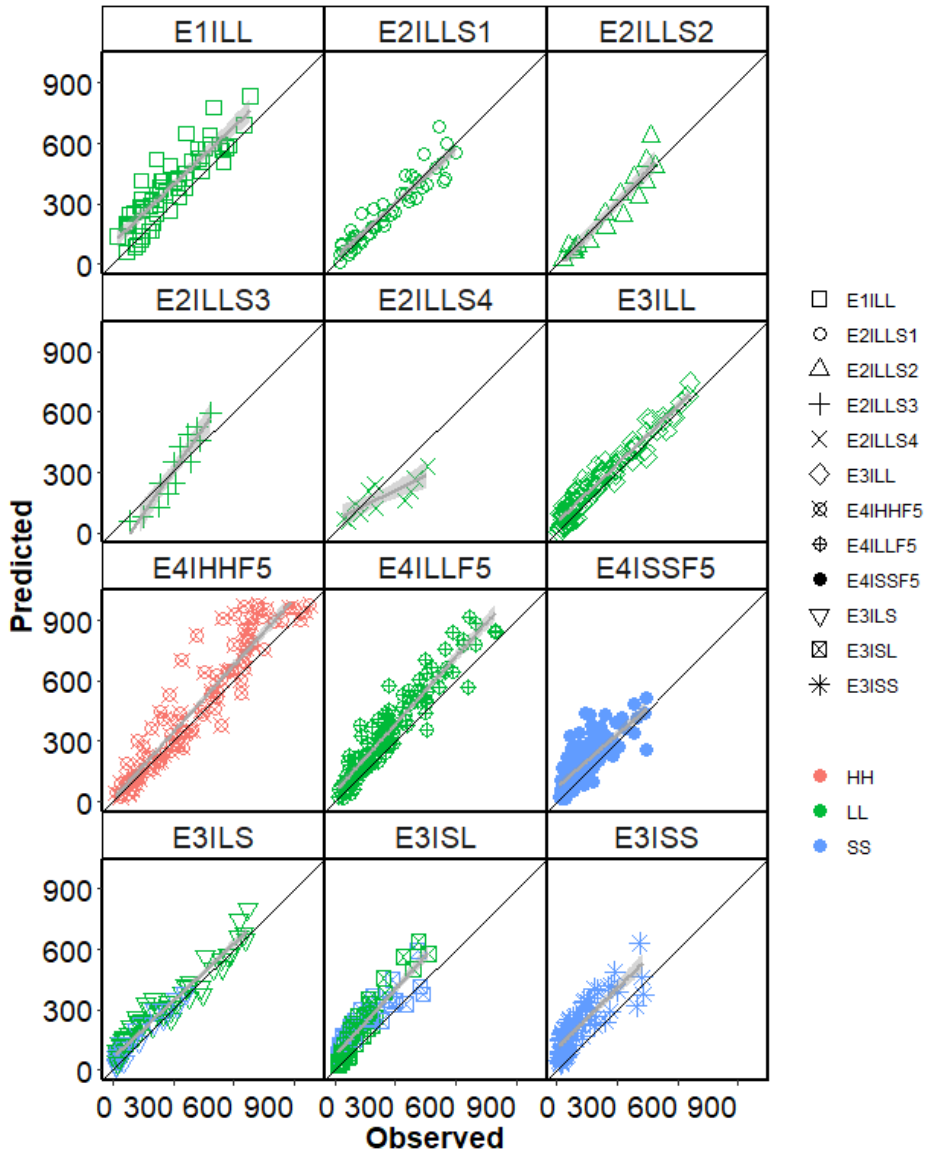

Figure 8.11. Predicted and observed values of plant height from four field experiments with multiple defoliation treatments [HH (84 day), LS (42, 28 day), SL (28, 42 day), and SS (28 day)] conducted between 2002 and 2019 at Lincoln University, Canterbury, New Zealand.

Table 8.3 Statistical measures of plant height from four field experiments with multiple defoliation treatments [HH (84 day), LS (42, 28 day), SL (28, 42 day), and SS (28 day)] conducted between 2002 and 2019 at Lincoln University, Canterbury, New Zealand. N = number of simulated and observed data pairs; R^2= coefficient of determination; R_RMSE = relative root mean square error (%); NSE = Nash-Sutcliffe efficiency; SB = Standard bias; NU = Nonunity slope; LC = Lack of correlation.

Treatment	N	R^2	R_RMSE	NSE	SB	NU	LC
Total	902	0.87	44.2	0.74	36.8	10.8	52.3
HH	162	0.90	32.8	0.8	21.3	27.6	51.2
LL	456	0.86	38.7	0.73	37.4	9.9	52.7
SS	284	0.65	77.2	0.12	50.1	9.8	40.1
Seedling	120	0.88	36.7	0.76	17	33.1	49.9
Regrowth	782	0.87	45.5	0.74	40.2	8.6	51.2
E1ILL	57	0.79	44.5	0.4	57.7	6.7	35.6
E2ILLS1	50	0.89	22.2	0.89	1	0.2	98.8
E2ILLS2	17	0.90	23.1	0.86	0.1	30.4	69.5
E2ILLS3	13	0.88	24.9	0.52	2.5	71.9	25.6
E2ILLS4	11	0.67	44.1	0.48	28.1	9.6	62.4
E3ILL	86	0.95	29.3	0.88	54.7	0.2	45
E4IHHF5	162	0.90	32.8	0.80	21.3	27.6	51.2
E4ILLF5	114	0.89	40.9	0.65	53.5	15.9	30.5
E4ISSF5	134	0.60	59.9	0.22	31.5	16.5	51.9
E3ILS	87	0.94	35.2	0.87	56	0	44
E3ISL	89	0.84	80.8	0.21	68	11.2	20.8
E3ISS	82	0.70	122.6	-0.52	72.7	7.9	19.5

8.4.1.6 Verification of fall dormancy classes

Different FD classes had different heightchron functions. Therefore, a separate set of parameters was needed to improve model simulation results for the FD2 and FD10 genotypes. The relationship between heightchron and mean Pp for FD2 and FD10 crops under the LL defoliation treatment showed a different response pattern (Figure 8.12). For the FD2 treatment, there was an exponential decay relationship between heightchron and Pp (R^2=0.78). Heightchron decreased from 2.8 ˚Cd mm^{-1} at 11 h of Pp to 1.13 ˚Cd mm^{-1} at 16.5 h of Pp. However, for FD10 lucerne crops, heightchron decreased with increased Pp; being 1.6 ˚Cd mm^{-1} at 10 h and 0.81 ˚Cd mm^{-1} at 16.5 h. The heightchron for FD10 was not different from FD5 as described in Section 8.3.1.2. The exponential decay functions had

three parameters for FD2: a=0.99, b=11740 and c=-1; and for FD10: a=0.82, b=25470 and c=-1.

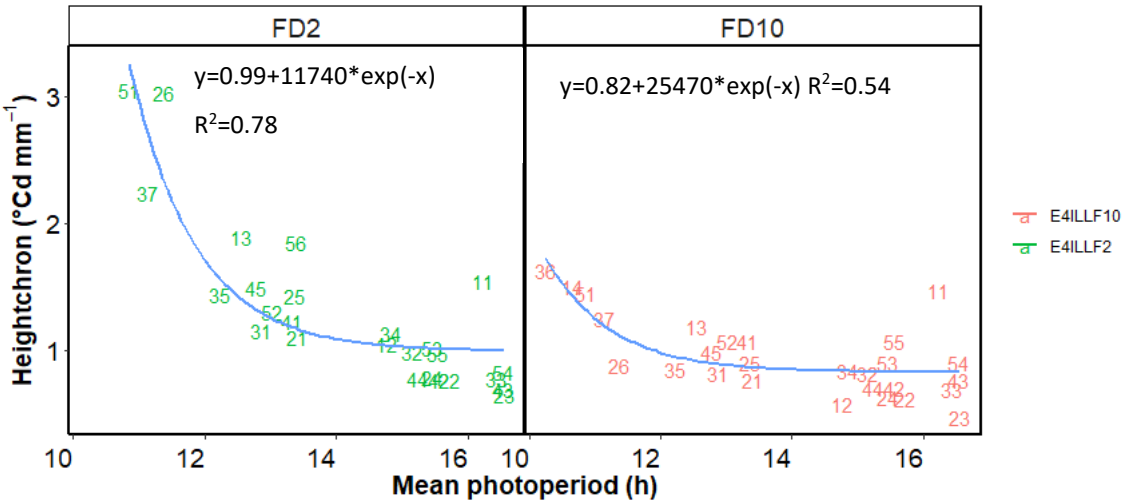

Figure 8.12. Heightchron against mean photoperiod (Pp) for FD2 and FD10 regrowth crops from Experiment 4 conducted at Lincoln University, Canterbury, New Zealand. The two dimension code represents growth years and regrowth cycles. The exponential decay functions with three parameters for FD2: a=0.99, b=11740 and c=-1; and for FD10: a=0.82, b=25470 and c=-1.

The verified height model was used to test FD2 and FD10 lucerne crops under different defoliation regimes. Overall, predicted and observed height values from Experiment 4 for two FD classes (FD2 and FD10) with multiple defoliation treatments (HH, LL, and SS) had good agreement, with NSE of 0.86 and R_RMSE of 31.8% (Figure 8.12 and Table 8.4). Both FD2 and FD10 had good agreement between predicted and observed values (NSE=0.82 and 0.88).

Among the three defoliation treatments, the HH and LL defoliation treatments had similar simulation results; R_RMSE values were 29.2% and 27.3% and NSE values were 0.81 and 0.83, whereas the SS treatment had the lowest agreement (R_RMSE=37.4%, NSE=0.71). Both FD2 and FD10 classes under the SS defoliation treatment had good agreement, with the highest R_RMSE value ~37% and NSE values ranging from 0.68 to 0.73.

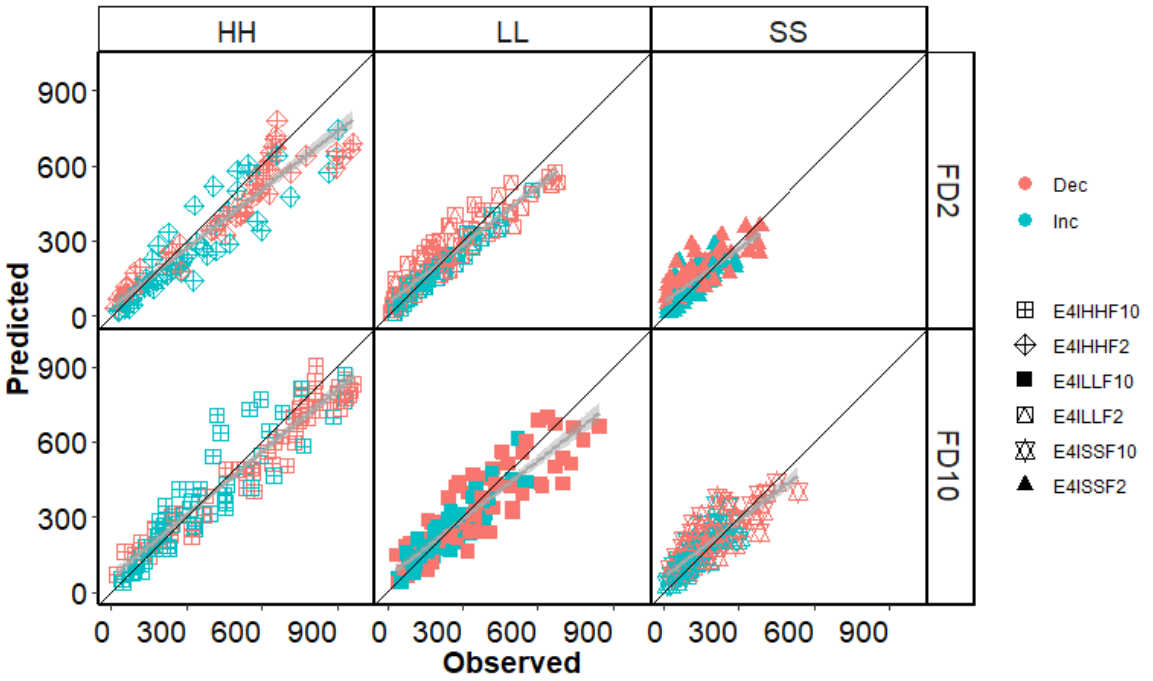

Figure 8.13. Predicted and observed values of plant height from Experiment 4 with three defoliation treatments [HH (84 day), LL (42 day) and SS (28 day)] and two fall dormancy (FD, FD2 and FD10) classes conducted between 2014 and 2019 at Lincoln University, Canterbury, New Zealand.

Table 8.4 Statistical measures of plant height from Experiment 4 with three defoliation treatments [HH (84 day), LL (42 day) and SS (28 day)] and two fall dormancy (FD, FD2 and FD10) classes conducted between 2014 and 2019 at Lincoln University, Canterbury, New Zealand. N = number of simulated and observed data pairs; R^2= coefficient of determination; R_RMSE = relative root mean square error (%); NSE = Nash-Sutcliffe efficiency; SB = Standard bias; NU = Nonunity slope; LC = Lack of correlation.

Treatment	N	R^2	R_RMSE	NSE	SB	NU	LC
Total	693	0.88	29.8	0.87	0.6	8	91.4
HH	217	0.88	25.6	0.85	11.7	5.3	82.9
LL	248	0.84	27	0.84	0.5	2.6	96.9
SS	228	0.69	41.9	0.64	13.3	1.3	85.4
FD2	346	0.88	33.8	0.86	1.5	14.3	84.2
FD10	347	0.89	26.6	0.88	0.1	5.2	94.6
Inc	313	0.84	34.5	0.83	1.1	1.7	97.2
Dec	380	0.90	26.9	0.89	0.4	15.7	83.9
E4IHHF2	108	0.87	30.6	0.81	20.4	8.7	70.8
E4IHHF10	109	0.90	21.3	0.88	4.7	6.3	89
E4ILLF2	124	0.88	26.2	0.87	0	9.6	90.4
E4ILLF10	124	0.80	26.9	0.79	1.4	0.3	98.3
E4ISSF2	114	0.64	47.9	0.58	12	2.2	85.7
E4ISSF10	114	0.72	37.4	0.67	14.5	0.7	84.8

8.4.2 **Leaf and stem quality simulation**

8.4.2.1 Leaf and stem CP simulation

A simple multiplication function based on leaf and stem N content for leaf and stem CP was used in the APSIM NextGen lucerne model. Therefore, the agreement of leaf and stem CP were the same as the leaf and stem N simulation (Appendix 57 for model structure of leaf and stem CP).

Overall, simulation results for predicting leaf and stem CP in each regrowth cycle of two Experiments 3 and 4 (Figure 8.14 and Figure 8.15; Table 8.5 and Table 8.6) showed fair overall agreement; R_RMSE values were 17.4% and 35%, respectively. However, prediction of leaf CP had a lower NSE value (0.18) compared with prediction of stem CP (0.42).

For leaf CP simulation, regrowth crops grown under the LL and SS treatments had fair agreement between predicted and observed values (NSE= 0.12 and 0.14). However, crops grown under the HH treatment had a poor agreement, with NSE of -0.34. Among the three

genotypes, simulation results showed fair agreement between predicted and observed values of leaf CP; NSE values ranged from 0.02 to 0.18.

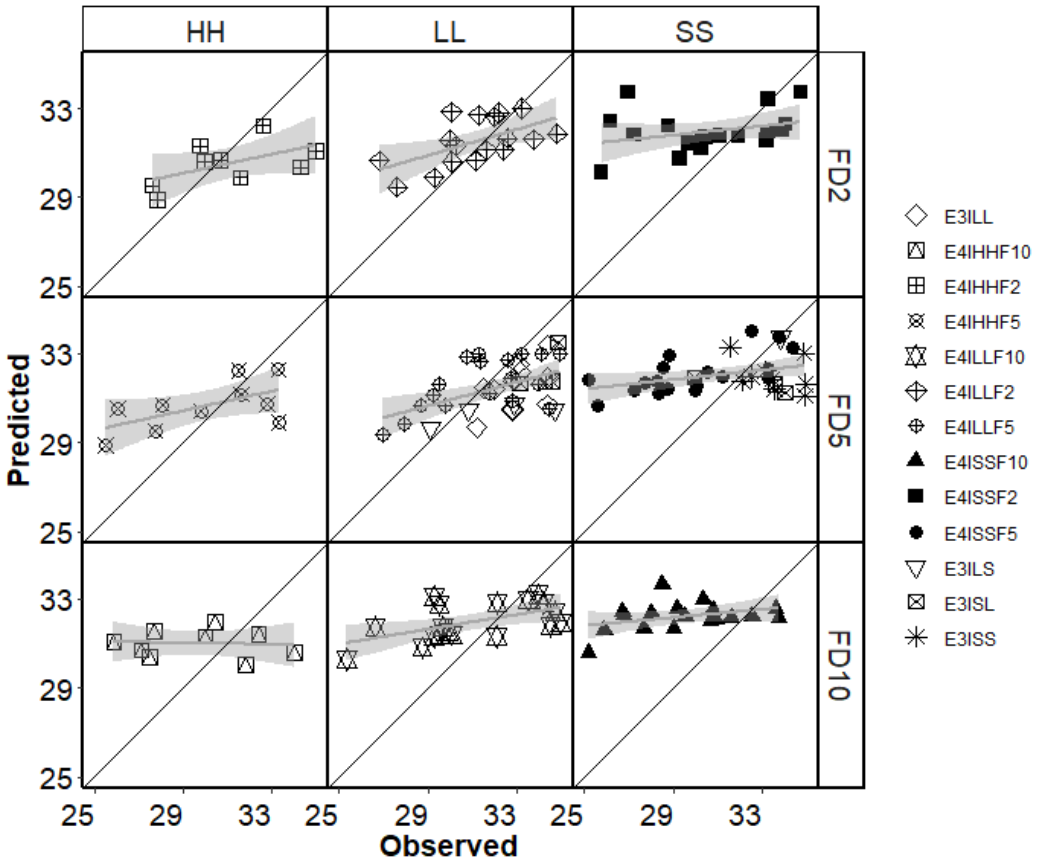

Figure 8.14. Predicted and observed values of leaf crude protein (CP, %) from Experiments 3 and 4 with multiple defoliation treatments [HH (84 day), LL (42 day), LS (42, 28 day), SL (28, 42 day), and SS (28 day)] and three fall dormancy (FD, FD2, FD5 and FD10) classes conducted between 2002 and 2019 at Lincoln University, Canterbury, New Zealand.

Table 8.5 Statistical measures of leaf crude protein (CP, %) values for Experiments 3 and 4 with multiple defoliation treatments [HH (84 day), LL (42 day), LS (42, 28 day), SL (28, 42 day), and SS (28 day)] and three fall dormancy (FD, FD2, FD5 and FD10) classes conducted from 2002 to 2019 at Iversen field, Lincoln University, Canterbury, New Zealand. n = number of simulated and observed data pairs; R^2= coefficient of determination; R_RMSE = relative root mean square error (%); NSE = Nash-Sutcliffe efficiency; SB = Standard bias; NU = Nonunity slope; LC = Lack of correlation.

Treatment	N	R^2	R_RMSE	NSE	SB	NU	LC
Total	269	0.33	17.4	0.18	1.8	16.7	81.5
HH	48	0.29	19.3	-0.34	40.1	7.1	52.8
LL	109	0.26	21.7	0.12	1.7	14.7	83.6
SS	112	0.21	11.8	0.14	1.7	6.8	91.6
FD2	64	0.29	13.1	0.16	7.4	7.6	85
FD5	139	0.34	19.6	0.18	0	19.3	80.7
FD10	66	0.39	15.6	0.02	21.8	16	62.2

For stem CP simulation, there was a fair overall agreement between predicted and observed values for regrowth crops grown under the three defoliation treatments; R_RMSE of 35%, and NSE of 0.42 (Figure 8.15 and Table 8.6).

Regrowth crops grown under the LL treatment had good agreement between predicted and observed values (NSE= 0.68). However, crops grown under the HH and SS treatment had poor to fair agreement, with NSE of -0.98 and 0.09. Among the three genotypes, FD5 had better simulation agreement compared with FD10 and FD2; NSE values ranged from 0.53 to -6.14.

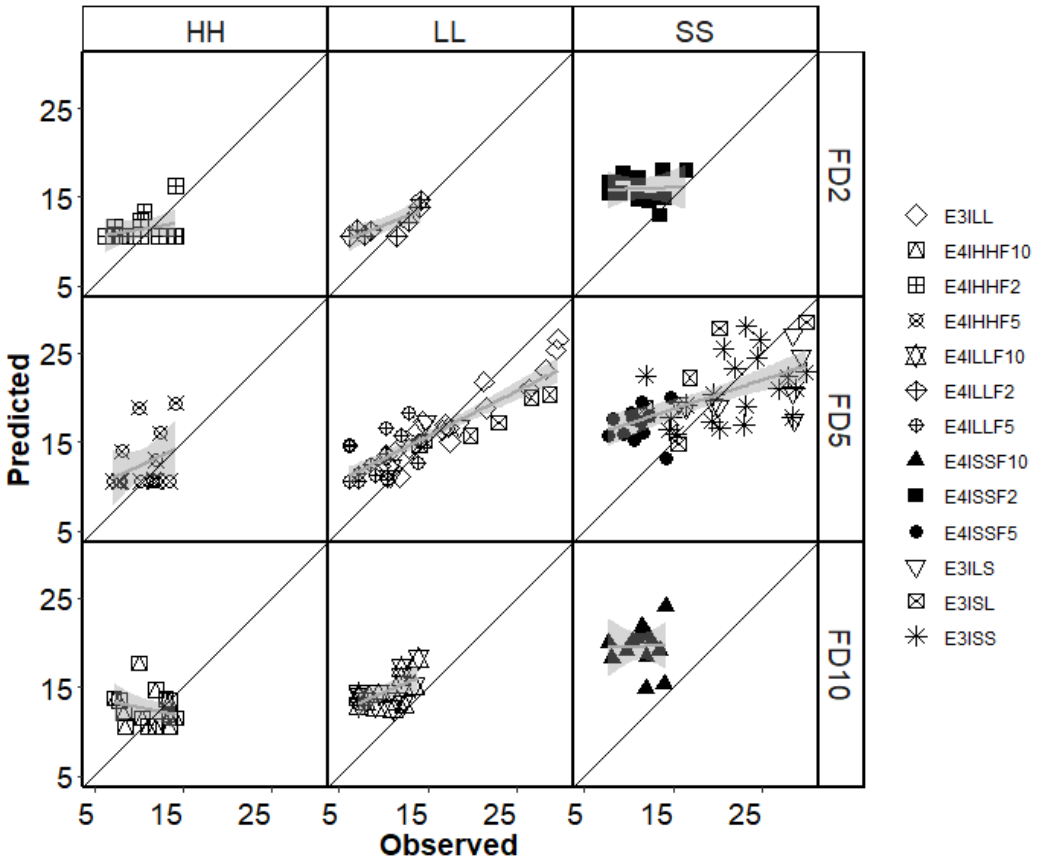

Figure 8.15. Predicted and observed values of stem crude protein (CP, %) from Experiments 3 and 4 with multiple defoliation treatments [HH (84 day), LL (42 day), LS (42, 28 day), SL (28, 42 day), and SS (28 day)] and three fall dormancy (FD, FD2, FD5 and FD10) classes conducted between 2002 and 2019 at Lincoln University, Canterbury, New Zealand.

Table 8.6 Statistical measures of stem crude protein (CP, %) values for Experiments 3 and 4 with multiple defoliation treatments [HH (84 day), LL (42 day), LS (42, 28 day), SL (28, 42 day), and SS (28 day)] and three fall dormancy (FD, FD2, FD5 and FD10) classes conducted from 2002 to 2019 at Iversen field, Lincoln University, Canterbury, New Zealand. n = number of simulated and observed data pairs; R^2= coefficient of determination; R_RMSE = relative root mean square error (%); NSE = Nash-Sutcliffe efficiency; SB = Standard bias; NU = Nonunity slope; LC = Lack of correlation.

Treatment	N	R^2	R_RMSE	NSE	SB	NU	LC
Total	192	0.52	35	0.42	16.4	1.0	82.6
HH	45	0.02	30.6	-0.98	15.1	35.3	49.5
LL	69	0.75	27.8	0.68	10.3	10.3	79.4
SS	78	0.32	39.2	0.09	23.7	1.1	75.2
FD2	33	0.11	35.1	-0.91	34.3	19	46.7
FD5	115	0.55	30	0.53	5.4	0.2	94.4
FD10	44	0.01	53.3	-6.14	52.9	33.2	13.9

8.4.2.2 Leaf and stem ME parameterization

Leaf ME ranged from 11 to 13 MJ kg^{-1} (Figure 8.16). Leaf ME decreased as leaf biomass increased. A broken-stick relationship was found between leaf ME and biomass for all treatments. Leaf ME declined from 12.5 MJ kg^{-1} at 100 kg ha^{-1} of leaf biomass (DM) to 11 MJ kg^{-1} with 2000 kg ha^{-1} leaf biomass. Leaf ME was consistent from 2000 to 4000 kg ha^{-1} of leaf biomass. Circled data were outliers from the late regrowth cycles of the HH treatment, which had senesced of leaf material in the samples (Appendix 58 for model structure of leaf ME).

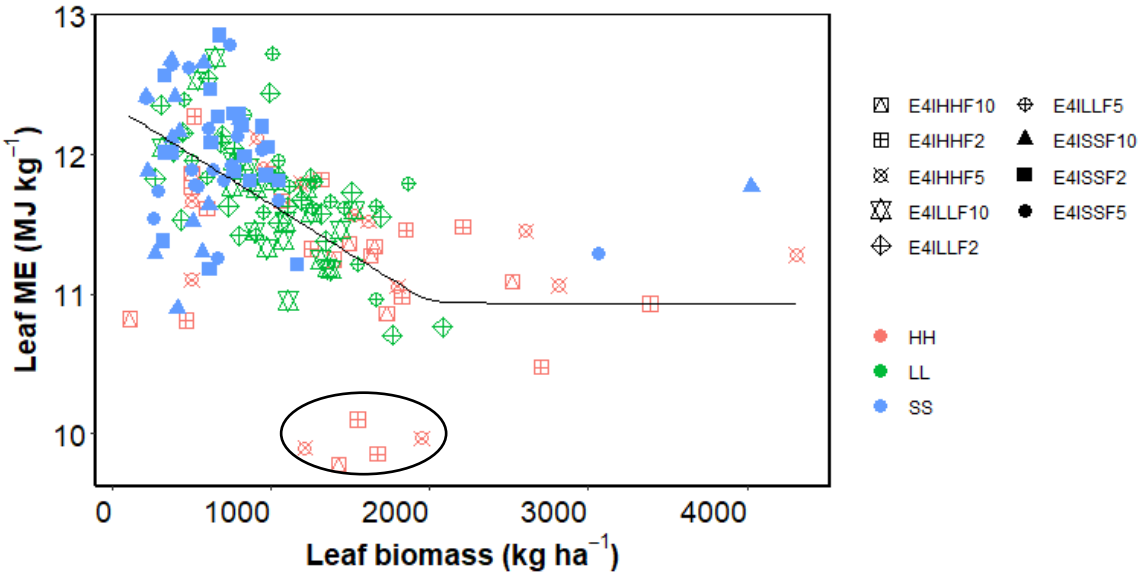

Figure 8.16. Leaf metabolisable energy (ME) against leaf biomass from Experiment 4 with three defoliation treatments [HH (84 day), LL (42 day) and SS (28 day)] and three fall dormancy (FD, FD2, FD5 and FD10) classes conducted from 2014 to 2019 at Lincoln University, Canterbury, New Zealand. The symbols represent combined treatments and the color represent defoliation treatments.

The ME thresholds for stem tissue ranged from 5.7 to 10.5 MJ kg^{-1} (Figure.8.17). Stem ME decreased as stem biomass increased. A broken-stick relationship was fitted between stem ME and biomass for all treatments. Stem ME declined from 9.5 MJ kg^{-1} at 100 kg ha^{-1} of stem biomass to 5.7 MJ kg^{-1} with 2600 kg ha^{-1} stem biomass. Stem ME was independent of stem biomass from 2600 to 6000 kg ha^{-1}. Circled data were outliers from the HH treatment which had senescence of stem material (Appendix 59 for model structure of stem ME).

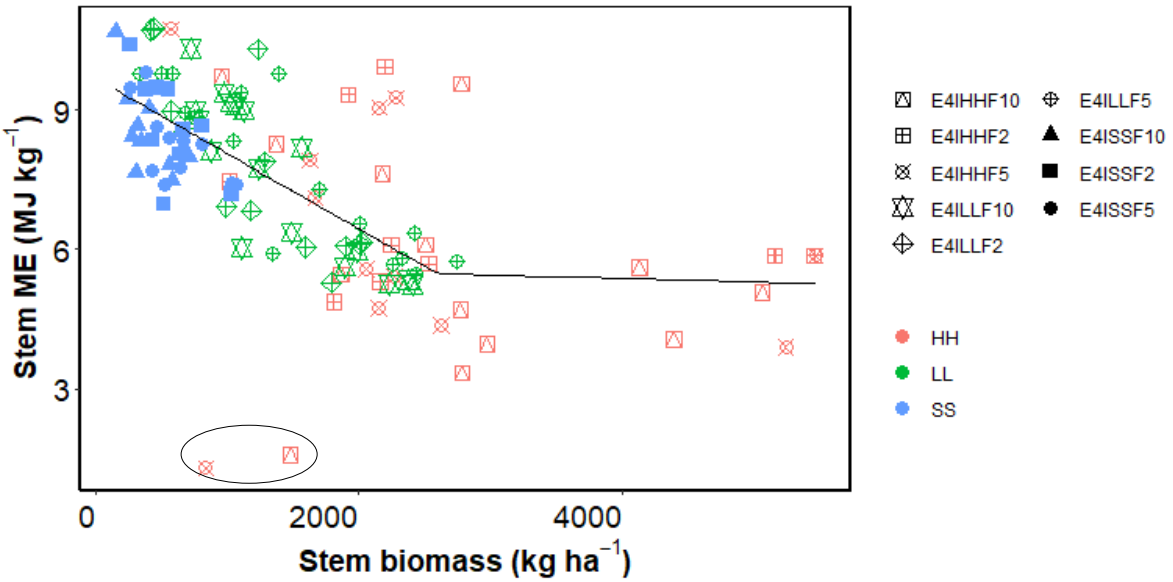

Figure 8.17. Stem metabolisable energy (ME) against stem biomass from Experiment 4 with three defoliation treatments [HH (84 day), LL (42 day) and SS (28 day)] and three fall dormancy (FD, FD2, FD5 and FD10) classes conducted at Lincoln University, Canterbury, New Zealand. The symbols represent combined treatments and the color represent defoliation treatments.

8.4.2.3 Leaf and stem ME simulation

Overall, predicted and observed leaf and stem ME values from Experiment 4 with multiple defoliation treatments (HH, LL and SS) for three FD classes (FD2, FD5 and FD10) had fair agreement, with NSE values of 0.38 and 0.49, respectively (Figures 8.18 and 8.19; Tables 8.7 and 8.8).

For leaf ME simulation, there was fair overall agreement between predicted and observed values (R_RMSE=3.8% and NSE=0.38). Most of the variation was from the SS treatment (NSE=-0.34). There was no difference among the three genotypes of FD classes in terms of prediction between predicted and observed values; R_RMSE values of ~3.8%, and NSE values of ~0.36.

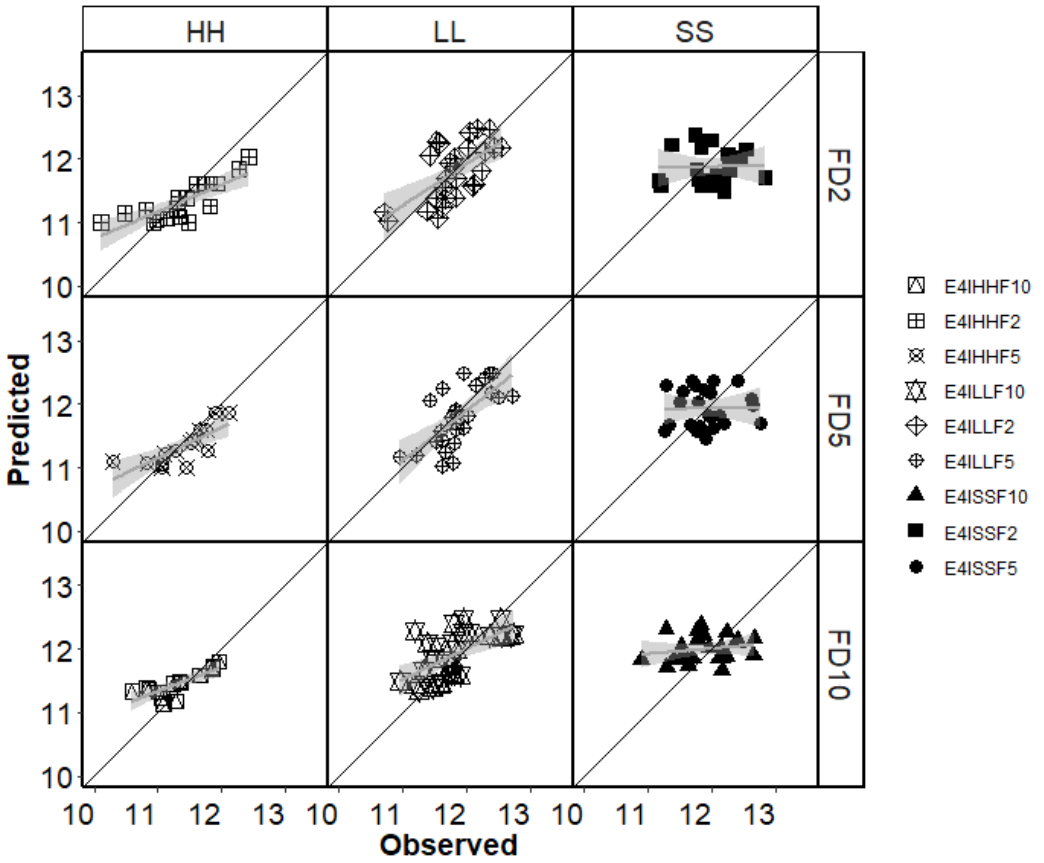

Figure 8.18. Predicted and observed values of leaf metabolisable energy (ME) from Experiment 4 with three defoliation treatments [HH (84 day), LL (42 day) and SS (28 day)] and three fall dormancy (FD, FD2, FD5 and FD10) classes conducted between 2014 and 2019 at Lincoln University, Canterbury, New Zealand.

Table 8.7 Statistical measures of leaf metabolisable energy (ME) values for Experiment 4 with three defoliation treatments [HH (84 day), LL (42 day) and SS (28 day)] and three fall dormancy (FD, FD2, FD5 and FD10) classes conducted from 2014 to 2019 at Iversen field, Lincoln University, Canterbury, New Zealand. n = number of simulated and observed data pairs; R^2= coefficient of determination; R_RMSE = relative root mean square error (%); NSE = Nash-Sutcliffe efficiency; SB = Standard bias; NU = Nonunity slope; LC = Lack of correlation.

Treatment	N	R^2	R_RMSE	NSE	SB	NU	LC
Total	199	0.39	3.8	0.38	0.7	2.2	97.2
HH	49	0.55	4.2	0.42	5.6	15.5	78.9
LL	81	0.39	3.2	0.25	0.2	17.5	82.4
SS	69	0.00	4.1	-0.34	0	25.5	74.5
FD2	66	0.42	3.8	0.41	0.6	1.7	97.7
FD5	66	0.39	3.8	0.36	0	4.5	95.5
FD10	67	0.43	3.7	0.36	10.3	0	89.7

For stem ME simulation, there was fair agreement between predicted and observed values among the three FD genotypes; R_RMSE values ranged from 15.7% to 19.4%, and NSE ranged from 0.55 to 0.40. For the three defoliation treatments, the HH treatment had closer agreement compared with the LL and SS treatments; R_RMSE values ranged from 10.9% to 21.6%, and NSE values ranged from 0.05 to 0.68.

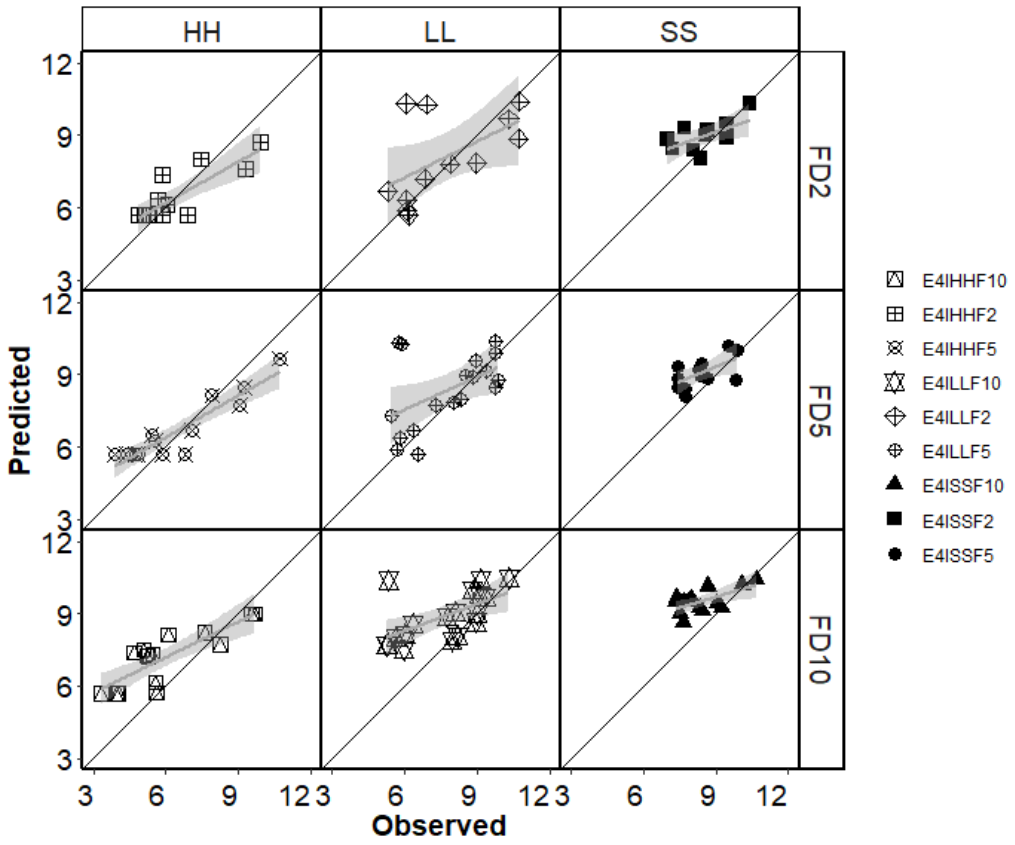

Figure 8.19. Predicted and observed values of stem metabolisable energy (ME) from Experiment 4 with three defoliation treatments [HH (84 day), LL (42 day) and SS (28 day)] and three fall dormancy (FD, FD2, FD5 and FD10) classes conducted between 2014 and 2019 at Lincoln University, Canterbury, New Zealand.

Table 8.8 Statistical measures of stem metabolisable energy (ME) values for Experiment 4 with three defoliation treatments [HH (84 day), LL (42 day) and SS (28 day)] and three fall dormancy (FD, FD2, FD5 and FD10) classes conducted from 2014 to 2019 at Iversen field, Lincoln University, Canterbury, New Zealand. n = number of simulated and observed data pairs; R^2= coefficient of determination; R_RMSE = relative root mean square error (%); NSE = Nash-Sutcliffe efficiency; SB = Standard bias; NU = Nonunity slope; LC = Lack of correlation.

Treatment	N	R^2	R_RMSE	NSE	SB	NU	LC
Total	130	0.55	17.3	0.49	8.9	2.7	88.4
HH	45	0.76	16.9	0.68	1.5	25.1	73.3
LL	48	0.26	21.6	0.05	7.6	14.7	77.8
SS	37	0.48	10.9	0.09	42.5	0.2	57.3
FD2	37	0.58	15.7	0.55	0	5.8	94.2
FD5	45	0.55	16.2	0.53	1.8	2.6	95.5
FD10	48	0.63	19.4	0.4	37.8	0.1	62

8.4.3 **Scenario testing**

8.4.3.1 Shoot yield

Stem height defoliation rules (300 mm for grazing or 450 mm for mechanical harvest) were applied to predict shoot long term biomass accumulation for the three locations (Alexandra, Lincoln and Napier). Predicted total annual shoot yields from 31-year establishment crops and regrowth crops for the three locations are shown in Figure 8.20. Overall, the 450 mm defoliation treatment resulted in higher annual shoot biomass, and regrowth crops produced more shoot biomass than seedling crops in the three locations.

Among the three locations, Napier had the highest predicted shoot biomass under the 450 mm defoliation treatment in both establishment and regrowth years. In contrast, at the Alexandra site, the lowest shoot biomass under 300 mm defoliation treatment was predicted in both establishment and regrowth years.

In Napier, there was a 50% probability of annual shoot biomass for establishment crops being below (or above) 14000 kg ha^{-1} under 300 mm defoliation treatment, and 16000 kg ha^{-1} under 450 mm defoliation treatment. For regrowth crops, a 50% probability was below (or above) 18000 kg ha^{-1} for 300 mm defoliation treatment and 21000 kg ha^{-1} for 450 mm defoliation treatment. In contrast, in Alexandra, there was a 50% probability of annual shoot biomass for establishment crops was below (or above) 11000 kg ha^{-1} under 300 mm and 12000 kg ha^{-1} under 450 mm defoliation treatments. For regrowth crops, there was a

50% probability of annual shoot biomass being below (or above) 14000 kg ha^{-1} for 300 mm defoliation and 17000 kg ha^{-1} for 450 mm defoliation treatment.

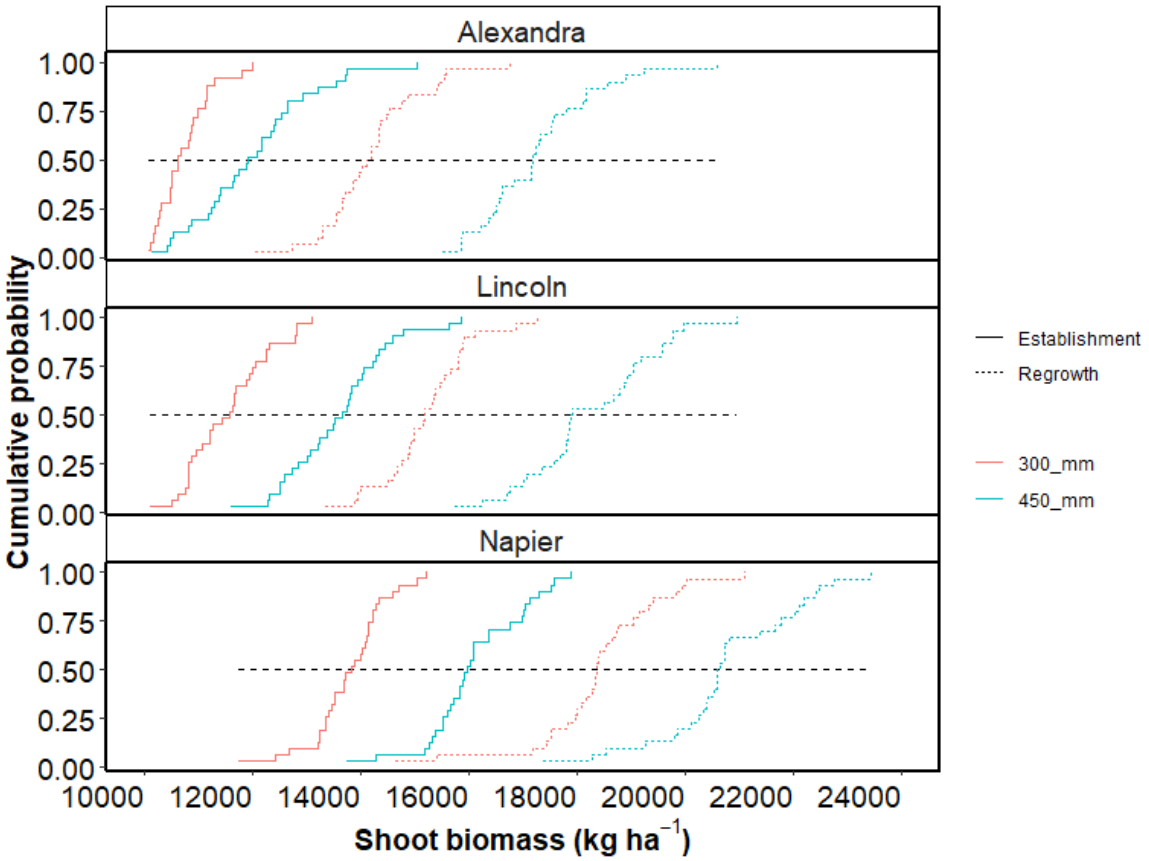

Figure 8.20. 31-year (1989-2019) predicted annual shoot biomass cumulative probability for establishment and regrowth years from three locations (Alexandra, Lincoln and Napier) in New Zealand.

Among the three locations, crops harvested at a 450 mm stem height resulted in a similar leaf biomass compared with harvest at 300 mm for both establishment and regrowth crops (Figure 8.21). However, crops harvested under the 450 mm defoliation treatment produced more stem biomass for both establishment and regrowth years. For example, Napier had the highest stem and leaf yield in regrowth years. For leaf biomass, a 50% probability was below (or above) ~11000 kg ha^{-1} for crops under both 300 and 450 mm defoliation treatments. In contrast, a 50% probability of stem biomass was below (or above) 8000 kg ha^{-1} under the 300 mm defoliation treatment and 10000 kg ha^{-1} under the 450 mm defoliation treatment. This result illustrates the trade-off between quantity and quality in gazing lucerne crops.

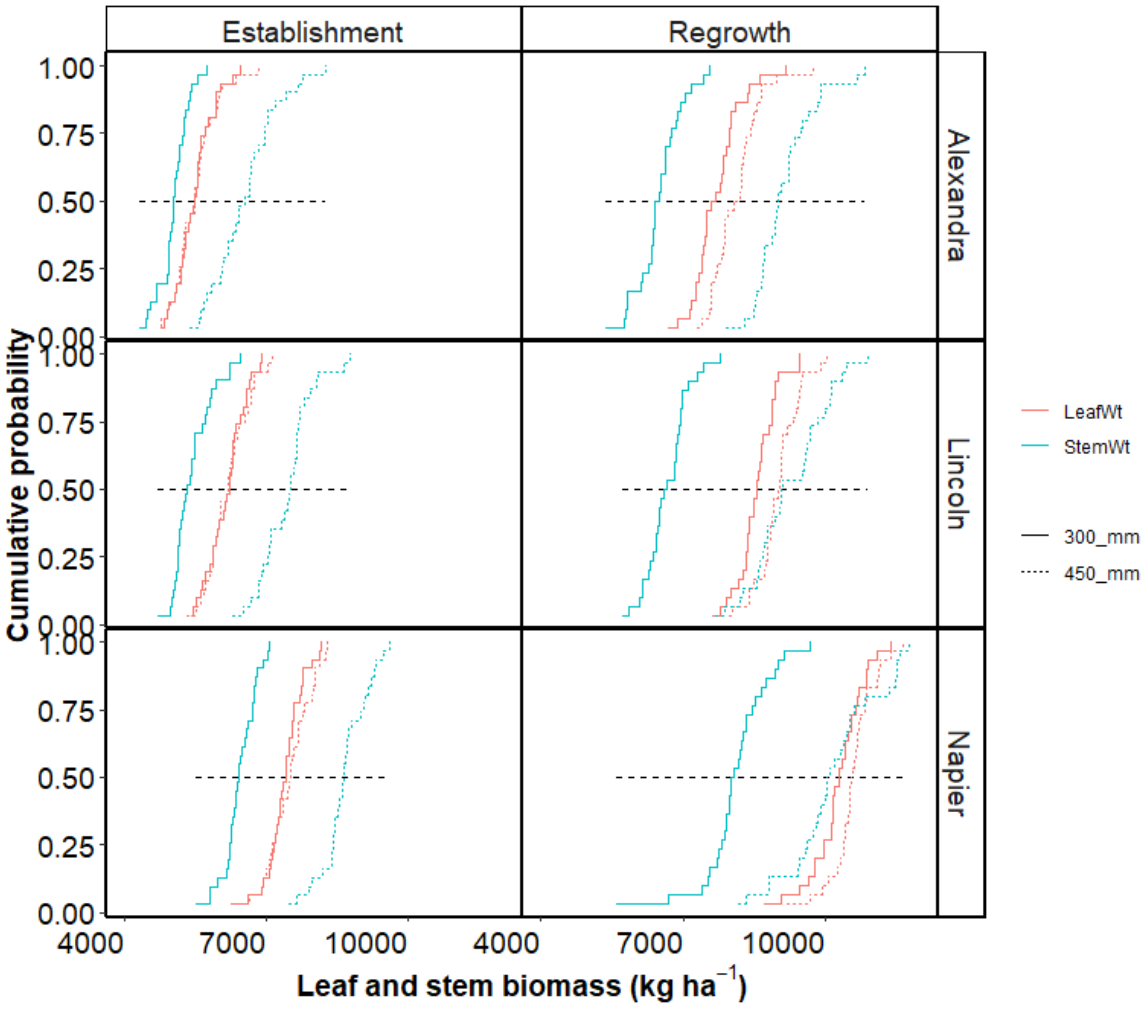

Figure 8.21. 31-year (1989-2019) predicted annual leaf and stem biomass cumulative probability for establishment and regrowth years from three locations (Alexandra, Lincoln and Napier) in New Zealand.

8.4.3.1 Crop regrowth cycles

The 300 mm of height defoliation treatment resulted in more regrowth cycles compared with the 450 mm defoliation treatment among the three locations. Regrowth years permitted crops to have more regrowth cycles compared with establishment years (Figure 8.22). Among the three locations, Napier had the most regrowth cycles for both establishment and regrowth year. For regrowth crops, a 50% probability was under (or above) 10 and 9 growth cycles under 300 and 450 mm treatments, respectively. In contrast, Alexandra had the lowest number of growth cycles for both establishment and regrowth years. For regrowth crops, there was a 50% probability of under (or above) 7 and 5 growth cycles under 300 and 450 mm treatments, respectively.

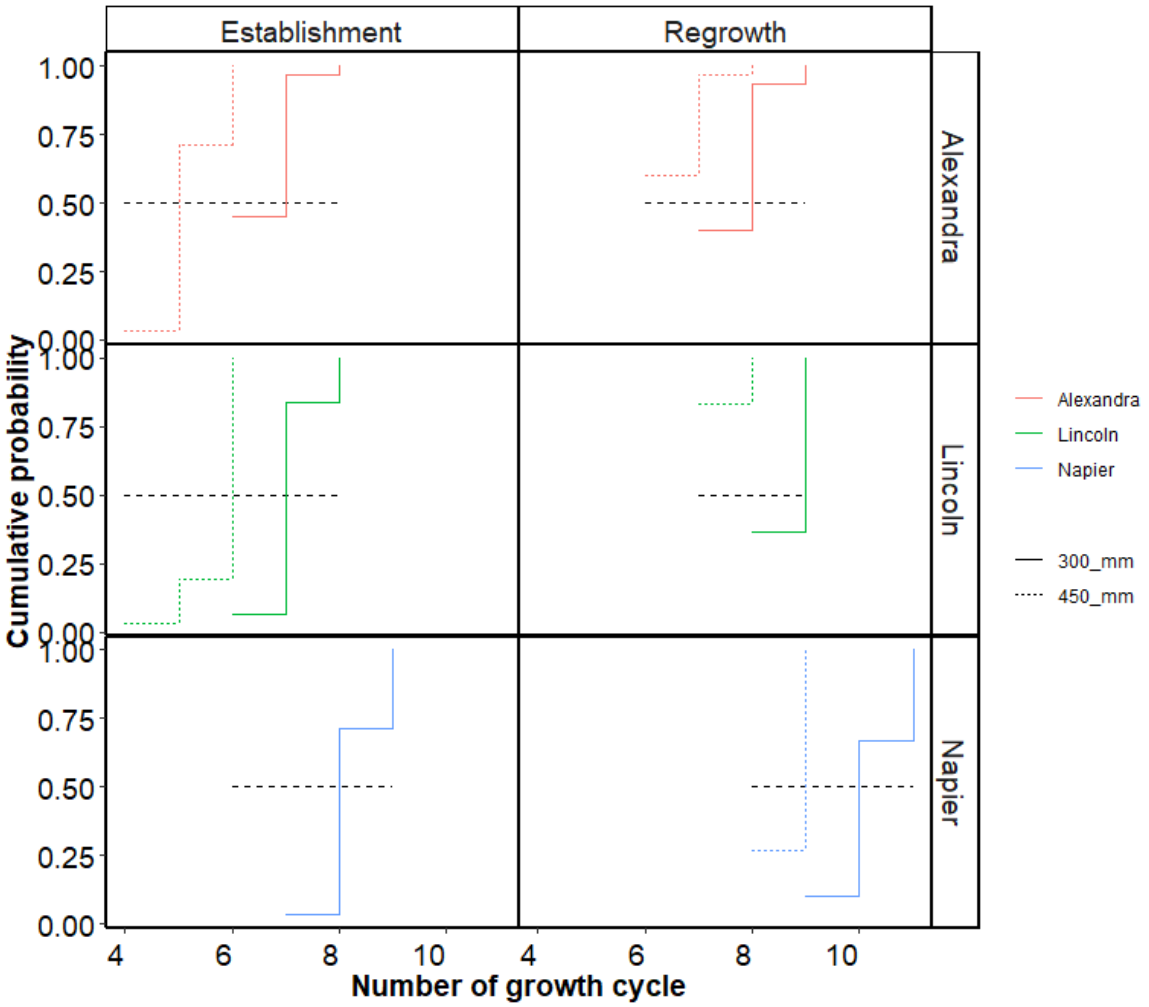

Figure 8.22. 31-year (1989-2019) prediction of number of growth cycle for establishment and regrowth years from three locations (Alexandra, Lincoln and Napier) in New Zealand.

8.4.3.2 Leaf and stem quality

Predicted leaf and stem CP and ME from 31-year establishment crops and 30-year regrowth crops for the three locations (Alexandra, Lincoln and Napier) is shown in Figures 8.23 and 8.24. Leaf CP values were higher than stem CP in all treatments and locations. The 450 mm defoliation treatment resulted in a higher total stem CP and ME compared with 300 mm defoliation treatment among the three locations. However, there was no difference in predicted total leaf CP and ME values for establishment and regrowth crops under 300 and 450 mm defoliation treatments. Higher total stem CP and ME resulted from increasing stem biomass.

Among the three locations, Napier had the highest total leaf and stem CP and ME under both the 300 and 450 mm defoliation treatments for establishment and regrowth crops.

For regrowth crops in Napier, a 50% probability of leaf CP was below (or above) ~3500 kg ha^{-1} for both the 300 and 450 mm defoliation treatments. However, the 450 mm defoliation treatment resulted in a 50% probability that total stem CP was below (or above) 2500 kg ha^{-1} compared with 2000 kg ha^{-1} under 300 mm defoliation treatment.

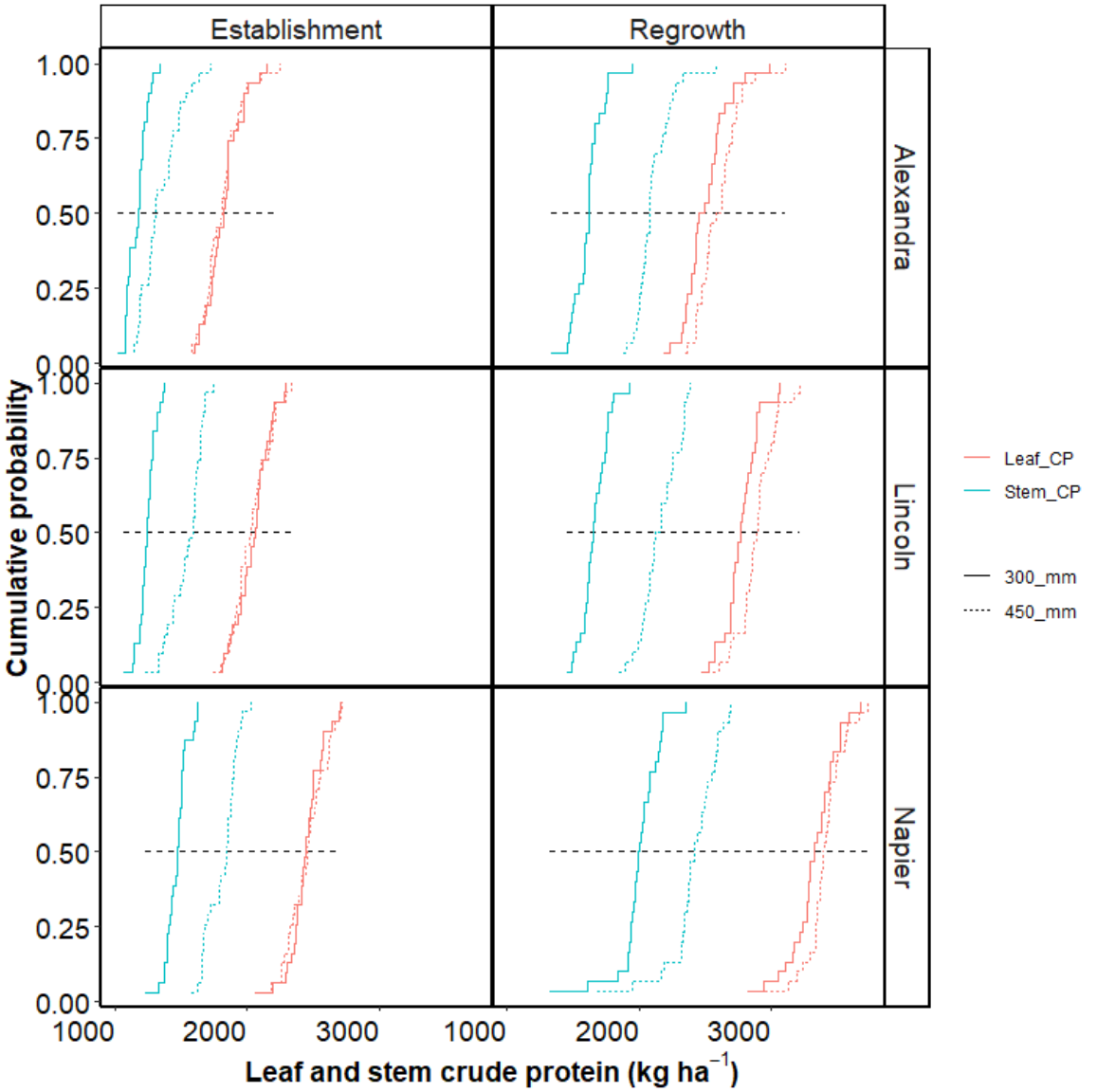

Figure 8.23. 31-year (1989-2019) predicted annual leaf and stem crude protein (CP) cumulative probability for establishment and regrowth years from three locations (Alexandra, Lincoln and Napier) in New Zealand.

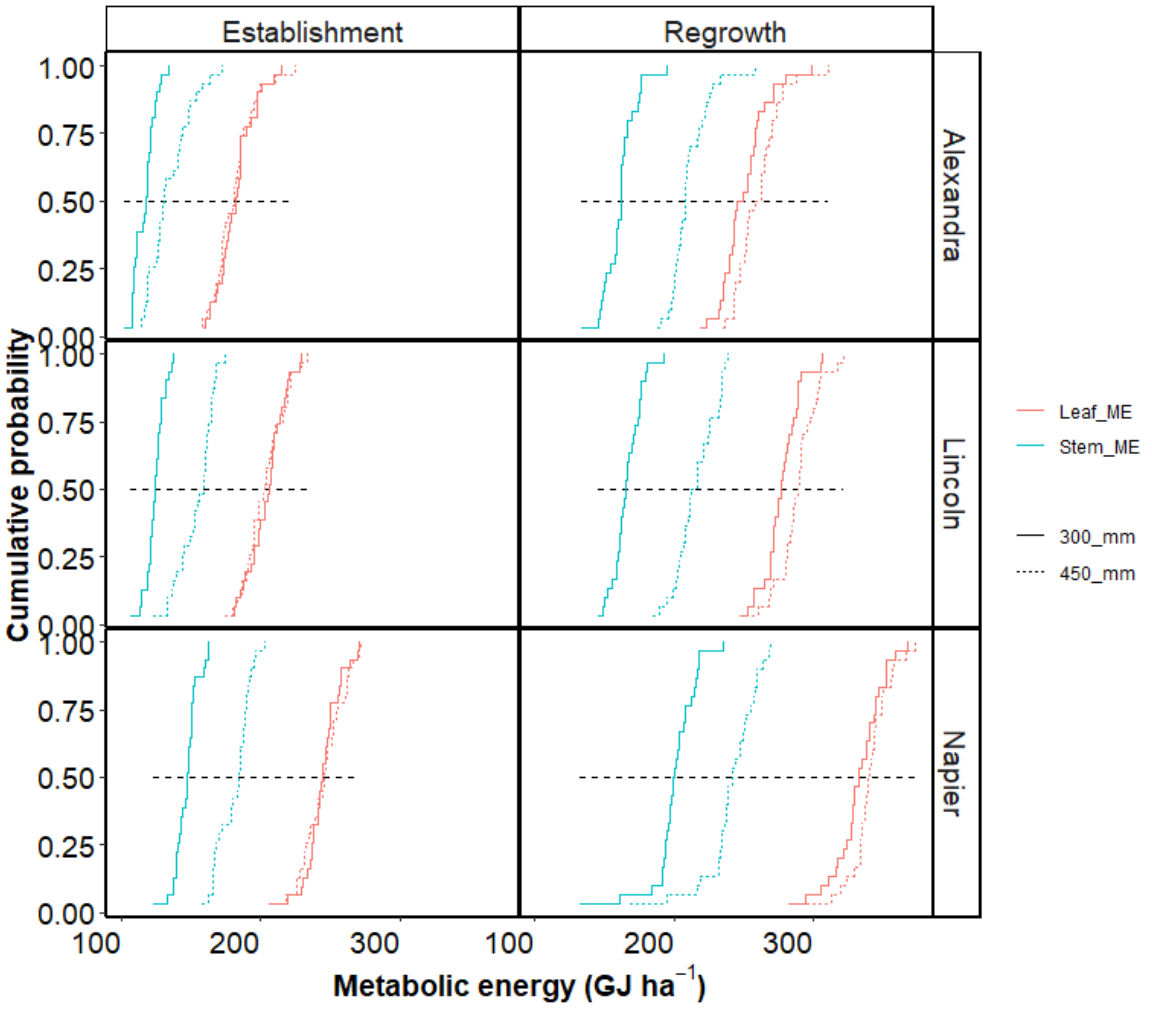

Figure 8.24. 31-year (1989-2019) predicted annual leaf and stem metabolisable energy (ME) cumulative probability for establishment and regrowth years from three locations (Alexandra, Lincoln and Napier) in New Zealand.

8.5 Discussion

Objective 5 of this thesis was to quantify and test the accuracy of prediction for forage quality, including plant height, crude protein (CP) and metabolisable energy (ME) of leaf and stem. The relationships for plant height derived from the FD5 genotype grown under the LL and HH defoliation treatment were successfully integrated into the model. These further tested using from FD2 and FD10 classes grown under different defoliation treatments to determine whether FD class or defoliation regime impacted lucerne plant height. Leaf and stem CP were calculated based on leaf and stem N concentration, and leaf and stem ME were calculated based on lab analysis values. The model was then used for scenario testing to compare forage yield and quality under two defoliation management in

three different lucerne growing regions (Canterbury, Central Otago and Hawkes Bay) in NZ under fully irrigated conditions.

8.5.1 Height and heightchron

For seedling and regrowth crops, plant height had a strong positive linear relationship with Tt. This suggests that temperature is the main driving factor for lucerne stem elongation under resource (water and N) unlimited conditions. This is consistent with response for both lucerne development (node appearance; Section 4.3.3) and leaf area expansion (Section 5.3.2). Heightchron was defined as the Tt requirement to elongate one mm of stem height. For regrowth crops, there was a strong exponential decay between heightchron and mean Pp. The rate decreased as Pp increased in both increasing and decreasing Pp conditions. This indicates that less Tt was required to elongate one mm of stem in long Pp conditions. For seedling crops, heightchron values were independent of Pp. However, heightchron values for seedling crops were higher than regrowth crops under the same Pp condition (Figure 8.4). This is consistent with seedling crops prioritizing partitioning to roots in the early growth stage (Sim, 2014; Ta et al., 2016). After plants reached the reproductive stage (50% buds visible), more Tt was required to elongate one mm of stem (Figure 8.8). $Heightchron_{rep}$ values were higher than in the vegetative stage, and also were independent of Pp. This could be explained by shifting carbon partitioning priority to reproductive organs and roots after plants reach in reproductive stage (Sinclair and Muchow, 1999; Ta, 2018). This is consistent with the demand and root partitioning rules, described in Chapter 6 (Sections 6.3.4.3 through 6.3.4.5). The base Pp for stem elongation was ~11 h. This confirmed that lucerne is a long day plant, and that stem elongation rate at and below 11 h was minimal.

Simulation of plant height showed good agreement between predicted and observed values for both seedling and regrowth crops grown under the LL treatment. Over-estimation was observed in E2ILLS3 treatments (sown in decreasing Pp condition; Figure 8.7). This was possibly due to a N limitation for seedling crop initial growth in autumn. This prediction agreement was improved after a N factor function was applied (NSE increased from -0.32 to 0.52). For the HH treatment, over-predictions were observed in mid-summer growth periods, most likely due to leaf senescence and lodging after the crop reached the reproductive stage. However, this response was not measured in the experiment. Thus,

more measured data for leaf senescence and lodging are needed for further model development.

8.5.1.1 Defoliation effect

The difference in prediction of height among defoliation regimes indicates that lucerne stem elongation was affected by defoliation treatments. This was consistent with the observation that different defoliation regimes created different root biomass and N reserves which affected plant regrowth (Teixeira et al., 2007c) (Chapters 6 and 7). Therefore, a simple linear model associated with root storage N was applied, which resulted in improved height predictions, especially in the SS treatment. This confirmed that plant height was affected by root storage N. However, the E3ISS treatment had poor prediction. This is because the SS defoliation was applied after it had been grown under a longer defoliation regime (LL) for two years. This suggests the E3ISS treatment had sufficient root N storage in the first regrowth year, and over-prediction was found in the first year simulation (Figure 8.9).

8.5.1.2 FD effect

Different FD classes had different heightchron functions (Figure 8.10). Exponential decay relationships were found between heightchron and Pp for both FD2 and FD10 genotypes. However, the FD2 genotypes showed a higher heightchron in short Pp (10-12 h) compared with FD10. This indicates that the FD10 required less Tt to elongate one mm of stem compared with the FD2 in a short Pp (early spring and late summer). This is consistent with the definition of FD, which is the reduction in shoot regrowth in the autumn, using plant height in autumn as the classification factor (Brummer et al., 2000; Teuber et al., 1998). In contrast, Ta et al. (2020) reported that FD10 produced more yield only in the first year, and this advantage was inconsistent over the next regrowth year. This could be explained by plant population declining in FD10 more rapidly than FD2, rather than plant height. A trade-off between internode length and node number of lucerne in response to FD was reported by Liu et al. (2015). However, our data showed no difference in node appearance rate among three the FD genotypes (Section 4.3.3.6), but plant height (internode length) among three the FD genotypes was different in response to a short Pp.

Predicted and observed values of plant height also had good agreement for both FD2 and FD10 under different defoliation treatments. This suggests that the APSIM NextGen lucerne model captured the height difference among the three FD genotypes. To our knowledge, no other lucerne model includes plant height for different lucerne FD genotypes.

8.5.2 Leaf and stem quality

Leaf CP values ranged from 25 to 33%. This is consistent with Brown and Moot (2004), who reported the lucerne palatable components (leaf and palatable stem) was 29%. Ta et al. (2020) reported that lucerne leaf contains the most nutritious components, with leaf CP constant at a value of 30%. Martiniello et al. (1997) compared leaf CP harvested at 40% bud and flowering stage, and found that leaf CP concentration was ~28% at 40% bud stage and ~25% at flowering stage.

In contrast, stem CP ranged from 7 to 27%. Similar results were reported by Ta et al. (2020), who reported soft stem (palatable) was 12% and hard stem was 7%. Data from different defoliation treatments showed that harvest frequency changed forage nutritive values regardless of the FD ranking. Specifically, the HH treatment had the lowest leaf and stem CP among all defoliation treatments. However, there were no differences among FD genotypes in terms of leaf and stem CP. In contrast, Rimi et al. (2012) reported that less non-dormant cultivars had higher CP than non-dormant and very non-dormant cultivars in the first two years, but showed no difference in the third year. Similar results were reported by Ta et al. (2020) (Experiment 4) that the yield and quality advantage of FD10 was only found in the first two years.

For leaf CP simulation, regrowth crops grown under the LL and SS treatments had closer agreement between predicted and observed values compared with crops grown under the HH treatment. This was due to fewer data points measured in the HH treatment, and its leaf CP values had a small range, from 25 to 33% (Figure 8.12). This also reflected the bias in the leaf N prediction (Section 7.3.6). Among the three genotypes, FD2 and FD5 had more accurate simulation agreement compared with FD10. This could be the consequence of poor agreement in N dynamics for FD10 (Section 7.3.7).

Leaf ME ranged from 9.5 to 13 MJ kg^{-1} (Figure 8.14). Similar results were reported by Brown and Moot (2004), in which the average ME of the lucerne palatable fraction was constant (~11.5 MJ kg^{-1}), and Ta et al. (2020) reported the average leaf ME was 11.7 MJ kg^{-1}. Leaf ME decreased as leaf biomass increased. A broken-stick relationship was found between leaf ME and biomass for all treatments. These results indicate that leaf ME decreased as leaf organ aged, especially for the HH treatment which had the lowest leaf ME at ~4000 kg DM ha^{-1} leaf biomass.

The ME thresholds for stem tissue ranged from 5.5 to 10.5 MJ kg^{-1} (Figure.8.15), which reflect the results were reported by Ta et al. (2020). The average ME of hard and soft stem were 5.3 and 8.5 MJ kg^{-1}, respectively. Stem ME decreased as stem biomass increased. A broken-stick relationship was fitted between stem ME and biomass for all treatments. This is consistent with increasing stem biomass resulting in lower shoot quality because of the increased lignification of stem tissue (Sadras and Lemaire, 2014). However, the APSIM NextGen lucerne model did not parameterize soft and hard stem separately, since the definition of soft and hard stem are subjective.

Simulation of leaf ME showed good agreement between predicted and observed values. Most of the variation was from the SS treatment (NSE=-0.32). This is because crops under the SS defoliation treatment had higher ME values, ranging from 11 to 13 MJ kg^{-1}. However, the leaf ME data showed a large variation which the linear regression model did not capture. There was no difference among the three genotypes tested in terms of predicted and observed values of leaf ME. For stem ME simulation, there was good agreement between predicted and observed values among the three FD genotypes. This suggests that a single function can be used to estimate lucerne quality among these three genotypes.

There are few lucerne models that simulate forage quality as CP and ME. In the DAFOSYM model (Rotz et al., 1989a), CP content of leaf and stem are calculated by separate relationships, which use growing degree days (GDD) as empirical models obtained from Fick and Onstad (1988). These empirical models only reflect the Tt impact on leaves and stem quality. They do not reflect N dynamics and CP changes within each regrowth cycle and across seasons, which is particularly important for grazing situations.

8.5.3 Scenario testing

The model was used for scenario testing to compare forage yield and quality under two defoliation managements in three different regions assuming unlimited conditions. As expected, Napier had the highest yield potential and Alexandra had the lowest yield potential. This is because Napier had the highest mean air temperature which lead to more accumulated thermal time (Tt) (Figure 8.1). Under the 450 mm defoliation treatment, 30 years establishment and regrowth shoot yield at 50% probability ranged from 13000 to 17000 kg ha^{-1} in Alexandra, 15000 to 18000 kg ha^{-1} in Lincoln and 18000 to 21000 kg ha^{-1} in Napier. These predicted shoot yield values were difficult to compare with published data from the same region due to different defoliation managements. Brash (1985) reported 15000 to 17000 kg ha^{-1} lucerne herbage yield for different cultivars under irrigated condition in Central Otago, which was similar to the predicted yield range in Alexandra. A range of yield from 12000 to 23000 kg ha^{-1} were been reported in Canterbury region (Brown et al., 2003; Ta et al., 2020; Teixeira et al., 2007a). The difference between our predicted yield in Lincoln and published data was due to different defoliation management. For example, defoliation management in scenario test simulation was based on plant height, whereas published data were from 42 day defoliation management. However, there is limited data on lucerne yields under irrigated conditions in the East Coast of North Island. McGowan et al. (2003) found that average yield ranged from 9600 to 12900 kg ha^{-1} depending on cultivars and season under dryland condition at Whatawhata research centre. Lucerne yield from their study was lower compared with predicted shoot yields in Napier, due to the summer water stress.

Another reason for the yield difference was that the number of growth cycle of harvestable crops were different among the three locations. For example, under the 450 mm defoliation treatment, nine or 10 growth cycles can be harvested in establishment, and regrowth years in Napier, whereas only 5 growth cycles can be harvested in establishment and 7 in regrowth years in Alexandra (Figure 8.22).

Harvest at 450 mm stem height resulted in higher shoot biomass compared with harvest at 300 mm for establishment and regrowth years in all three locations. This is because the longer regrowth duration allowed plants to accumulate more biomass. However, the increase of biomass was mostly observed in stem biomass, while leaf biomass remain

constant (Figure 8.21). This means that the increasing 150 mm of stem height resulted mostly from an increase in stem proportion in shoots. This suggests that as plants become taller, structural tissues of stems become a higher proportion of the shoot biomass and they contain less N (Chapter 7, Section 7.3.3).

Defoliation management based on stem height is an effective approach to maximize forage yield and quality. With the addition of plant height, leaf and stem quality module, the APSIM NextGen lucerne model is now more useful to estimate potential animal nutrition in farming systems. The model can be used to optimize stem height and forage quality, which allows users to estimate forage yield and quality to match animal needs and make informed decisions in both gazing and cut and carry systems.

8.6 Conclusions

The results of this chapter permit the following conclusions:

- Plant height had a strong positive linear relationship with Tt. Greater Tt was required for plants to grow one mm of height in a short Pp and in the reproductive phase.
- The difference of predicting height among all defoliation regimes indicates that lucerne stem elongation was affected by defoliation treatments. The reason for this was that different defoliation regimes created different root biomass and N reserves.
- Leaf CP ranged from 25 to 36%, and stem CP ranged from 10% to 25%. Leaf ME ranged from 11 to 12.5 MJ kg^{-1}. Leaf ME decreased as leaf biomass increased. The ME thresholds for stem tissue ranged from 5.5 to 10.5 MJ kg^{-1}. Stem ME decreased as stem biomass increased.
- The APSIM NextGen lucerne model had good to fair predictions of plant height, leaf and stem CP and ME under LL and HH defoliation for genotype FD2 and FD5. FD10 under the SS treatment had poor agreement due to poor prediction of biomass (Chapter 6) and N dynamics in Chapter 7.
- In the scenario testing, Napier had the highest yield potential among the three locations due to higher air temperature and therefore accumulated Tt. The 450 mm

compared with the 300 mm defoliation treatment, resulted in increasing stem biomass, which lead to increased low quality biomass.

9 GENERAL DISSCUSSION

9.1 Overview

The aim of this thesis was to develop a lucerne model in APSIM next generation (APSIM NextGen) that can accurately simulates the growth, development and quality of lucerne cultivars grown under different defoliation managements (Section 1.2). To achieve this, long-term datasets from three genotypes of three fall dormancy classes (FD; FD2, FD5 and FD10) grown under irrigated and multiple defoliation treatments (LL, LS, SL, SS and HH) were assembled from previous Experiments 1-3 and measured from a current field Experiment 4 (Section 3.1). These data were used for model calibration and verification. Specifically, datasets from long regrowth cycles (LL and HH treatments) with a semi-dormant genotype (FD5) were used for model calibration. Additional datasets that included multiple defoliation regimes and FD classes were used for model verification.

The APSIM NextGen lucerne model focuses on simulation of lucerne crops growth and development processes. The model proposed a mechanism for root carbon (C) and nitrogen (N) remobilization in spring and partitioning in autumn, which captured root C and N seasonal patterns and simulated the impact on shoot regrowth for perennial crops. The model structure can be segmented into six major physiological processes: (i) Crop development stages and phenology, (ii) Canopy expansion and radiation interception, (iii) Total radiation use efficiency (RUE), (iv) Biomass (or dry matter; DM) demand/partitioning of leaf, stem and root, (v) N supply (N uptake and N_2 fixation), and (vi) N demand/partitioning of leaf, stem and root.

The phenology module was parameterized as the crop response of thermal time (Tt) and photoperiod (Pp). The yield module was constructed based on the yield framework proposed by Monteith (1994) and modified by Teixeira et al. (2008) for perennial crops. In this framework, total biomass was estimated as the product of accumulated intercepted total radiation and radiation use efficiency (RUE_{total}, g DM MJ^{-1}), accumulated biomass was then allocated based on demand /partitioning of leaf, stem and root. The N module was associated with biomass in the Plant Modelling Framework (PMF) in APSIM NextGen. N supply includes N uptake (Root) and N_2 fixation (Nodules), whereas N demand and partitioning was built as a demand function for each organ.

To be a useful tool for animal nutrition in farming systems, the APSIM NextGen lucerne model also includes plant height, leaf and stem quality modules, which allow users to estimate forage yield and quality to match animal needs. Figure 9.1 shows a figure for the APSIM NextGen lucerne model structure and the main variables and parameters from each process are listed in Table 9.1. The calculated processes and variables, flow of energy or biomass and N (solid arrows) and relationships among components (dashed arrows) are discussed in this chapter. In addition, strengths and weakness and potential application of each model approach are also discussed.

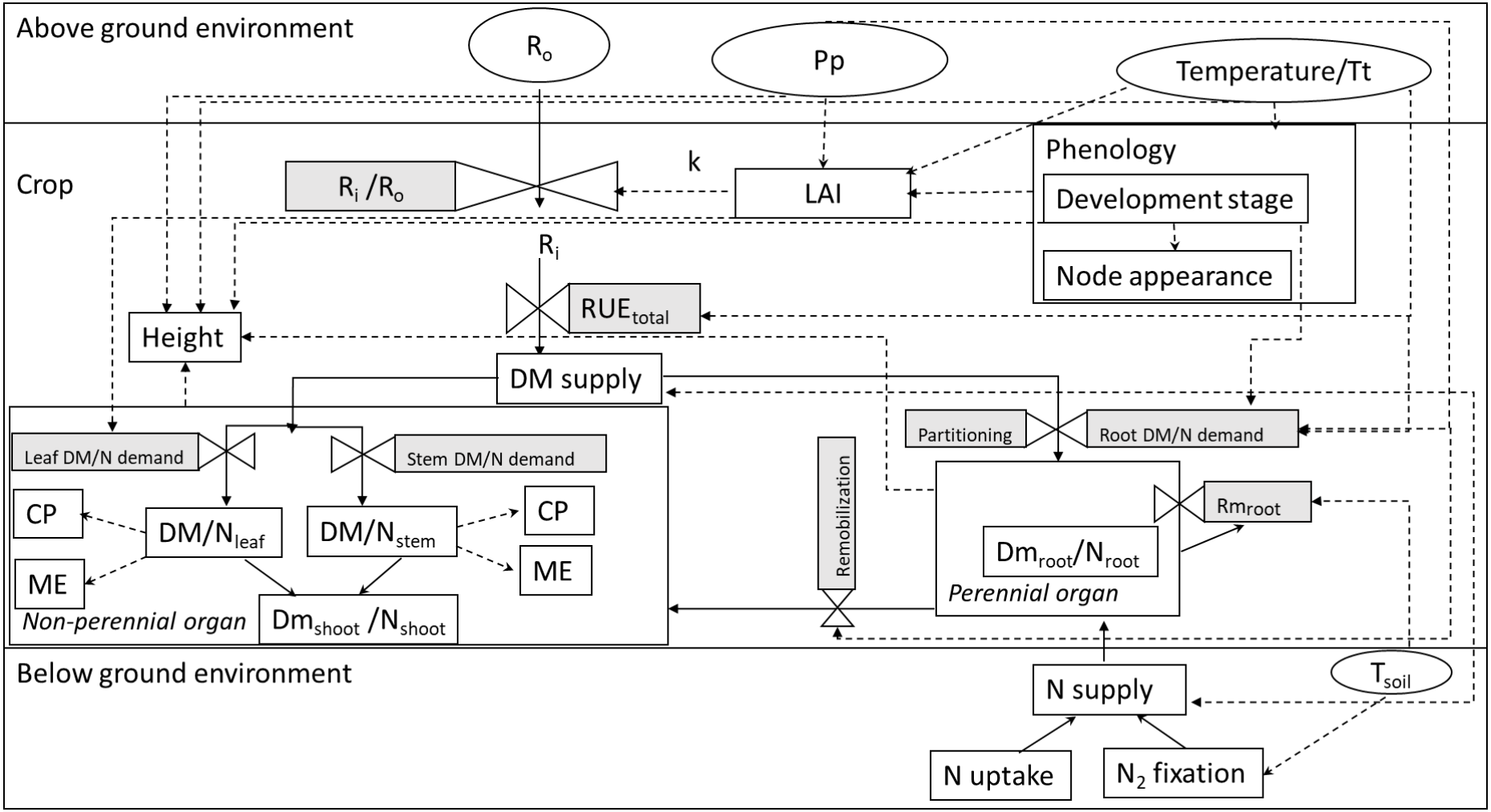

Figure 9.1. Structure of the APSIM NextGen lucerne model. Model components are represented as input variables (oval boxes) or state variables (rectangles). Processes are represented by grey boxes. Solid arrows indicate flow of energy or biomass and dashed arrows indicate relationships among components.

Table 9.1 Variables for the APSIM NextGen lucerne model developed using lucerne crop grown at Lincoln University, Canterbury, New Zealand.

Variable name	Definition	Units
	Environmental variables	
T_{max}	Daily max. air temperature	˚C
T_{min}	Daily min. air temperature	˚C
T_{mean}	Daily mean air temperature	˚C
T_{soil}	Daily mean soil temperature (100 mm)	˚C
Pp	Photoperiod	h day^{-1}
R_O	Total radiation	MJ m^{-2}
R_i/R_O	Fractional total radiation interception	-
	State variables	
DM supply	Dry matter supply from photosynthesis	g DM m^{-2}
DM_{leaf}	Accumulated leaf dry matter	g DM m^{-2}
N_{leaf}	Leaf N concentration	%
DM_{stem}	Accumulated stem dry matter	g DM m^{-2}
N_{stem}	Stem N concentration	%
CP	Leaf and stem crude protein	%
ME	Leaf and stem metabolisable energy	MJ g^{-1}
DM_{shoot}	Accumulated shoot dry matter	g DM m^{-2}
N_{shoot}	Shoot N concentration	%
Height	Stem height	mm
DM_{root}	Accumulated root dry matter	g DM m^{-2}
N_{root}	Root N concentration	%
LAI	Leaf area index	m^2 m^{-2}
Phenology	Development stage	-
N supply	N uptake and N_2 fixation	g N ha^{-1}
	Calculated variables	
k	Extinction coefficient	-
RUE_{total}	Total radiation use efficiency	g DM MJ^{-1}
Leaf DM/N demand	Leaf biomass and N demand	
Stem DM/N demand	Stem biomass and N demand	
Root DM/N demand	Root biomass and N demand	
Remobilization	Root biomass and N remobilization	
Rm_{root}	Root maintenance respiration	g g^{-1} day^{-1}

9.2 Modelling parameters and performance

9.2.1 Phenological model parameters and performance

The first step to build the APSIM NextGen lucerne model was to create a phenology module. Lucerne phenological development was affected by Tt and modified by Pp (Hanson et al., 1988). The Moot model with a T_b of 1 ˚C was the most accurate method for estimating Tt accumulation. Parameters for phenological development are shown in Table 9.2.

Development stage was parameterized as Tt targets and modified by a Pp response in the APSIM NextGen lucerne model. Seedling crops required a juvenile phase (Tt_{juv}; not respond to Pp) before they reached the bud visible stage. Therefore, a higher Tt accumulation was required for seedling crops to reach the bud visible phase compared with regrowth crops grown in the same temperature and Pp conditions. For both seedling and regrowth crops, the Tt to reach 50% buds visible ($Tt_{0\text{-}bv}$) increased as Pp shortened in autumn, a minimum of 278 ˚Cd for the basic vegetative (Tt_{BVP}) period was required at Pp >14h for regrowth crops. Once the reproductive organ (bud) initiated, temperature was the only driver (Teixeira et al., 2011). Pp had no influence on the duration between the bud visible and the flowering stage. $Tt_{bv\text{-}fl}$ of 310 ˚Cd was the only requirement to reach the flowering stage.

Phyllochron is the Tt requirement to develop one main stem leaf. Seedling crops had a consistent $phyllochron_{seedling}$ (~50 ˚Cd main stem $node^{-1}$). $Phyllochron_{veg}$ was constant (~31 ˚Cd main stem $node^{-1}$) in increasing Pp (spring), but responsive to decreasing Pp in autumn, from 49 to 35 ˚Cd main stem $node^{-1}$ as Pp decreased from 16 to 10 h. $Phyllochron_{rep}$ values doubled (~69 ˚Cd main stem $node^{-1}$) compared with the vegetative stage. In seedling and reproductive stages and autumn, lucerne crops had a higher phyllochron due to partitioning more biomass to roots. No Pp response was detected in seedling crops or when the crops were in the reproductive stage. This indicates that there is a more universal relationship between phyllochron and partitioning than Pp, and partitioning is more likely the dominant driver (Chapter 6).

Simulation results showed good agreement between predicted and observed values of days to buds visible, flowering stages and number of main stem nodes under different defoliation regimes and FD classes. Functions and parameters for phenological

development were not affected by defoliation regime and FD class. Therefore, no new parameter was needed for FD2 and FD10 genotypes (Table 9.2).

Table 9.2 Parameters for phenological development in the APSIM NextGen lucerne model.

Parameter name	Parameter description	Units	FD5	FD2	FD10
T_b	Base temperature	˚C	1	-	-
T_{opt}	Optimal temperature	˚C	30	-	-
T_{max}	Maximum temperature	˚C	40	-	-
Tt_{Juv}	Tt requirement to reach juvenile stage	˚Cd	215 to 547	-	-
Tt_{BVP}	basic vegetative phase	˚Cd	278	-	-
$Tt_{0\text{-}bv}$	Tt requirement to reach buds visible stage for regrowth crops	˚Cd	278 to 644	-	-
$Tt_{bv\text{-}fl}$	Tt requirement from buds visible stage to flowering stage	˚Cd	310	-	-
$Phyllochron_{seedling}$	Tt requirement to develop one main stem leaf in seedling crops	˚Cd node^{-1}	50	-	-
$Phyllochron_{veg}$	Tt requirement to develop one main stem leaf in vegetative stage	˚Cd node^{-1}	31 to 49	-	-
$Phyllochron_{rep}$	Tt requirement to develop one main stem leaf in regrowth stage	˚Cd node^{-1}	69	-	-

Note: symbol – represents the same parameter as for FD5.

9.2.2 Phenological model strengths and weaknesses

The accurate simulation of lucerne development stages is important because theseaffected several processes in the APSIM NextGen lucerne model (Figure 9.1). For example, node appearance is one of the components of the canopy. It was parameterized as a function of development stages (Chapter 4 and 5). Root demand and partitioning were also dependent on development stage. Root remobilization and demand changed when plants reached the reproductive stage (Chapter 6). This phenology module provides a framework to model buds visible and flowering stages for other perennial legume crops in APSIM NextGen.

The weakness in the phenology module, however, is that there were inefficient data points with daylengths of less than 12 hours for calibration. Hence more data at this end may

change this relationship dramatically. For example, the breakpoint could be at 12 hours to capture the data from E4IHHF5 treatment, but there was no further points between them to fit the function. Future phenology (day to buds visible) data collection is needed in daylengths of less than 12 hours.

9.2.3 Canopy expansion model parameters and performance

The ability to quantify canopy expansion is essential to simulate radiation interception and combine with RUE to estimate crop yield (Chapter 5). LAI was used as a crop factor to quantify canopy expansion. LAI showed a linear response to Tt (Figure 5.2). The slope of the linear regression represents the leaf area expansion rate (LAER). LAER showed a seasonal response pattern in increasing and decreasing Pp. In autumn, LAER declined as Pp decreased ($p<0.0001$). However, no Pp response in LAER was observed in seedling crops or regrowth crops in increasing Pp conditions. In addition, the three FD classes had different LAER functions (Table 9.3). In decreasing Pp, LAER decreased with decreased Pp for FD2, whereas LAER was constant (~0.01) for FD10 (Figure 5.9). This indicates that the FD2 genotype responded to Pp in decreasing Pp. In contrast, the FD10 was independent of Pp. This suggests that partitioning was possibly the dominant driver of this seasonal pattern (Chapter 6) which is not accounted for in the current empirical model.

The APSIM NextGen lucerne model used the LAER response to Pp functions to predict LAI expansion. Parameters for canopy expansion are shown in Table 9.3. However, this approach averaged the canopy response to temperature within each regrowth cycle into one value, which ignored the different growth phases within each regrowth cycle. Specifically, regrowth crops showed a slow regrowth phase before crops reach their linear growth phase at the beginning of each cycle. The x-intercept values from the linear regression between LAI and Tt ranged from ~-50 to ~200 ˚Cd. This indicates that some regrowth cycles (-50 to 0 ˚Cd) had leaves (basal buds) present before defoliation occurred. In contrast, some regrowth cycles required about 200 ˚Cd to reach the calculated LAER, described as a lag phase. Therefore, a lag phase function (Section 5.3.2.1) and a basal buds function (Section 5.3.2.3) were tested to improve to the accuracy of the model.

The lag phase function was parameterized as a linear function between Tt since defoliation date and a lag phase reduce factor (LRF). Tt since defoliation date increased from 0 to 200 ˚Cd as LRF increased from 0 to 1 (Section 5.3.2.1). A basal buds module was tested under

the assumption that crop starts to produce basal buds when they reach their reproductive stage in the prior regrowth cycle. The model simulation results suggest that the basal buds expansion rate was 20% of the potential LAER before defoliation occurred (Figure 5.5). However, to investigate whether basal buds might link in with the lag phase, more field observations are required from the early regrowth cycles to understand the timing and influence of basal bud initiation and expansion.

A senescence function was applied to model canopy senescence in the 84 day (HH) defoliation treatment. This showed a steep decline in LAI after peaked (Figure 5.7). However, more measurements of leaf senescence are required in the later regrowth cycle to validate this senescence function.

Applying the lag phase, basal buds and canopy senescence functions improved prediction accuracy of LAI. However, it is important to acknowledge that the average LAER values were from four different experiments. Subsequent analyses suggest the E4ILLF5 had water stress in some summer regrowth cycles (Ta et al., 2020). Therefore, LAER values from those regrowth cycles were lower than other treatments. Using the same LAER values resulted in overestimated LAI in the E4ILLF5 but underestimated in the E3ILL treatment (Figure 5.6). This issue should be addressed when a soil water module is applied in future model improvement, with values from E3ILL considered most accurate for estimating the maximum LAER.

Defoliation treatment also affected canopy expansion. Attempts to predict LAI from a function that varies LAER against Pp resulted in acceptable predictions between experiments under the LL and HH defoliation treatments. However, the model had a fair LAI prediction for the short defoliation treatment (SS) due to low root C and N reserves (Chapter 6 and 7).

The extinction coefficient (k) was the same for seedling and regrowth crops (0.81), and it was not affected by defoliation management or FD class.

Table 9.3 Parameters for canopy expansion in the APSIM NextGen lucerne model.

Parameter	Parameter description	Units	FD5	FD2	FD10
T_b	Base temperature for leaf area expansion	˚C	2	-	-
LAER	Leaf area expansion rate	$m^2\ m^{-2}\ ˚Cd^{-1}$	0.008 to 0.022	0.01 to 0.022	0.01 to 0.018
Lag phase	Leaf area expansion before reach LAER	˚Cd	0-200	-	-
LRF	lag reduce factor	%	0 to 1	-	-
BBF	Basal buds factor	%	0.2	-	-
k	Extinction coefficient		0.81	-	-

Note: symbol – represents the same parameter as for FD5.

9.2.4 Canopy expansion model strengths and weaknesses

Lucerne LAI components include main stem node appearance, branching, leaf expansion and senescence. All components respond to environmental factors differently throughout the season (Brown et al., 2005). LAER is an empirical approach to simulate canopy expansion which assume LAER changes in relation to Pp direction. This method integrates the crop canopy, but does not consider each component of the canopy, which includes nodes, branching, and leaf senescence (Brown et al., 2005). This is predominantly because detailed canopy component data are difficult to obtain in the field, and the challenge is to represent the complexity of different leaf and branching through the available model structure. However, the goal for canopy expansion simulation was to predict radiation interception. The critical LAI (LAI_{crit}) for lucerne was approximately 3.65 (Figure 5.12). Therefore, changes in LAI above LAI_{crit} will have little influence on radiation interception and subsequent growth simulations. Thus, a simple but robust model for canopy expansion is critical before crops reach the LAI_{crit}. Therefore, an empirical model was used in APSIM NextGen Lucerne model.

Changes in LAER in response to Pp was driven by the substantial proportion of total biomass and N that was translocated below-ground under a decreasing Pp (Teixeira et al., 2007b). This is because photosynthesis does not respond to Pp changes biologically, but Pp

direction changes lucerne C and N partitioning priority (Luo et al., 1995). Therefore, the LAER against Pp relationship is a surrogate for changes in C and N partitioning. The limitation of this empirical approach of modelling canopy expansion was also reflected in the SS treatment. For example, slower LAER under the SS treatment was due to low C and N reverses in perennial organs. However, the empirical model of LAER only considered temperature and Pp effects. Overestimation of LAI was found under the SS defoliation treatment (Figure 5.7). This issue will become more problematic in water stress and low plant population conditions. Therefore, a more mechanistic approach that links LAER with C and N availability is needed for further model development.

9.2.5 DM accumulation and partitioning model parameters and performance

Total shoot and root yield are determined primarily by the amount of radiation intercepted by the canopy and how efficiently it is used (Brown et al., 2006). The model is structured around the following assumptions; 1) total biomass assimilation is a function of radiation interception and total radiation use efficiency, 2) assimilated biomass can be partitioned to leaf, stem and root (crown and taproots), 3) root organ has structural and storage components, and storage biomass of perennial organs increases due to partitioning at certain times of the year and at defined stages of the regrowth cycle; and 4) perennial organ biomass can be reduced by maintenance respiration throughout the year, or remobilized to facilitate shoot regrowth.

The APSIM NextGen lucerne model used radiation interception and total RUE (RUE_{total}) to calculate total dry matter supply (Chapter 6, parameters are shown in Table 9.4). RUE_{total} was parameterized as a temperature response function, being 0 at 0 ˚C, and 1.1 MJ g^{-1} at 18 ˚C. An optimal temperature of 30 ˚C and a maximum temperature of 40 ˚C for photosynthesis was used, RUE_{total} was constant at 1.1 MJ g^{-1} from 18 to 30 ˚C, then declined to 0 at 40 ˚C. In this study, the RUE_{total} value was 1.1 g DM MJ^{-1} total radiation at 18 ˚C, lower than that previously reported (Brown et al., 2006; Teixeira et al., 2008; Thiébeau et al., 2011). The lower RUE_{total} reported in our experiment was the main factor responsible for lower shoot yields in the E4ILLF5 treatment (Figure 4b) and probably was due to summer water stress, despite efforts to fully irrigated the crops (Ta, 2018).

Total biomass supply was then allocated based on leaf, stem and root demand in the PMF (Brown et al., 2014). Specifically, leaf biomass demand was parameterized as a positive

power function between leaf biomass (g m^{-2}) and LAI (m^2 m^{-2}) (Figure 6.3). Stem biomass demand were parameterized as a positive power relationship between stem and shoot biomass (Figure 6.4). This indicates that lucerne crops invest a greater proportion of structural tissues as plants grow taller, to maintain an erect stature. However, root biomass decreased from spring to mid- summer and then increased to late autumn due to changes in partitioning to roots that occurred in the decreasing Pp (Figure 6.5 and 6.6).

To model this seasonal pattern, the APSIM NextGen lucerne model provided a mechanistic framework to model root biomass dynamics with structural and storage components. The storage component represents the dynamic fraction, which had different biomass demand in increasing and decreasing Pp. Structural root biomass (~2500 kg ha^{-1}) was defined and calculated as the x-intercept value of the linear regression between calculated root respiration and initial root biomass in winter, based on the assumption that structural root biomass does not respire (Figure 6.7). Storage root biomass demand was calculated as a ratio of structural root biomass. The ratios of storage to structural root differed among development stages and FD classes (Table 9.4).

Remobilization and partitioning among each organ were regulated by seasonal signals (Cunningham and Volenec, 1998). In increasing Pp, little carbon assimilate was transported from above-ground to below-ground (no storage root demand). The decrease of root biomass during this period was due to remobilization from below-ground to above-ground and maintenance respiration. For FD5, a remobilization coefficient value of 0.05 (5% of storage root biomass per day) was used to calculate root remobilization in increasing Pp. The regrowth coefficient function includes two parameters: remobilization duration and remobilization rate. This was used to test the null hypothesis that remobilization remained constant throughout the regrowth period. In increasing Pp, storage roots had no demand, but remobilization from root to shoot occurred within the first 300-350 ˚Cd in each regrowth cycle (remobilization rate being 1.5 from 0 to 300 ˚Cd; decreasing to 0 at 350 ˚Cd). In a decreasing Pp, storage roots had no demand in the first 300-350 ˚Cd in each regrowth cycle, shoot had the priority to DM allocation. However, 350 ˚Cd after harvest in each regrowth cycle, storage root had maximal demand. This mechanistic approach realistically represents the biological processes of remobilization in the regrowth cycle. A

constant root maintenance respiration coefficient (Rm_root_day) of 0.0005 g g^{-1}.day^{-1} was applied to model root storage maintenance loss.

For FD2 and FD10, the same remobilization coefficient value of 0.01 (1% of storage root biomass per day) was used to calculate root remobilization in increasing Pp. However, FD2 had the shortest remobilization duration of 250-300 ˚Cd within each regrowth cycle, whereas FD10 had the longest remobilization duration of 500-550 ˚Cd.

Table 9.4 Parameters for DM accumulation and partitioning in the APSIM NextGen lucerne model

Parameter name	Parameter description	Units	FD5	FD2	FD10
RUE_{total}	Radiation Use Efficiency for total biomass	g MJ^{-1}	0-1.1	-	-
Leaf demand	Two parameters from leaf demand power function		0.14 and 1.23	-	-
Stem demand	Two parameters from stem demand power function		39.5 and 0.85	-	-
Structural root demand	Structural root biomass	kg ha^{-1}	2500	-	-
Storage root biomass ratio	Storage to structural root ratio	%	Juvenile: 3; Vegetative: 1.6; Reproductive : 2.3.	Juvenile: 3; Vegetative: 1.6; Reproductive : 2.3.	Juvenile: 3; Vegetative: 2.5; Reproductive : 2.5.
Remobilization coefficient	Remobilization percentage of storage root per day	%	5	1	1
Remobilization rate	Remobilization coefficient adjust values		0-1.5	0-1.5	0-1.5
Remobilization duration	Tt since defoliation	˚Cd	300-350	250-300	500-550
Rm_root_day	Root respiration coefficient	g g^{-1} day^{-1}	0.0005	-	-

Note: symbol – represents the same parameter as for FD5.

9.2.6 DM accumulation and partitioning model strengths and weaknesses

The APSIM NextGen lucerne model implements perennial crop physiology, and models leaf, stem and perennial organs separately. To our knowledge, this is the first attempt to simulate lucerne perennial biomass remobilization and partitioning with seasonal signal changes. This modelling approach uses structural and storage components to represent source and sink relationships and mobilization among organs (Cannell and Thornley, 2000). This aspect is more important for analysing strong seasonality in root dynamics of perennial than annual crops. This framework can be used in other perennial crop modelling.

The APSIM NextGen lucerne model was able to capture root biomass seasonal changes under the HH and LL treatments. However, the current model does not capture root biomass dynamics under the SS defoliation treatment. This is possibly due to lower perennial organ N reserve levels which resulted from the SS defoliation treatment (Chapter 7). This suggest that further understanding of N dynamics in lucerne plants will be required to model the effects of defoliation regimes on lucerne biomass.

Lower RUE_{total} value used in the current model might result in underestimation of total biomass for no water stress conditions. An estimate of the maximum RUE_{total} value can be gained by fitting the regression through the upper bound in Figure 6.2 which would suggest a RUE_{total} of 1.52 at 18 ˚C is possible in this environment. Further model development is needed to test the RUE_{total} function under different plant available water level. In addition, the temperature from 19 to 40 ˚C was out of our measured range, thus this function should be tested in different locations with different temperature ranges.

The structural root biomass (~2500 kg ha^{-2}) was calculated from field experiments which had sufficient plant population (minimal plant population was ~200 m^{-2}). However, at lower plant populations, structural root biomass could be lower. It is important to acknowledge that root remobilization and partitioning related parameters were not direct measurements from field or lab. However, the model fitting processes were based on the understanding of plant biology of remobilization and partitioning. To validate and test these parameters, more field and lab data from different locations are required.

9.2.7 N accumulation and partitioning model parameters and performance

The hypothesis is that root biomass decreases resulted from N remobilization during early regrowth. Therefore lower root N reserves occur due to frequent defoliation, which leads

to slower regrowth (Teixeira et al., 2007c). Thus, the APSIM NextGen lucerne model includes an N module to quantify N dynamics and test the link between carbon (C) and nitrogen (N) (Chapter 7, parameters are shown in Table 9.5). The model is structured around the following assumptions; 1) total N assimilation is a function of N contraction of total biomass and photosynthesis rate; 2) assimilated biomass can be partitioned to leaf, stem and root (crown and taproots) based on N demand of each organ, and 3) root organ has structural and storage components, and storage N of perennial organs increases due to partitioning at certain times of the year and at defined stages of the regrowth cycle which are the same time as biomass partitioning; and 4) perennial organ N can be reduced remobilized to facilitate shoot regrowth.

An empirical model was used to estimate N supply as 2.5% of photosynthesis rate. N demand for each organ was parameterized by N concentration thresholds of leaf, stem and root. Specifically, leaf N concentration ranged from 3.6% to 6.8% (Figure 7.2), and N concentration decreased as leaf biomass increased in both increasing and decreasing Pp conditions, although this change was minor. Leaf N concentration was unaffected by defoliation or FD treatments. Stem N concentration ranged from 1% to 5.5% (Figure 7.4), and showed an allometric relationship with stem biomass. However, root as a reserve organ, showed a strong seasonal pattern which was consistent with biomass seasonal patterns. Root N concentration also varied with defoliation regimes and FD treatments (Figure 7.5).

Root N remobilization was parameterized as a function of three parameters, including the N remobilization coefficient and N regrowth coefficient function (remobilization duration and remobilization rate which were the same as biomass regrowth coefficient function). For FD5, 2% of storage root N per day was used as the N remobilization coefficient value for remobilization calculations in an increasing Pp (Figure 7.6). However, FD2 and FD10 had the same remobilization coefficient (0.5%), but FD10 had a longer remobilization duration (250-300 ˚Cd) compared with FD2 (500-550 ˚Cd) (Section 7.3.7).

Simulation results from the APSIM NextGen lucerne model showed fair agreement between predicted and observed values of leaf, stem and root N concentration. Leaf N values differed across leaf biomass, and there was no clear pattern within those data (Figure 7.8). Therefore, using leaf biomass to parameterize leaf N thresholds resulted in

systematic bias for leaf N prediction. This is an area that needs additional field measurement and a more effective approach of parameterization in the PMF. Stem N simulation had poor agreement probably due to insufficient measured stem N data for the HH and SS treatments. For root N simulation, the HH treatment showed good agreement between predicted and observed values. This indicated that the N module in APSIM NextGen was able to capture the seasonal pattern of N allocation in root. However, for the LL and SS treatments, prediction of root N had poor agreement. This could be because crops grown under the LL and SS treatments did not partition sufficient dry matter to nodules, which could down regulate N_2 fixation, which is not account for correctly.

Table 9.5 Parameters for N dynamics in leaf, stem and root in the APSIM NextGen lucerne model.

Parameter name	Parameter description	Units	FD5	FD2	FD10
N supply rate	Total dry matter	%	2.5	-	-
Leaf N_{max}	Maximum leaf N concentration	%	4-6	-	-
Leaf N_{crit}	Critical leaf N concentration	%	3.5-5.5	-	-
Leaf N_{min}	Minimum leaf N concentration	%	3.5-5.5	-	-
Stem N_{max}	Maximum stem N concentration	%	1.7-5	-	-
Stem N_{crit}	Minimum to maximum stem N concentration ratio	%	0.55	-	-
Stem N_{min}	Minimum to maximum stem N concentration ratio	%	0.55	-	-
Root N_{max}	Maximum root N concentration	%	1.5-2.5	-	-
Root N_{crit}	Critical root N concentration	%	0.9	-	-
Root N_{min}	Minimum root N concentration	%	0.9	-	-
N Remobilization coefficient	Remobilization percentage of storage root per day	% per day	2	0.5	0.5
N Remobilization rate	Remobilization coefficient adjust values		0-1.5	0-1.5	0-1.5
N Remobilization duration	Tt since defoliation	˚Cd	300-350	250-300	500-550

Note: symbol – represents the same parameter as for FD5.

9.2.8 N accumulation and partitioning model strengths and weaknesses

The APSIM NextGen lucerne model implements perennial crop physiology, and models leaf, stem and root N dynamics under different defoliation and FD treatment. Model structure was based on the assumption that lucerne perennial biomass seasonal patterns were driven by N remobilization and partitioning. Fitting a N dynamic improved biomass prediction, especially for the SS treatment. This framework of N dynamic simulation can be used in other perennial crop modelling in APSIM.

However, an empirical model was used to estimate N supply. This was because a lack of measured data from N_2 fixation to parameterize N supply (N uptake and N_2 fixation). Using 2.5% N of total biomass over-estimated N supply in the SS treatments. Future research is needed to model N_2 fixation in the APSIM NextGen lucerne model, especially for perennial crops. The APSIM NextGen lucerne model showed poor to fair agreement for leaf N, stem N and root. Those functions need further testing in different environmental conditions. Additional field measurement and a more effective approach of parameterization is needed in the PMF.

9.2.9 Forage quality model parameters and performance

Chapter 8 focused on lucerne forage quality and scenario testing, with parameters shown in Table 9.6. Forage quality includes plant height, leaf and stem crude protein (CP) and metabolisable energy (ME).

Plant height had a strong positive linear relationship with Tt. The slope of the linear regression (heightchron) was defined as the Tt requirement for stem to elongate one mm in height. Greater Tt was required for plants to grow one mm of height in short Pp, and in the reproductive phase. Plant height parameterized as an exponential decay function for the three FD genotypes. However, the FD2 genotypes showed a higher heightchron in short Pp (10-12 h) compared with FD10. This indicates that the FD10 required less Tt to elongate one mm stem compared with the FD2 in a short Pp (early spring and late summer) (Table 9.6).

The difference of predicting height among all defoliation regimes indicates that lucerne stem elongation was affected by defoliation treatments. The reason for this was that different defoliation regimes created different root biomass and N reserves which impacted stem elongation (Section 8.4.1.1).

Leaf and stem CP were parameterized as leaf and stem N concentration multiplied by 6.25. Leaf CP values had a small range, from 25 to 33% (Figure 8.12). Regrowth crops grown under the LL and SS treatments had closer agreement between predicted and observed values compared with crops grown under the HH treatment. This was due to fewer data points measured in the HH treatment. Among the three genotypes, FD2 and FD5 had closer agreement than FD10. This could be the consequence of poor agreement in leaf and stem N concentration for FD10 (Chapter 7.3.7).

Leaf ME ranged from 11 to 12.5 MJ kg^{-1} (Figure 8.14), and the ME thresholds for stem tissue ranged from 5.7 to 10.5 MJ kg^{-1} (Figure.8.15). A broken-stick relationship was found between leaf and stem ME and leaf and stem biomass for all treatments. This is consistent with increasing stem biomass resulting in lower shoot quality because of the increased lignification of stem tissue (Sadras and Lemaire, 2014).

Simulation of leaf ME showed fair agreement between predicted and observed values. However, most of the variation was from the SS treatment (NSE=-0.32). This is because crops under the SS defoliation treatment had higher ME values, ranging from 11 to 13 MJ kg^{-1}. However, the leaf ME data had large variation which the linear regression model did not represent. There was no difference among the three genotypes tested for predicted and observed values of leaf ME. For stem ME simulation, there was fair agreement between predicted and observed values among the three FD genotypes.

The APSIM NextGen lucerne model had good prediction of plant height, and fair and poor prediction of leaf and stem CP and ME under LL and HH defoliation for genotype FD2 and FD5. FD10 under the SS treatment had poor agreement due to poor prediction of biomass (Chapter 6) and N concentration in Chapter 7.

Table 9.6 Parameters for plant height and forage quality in the APSIM NextGen lucerne model.

Parameter name	Parameter description	Units	FD5	FD2	FD10
Heightchron$_{veg}$	Tt requirement to elongate one mm stem height in vegetative stage (exponential decay function with three parameters: a, b and c)	-	a = 0.62; b = 97660; c = -1	a = 0.99; b = 117400; c = -1	a = 0.82; b = 25470; c = -1
Heightchron$_{rep}$	Tt requirement to elongate one mm stem height in reproductive stage	-	2.5	-	-
N limitation factor	Percentage of heightchron	%	0-0.7	-	-
Crude protein	N concentration	%	6.25	6.25	6.25
Leaf ME	Leaf metabolisable energy		11 to 12.5	-	-
Stem ME	Stem metabolisable energy	Kg ha^{-1}	5.7 to 10.5	-	-

Note: symbol – represents the same parameter as for FD5.

9.2.10 Forage quality model strengths and weaknesses

A goal for building the APSIM NextGen lucerne model has been to predict lucerne forage yield and quality. The APSIM NextGen lucerne model is able to predict plant height, leaf and stem quality (CP and ME) under non-limiting environmental conditions. The model can be used to optimize stem height and forage quality, which allows users to estimate forage yield and quality to match animal needs and make informed decisions in both gazing and cut and carry systems. It can also help to estimate potential animal nutrition in farming systems.

Heightchron was an empirical function associated with Tt and Pp. However, stem elongation is driven by C and N availability. This limitation was reflected in the SS defoliation treatment, which was improved by applying the N restriction function (Section 8.4.1.4). The heightchron function should also be tested in water stress conditions for further model development.

Leaf and stem CP and ME were parametrized using leaf and stem biomass. However, phenology and the age of the material of crops also affect forage quality (CP and ME). Once

a crop starts to senesce leaf, the relationship between leaf quality and biomass might be different. Therefore, further model development should test leaf and stem CP and ME in different defoliation management and environmental conditions.

9.3 Model limitation and future work

It is important to acknowledge that calibration and validation of the APSIM NextGen lucerne model is an ongoing process. The work from this thesis is the first step towards the release of a comprehensive APSIM NextGen lucerne model. The modelling processes in each results chapter indicates areas where further research is needed to understand lucerne physiology and improve the current APSIM NextGen lucerne model. Some of the points that deserve future investigation follow.

9.3.1 Model validation in different environment

The next step for model improvement is to validate the APSIM NextGen lucerne model using data from different locations. The APSIM NextGen lucerne model was calibrated from data only collected in Lincoln University, Canterbury, New Zealand. Parameters and functions were then verified using data from different defoliation and FD treatments in the same location. Therefore, some important environmental factors included temperature and Pp were in a limited range. For example, the RUE_{total} function was only tested in the mean air temperature of 5 to 18 ˚C. This could be an issue for the model using in locations where temperatures are out of this range. Lucerne root seasonal pattern was regulated by Pp, remobilization and partitioning functions were related to Pp (average Pp ranged from 10 to 16.5 h in Lincoln). However, it is not clear if those functions are effective in a tropical region where the annual Pp change is smaller, or at higher latitudes where daylengthes are longer or shorter.

9.3.2 Dryland and water stress condition

All experiments used for creating the APSIM NextGen lucerne model were conducted under irrigated conditions with sufficient plant population. All parameters and functions generated from each results chapter did not consider water stress. Thus, it is necessary to test the current model under different water stress conditions. For example, parameters (e.g. LAER) sensitive to soil water content need to modified to cope water stress conditions.

9.3.3 Plant population and crop persistence

Crop persistence is an important characteristic for perennial crops, such as lucerne. Self-thinning of shoots is affected by both environmental factors and management (Teixeira et al., 2007a). However, the current APSIM NextGen lucerne model does not include a plant or stem population module to estimate crop persistence. Therefore, future work is needed to integrate lucerne plant and shoot population dynamics into the APSIM NextGen lucerne model.

9.3.4 Sensitivity and uncertainty test for estimated parameters

Model calibration in this thesis used two different approaches. The first approach used different data analyses to quantify the response functions and generate parameters, where data are available. The second optimization approach was used to estimate parameters when observed data were not measured. Several model optimization exercises were conducted to test different parameters in different physiological processes in this thesis. For example, the parameters involved in N supply, biomass and N remobilization and partitioning processes. Thus, sensitivity and uncertainty analysis for all parameters are necessary to improve the accuracy of model prediction.

9.4 Conclusions

The integration of crop physiological knowledge into the APSIM NextGen lucerne model to develop and verify a comprehensive process-based model was relatively successful to simulate crop development stage, canopy expansion, yield and quality under different defoliation regimes and among genotypes of FD classes. However, parameters and functions generated from model optimization need further testing and validation. The main findings in each chapter were:

- Chapter 4: Lucerne phenological development was driven by Tt and modified by Pp. Using Tt and Pp response functions can accurate simulate crop develop stage and node appearance. These functions were not affected by defoliation and FD treatments.

- Chapter 5. Attempts to predict LAI from a function that varies LAER against Pp, resulted in acceptably predictions between experiments under the LL and HH defoliation treatments. Applying the lag phase, basal buds and canopy senescence

functions improved prediction of LAI. However, more measurements are required in the early regrowth cycle to understand the relationship between basal buds initiation and expansion. However, this relationship is empirical and requires a more mechanistic approach.

- Chapter 6. A key step for modelling perennial crops is to simulate the seasonal dynamics of perennial organ biomass. The APSIM NEXTGEN model provided a feasible framework to simulate sink and source relationships among organs. For FD5, in an increasing Pp, a remobilization rate of 0.05 (remobilization coefficient: 5% of storage root biomass per day) was applied during the first 300-350 ˚Cd (remobilization duration). In a decreasing Pp, storage roots exhibited little remobilization but maximal demand.

- Chapter 7. Perennial biomass remobilization and partitioning are associated with N dynamics. Simulating N concentration of each organ improved biomass prediction, with the SS treatment most effectively predicted. The APSIM NextGen lucerne model had a fair prediction of N concentration among each organ of FD5, and a poor prediction of FD2 and FD10.

- Chapter 8. The APSIM NextGen lucerne model had good to fair prediction of plant height, leaf and stem CP and ME under the LL and HH defoliation for genotype FD2 and FD5. FD10 under the SS treatment had poor agreement due to poor prediction of biomass and N dynamics.

This thesis provides a framework used to build a perennial crop model in the PMF in APSIM NextGen. The APSIM NextGen lucerne model integrated knowledge about the response of lucerne crops to environmental factors and also the influence of defoliation and genotype of FD class treatments on these relationships. The simulation results demonstrated the current model is robust under non-limited environmental conditions to allow testing new hypotheses and identifying future research area.

REFERENCES

Andreucci, M. P., Black, A. D., and Moot, D. J. (2012). Cardinal temperatures and thermal time requirements for germination of forage brassicas. *Agronomy New Zealand* **42**, 181-191.

Atkin, O. K., Edwards, E. J., and Loveys, B. R. (2000). Response of root respiration to changes in temperature and its relevance to global warming. *The New Phytologist* **147**, 141-154.

Avice, J. C., Lemaire, G., Ourry, A., and Boucaud, J. (1997a). Effects of the previous shoot removal frequency on subsequent shoot regrowth in two Medicago sativa L. cultivars. *Plant and Soil* **188**, 189-198.

Avice, J. C., Ourry, A., Lemaire, G., and Boucaud, J. (1996). Nitrogen and carbon flows estimated by ^{15}N and ^{13}C pulse-chase labeling during regrowth of alfalfa. *Plant Physiology* **112**, 281-290.

Avice, J. C., Ourry, A., Lemaire, G., Volenec, J. J., and Boucaud, J. (1997b). Root protein and vegetative storage protein are key organic nutrients for alfalfa shoot regrowth. *Crop Science* **37**, 1187-1193.

Baruah, D., and Baruah, D. C. (2014). Modeling of biomass gasification: A review. *Renewable and Sustainable Energy Reviews* **39**, 806-815.

Baysdorfer, C., and Bassham, J. A. (1985). Photosynthate supply and utilization in alfalfa: A developmental shift from a source to a sink limitation of photosynthesis. *Plant Physiology* **77**, 313-317.

Beaudoin, N., Mary, B., Launay, M., and Brisson, N. (2009). Conceptual basis, formalisations and parameterization of the STICS crop model, Editions Quae, Versailles Cedex, pp. 304.

Belanger, G., Kunelius, T., McKenzie, D., Papadopoulos, Y., Thomas, B., McRae, K., Fillmore, S., and Christie, B. (1999). Fall cutting management affects yield and persistence of alfalfa in Atlantic Canada. *Canadian Journal of Plant Science* **79**, 57-63.

Ben-Younes, M. (1992). Modeling the temperature-mediated phenological development of alfalfa (*Medicago sativa* L.). Ph.D thesis, Oregon State University, Corvallis, Oregon, USA.

Black, A. D., Moot, D. J., and Lucas, R. J. (2006). Development and growth characteristics of Caucasian and white clover seedlings, compared with perennial ryegrass. *Grass and Forage Science* **61**, 442-453.

Bonhomme, R. (2000). Bases and limits to using 'degree.day' units. *European Journal of Agronomy* **13**, 1-10.

Bourgeois, G., Savoie, P., and Girard, J. M. (1990). Evaluation of an alfalfa growth simulation model under Québec conditions. *Agricultural Systems* **32**, 1-12.

Brash, D. (1985). Lucerne cultivar comparisons: Herbage yields under irrigation and on dryland in Central Otago. *Proceedings of the New Zealand Agronomy Society* **15**, 121-125.

Brouwer, B., Ziolkowska, A., Bagard, M., Keech, O., and Gardestrom, P. (2012). The impact of light intensity on shade-induced leaf senescence. *Plant, Cell & Environment* **35**, 1084-1098.

Brown, H., Huth, N., and Holzworth, D. (2018). Crop model improvement in APSIM: Using wheat as a case study. *European Journal of Agronomy* **100**, 141-150.

Brown, H., Moot, D., and Pollock, K. (2003). Long term growth rates and water extraction patterns of dryland chicory, lucerne and red clover. *In* Legumes for Dryland Pastures (D. Moot, ed.). New Zealand Grassland Association, 11,91-99.

Brown, H. E. (2004). Understanding yield and water use of dryland forage crops in New Zealand. Ph.D thesis, Lincoln University, Canterbury, New Zealand.

Brown, H. E., Huth, N. I., Holzworth, D. P., Teixeira, E. I., Wang, E., Zyskowski, R. F., and Zheng, B. (2019). A generic approach to modelling, allocation and redistribution of biomass to and from plant organs. *in silico Plants* **1**.

Brown, H. E., Huth, N. I., Holzworth, D. P., Teixeira, E. I., Zyskowski, R. F., Hargreaves, J. N. G., and Moot, D. J. (2014). Plant Modelling Framework: Software for building and running crop models on the APSIM platform. *Environmental Modelling & Software* **62**, 385-398.

Brown, H. E., and Moot, D. J. (2004). Quality and quantity of chicory, lucerne and red clover production under irrigation. *Proceedings of the New Zealand Grassland Association* **66**, 257-264.

Brown, H. E., Moot, D. J., and Teixeira, E. I. (2005). The components of lucerne (*Medicago sativa* L.) leaf area index respond to temperature and photoperiod in a temperate environment. *European Journal of Agronomy* **23**, 348-358.

Brown, H. E., Moot, D. J., and Teixeira, E. I. (2006). Radiation use efficiency and biomass partitioning of lucerne (*Medicago sativa* L.) in a temperate climate. *European Journal of Agronomy* **25**, 319-327.

Brummer, E. C., Moore, K. J., and Bjork, N. C. (2002). Agronomic consequences of dormant–nondormant alfalfa mixtures. *Agronomy Journal* **94**, 782-785.

Brummer, E. C., Shah, M. M., and Luth, D. (2000). Reexamining the relationship between fall dormancy and winter hardiness in alfalfa. *Crop Science* **40**, 971-977.

Cannell, M. G. R., and Thornley, J. H. M. (2000). Modelling the components of plant respiration: Some guiding principles. *Annals of Botany* **85**, 45-54.

Carlsson, G., and Huss-Danell, K. (2003). Nitrogen fixation in perennial forage legumes in the field. *Plant and Soil* **253**, 353-372.

Christian, K. R. (1977). Effects of the environment on the growth of alfalfa. *In* Advances in Agronomy (N. C. Brady, ed.), Vol. 29, pp. 183-227. Academic Press.

Cichota, R., McAuliffe, R., Lee, J., Minnee, E., Martin, K., Brown, H. E., Moot, D. J., and Snow, V. O. (2020). Forage chicory model: Development and evaluation. *Field Crops Research* **246**, 107633.

Confalonieri, R., and Bechini, L. (2004). A preliminary evaluation of the simulation model CropSyst for alfalfa. *European Journal of Agronomy* **21**, 223-237.

Confalonieri, R., Bellocchi, G., Bregaglio, S., Donatelli, M., and Acutis, M. (2010). Comparison of sensitivity analysis techniques: A case study with the rice model WARM. *Ecological Modelling* **221**, 1897-1906.

Cunningham, S. M., Gana, J. A., Volenec, J. J., and Teuber, L. R. (2001). Winter hardiness, root physiology, and gene expression in successive fall dormancy selections from 'Mesilla' and 'CUF 101' alfalfa. *Crop Science* **41**, 1091-1098.

Cunningham, S. M., and Volenec, J. J. (1996). Purification and characterization of vegetative storage proteins from alfalfa (*Medicago sativa* L.) taproots. *Journal of Plant Physiology* **147**, 625-632.

Cunningham, S. M., and Volenec, J. J. (1998). Seasonal carbohydrate and nitrogen metabolism in roots of contrasting alfalfa (*Medicago sativa* L.) cultivars. *Journal of Plant Physiology* **153**, 220-225.

Cunningham, S. M., Volenec, J. J., and Teuber, L. R. (1998). Plant survival and root and bud composition of alfalfa populations selected for contrasting fall dormancy. *Crop Science* **38**, 962-969.

Denison, R. F., and Loomis, R. S. (1989). An integrative physiological model of alfalfa growth and development, University of California, Division of Agriculture and Natural Resources, Oakland, California, pp. 73.

Dougherty, C. T. (1976). Water in the crop model SIMED 2. *In* Soil and plant water symposium. Proceedings of soil and plant water symposium, 126, 103-110.

Douglas, J. A. (1986). The production and utilization of lucerne in New Zealand. *Grass and Forage Science* **41**, 81-128.

Eyduran, E., Zaborski, D., Waheed, A., Celik, S., Karadas, K., and Grzesiak, W. (2017). Comparison of the predictive capabilities of several data mining algorithms and multiple linear regression in the prediction of body weight by means of body

measurements in the indigenous Beetal goat of Pakistan. *Pakistan Journal of Zoology* **49**.

Fairey, D. T., Fairey, N. A., and Lefkovitch, L. P. (1996). The relationship between fall dormancy and germplasm source in North American alfalfa cultivars. *Canadian Journal of Plant Science* **76**, 429-433.

Fick, G. W. (1975). ALSIM 1-Level 1 User's Manual, Agronomy Mimeo 75-20, Department of Agronomy, Cornell University, Ithaca, New York, USA.

Fick, G. W. (1977). The mechanism of alfalfa regrowth: A computer simulation approach. *Search Agriculture* **7**, 1-28.

Fick, G. W. (1981). ALSIM 1-Level 2 user's Manual, Agronomy Mimeo 81-35, Department of Agronomy, Cornell University, Ithaca, New York, USA.

Fick, G. W., Holt, D. A., and Lugg, D. G. (1988). Environmental physiology and crop growth. *In* Alfalfa and alfalfa improvement (A. A. Hanson, D. K. Barnes and R. R. Hill, eds.), pp. 163-194. American Society of Agronomy, Madison, Wisconsin.

Fick, G. W., and Onstad, D. W. (1988). Statistical models for predicting alfalfa herbage quality from morphological or weather data. *Journal of Production Agriculture* **1**, 160-166.

Fishbeck, K. A., Heichel, G. H., and Vance, C. P. (1987). Dry matter, nitrogen distribution, and dinitrogen fixation in contrasting alfalfa symbioses. *Crop Science* **27**, 1205-1209.

Gallagher, J. N., Biscoe, P. V., and Wallace, J. S. (1979). Field studies of cereal leaf growth: IV. winter wheat leaf extension in relation to temperture and leaf water status. *Journal of Experimental Botany* **30**, 657-668.

Gao, L., and Hannaway, D. B. (1985). ALFAMOD: An agroclimatological computer model of alfalfa production. *Jiangsu Journal of Agricultural Sciences* **2**, 1-11.

Ghiocel, C. D., Dragomir, N., Dragomir, C., Schipor, R., Moraru, N., and Văcariu, D. (2013). Nitrogen fertilisation and nodosity-forming capacity in alfalfa. *Scientific Papers Animal Science and Biotechnologies* **46**, 169-171.

Gosse, G., Lemaire, G., Chartier, M., and Balfourier, F. (1988). Structure of a lucerne population (*Medicago sativa* L.) and dynamics of stem competition for light during regrowth. *Journal of Applied Ecology* **25**, 609-617.

Gramshaw, D., Lowe, K., and Lloyd, D. (1993). Effect of cutting interval and winter dormancy on yield, persistence, nitrogen concentration, and root reserves of irrigated lucerne in the Queensland subtropics. *Australian Journal of Experimental Agriculture* **33**, 847-854.

Halbleib, M. D., Daly, C., and Hannaway, D. B. (2012). Nationwide crop suitability modeling of biomass feedstocks. *In* Sun Grant Initiative National Conference, New Orleans, Los Angeles. Science for Biomass Feedstock Production and Utilization, 2-5.

Hammer, G. L. (1998). Crop modelling: current status and opportunities to advance. *Acta Horticulturae* **456**, 27-36.

Hannaway, D. B., and Shuler, P. E. (1993). Nitrogen fertilization in alfalfa production. *Journal of Production Agriculture* **6**, 80-85.

Hanson, A. A., Barnes, D., Hill, R. R., Heichel, G. H., Leath, K., Hunt, O., Marten, G., Tesar, M., Mickelson, S., and Holtgraver, K. (1988). Alfalfa and alfalfa improvement, American society of agronomy, Madison, Wisconsin, pp. 1084.

Hay, R. K., and Porter, J. R. (2006). The physiology of crop yield, 2nd/Ed. Blackwell Publishing, Cambridge, UK., pp. 314.

Hay, R. K., and Walker, A. J. (1989). Introduction to the physiology of crop yield, Longman Scientific & Technical, New York.

He, W., Grant, B. B., Smith, W. N., VanderZaag, A. C., Piquette, S., Qian, B., Jing, Q., Rennie, T. J., Bélanger, G., Jégo, G., and Deen, B. (2019). Assessing alfalfa production under historical and future climate in eastern Canada: DNDC model development and application. *Environmental Modelling & Software* **122**, 104540.

Hewitt, A. E. (2010). New Zealand soil classification, 3th/Ed. Manaaki Whenua - Landcare Research, Lincoln, New Zealand, pp. 136.

Hodges, T. (1990). Predicting crop phenology, 1st/Ed. CRC Press, Boca Raton, Ann Arbor, Boston, pp. 233.

Holt, D., Miles, G., Bula, R., Schreiber, M., and Peart, R. (1976). SIMED, a crop simulation model, as a tool for teaching crop physiology. *Journal of Agronomic Education* **5**, 53-56.

Holt, D. A. (1975). Environmental physiology, modeling and simulation of alfalfa growth. pp. 26. Agricultural Experiment Station, Purdue University.

Holzworth, D., Huth, N. I., Fainges, J., Brown, H., Zurcher, E., Cichota, R., Verrall, S., Herrmann, N. I., Zheng, B., and Snow, V. (2018). APSIM Next Generation: Overcoming challenges in modernising a farming systems model. *Environmental Modelling & Software* **103**, 43-51.

Holzworth, D. P., Huth, N. I., deVoil, P. G., Zurcher, E. J., Herrmann, N. I., McLean, G., Chenu, K., van Oosterom, E. J., Snow, V., Murphy, C., Moore, A. D., Brown, H., Whish, J. P. M., Verrall, S., Fainges, J., Bell, L. W., Peake, A. S., Poulton, P. L., Hochman, Z., Thorburn, P. J., Gaydon, D. S., Dalgliesh, N. P., Rodriguez, D., Cox, H., Chapman, S., Doherty, A., Teixeira, E., Sharp, J., Cichota, R., Vogeler, I., Li, F. Y.,

Wang, E., Hammer, G. L., Robertson, M. J., Dimes, J. P., Whitbread, A. M., Hunt, J., van Rees, H., McClelland, T., Carberry, P. S., Hargreaves, J. N. G., MacLeod, N., McDonald, C., Harsdorf, J., Wedgwood, S., and Keating, B. A. (2014). APSIM – Evolution towards a new generation of agricultural systems simulation. *Environmental Modelling & Software* **62**, 327-350.

Jamieson, P. D., Porter, J. R., and Wilson, D. R. (1991). A test of the computer simulation model ARCWHEAT1 on wheat crops grown in New Zealand. *Field Crops Research* **27**, 337-350.

Jáuregui, J. M., Mills, A., Black, D. B. S., Wigley, K., Ridgway, H. J., and Moot, D. J. (2019). Yield components of lucerne were affected by sowing dates and inoculation treatments. *European Journal of Agronomy* **103**, 1-12.

Jego, G., Rotz, C. A., Belanger, G., Tremblay, G. F., Charbonneau, E., and Pellerin, D. (2015). Simulating forage crop production in a northern climate with the Integrated Farm System Model. *Canadian Journal of Plant Science* **95**, 745-757.

Jing, Q., Qian, B., Bélanger, G., VanderZaag, A., Jégo, G., Smith, W., Grant, B., Shang, J., Liu, J., He, W., Boote, K., and Hoogenboom, G. (2020). Simulating alfalfa regrowth and biomass in eastern Canada using the CSM-CROPGRO-perennial forage model. *European Journal of Agronomy* **113**, 125971.

Jones, C. A., Ritchie, J. T., Kiniry, J. R., and Godwin, D. C. (1986). CERES-Maize: A simulation model of maize growth and development, Texas A&M University Press, Texas, USA, pp. 194.

Jones, J. W., Hoogenboom, G., Porter, C. H., Boote, K. J., Batchelor, W. D., Hunt, L. A., Wilkens, P. W., Singh, U., Gijsman, A. J., and Ritchie, J. T. (2003). The DSSAT cropping system model. *European Journal of Agronomy* **18**, 235-265.

Justes, E., Thiébeau, P., Avice, J. C., Lemaire, G., Volenec, J. J., and Ourry, A. (2002). Influence of summer sowing dates, N fertilization and irrigation on autumn VSP accumulation and dynamics of spring regrowth in alfalfa (*Medicago sativa* L.). *Journal of Experimental Botany* **53**, 111-121.

Kallenbach, R. L., Nelson, C. J., and Coutts, J. H. (2002). Yield, quality, and persistence of grazing- and hay-type alfalfa under three harvest frequencies. *Agronomy Journal* **94**, 1094-1103.

Kalu, B. A., and Fick, G. W. (1981). Quantifying morphological development of alfalfa for studies of herbage quality. *Crop Science* **21**, 267-271.

Kalu, B. A., and Fick, G. W. (1983). Morphological stage of development as a predictor of alfalfa herbage quality. *Crop Science* **23**, 1167-1172.

Keating, B. A. (2020). Crop, soil and farm systems models – science, engineering or snake oil revisited. *Agricultural Systems* **184**, 102903.

Keating, B. A., Carberry, P. S., Hammer, G. L., Probert, M. E., Robertson, M. J., Holzworth, D., Huth, N. I., Hargreaves, J. N. G., Meinke, H., Hochman, Z., McLean, G., Verburg, K., Snow, V., Dimes, J. P., Silburn, M., Wang, E., Brown, S., Bristow, K. L., Asseng, S., Chapman, S., McCown, R. L., Freebairn, D. M., and Smith, C. J. (2003). An overview of APSIM, a model designed for farming systems simulation. *European Journal of Agronomy* **18**, 267-288.

Khaiti, M., and Lemaire, G. (1992). Dynamics of shoot and root growth of lucerne after seeding and after cutting. *European Journal of Agronomy* **1**, 241-247.

Kim, T., Ourry, A., Boucaud, J., and Lemaire, G. (1991). Changes in source-sink relationship for nitrogen during regrowth of lucerne (*Medicago sativa* L.) following removal of shoots. *Functional Plant Biology* **18**, 593-602.

Kiniry, J. R., Williams, J., Gassmann, P., and Debaeke, P. (1992). A general, process-oriented model for two competing plant species. *Transactions of the ASAE* **35**, 801-810.

Kobayashi, K., and Salam, M. (2000). Comparing simulated and measured values using mean squared deviation and its components. *Agronomy Journal* **92**, 345-352.

Lemaire, G., and Belanger, G. (2020). Allometries in plants as drivers of forage nutritive value: A review. *Agriculture* **10**, 5.

Lemaire, G., Khaity, M., Onillon, B., Allirand, J. M., Chartier, M., and Gosse, G. (1992). Dynamics of accumulation and partitioning of N in leaves, stems and roots of lucerne (*Medicago sativa* L.) in a dense canopy. *Annals of Botany* **70**, 429-435.

Lemaire, G., Oosterom, E. v., Sheehy, J., Jeuffroy, M. H., Massignam, A., and Rossato, L. (2007). Is crop N demand more closely related to dry matter accumulation or leaf area expansion during vegetative growth? *Field Crops Research* **100**, 91-106.

Liu, Z., Li, X., Wang, Z., and Sun, Q. (2015). Contrasting strategies of alfalfa stem elongation in response to fall dormancy in early growth stage: the tradeoff between internode length and internode number. *PLOS One* **10**, e0135934.

Liu, Z. Y., Yang, G. F., Li, X. L., Yan, Y. F., Sun, J., Gao, R., Sun, Q. Z., and Wang, Z. L. (2016). Autumn dormancy regulates the expression of cas18, vsp and corF genes during cold acclimation of lucerne (*Medicago sativa* L.). *Crop and Pasture Science* **67**, 666-678.

Lu, X., Ji, S., Hou, C., Qu, H., Li, P., and Shen, Y. (2018). Impact of root C and N reserves on shoot regrowth of defoliated alfalfa cultivars differing in fall dormancy. *Grassland science* **64**, 83-90.

Luo, Y., Meyerhoff, P. A., and Loomis, R. S. (1995). Seasonal patterns and vertical distributions of fine roots of alfalfa (*Medicago sativa* L.). *Field Crops Research* **40**, 119-127.

Major, D. J., Hanna, M. R., and Beasley, B. W. (1991). Photoperiod response characteristics of alfalfa (*Medicago sativa* L) cultivars. *Canadian Journal of Plant Science* **71**, 87-93.

Malik, W., Boote, K. J., Hoogenboom, G., Cavero, J., and Dechmi, F. (2018). Adapting the CROPGRO model to simulate alfalfa growth and yield. *Agronomy Journal* **110**, 1777-1790.

Marcelis, L. F. M., Heuvelink, E., and Goudriaan, J. (1998). Modelling biomass production and yield of horticultural crops: A review. *Scientia Horticulturae* **74**, 83-111.

Martiniello, P., Paoletti, R., and Berardo, N. (1997). Effect of phenological stages on dry matter and quality components in lucerne. *European Journal of Agronomy* **6**, 79-87.

Mattera, J., Romero, L. A., Cuatrín, A. L., Cornaglia, P. S., and Grimoldi, A. A. (2013). Yield components, light interception and radiation use efficiency of lucerne (*Medicago sativa* L.) in response to row spacing. *European Journal of Agronomy* **45**, 87-95.

McCree, K. J. (1974). Equations for the rate of dark respiration of white clover and grain sorghum, as functions of dry weight, photosynthetic rate, and temperature. *Crop Science* **14**, 509-514.

McGowan, A., Sheath, G., and Webby, R. (2003). Lucerne for high quality summer feed in North Island hill country. *In* Legumes for dryland pastures, Grassland Research and Practice Series No. 11. (D. J. Moot, ed.). New Zealand Greassland Association, Lincoln, Canterbury, New Zealand,169-174.

Meuriot, F., Decau, M. L., Morvan-Bertrand, A., Prud'Homme, M. P., Gastal, F., Simon, J. C., Volenec, J. J., and Avice, J. C. (2005). Contribution of initial C and N reserves in Medicago sativa recovering from defoliation: lmpact of cutting height and residual leaf area. *Functional Plant Biology* **32**, 321-334.

Michaud, R., Lehman, W. F., and Rumbaugh, M. D. (1988). World distribution and historical development. *In* Alfalfa and Alfalfa Improvement (A. A. Hanson, D. K. Barnes and R. R. Hill, eds.), Vol. 29, pp. 25-91. American Society of Agronomy, Madison, USA.

Monks, D. P., SadatAsilan, K., and Moot, D. J. (2009). Cardinal temperatures and thermal time requirements for germination of annual and perennial temperate pasture species. *Agronomy New Zealand* **39**, 95-109.

Monsi, M., and Saeki, T. (2005). On the factor light in plant communities and its importance for matter production. *Annals of Botany* **95**, 549-567.

Monteith, J. L. (1994). Validity of the correlation between intercepted radiation and biomass. *Agricultural and Forest Meteorology* **68**, 213-220.

Moot, D., Hargreaves, J., Brown, H., and Teixeira, E. (2015). Calibration of the APSIM-Lucerne model for 'Grasslands Kaituna' lucerne crops grown in New Zealand. *New Zealand Journal of Agricultural Research* **58**, 190-202.

Moot, D. J. (2012). An overview of dryland legume research in New Zealand. *Crop and Pasture Science* **63**, 726-733.

Moot, D. J., Bennett, S., Mills, A., and Smith, M. C. (2016). Optimal grazing management to achieve high yields and utilisation of dryland lucerne. *Journal of New Zealand Grasslands* **78**, 27-33.

Moot, D. J., Brown, H. E., Teixeira, E. I., and Pollock, K. M. (2003). Crop growth and development affect seasonal priorities for lucerne management. *In* Legumes for dryland pastures (D. J. Moot, ed.). New Zealand Grassland Association, Lincoln, Canterbury, New Zealand, Grassland Research and Practice Series No. 11.,201-208.

Moot, D. J., Robertson, M. J., and Pollock, K. M. (2001). Validation of the APSIM-Lucerne model for phenological development in a cool-temperate climate. *In* Australian Agronomy Conference, Hobart, 1-5.

Morari, F., Lugato, E., and Borin, M. (2004). An integrated non-point source model-GIS system for selecting criteria of best management practices in the Po Valley, North Italy. *Agriculture, Ecosystems & Environment* **102**, 247-262.

Moriasi, D. N., Arnold, J. G., Van Liew, M. W., Bingner, R. L., Harmel, R. D., and Veith, T. L. (2007). Model evaluation guidelines for systematic quantification of accuracy in watershed simulations. *Transactions of the ASABE* **50**, 885-900.

Nash, J. E., and Sutcliffe, J. V. (1970). River flow forecasting through conceptual models part I—A discussion of principles. *Journal of hydrology* **10**, 282-290.

Noquet, C., Avice, J. C., Ourry, A., Volenec, J. J., Cunningham, S. M., and Boucaud, J. (2001). Effects of environmental factors and endogenous signals on N uptake, N partitioning and taproot vegetative storage protein accumulation in Medicago sativa. *Functional Plant Biology* **28**, 279-287.

Onstad, D. W., and Shoemaker, C. A. (1984). Management of alfalfa and the alfalfa Weevil (*Hypera postica*): An example of systems analysis in forage production. *Agricultural Systems* **14**, 1-30.

Parsch, L. D. (1987). Validation of ALSIM1 (Level 2) under Michigan conditions. *Agricultural Systems* **25**, 145-157.

Pearson, C., and Hunt, L. (1972). Effects of temperature on primary growth of alfalfa. *Canadian Journal of Plant Science* **52**, 1007-1015.

Reynolds, J. R., and Smith, D. (1962). Trend of carbohydrate reserves in alfalfa, smooth bromegrass, and timothy grown under various cutting schedules. *Crop Science* **2**, 333-336.

Riaz, S., Chaudhry, Q. A., and Siddiqui, S. (2016). Mathematical modeling and optimization of complex structures: A review. *Complex Adaptive Systems Modeling* **4**, 1-3.

Riday, H., and Brummer, E. C. (2002). Heterosis of agronomic traits in alfalfa. *Crop Science* **42**, 1081-1087.

Rimi, F., Macolino, S., Leinauer, B., Lauriault, L. M., and Ziliotto, U. (2010). Alfalfa yield and morphology of three fall-dormancy categories harvested at two phenological stages in a subtropical climate. *Agronomy Journal* **102**, 1578-1585.

Rimi, F., Macolino, S., Leinauer, B., Lauriault, L. M., and Ziliotto, U. (2012). Fall dormancy and harvest stage effects on alfalfa nutritive value in a subtropical climate. *Agronomy Journal* **104**, 415-422.

Rimi, F., Macolino, S., Leinauer, B., Lauriault, L. M., and Ziliotto, U. (2014). Fall dormancy and harvest stage impact on alfalfa persistence in a subtropical climate. *Agronomy Journal* **106**, 1258-1266.

Ritchie, J. T., and Nesmith, D. S. (1991). Temperature and crop development, American Society of Agronomy, Madison, Wisconsin, USA., pp. 5-29.

Robertson, M. J., Carberry, P. S., Huth, N. I., Turpin, J. E., Probert, M. E., Poultron, P. L., Bell, M. J., Wright, G. C., Yeates, S. J., and Brinsmead, R. B. (2002). Simulation of growth and development of diverse legumes species in APSIM. *Australian Journal of Agricultural Research* **53**, 429-446.

Rotz, C. A. (2005). The integrated farm system model: A tool for whole farm nutrient management analysis. *In* NRAES manure management conference, Pennsylvania, USA. USDA / Agricultural Research Service, University Park, 6.

Rotz, C. A., Black, J. R., Mertens, D. R., and Buckmaster, D. R. (1989a). DAFOSYM: A model of the dairy forage system. *Journal of Production Agriculture* **2**, 83-91.

Rotz, C. A., Buckmaster, D. R., Mertens, D. R., and Black, J. R. (1989b). DAFOSYM: A dairy forage system model for evaluating alternatives in forage conservation. *Journal of Dairy Science* **72**, 3050-3063.

Rotz, C. A., Corson, M. S., Chianese, D. S., Montes, F., and Hafner, S. D. (2012). The integrated farm system model. *In* Natural resource, agriculture and engineering service. Dairy manure management: Treatment, handling, and community relations. Pasture Systems & Watershed Management Research, University Park, Pennsylvania, USA.

Rotz, C. A., Hesterman, O. B., and Ritchie, J. T. (1986). Alfalfa growth simulation model, Michigan State University and USA Dairy Forage Research, Center East Lansing, Michigan State, USA.

Rymph, S. J. (2004). Modeling growth and composition of perennial tropical forage grasses. Ph.D thesis, University of Florida, Gainesville.

Sadras, V. O., and Lemaire, G. (2014). Quantifying crop nitrogen status for comparisons of agronomic practices and genotypes. *Field Crops Research* **164**, 54-64.

Sanderson, M. A. (1992). Predictors of alfalfa forage quality: validation with field data. *Crop Science* **32**, 245-250.

Selirio, I. S., and Brown, D. M. (1979). Soil moisture-based simulation of forage yield. *Agricultural Meteorology* **20**, 99-114.

Sharifiamina, S., Moot, D., and Bloomberg, M. (2016). Calculating "Hydrothermal time" to quantify seed germination of tall fescue. *Proceedings of the New Zealand Grassland Association* **78**, 163-168.

Sharratt, B. S., Sheaffer, C. C., and Baker, D. G. (1989). Base temperature for the application of the growing-degree-day model to field-grown alfalfa. *Field Crops Research* **21**, 95-102.

Sim, R. E. (2014). Water extraction and use of seedling and established dryland lucerne crops. Ph.D thesis, Lincoln University, Canterbury, New Zealand.

Sim, R. E., Brown, H. E., Teixeira, E. I., and Moot, D. J. (2016). Soil water extraction patterns of lucerne grown on stony soils. *Plant and Soil* **414**, 95-112.

Sim, R. E., Moot, D. J., Brown, H. E., and Teixeira, E. I. (2015). Sowing date affected shoot and root biomass accumulation of lucerne during establishment and subsequent regrowth season. *European Journal of Agronomy* **68**, 69-77.

Sinclair, T. R., and Muchow, R. C. (1999). Radiation use efficiency. *In* Advances in Agronomy (D. L. Sparks, ed.), Vol. 65, pp. 215-265. Academic Press.

Smith, A. P., Moore, A. D., Boschma, S. P., Hayes, R. C., Nie, Z., and Pembleton, K. G. (2017). Modelling of lucerne (*Medicago sativa* L.) for livestock production in diverse environments. *Crop and Pasture Science* **68**, 74-91.

Steduto, P., Hsiao, T. C., Raes, D., and Fereres, E. (2009). AquaCrop—The FAO crop model to simulate yield response to water: I. Concepts and underlying principles. *Agronomy Journal* **101**, 426-437.

Stockle, C., and Nelson, R. (1998). CropSyst user's manual, Biological Systems Engineering Department, Washington State University, Pullman, Washington, USA.

Stöckle, C. O., Donatelli, M., and Nelson, R. (2003). CropSyst, a cropping systems simulation model. *European Journal of Agronomy* **18**, 289-307.

Streck, N. A., de Paula, F. L. M., Bisognin, D. A., Heldwein, A. B., and Dellai, J. (2007). Simulating the development of field grown potato (*Solanum tuberosum* L.). *Agricultural and Forest Meteorology* **142**, 1-11.

Streck, N. A., Weiss, A., Xue, Q., and Stephen, B. P. (2003). Improving predictions of developmental stages in winter wheat: A modified Wang and Engel model. *Agricultural and Forest Meteorology* **115**, 139-150.

Strullu, L., Beaudoin, N., Thiébeau, P., Julier, B., Mary, B., Ruget, F., Ripoche, D., Rakotovololona, L., and Louarn, G. (2020). Simulation using the STICS model of C&N dynamics in alfalfa from sowing to crop destruction. *European Journal of Agronomy* **112**, 125948.

Summers, C. G., and Putnam, D. H. (2008). Irrigated alfalfa management for Mediterranean and desert zones, Bowles Farming Company, Inc., Los Banos, California.

Szeicz, G. (1974). Solar radiation for plant growth. *Journal of Applied Ecology* **11**, 617-636.

Ta, H. T. (2018). Growth and development of lucerne with different fall dormancy ratings. Ph.D thesis, Lincoln University, Canterbury, New Zealand.

Ta, H. T., Teixeira, E., and Moot, D. J. (2016). Impact of autumn (fall) dormancy rating on growth and development of seedling lucerne. *Journal of New Zealand Grasslands* **78**, 169-176.

Ta, H. T., Teixeira, E. I., Brown, H. E., and Moot, D. J. (2020). Yield and quality changes in lucerne of different fall dormancy ratings under three defoliation regimes. *European Journal of Agronomy* **115**, 126012.

Ta, T. C., Macdowall, F. D. H., and Faris, M. A. (1990). Utilization of carbon and nitrogen reserves of alfalfa roots in supporting N_2-fixation and shoot regrowth. *Plant and Soil* **127**, 231-236.

Teixeira, E. I. (2006). Understanding growth and development of lucerne crops (*Medicago sativa* L.) with contrasting levels of perennial reserves. Ph.D thesis, Lincoln University, Canterbury, New Zealand.

Teixeira, E. I., Brown, H. E., Meenken, E. D., and Moot, D. J. (2011). Growth and phenological development patterns differ between seedling and regrowth lucerne crops (*Medicago sativa* L.). *European Journal of Agronomy* **35**, 47-55.

Teixeira, E. I., Moot, D. J., and Brown, H. E. (2008). Defoliation frequency and season affected radiation use efficiency and dry matter partitioning to roots of lucerne (*Medicago sativa* L.) crops. *European Journal of Agronomy* **28**, 103-111.

Teixeira, E. I., Moot, D. J., and Brown, H. E. (2009). Modeling seasonality of dry matter partitioning and root maintenance respiration in lucerne (*Medicago sativa* L.) crops. *Crop and Pasture Science* **60**, 778-784.

Teixeira, E. I., Moot, D. J., Brown, H. E., and Fletcher, A. L. (2007a). The dynamics of lucerne (*Medicago sativa* L.) yield components in response to defoliation frequency. *European Journal of Agronomy* **26**, 394-400.

Teixeira, E. I., Moot, D. J., Brown, H. E., and Pollock, K. M. (2007b). How does defoliation management impact on yield, canopy forming processes and light interception of lucerne (*Medicago sativa* L.) crops? *European Journal of Agronomy* **27**, 154-164.

Teixeira, E. I., Moot, D. J., and Mickelbart, M. V. (2007c). Seasonal patterns of root C and N reserves of lucerne crops (*Medicago sativa* L.) grown in a temperate climate were affected by defoliation regime. *European Journal of Agronomy* **26**, 10-20.

Teuber, L., Taggard, K., Gibbs, L., McCaslin, M., Peterson, M., and Barnes, D. (1998). Fall dormancy. Standard tests to characterize alfalfa cultivars,A-1.

Thiébeau, P., Beaudoin, N., Justes, E., Allirand, J. M., and Lemaire, G. (2011). Radiation use efficiency and shoot:root dry matter partitioning in seedling growths and regrowth crops of lucerne (*Medicago sativa* L.) after spring and autumn sowings. *European Journal of Agronomy* **35**, 255-268.

Thornley, J. H., and Johnson, I. R. (1990). Plant and crop modelling--A mathematical approach to plant and crop physiology, Clarendon Press, Oxford, pp. 660.

Undersander, D., Cosgrove, D., Cullen, E., Rice, M. E., Renz, M., Sheaffer, C., Shewmaker, G., and Sulc, M. (2011). Alfalfa management guide, Wiley Online Library.

Vallet, C., Chabbert, B., Czaninski, Y., Lemaire, G., and Monties, B. (1997). Extractibility of structural carbohydrates and lignin deposition in maturing alfalfa internodes. *International Journal of Biological Macromolecules* **21**, 201-206.

Vallet, C., Lemaire, G., Monties, B., and Chabbert, B. (1998). Cell wall fractionation of alfalfa stem in relation to internode development: Biochemistry aspect. *Journal of Agricultural and Food Chemistry* **46**, 3458-3467.

Van Keuren, R. W., and Matches, A. G. (1988). Pasture production and utilization. *In* Alfalfa and Alfalfa Improvement (A. A. Hanson, D. K. Barnes and R. R. Hill, eds.), pp. 515-538. American Society of Agronomy, Madison, Wisconsin, USA.

Ventroni, L. M., Volenec, J. J., and Cangiano, C. A. (2010). Fall dormancy and cutting frequency impact on alfalfa yield and yield components. *Field Crops Research* **119**, 252-259.

Wallach, D., Makowski, D., and Jones, J. W. (2006). Working with dynamic crop models: Evaluating, analyzing, parameterizing, and applications, Elsevier Science, The Netherland, pp. 462.

Wang, E., and Engel, T. (1998). Simulation of phenological development of wheat crops. *Agricultural Systems* **58**, 1-24.

Watt, J., and Burgham, S. (1992). Physical properties of eight soils of the Lincoln area, Canterbury, DSIR Land Resources Technical Record, pp. 134.

Whisler, F. D., Acock, B., Baker, D. N., Fye, R. E., Hodges, H. F., Lambert, J. R., Lemmon, H. E., McKinion, J. M., and Reddy, V. R. (1986). Crop simulation models in agronomic systems. *Advances in Agronomy* **40**, 141-208.

Williams, J., Jones, C., Kiniry, J., and Spanel, D. (1989). The EPIC crop growth model. *Transactions of the ASAE* **32**, 497-511.

Wilson, D. R., Muchow, R. C., and Murgatroyd, C. J. (1995). Model analysis of temperature and solar radiation limitations to maize potential productivity in a cool climate. *Field Crops Research* **43**, 1-18.

Wivstad, M., Mårtensson, A. M., and Ljunggren, H. D. (1987). Field measurement of symbiotic nitrogen fixation in an established lucerne ley using ^{15}N and an acetylene reduction method. *Plant and Soil* **97**, 93-104.

Yolcu, H., Tan, M., and Serin, Y. (2006). Effects of early cutting time and stubble height on yield and quality in lucerne. *New Zealand Journal of Agricultural Research* **49**, 201-206.

Zaka, S., Ahmed, L. Q., Escobar-Gutiérrez, A. J., Gastal, F., Julier, B., and Louarn, G. (2017). How variable are non-linear developmental responses to temperature in two perennial forage species? *Agricultural and Forest Meteorology* **232**, 433-442.

Zaka, S., Frak, E., Julier, B., Gastal, F., and Louarn, G. (2016). Intraspecific variation in thermal acclimation of photosynthesis across a range of temperatures in a perennial crop. *AoB Plants* **8**, plw035.

Zhu, Y., Feng, L., Yi, P., Yang, X., and Hu, Y. (2007). A dynamic model simulating photosynthetic production and dry matter accumulation for alfalfa (*Medicago sativa* L.). *Acta Agronomica Sinica* **10**, 1682-1687.

APPENDICES

Appendix 1 Soil paremeters for Iverson field, Lincoln University, New Zealand. BD = Bulk Density; AD = Air Dry; LL15 = Lower Limit (-15 bar); DUL = Drained Uper Limit; SAT= Saturation; LL = Lower Limit; KL = Franction of plant available water able to be extracted /day from a particular soil layer. PAWC = Plant Available Water Capacity.

Depth (CM)	BD (g/cc)	AD (mm/mm)	LL15 (mm/mm)	DUL (mm/mm)	SAT (mm/mm)	LL (mm/mm)	KL (/day)	PAWC (mm/mm)
0-10	1.26	0.05	0.075	0.35	0.38	0.1	0.06	0.25
10-20	1.26	0.06	0.078	0.35	0.38	0.13	0.06	0.22
20-30	1.26	0.07	0.07	0.32	0.39	0.12	0.03	0.2
30-40	1.44	0.07	0.07	0.29	0.32	0.12	0.03	0.17
40-50	1.44	0.069	0.07	0.27	0.3	0.11	0.03	0.16
50-60	1.44	0.07	0.07	0.31	0.32	0.08	0.03	0.23
60-70	1.57	0.07	0.07	0.33	0.34	0.08	0.03	0.25
70-80	1.57	0.07	0.07	0.35	0.35	0.08	0.03	0.27
80-90	1.57	0.07	0.07	0.34	0.35	0.09	0.03	0.25
90-100	1.58	0.07	0.07	0.34	0.35	0.11	0.03	0.23
100-110	1.58	0.07	0.07	0.34	0.35	0.12	0.03	0.22
110-120	1.58	0.07	0.07	0.34	0.35	0.15	0.03	0.19
120-130	1.58	0.08	0.08	0.34	0.35	0.15	0.03	0.19
130-140	1.59	0.078	0.08	0.33	0.35	0.15	0.03	0.18
140-150	1.59	0.08	0.08	0.33	0.35	0.16	0.03	0.17
150-160	1.59	0.087	0.09	0.32	0.34	0.2	0.03	0.12
160-170	1.59	0.09	0.09	0.3	0.33	0.25	0.03	0.05
170-180	1.59	0.09	0.09	0.3	0.33	0.25	0.03	0.05
180-190	1.59	0.09	0.09	0.3	0.33	0.25	0.03	0.05
190-200	1.59	0.08	0.08	0.31	0.33	0.25	0.03	0.06
200-210	1.59	0.09	0.09	0.31	0.33	0.23	0.03	0.08

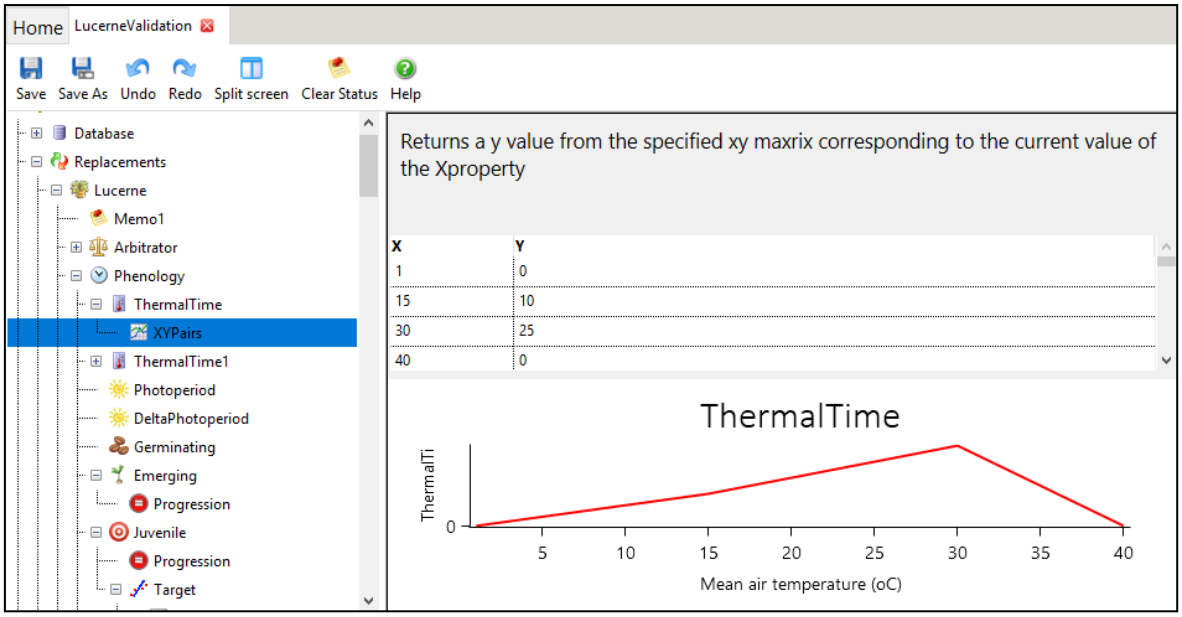

Appendix 2. Thermal time (Tt) function for phenological development in APSIM NextGen lucerne model.

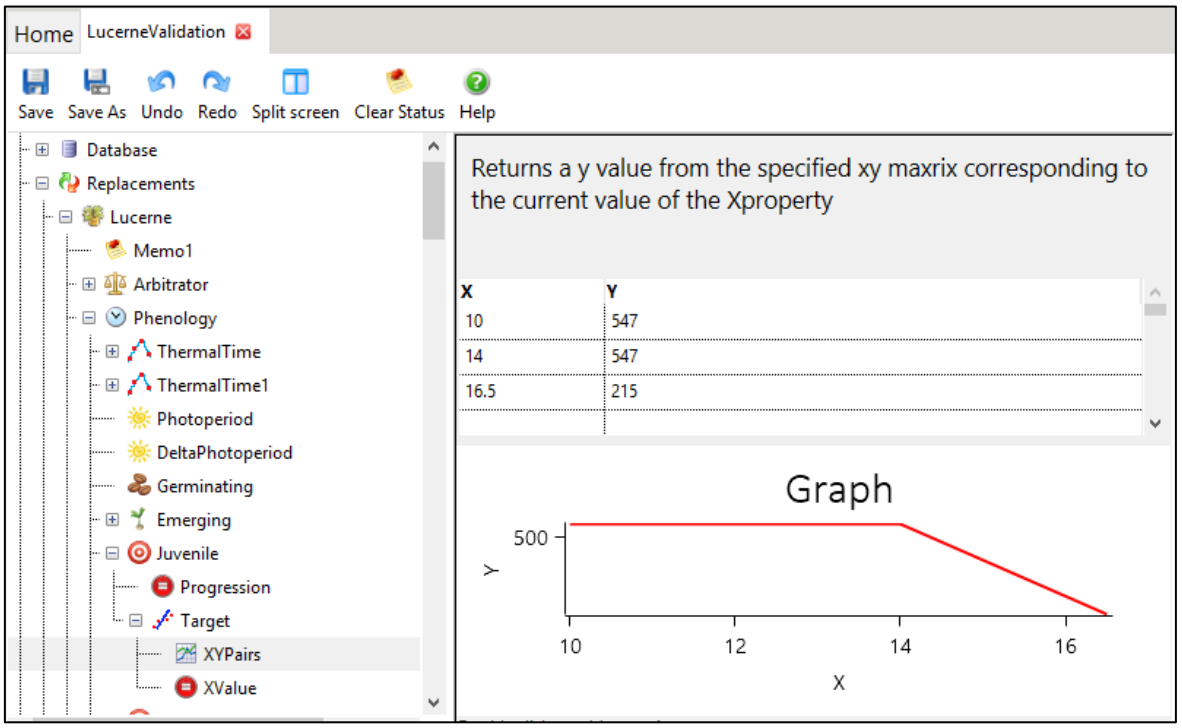

Appendix 3**.** Model structure for juvenile stage in APSIM NextGen lucerne model.

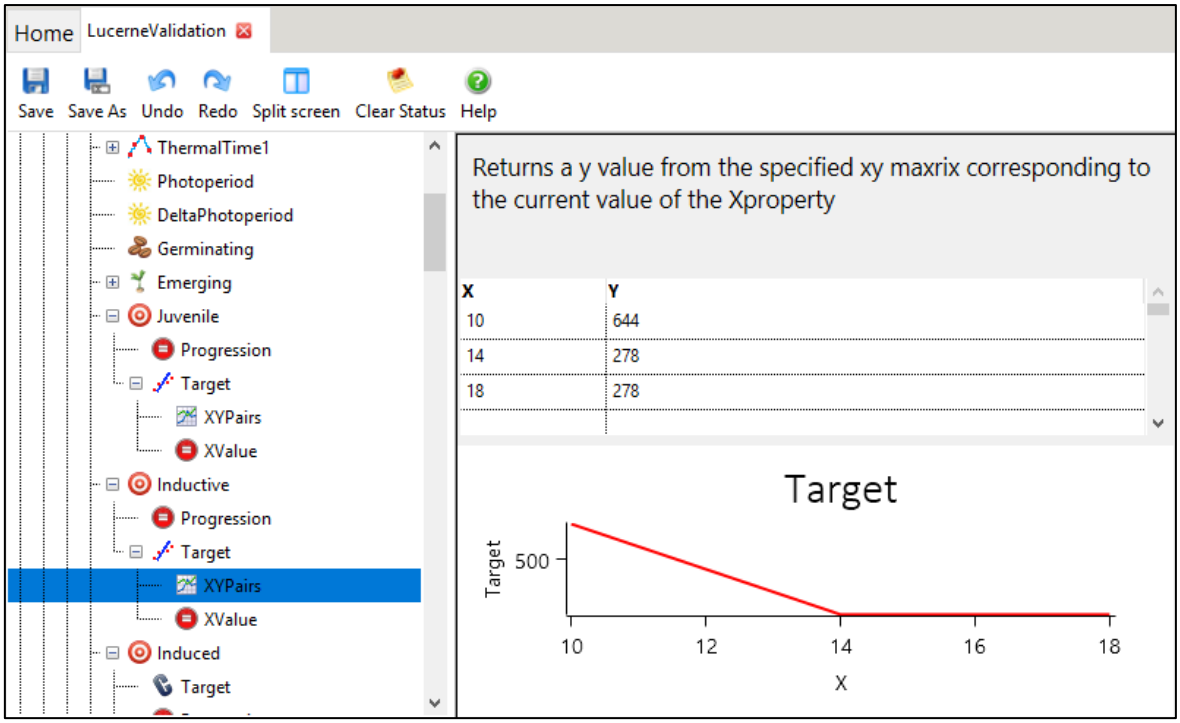

Appendix 4. Model structure for inductive stage in APSIM NextGen lucerne model.

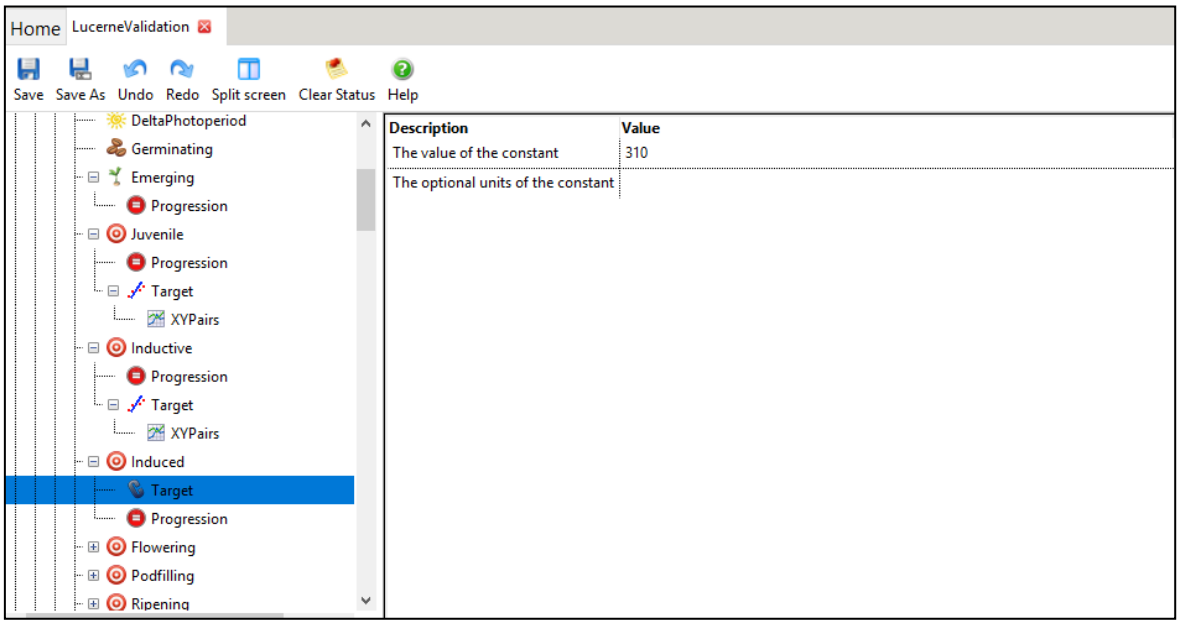

Appendix 5. Model structure for induced stage in APSIM NextGen lucerne model.

Appendix 6. Statistical measures of linear relationship between number of main stem nodes and thermal time for four field experiments conducted within 1997 to 2019 at Lincoln University, Canterbury, New Zealand.

Stage	ID	Growth season	Regrowth cycle	R^2	Slope	Intercept	p
Seedling	E2ILLS1	1	1	0.99	0.022	-2.83	<0.0001
	E2ILLS2	1	1	0.98	0.020	-2.56	<0.0001
	E2ILLS3	1	1	0.99	0.017	-1.82	<0.0001
	E2ILLS4	1	1	0.99	0.020	-3.10	<0.0001
	E2ILLS1	1	2	0.99	0.023	2.14	<0.0001
	E2ILLS2	1	2	0.92	0.016	4.67	<0.0001
	E2ILLS3	1	2	0.97	0.017	3.14	<0.0001
	E2ILLS1	1	3	0.99	0.017	4.25	<0.0001
	E2ILLS4	1	2	0.98	0.021	3.14	<0.0001
	E2ILLS1	1	4	0.96	0.019	3.06	0.135
	E2ILLS2	1	3	0.99	0.018	4.29	0.032
	E4ILLF5	1	1	0.99	0.025	-5.03	<0.0001
	E4ILLF5	1	2	0.99	0.031	-0.76	<0.0001
	E4ILLF5	1	3	0.99	0.025	-0.32	<0.0001
	E4ILLF5	1	4	0.99	0.026	-0.12	<0.0001
Regrowth	E1ILL	2	2	0.99	0.033	-0.16	0.0004
	E1ILL	2	3	0.99	0.029	0.22	0.06
	E1ILL	2	4	0.99	0.026	-0.002	0.05
	E1ILL	2	5	0.99	0.021	-0.57	0.04
	E1ILL	2	6	1.00	0.020	-0.09	NA
	E1ILL	3	2	1.00	0.032	-1.78	NA
	E1ILL	3	4	1.00	0.028	-0.99	NA
	E1ILL	3	5	0.97	0.026	-0.81	0.016
	E1ILL	4	1	0.99	0.027	1.41	0.0398
	E1ILL	4	2	0.99	0.027	0.45	<0.0001
	E1ILL	4	3	0.99	0.027	0.82	<0.0001
	E1ILL	4	4	0.96	0.032	0.098	<0.0001
	E1ILL	4	5	0.99	0.025	1.56	<0.0001
	E1ILL	4	6	0.99	0.022	1.49	0.004
	E1ILL	5	1	0.97	0.020	0.09	0.0004
	E1ILL	5	2	0.93	0.049	-2.23	0.008
	E1ILL	5	3	0.98	0.038	-1.25	0.008
	E1ILL	5	4	0.99	0.031	-0.94	0.003

E1ILL	5	5	0.96	0.025	0.34	0.0006
E1ILL	5	6	0.99	0.020	4.12	0.035
E1ILL	5	7	0.94	0.023	1.82	0.032
E2ILLS1	2	1	0.98	0.038	-2.30	0.0016
E2ILLS1	2	2	0.98	0.027	0.61	0.0001
E2ILLS1	2	3	0.99	0.033	-0.43	0.0049
E2ILLS1	2	4	0.99	0.029	0.35	0.0005
E2ILLS1	2	5	0.98	0.025	3.47	0.0815
E2ILLS1	2	6	0.98	0.022	3.55	0.0078
E3ILL	3	1	0.98	0.020	0.37	<0.0001
E3ILL	3	2	0.98	0.032	1.36	0.0002
E3ILL	3	3	0.99	0.029	0.93	0.0005
E3ILL	3	4	0.99	0.025	2.90	0.002
E3ILL	3	5	0.99	0.025	3.10	<0.0001
E3ILL	3	6	0.99	0.026	2.49	0.001
E3ILL	3	7	0.98	0.017	1.75	0.009
E3ILL	4	1	0.98	0.017	1.09	<0.0001
E3ILL	4	2	0.99	0.027	0.49	0.0007
E3ILL	4	3	0.99	0.031	-0.22	<0.0001
E3ILL	4	4	0.96	0.023	2.47	0.019
E3ILL	4	5	0.99	0.025	1.02	0.0000
E3ILL	4	6	0.99	0.025	0.88	<0.0001
E3ILL	4	7	0.99	0.021	1.26	0.008
E3ILL	5	1	0.96	0.017	2.46	0.0001
E4ILLF5	2	1	0.97	0.034	1.24	0.002
E4ILLF5	2	2	0.99	0.038	0.06	<0.0001
E4ILLF5	2	3	0.99	0.033	2.11	0.0008
E4ILLF5	2	4	0.99	0.028	-0.19	<0.0001
E4ILLF5	2	5	0.99	0.027	0.26	0.0005
E4ILLF5	2	6	0.97	0.024	1.97	0.0025
E4ILLF5	3	1	0.99	0.038	0.08	<0.0001
E4ILLF5	3	2	0.99	0.033	-0.06	<0.0001
E4ILLF5	3	3	0.99	0.030	-0.06	<0.0001
E4ILLF5	3	4	0.99	0.017	0.87	0.07
E4ILLF5	3	5	0.99	0.026	0.44	0.005
E4ILLF5	3	6	0.88	0.019	2.10	0.06
E4ILLF5	3	7	0.99	0.053	0.20	0.003

E4ILLF5	4	1	0.96	0.026	2.64	0.12
E4ILLF5	4	2	0.95	0.022	3.58	0.024
E4ILLF5	4	3	0.99	0.029	0.54	0.03
E4ILLF5	4	4	0.99	0.029	-0.22	0.07
E4ILLF5	4	5	0.96	0.023	1.7	0.13
E4ILLF5	5	2	0.98	0.031	1.45	0.09
E4ILLF5	5	4	0.99	0.033	1.89	0.006
E4ILLF5	5	6	0.99	0.010	5.31	NA

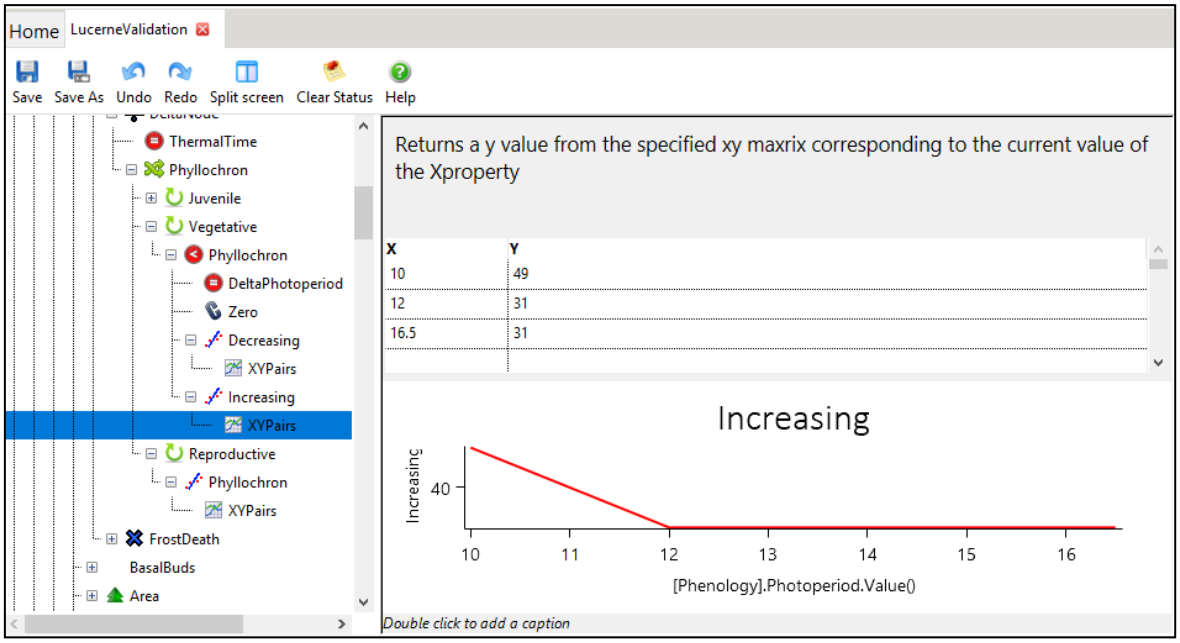

Appendix 7. Phyllochron$_{veg}$ function in increasing photoperiod (Pp) in APSIM NextGen lucerne model.

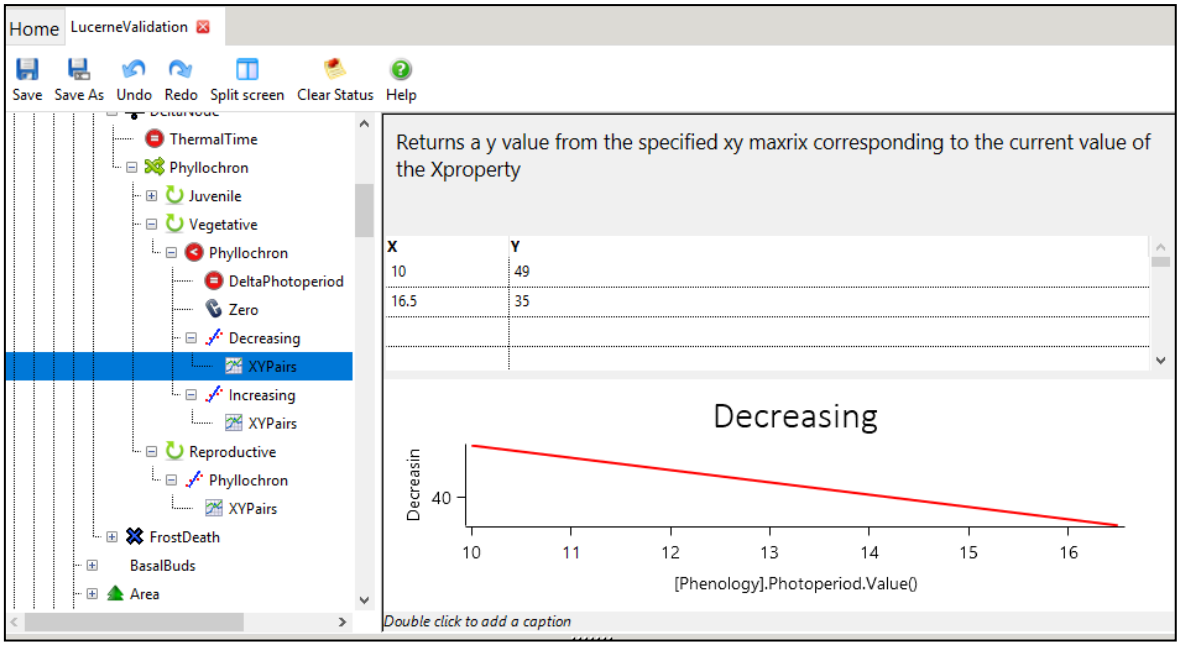

Appendix 8. Phyllochron$_{veg}$ function in decreasing photoperiod (Pp) in APSIM NextGen lucerne model.

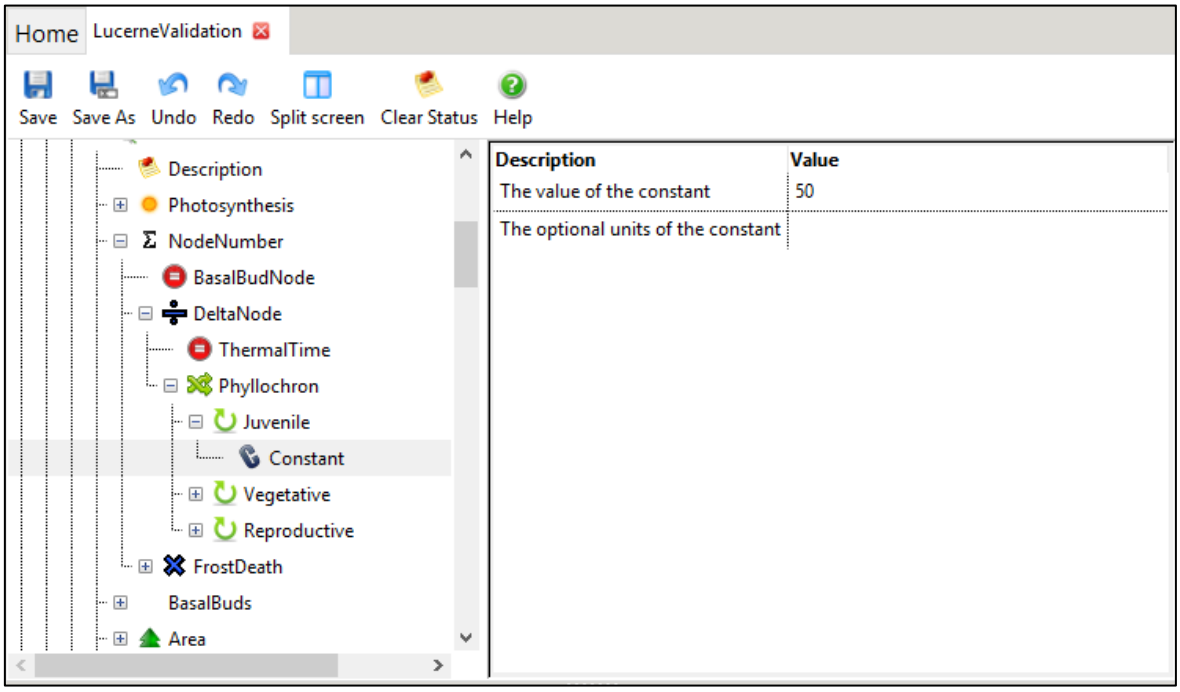

Appendix 9. Phyllochron function for seedling crops in APSIM NextGen lucerne model.

Appendix 10. Statistical measures of linear relationship between number of main stem nodes and thermal time for one field experiments with 84 day (HH) defoliation treatment conducted within 2014 to 2019 at Lincoln University, Canterbury, New Zealand.

Stage	ID	Growth season	Regrowth cycle	R^2	Slope	Intercept	p
Regrowth	E4IHHF5	1	2	0.97	24.80	27.50	0.11
Vegetative	E4IHHF5	1	3	0.90	21.23	4.15	0.21
	E4IHHF5	2	1	1.00	15.79	5.36	0.00
	E4IHHF5	2	2	1.00	22.94	15.87	0.00
	E4IHHF5	2	3	0.99	30.89	14.01	0.01
	E4IHHF5	3	1	0.95	33.82	-18.01	0.00
	E4IHHF5	3	2	1.00	25.07	4.34	0.00
	E4IHHF5	3	3	1.00	38.46	14.71	NaN
	E4IHHF5	3	4	1.00	23.71	8.25	0.01
	E4IHHF5	4	1	0.98	20.29	-6.36	0.00
	E4IHHF5	4	2	0.98	19.75	0.17	0.01
	E4IHHF5	4	3	0.99	43.40	24.45	0.05
	E4IHHF5	5	1	1.00	27.80	3.25	0.01
	E4IHHF5	5	2	0.95	68.02	-377.90	0.03
Regrowth	E1ILL	1	2	0.98	75.89	-631.92	0.00
Reproductive	E1ILL	2	1	1.00	39.01	-191.70	0.00
	E1ILL	2	2	1.00	65.60	-472.16	0.00
	E1ILL	2	3	0.99	60.18	-347.65	0.00
	E1ILL	3	2	1.00	60.71	-540.46	0.00
	E1ILL	3	3	0.93	93.02	-1037.82	0.03
	E1ILL	4	2	1.00	71.27	-815.64	NaN
	E1ILL	4	3	1.00	73.98	-626.27	NaN
	E1ILL	5	2	1.00	77.52	-609.66	NaN
	E1ILL	5	3	0.94	225.36	-2411.57	0.03

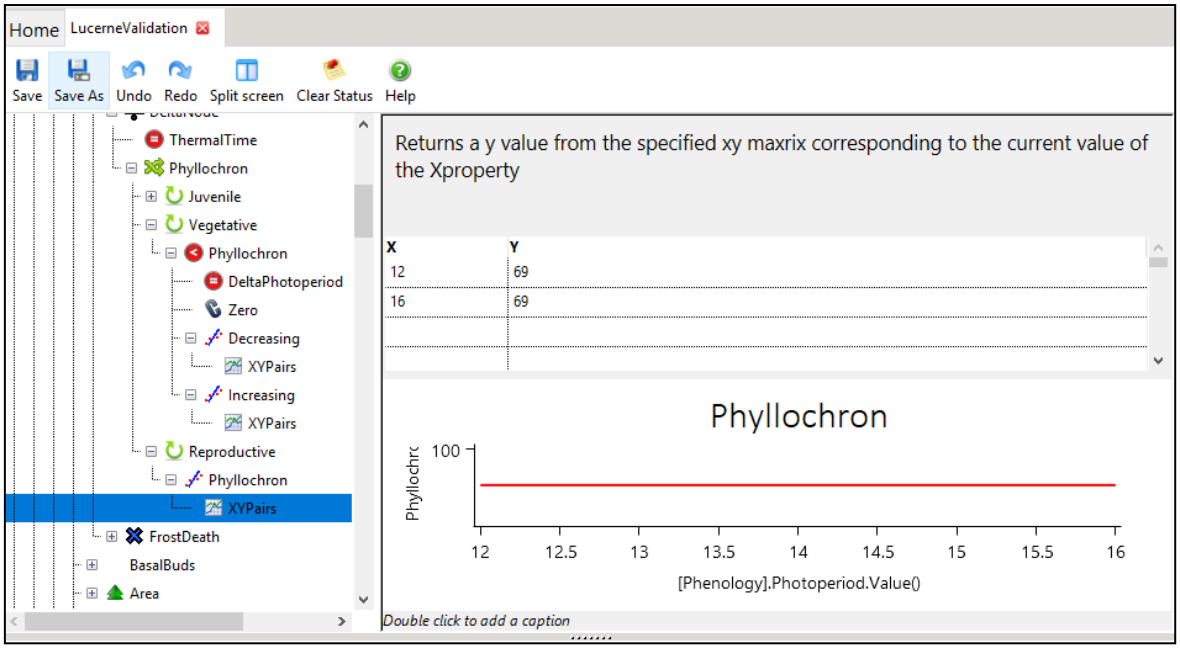

Appendix 11. Phyllochron function for the reproductive stage ($phyllochron_{rep}$) in APSIM NextGen lucerne model.

Appendix 12. Statistical measures of linear relationship between leaf are index (LAI) and thermal time for four field experiments conducted within 1997 to 2019 at Lincoln University, Canterbury, New Zealand. Pp represent photoperiod direction of each regrowth cycle.

Stage	ID	Growth season	Regrowth cycle	R^2	Slope	Intercept	p	x-intercept	Pp
Seedling	E2ILLS1	1	1	0.97	0.01	-7.04	0.11	494.53	Inc
	E2ILLS1	1	2	0.99	0.02	-1.40	<0.001	66.60	Dec
	E2ILLS1	1	3	0.97	0.02	-0.51	0.01	28.92	Dec
	E2ILLS2	1	1	0.99	0.01	-4.41	<0.001	427.08	Dec
	E2ILLS2	1	2	0.98	0.03	-1.66	0.01	65.34	Dec
	E2ILLS3	1	1	0.96	0.01	-2.94	<0.001	337.15	Dec
	E2ILLS3	1	2	0.98	0.02	-1.10	0.08	49.57	Dec
	E2ILLS4	1	1	0.98	0.01	-6.63	<0.001	451.31	Dec
	E2ILLS4	1	2	0.89	0.01	-0.85	0.21	57.27	Dec
	E2ILLS1	1	1	0.97	0.01	-7.04	0.11	494.53	Inc
	E2ILLS1	1	2	0.99	0.02	-1.40	<0.001	66.60	Dec
	E4ILLF5	1	1	0.88	0.00	-1.69	0.22	385.05	Inc
	E4ILLF5	1	2	0.99	0.01	-0.27	<0.001	24.03	Dec
	E4ILLF5	1	3	0.99	0.01	-0.08	<0.001	12.50	Dec
	E4ILLF5	1	4	0.99	0.01	-0.06	<0.001	11.26	Dec
Regrowth	E1ILL	2	4	0.99	0.02	-2.79	0.04	129.88	Dec
	E1ILL	2	5	0.99	0.02	-3.12	NA	184.43	Dec
	E1ILL	2	6	0.99	0.01	-1.52	NA	120.52	Dec
	E1ILL	3	2	0.99	0.01	0.88	NA	-66.34	Inc
	E1ILL	3	4	0.99	0.02	-2.37	NA	111.74	Dec
	E1ILL	3	5	0.99	0.02	-2.24	<0.001	106.28	Dec
	E1ILL	3	6	0.90	0.01	-1.62	0.21	116.65	Dec
	E1ILL	5	1	0.99	0.02	-5.54	<0.001	338.77	Inc
	E1ILL	5	2	0.98	0.02	-3.49	0.08	162.65	Inc
	E1ILL	5	3	0.99	0.02	-3.26	0.01	145.63	Inc
	E1ILL	5	4	0.99	0.02	-3.20	<0.001	151.80	Dec
	E1ILL	5	5	0.97	0.02	-2.22	0.02	137.28	Dec
	E1ILL	5	6	0.99	0.01	-0.78	<0.001	65.32	Dec
	E1ILL	6	1	0.99	0.02	-5.79	<0.001	272.02	Inc
	E2ILLS1	2	1	0.99	0.02	-4.80	<0.001	203.14	Inc
	E2ILLS1	2	2	0.99	0.02	-2.74	<0.001	118.90	Inc
	E2ILLS1	2	3	0.99	0.02	-3.60	<0.001	157.36	Inc

E2ILLS1	2	4	0.95	0.02	-2.06	0.02	133.69	Dec
E2ILLS1	2	5	0.94	0.02	-0.77	0.03	41.90	Dec
E2ILLS1	2	6	0.99	0.01	-1.44	NA	125.99	Dec
E2ILLS2	2	1	0.98	0.03	-5.08	<0.001	196.59	Inc
E2ILLS3	2	1	0.99	0.02	-4.87	<0.001	218.69	Inc
E2ILLS4	2	1	0.98	0.02	-4.28	<0.001	201.49	Inc
E2ILLS1	2	1	0.99	0.02	-4.80	<0.001	203.14	Inc
E3ILL	3	1	0.98	0.01	-2.67	0.01	266.41	Inc
E3ILL	3	2	0.98	0.02	-1.52	<0.001	62.62	Inc
E3ILL	3	3	0.98	0.02	-1.61	<0.001	72.77	Inc
E3ILL	3	4	0.96	0.01	0.68	<0.001	-45.84	Dec
E3ILL	3	5	0.98	0.02	0.22	<0.001	-12.88	Dec
E3ILL	3	6	0.97	0.01	0.07	<0.001	-4.69	Dec
E3ILL	3	7	0.98	0.00	-0.01	0.09	2.87	Dec
E3ILL	4	1	0.99	0.01	-3.36	<0.001	242.25	Inc
E3ILL	4	2	0.98	0.03	-1.97	0.01	73.88	Inc
E3ILL	4	3	0.99	0.03	-1.92	<0.001	76.11	Inc
E3ILL	4	4	0.94	0.01	0.03	0.01	-2.72	Dec
E3ILL	4	5	0.99	0.02	-1.13	<0.001	52.49	Dec
E3ILL	4	6	0.90	0.01	-0.77	0.01	59.59	Dec
E3ILL	4	7	0.99	0.01	-0.02	0.01	3.59	Dec
E3ILL	5	1	0.97	0.01	-2.19	<0.001	230.50	Inc
E4ILLF5	2	1	0.96	0.02	0.15	<0.001	-9.42	Inc
E4ILLF5	2	2	0.99	0.01	-0.31	<0.001	23.82	Inc
E4ILLF5	2	3	0.99	0.02	-0.20	<0.001	12.04	Dec
E4ILLF5	2	4	0.99	0.01	-1.86	<0.001	143.01	Dec
E4ILLF5	2	5	0.99	0.01	-0.14	<0.001	14.68	Dec
E4ILLF5	2	6	0.99	0.01	-0.21	<0.001	35.35	Dec
E4ILLF5	2	7	0.92	0.00	-0.15	0.01	77.43	Dec
E4ILLF5	3	1	0.99	0.01	0.07	<0.001	-4.77	Inc
E4ILLF5	3	2	0.99	0.01	-0.01	<0.001	0.89	Inc
E4ILLF5	3	3	0.98	0.02	-1.04	0.01	65.01	Dec
E4ILLF5	3	4	0.99	0.01	-0.13	NA	14.66	Dec
E4ILLF5	3	5	0.86	0.02	-1.69	0.25	104.92	Dec
E4ILLF5	4	1	0.99	0.02	-2.45	NA	125.99	Inc
E4ILLF5	4	2	0.99	0.01	-0.59	0.03	43.69	Inc
E4ILLF5	4	3	0.92	0.01	-0.73	0.18	69.49	Dec

E4ILLF5	4	4	0.91	0.01	-0.37	0.19	27.80	Dec
E4ILLF5	4	5	0.99	0.01	-0.13	NA	10.78	Dec
E4ILLF5	5	2	0.91	0.01	-1.46	0.19	102.23	Inc
E4ILLF5	5	3	0.82	0.01	0.72	0.28	-75.55	Inc
E4ILLF5	5	4	0.99	0.01	-0.23	0.07	21.56	Inc
E4ILLF5	5	5	0.99	0.01	-0.08	NA	10.69	Dec
E4ILLF5	5	6	0.99	0.02	-1.54	NA	96.74	Dec

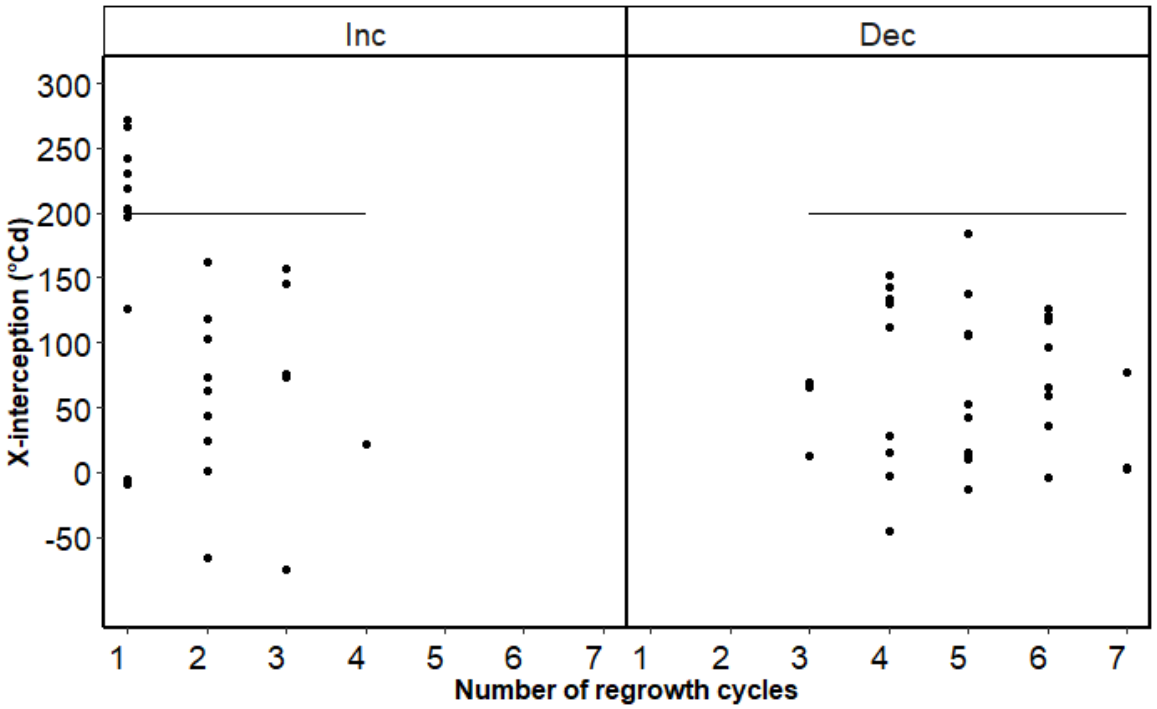

Appendix 13. X-interception values of linear regression between leaf area index (LAI) and thermal time (Tt) of each regrowth cycle from four field experiments conducted within 1997 to 2019 at Lincoln University, Canterbury, New Zealand. Inc and Dec represent increasing and decreasing photoperiod (Pp).

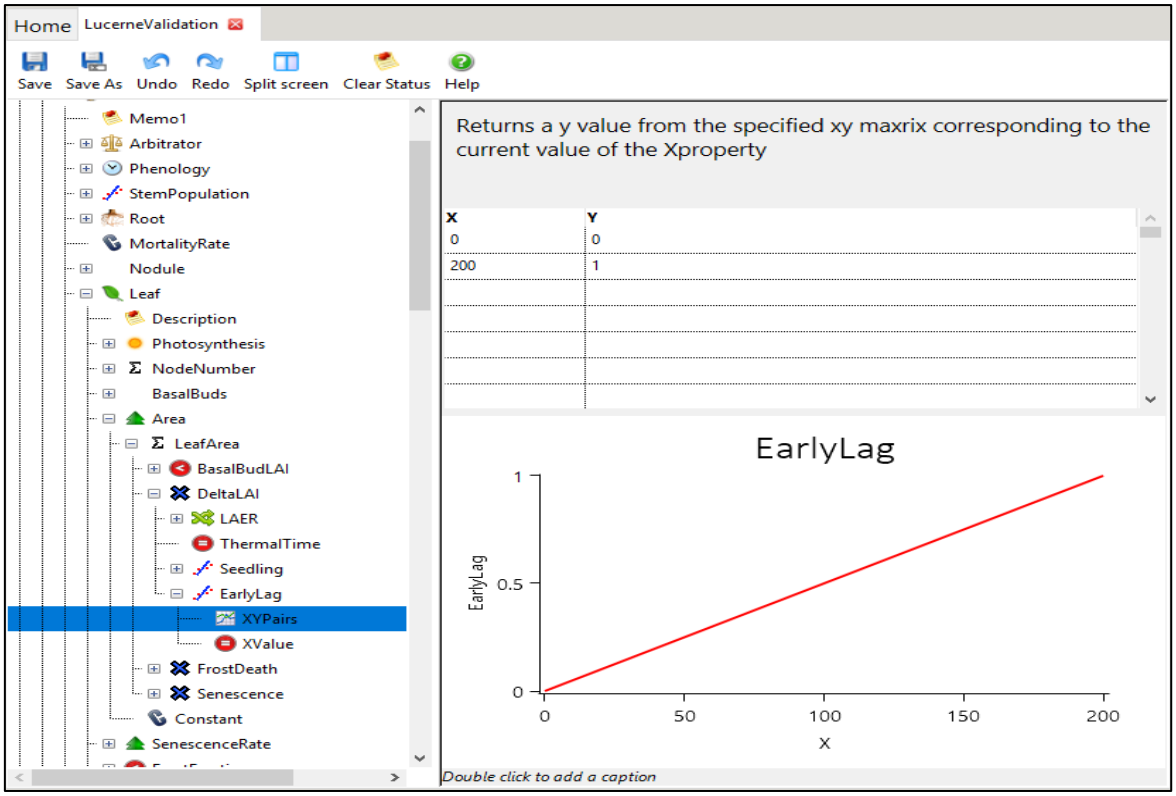

Appendix 14. Model structure for the lag function of leaf area expansion rate (LAER) in APSIM NextGen lucerne model.

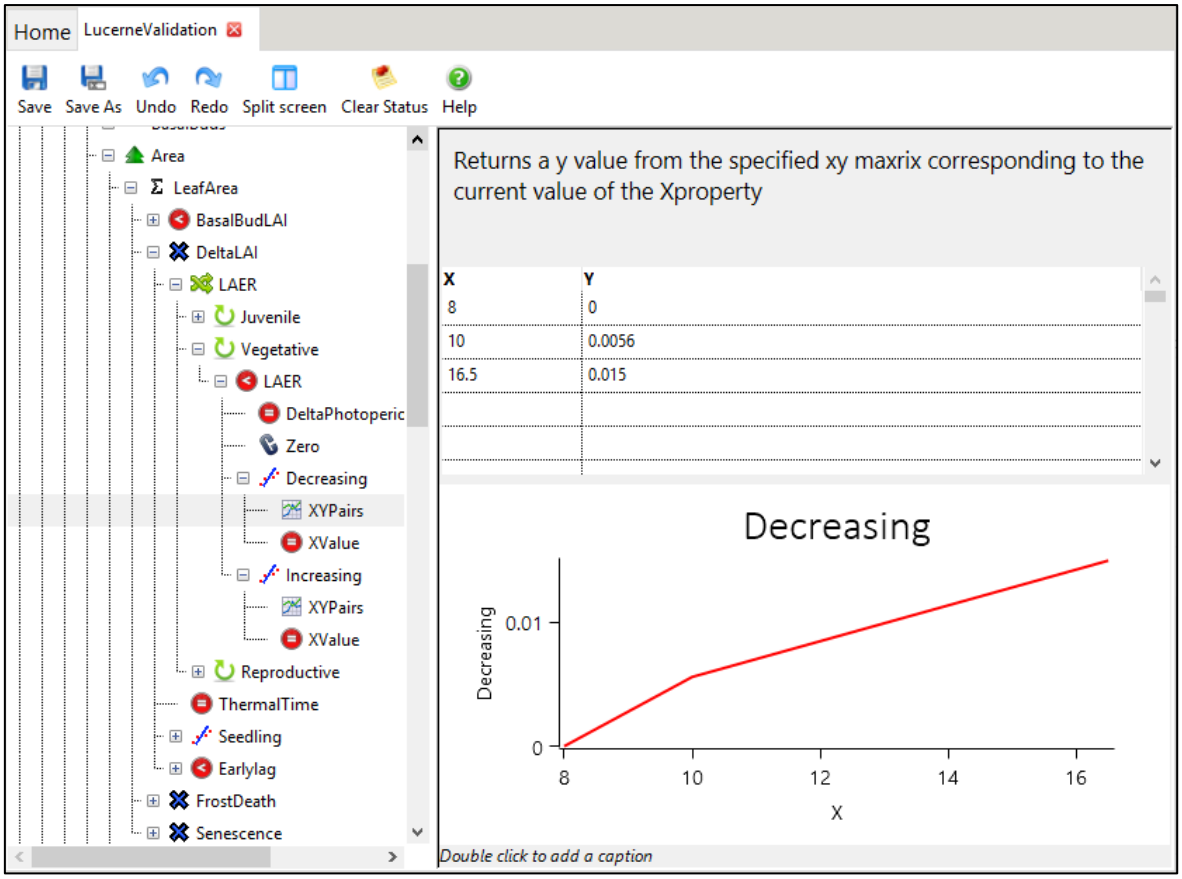

Appendix 15. Model structure for leaf area expansion rate (LAER) function in a decreasing photoperiod (Pp) in APSIM NextGen lucerne model.

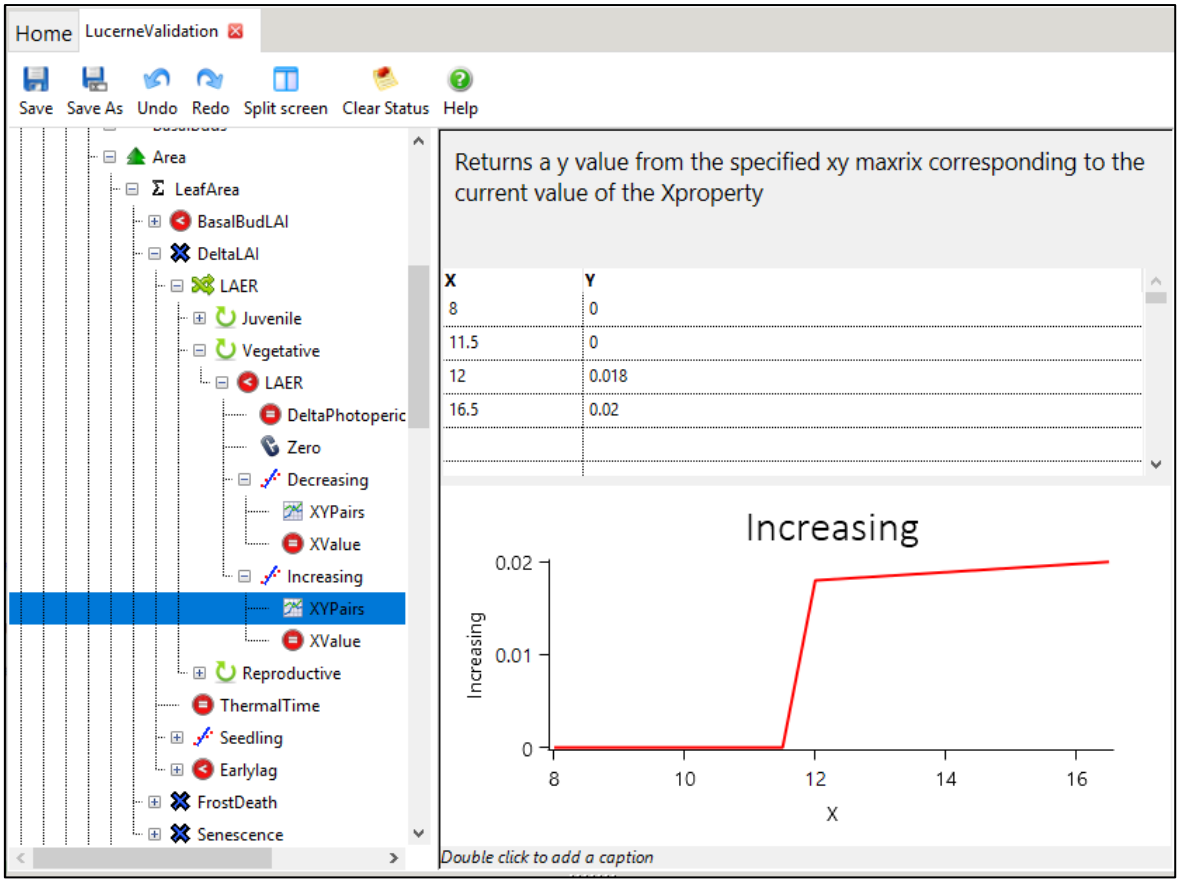

Appendix 16. Model structure for leaf area expansion rate (LAER) function in an increasing photoperiod (Pp) in APSIM NextGen lucerne model.

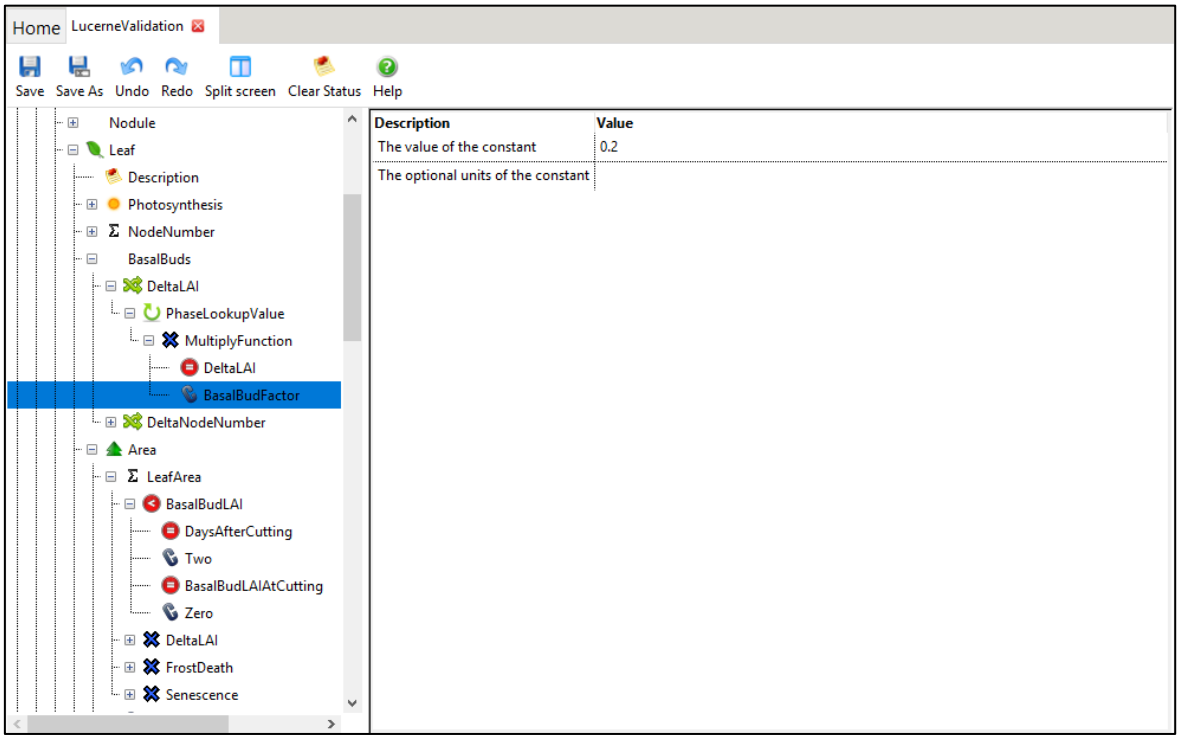

Appendix 17. Model structure for the basal buds function in APSIM NextGen lucerne model.

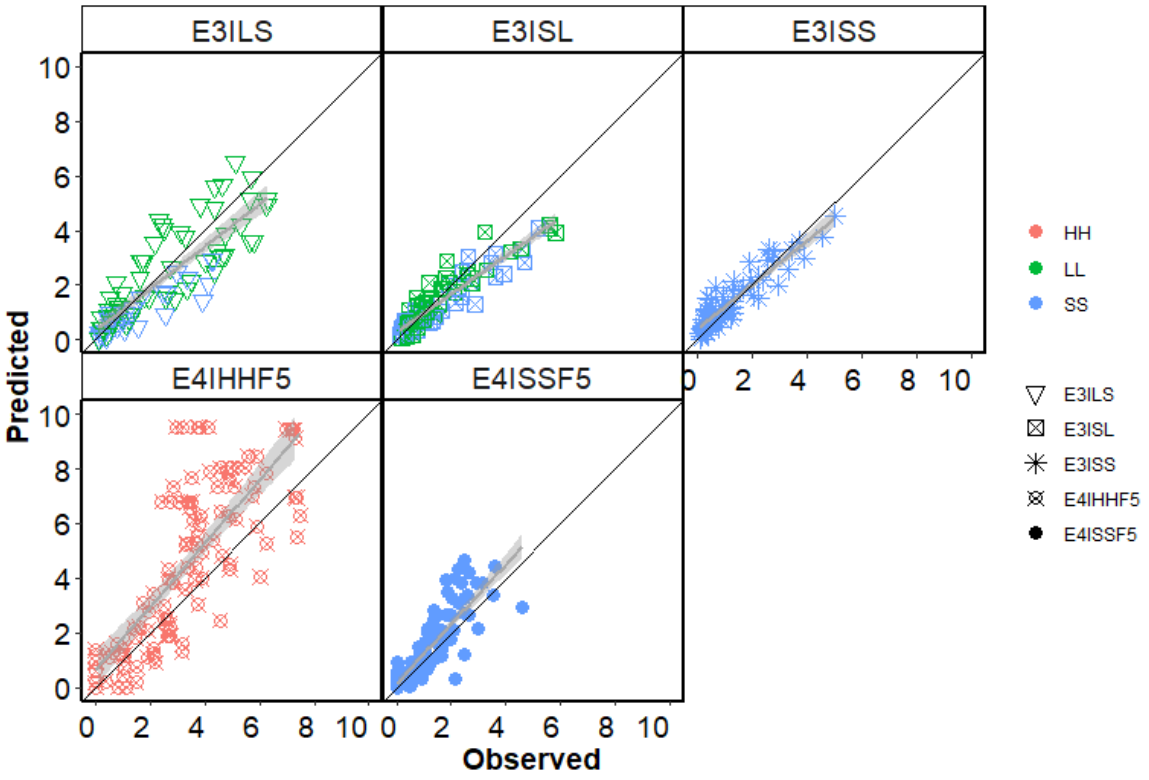

Appendix 18. Predicted and observed Leaf area index (LAI) values before apply the SenescenceRate function from two field experiments with multiple defoliation treatments [HH (84 day), LS (42, 28 day), SL (28, 42 day), and SS (28 day)] conducted between 2002 and 2019 at Iversen field, Lincoln University, Canterbury, New Zealand.

Appendix 19. Statistical measures of leaf are index (LAI) before apply the SenescenceRate function from two field experiments with multiple defoliation treatments [HH (84 day), LS (42, 28 day), SL (28, 42 day), and SS (28 day)] conducted between 2002 and 2019 at Iversen field, Lincoln University, Canterbury, New Zealand. N = number of simulated and observed data pairs; R2= coefficient of determination; R_RMSE = relative root mean square error (%); NSE = Nash-Sutcliffe efficiency; SB = Standard bias; NU = Nonunity slope; LC = Lack of correlation.

Treatment	N	R^2	R_RMSE	NSE	SB	NU	LC
E3ILS	86	0.72	43.5	0.7	3	2.4	94.6
E3ISL	82	0.84	43.7	0.76	12.9	20.2	66.8
E3ISS	67	0.82	44.2	0.79	9.3	2.3	88.4
E4IHHF5	101	0.58	65.2	-0.63	31.1	43.1	25.8
E4ISSF5	92	0.71	52.7	0.32	16.2	41.8	42

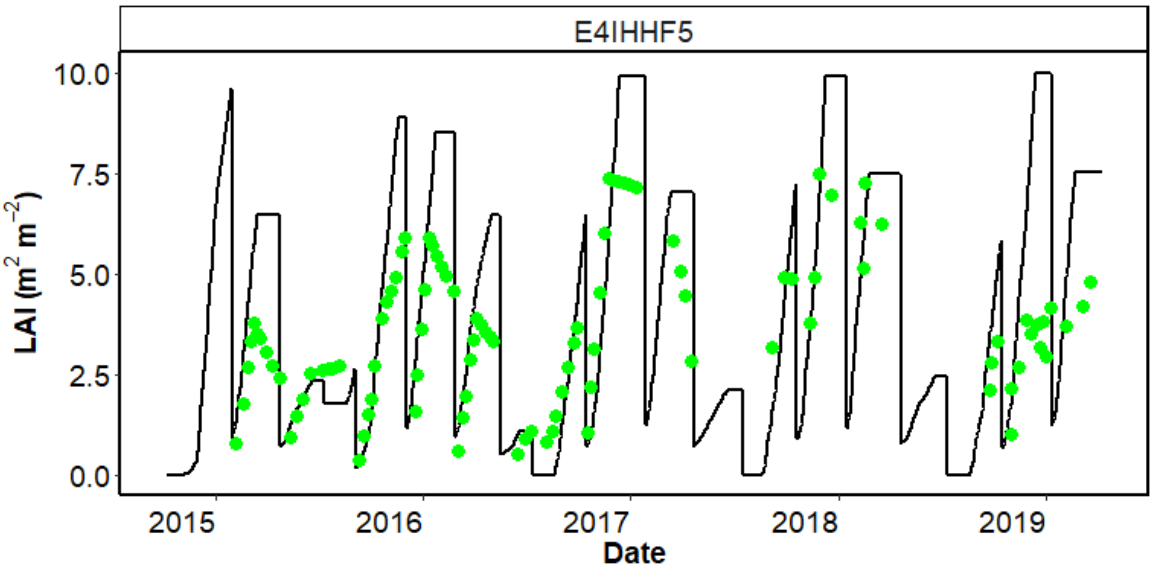

Appendix 20. Predicted and observed leaf area index (LAI) values before apply the SenescenceRate function for a field experiment with an 84 day defoliation treatment (HH) conducted between 2014 and 2019 at Iversen field, Lincoln University, Canterbury, New Zealand.

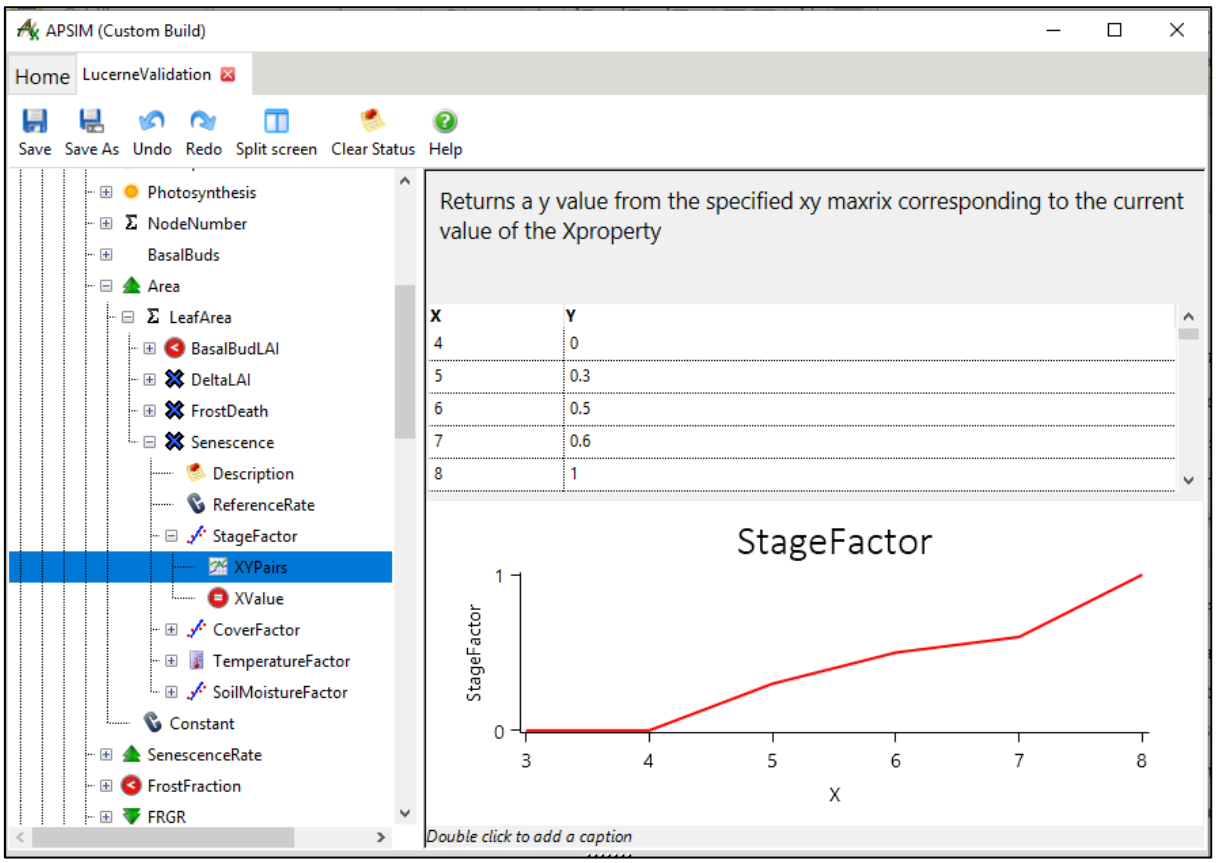

Appendix 21. Model structure for leaf area senescence function in APSIM NextGen lucerne model.

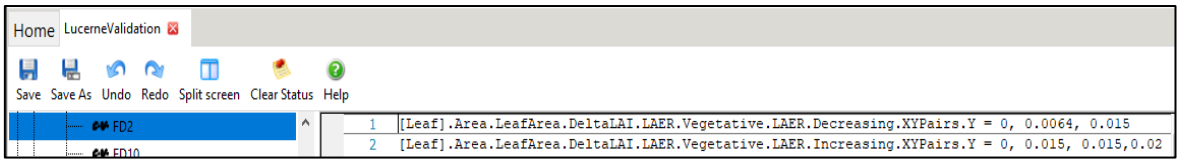

Appendix 22. Model structure for leaf area expansion rate (LAER) of FD2 in APSIM NextGen lucerne model.

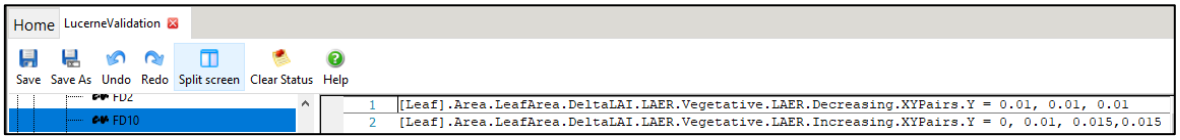

Appendix 23. Model structure for leaf area expansion rate (LAER) of FD10 in APSIM NextGen lucerne model.

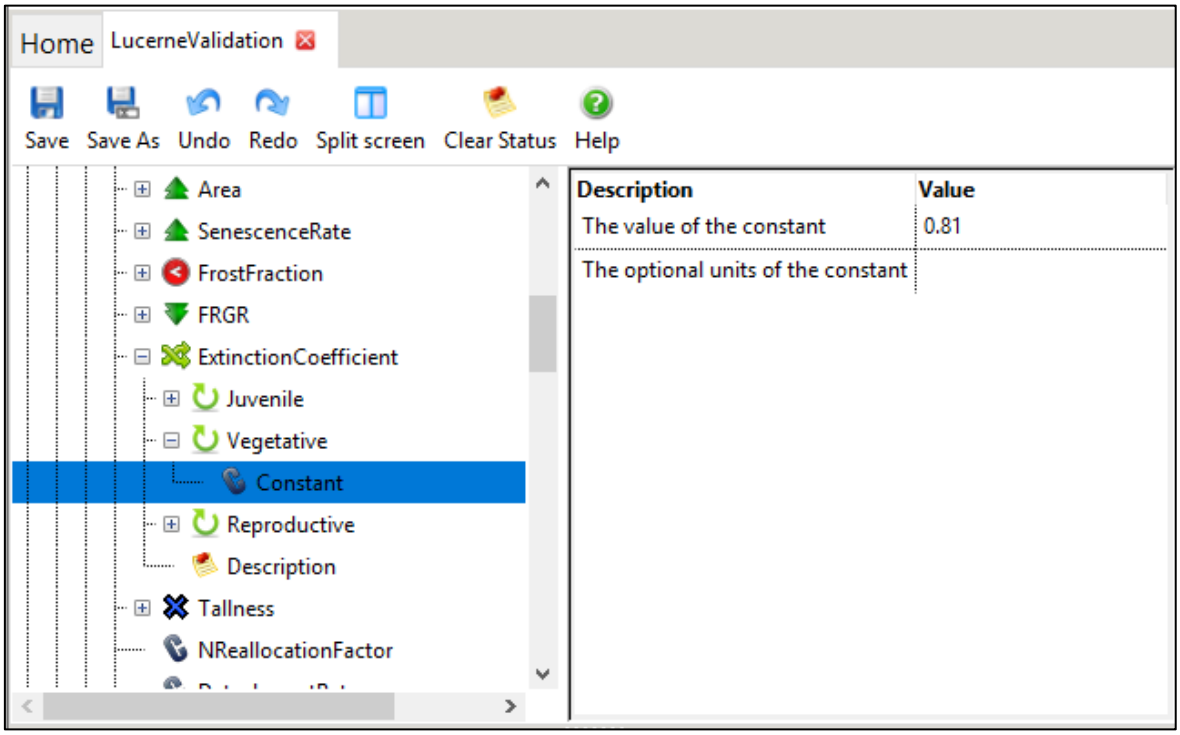

Appendix 24. Model structure for Extinction coefficient in APSIM NextGen lucerne model.

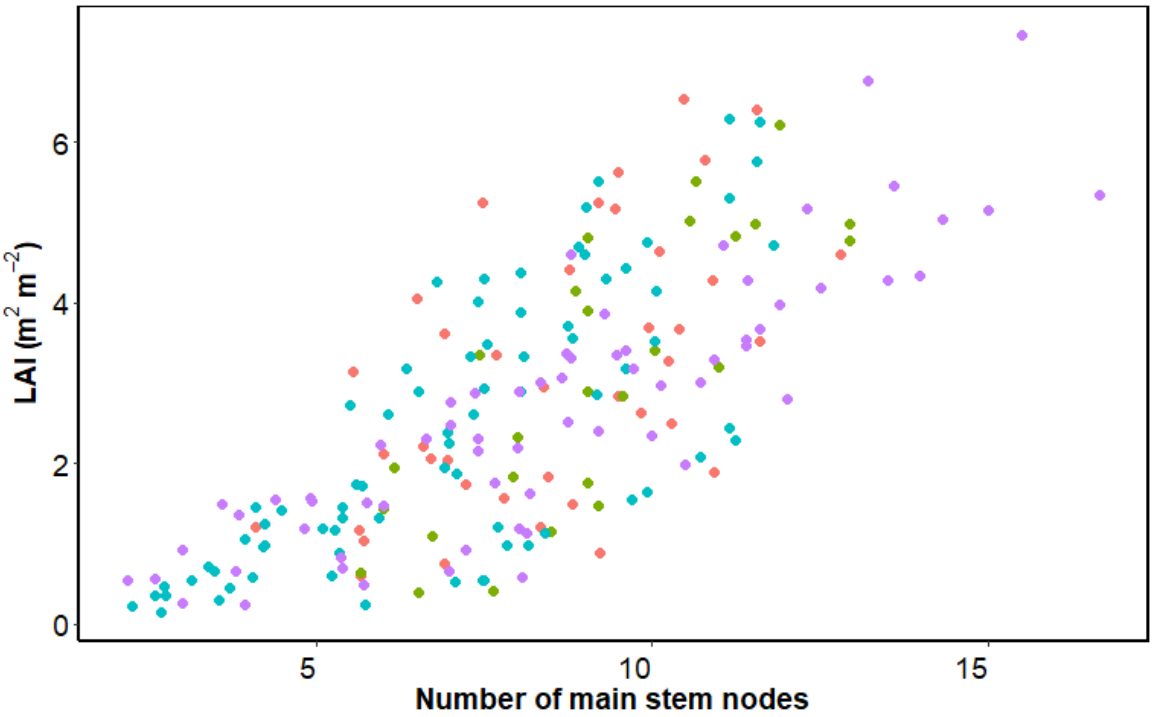

Appendix 25. Relationship between leaf area index (LAI) and number of main stem nodes.

Appendix 26. Statistical measures of total biomass (shoot and root; g DM m^{-2}) against accumulated total radiation (MJ m^{-2}) from two field experiments conducted from 2002-2019 at Iversen field, Lincoln University, Canterbury, New Zealand.

ID	Growth season	Regrowth cycle	R^2	Slope	Intercept	p
E4ILLF5	1	1	0.99	0.66	-70.45	0.07
E4ILLF5	1	2	1	1.15	306.97	NA
E4ILLF5	2	1	1	0.12	625.6	NA
E4ILLF5	2	2	1	0.71	435.09	NA
E4ILLF5	2	3	1	0.78	562.7	NA
E4ILLF5	2	4	1	1.09	509.02	0.01
E4ILLF5	2	5	1	1.01	495.19	NA
E4ILLF5	3	1	1	0.73	487.85	NA
E4ILLF5	3	2	1	0.48	494.62	NA
E4ILLF5	3	3	1	0.92	541.93	NA
E4ILLF5	3	4	1	1.06	863.62	NA
E4ILLF5	4	1	1	0	661.8	NA
E4ILLF5	4	2	1	0.34	519.11	NA
E4ILLF5	4	3	1	0.95	546.46	NA
E4ILLF5	4	4	1	0.66	669.88	NA
E4ILLF5	4	5	1	0.8	659.23	NA
E4ILLF5	5	3	1	0.68	498.31	NA
E4ILLF5	5	4	1	0.47	584.21	NA
E4ILLF5	5	5	1	0.91	466.09	NA
E4ILLF5	5	6	1	1.03	503.02	NA
E3ILL	3	1	0.71	0.48	579.34	0.07
E3ILL	3	2	1	0.74	475.8	0.02
E3ILL	3	3	0.96	0.66	435.23	0
E3ILL	3	4	0.97	1.09	308.33	0
E3ILL	3	5	0.85	0.75	542.03	0.08
E3ILL	3	6	0.53	0.39	733.18	0.16
E3ILL	3	7	0.9	2.51	586.92	0.21
E3ILL	4	1	0.92	0.7	556.13	0.04
E3ILL	4	2	0.82	0.53	552.43	0.03
E3ILL	4	3	0.78	0.99	501.27	0.05
E3ILL	4	4	0.99	1.38	438.36	0.01
E3ILL	4	5	0.96	1.3	488.32	0
E3ILL	4	6	0.77	1.56	411.87	0.05

E3ILL	4	7	1	1.08	667.81	NA
E3ILL	5	1	1	0.3	580.07	NA

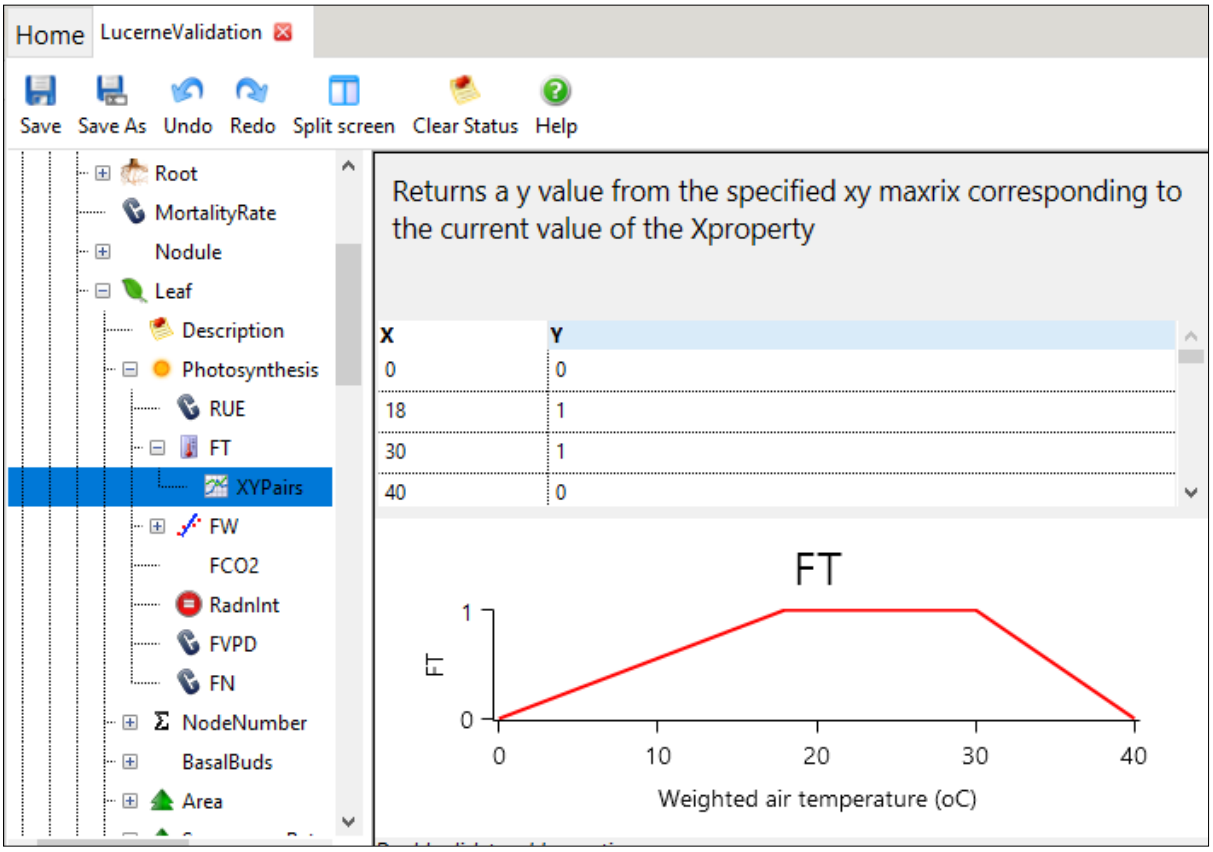

Appendix 27. Model structure for total radiation use efficiency (RUE_{total}; g MJ^{-1}) function in APSIM NextGen lucerne model.

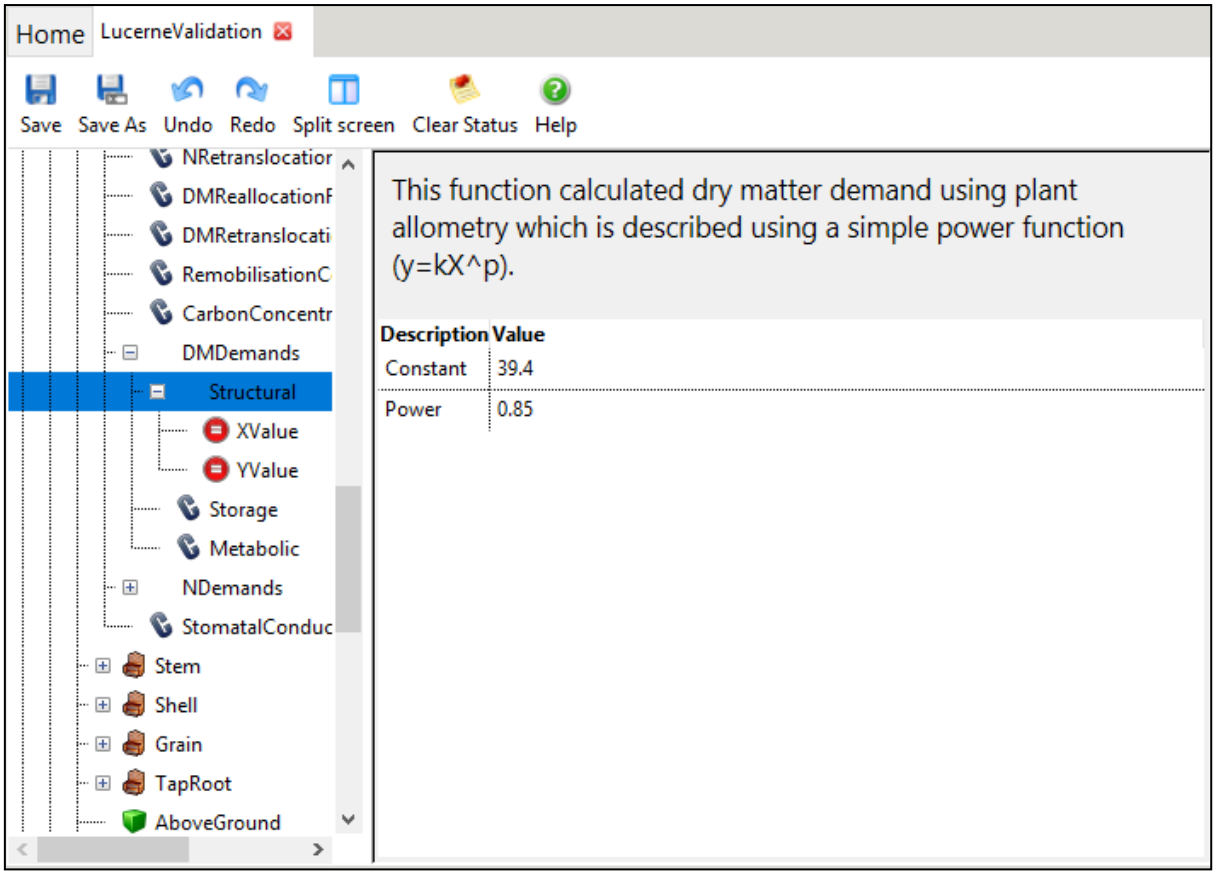

Appendix 28. Model structure for leaf biomass demand function in APSIM NextGen lucerne model.

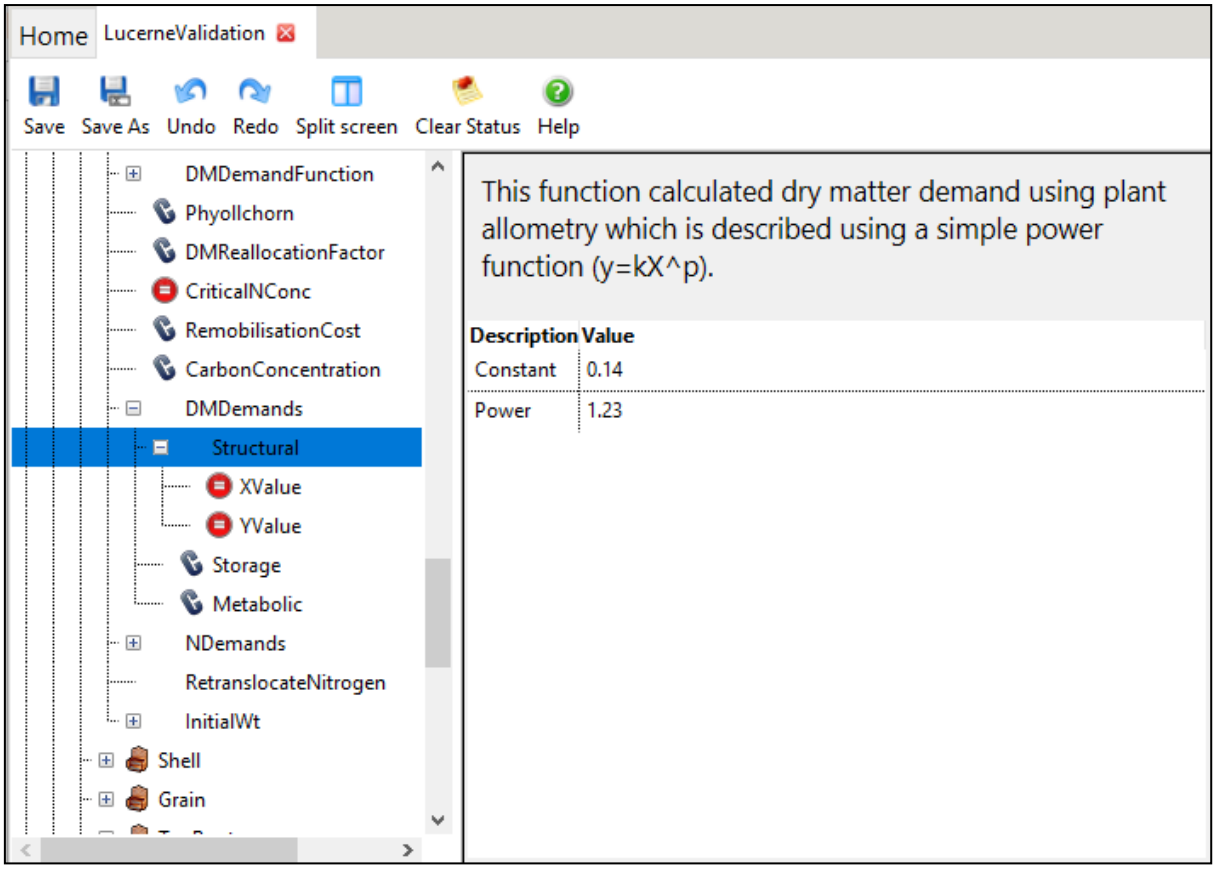

Appendix 29. Model structure for stem biomass demand function in APSIM NextGen lucerne model.

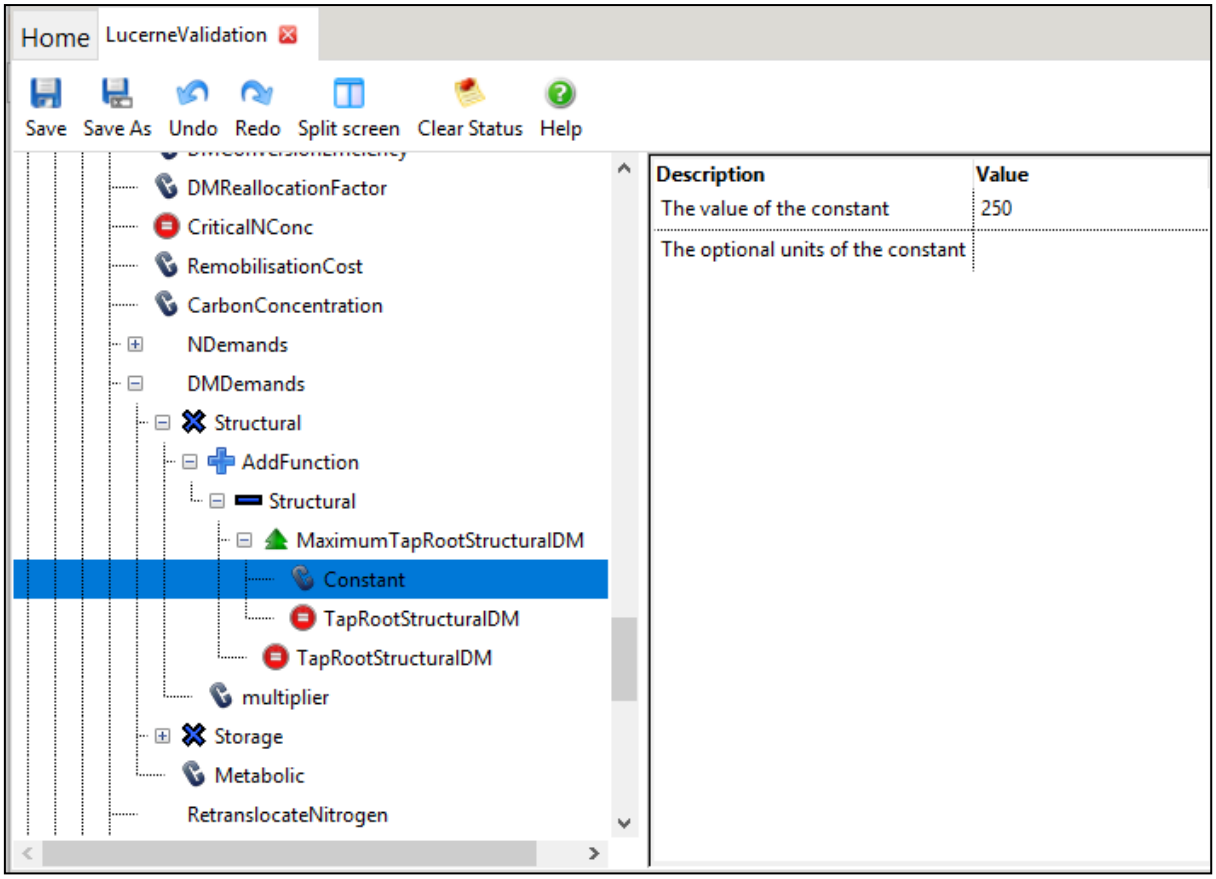

Appendix 30. Model structure for root structural demand in APSIM NextGen lucerne model.

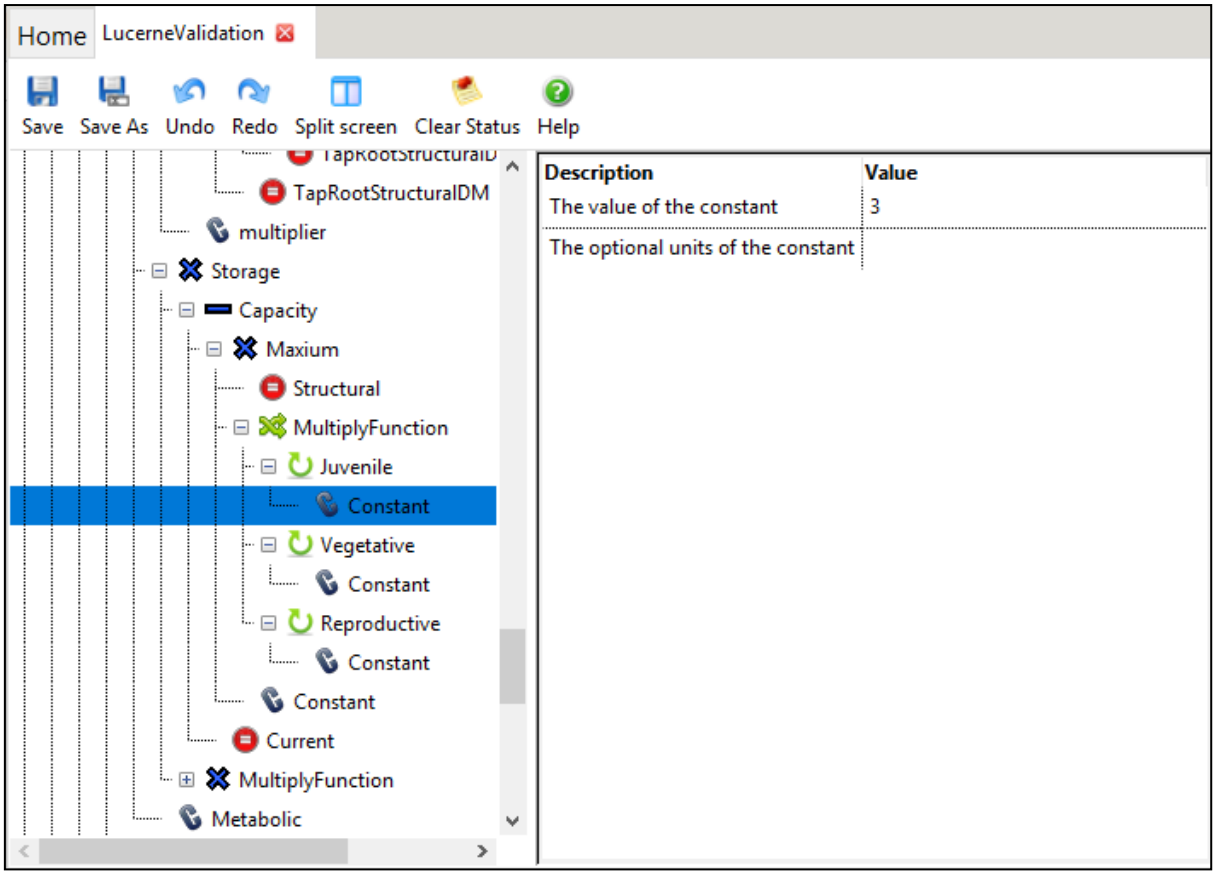

Appendix 31. Model structure for root storage demand function in APSIM NextGen lucerne model.

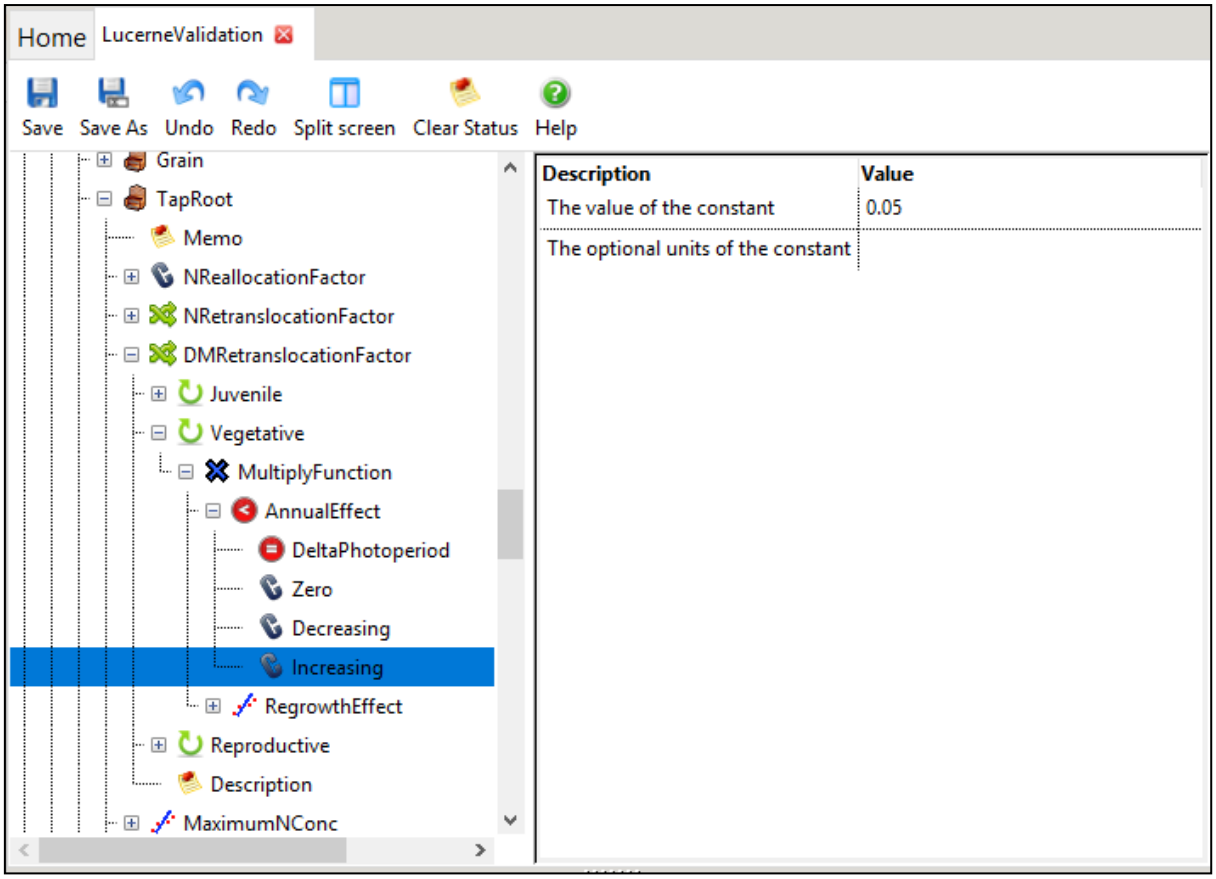

Appendix 32. Model structure for root remobilization function in APSIM NextGen lucerne model.

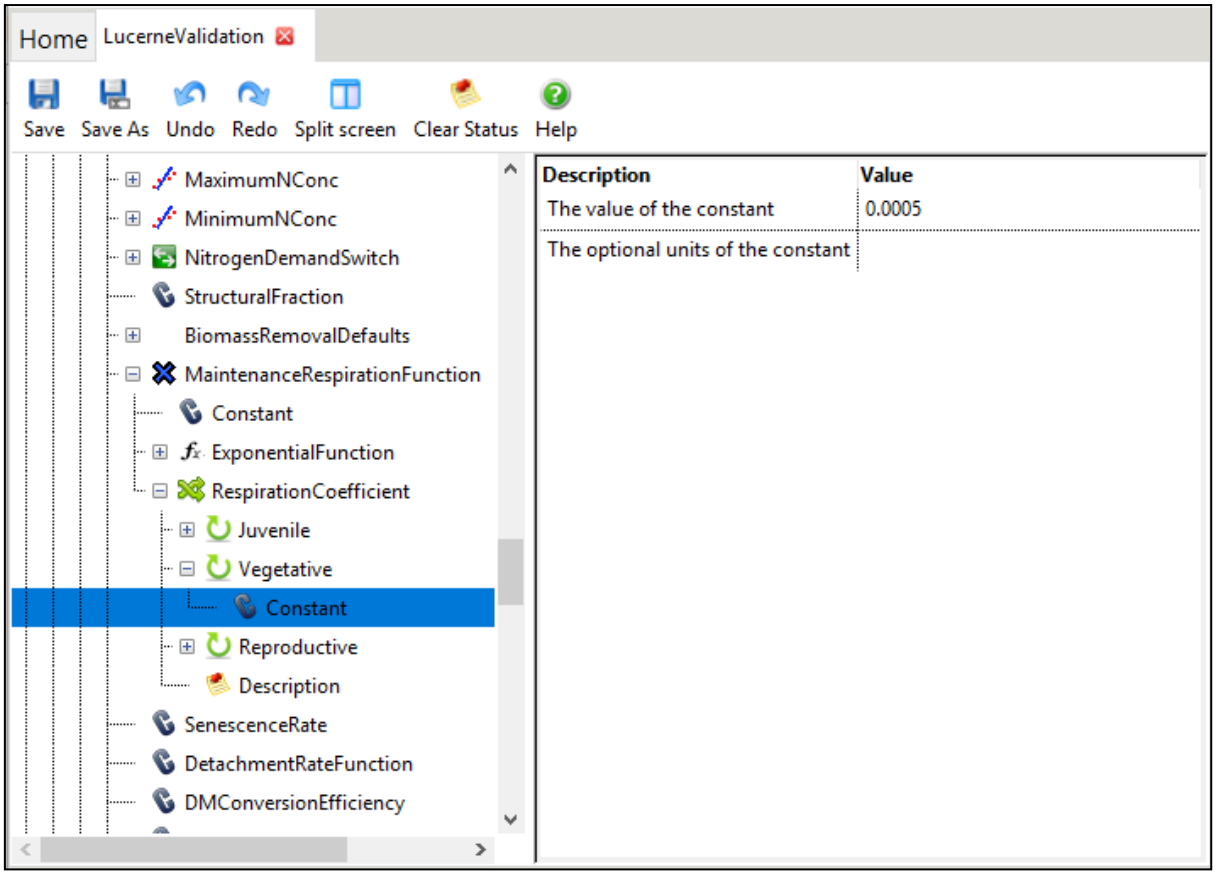

Appendix 33. Model structure for root maintenance respiration function in APSIM NextGen lucerne model.

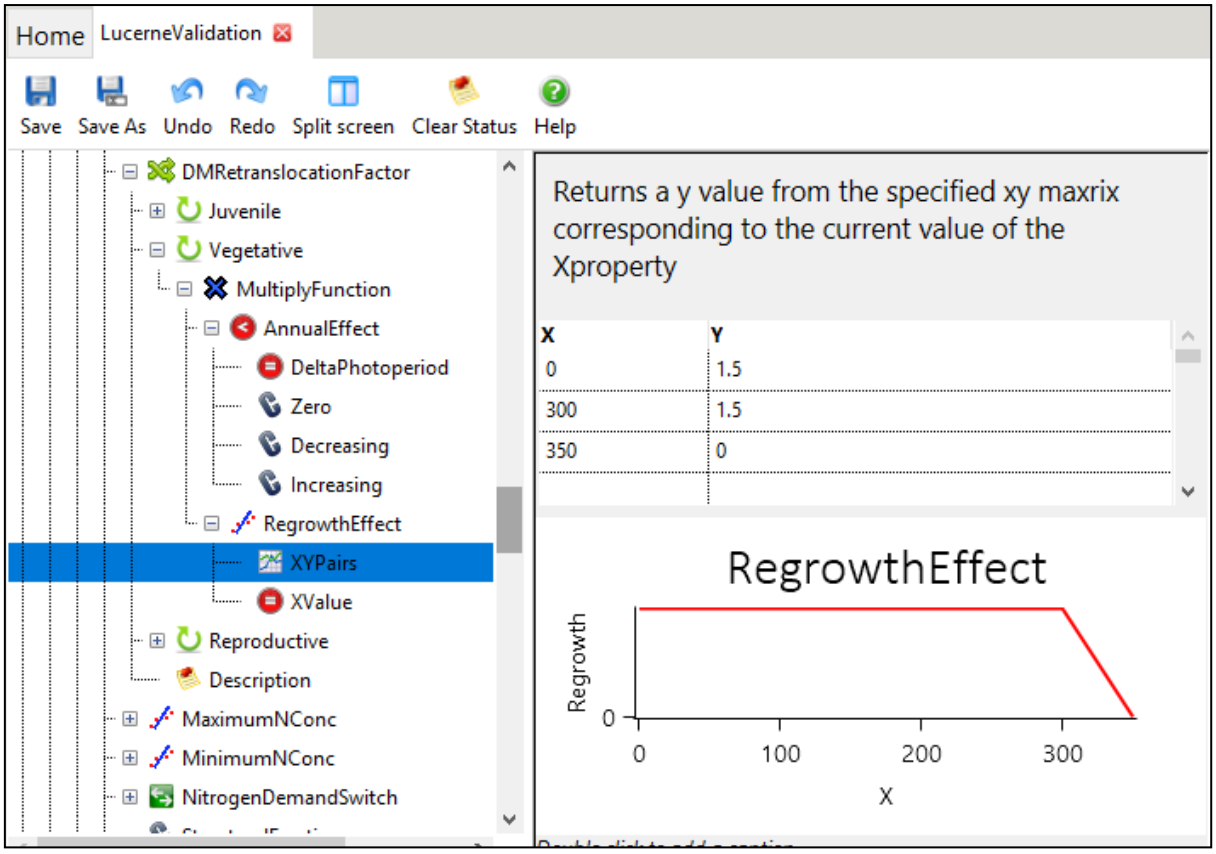

Appendix 34. Model structure for root remobilization coefficient function in APSIM NextGen lucerne model.

Appendix 35 Statistical measures of biomass remobilization coefficient values for fall dormancy 2 (FD2) experiments conducted from 2014 to 2019 at Iversen field, Lincoln University, Canterbury, New Zealand. N = number of simulated and observed data pairs; R^2= coefficient of determination; R_RMSE = relative root mean square error (%); NSE = Nash-Sutcliffe efficiency; SB = Standard bias; NU = Nonunity slope; LC = Lack of correlation.

Prediction	C remobilization coefficient	N	R^2	R_RMSE	NSE	SB	NU	LC
Predicted0	shoot	56	0.76	68.2	0.43	18.8	39.3	41.9
(0)	root	44	0.49	35.86	-0.01	35.6	14.1	50.3
Predicted1	shoot	56	0.75	70.42	0.39	23.8	34.9	41.2
(0.005)	root	44	0.49	28.51	0.36	9.7	11.2	79.1
Predicted2	shoot	56	0.75	**70.45**	**0.39**	24.3	34.8	41
(0.01)	root	44	0.48	**28.26**	**0.37**	4.8	12.3	82.9
Predicted3	shoot	56	0.75	70.46	0.39	24.3	34.7	40.9
(0.015)	root	44	0.48	28.19	0.37	4.1	12.4	83.6
Predicted4	shoot	56	0.75	70.47	0.39	24.4	34.7	40.9
(0.02)	root	44	0.48	28.16	0.37	3.7	12.4	83.9
Predicted5	shoot	56	0.75	70.47	0.39	24.4	34.7	40.9
(0.025)	root	44	0.48	28.14	0.38	3.5	12.4	84.1
Predicted6	shoot	56	0.75	70.47	0.39	24.4	34.7	40.9
(0.03)	root	44	0.47	28.14	0.38	3.4	12.4	84.2
Predicted7	shoot	56	0.75	70.47	0.39	24.4	34.7	40.9
(0.035)	root	44	0.47	28.13	0.38	3.3	12.4	84.3
Predicted8	shoot	56	0.75	70.47	0.39	24.4	34.7	40.9
(0.04)	root	44	0.47	28.13	0.38	3.3	12.4	84.3
Predicted9	shoot	56	0.75	70.47	0.39	24.4	34.7	40.9
(0.045)	root	44	0.47	28.13	0.38	3.2	12.4	84.4

Appendix 36 Statistical measures of biomass remobilization coefficient values for fall dromancy 10 (FD10) experiments conducted from 2014 to 2019 at Iversen field, Lincoln University, Canterbury, New Zealand. N = number of simulated and observed data pairs; R^2= coefficient of determination; R_RMSE = relative root mean square error (%); NSE = Nash-Sutcliffe efficiency; SB = Standard bias; NU = Nonunity slope; LC = Lack of correlation.

Prediction	C remobilization coefficient	N	R^2	R_RMSE	NSE	SB	NU	LC
Predicted0	shoot	56	0.76	42.5	0.72	0	13	87
(0)	root	44	0.20	56.7	-0.88	43.1	14.4	42.5
Predicted1	shoot	56	0.72	45.4	0.68	0.6	12.4	87.1
(0.005)	root	44	0.24	50	-0.46	34	14.2	51.9
Predicted2	shoot	56	0.73	**45.3**	**0.68**	0.6	12.3	87.1
(0.01)	root	44	0.24	**49.5**	**-0.43**	31.4	15.4	53.2
Predicted3	shoot	56	0.73	45.3	0.68	0.6	12.2	87.2
(0.015)	root	44	0.23	49.6	-0.44	29.6	16.7	53.7
Predicted4	shoot	56	0.73	45.3	0.68	0.6	12.2	87.2
(0.02)	root	44	0.23	49.6	-0.44	29	17.2	53.8
Predicted5	shoot	56	0.73	45.3	0.68	0.6	12.2	87.2
(0.025)	root	44	0.23	49.6	-0.44	29	17.2	53.8
Predicted6	shoot	56	0.73	45.3	0.68	0.6	12.2	87.2
(0.03)	root	44	0.23	49.6	-0.44	28.9	17.2	53.8
Predicted7	shoot	56	0.73	45.3	0.68	0.6	12.2	87.2
(0.035)	root	44	0.23	49.6	-0.44	28.9	17.3	53.8
Predicted8	shoot	56	0.73	45.3	0.68	0.6	12.2	87.2
(0.04)	root	44	0.23	49.6	-0.44	28.9	17.3	53.8
Predicted9	shoot	56	0.73	45.3	0.68	0.6	12.2	87.2
(0.045)	root	44	0.23	49.6	-0.44	28.9	17.3	53.8

Appendix 37 Statistical measures of shoot and root biomass for remobilization duration values of fall dormancy 2 (FD2) from a field experiments conducted from 2014 to 2019 at Iversen field, Lincoln University, Canterbury, New Zealand. N = number of simulated and observed data pairs; R2= coefficient of determination; R_RMSE = relative root mean square error (%); NSE = Nash-Sutcliffe efficiency; SB = Standard bias; NU = Nonunity slope; LC = Lack of correlation.

Regrowth coefficient	Biomass	N	R^2	R_RMSE	NSE	SB	NU	LC
Predicted0	shoot	125	0.70	62.5	0.58	16.5	11.0	72.5
(0)	root	113	0.50	31.9	0.47	5.9	0.0	94.1
Predicted1	shoot	125	0.70	61.0	0.60	11.0	13.6	75.4
(0-50)	root	113	0.33	44.3	-0.02	33.3	1.3	65.4
Predicted2	shoot	125	0.70	60.9	0.61	11.6	13.1	75.3
(50-100)	root	113	0.39	41.3	0.11	30.1	0.8	69.0
Predicted3	shoot	125	0.71	60.8	0.61	12.5	12.4	75.1
(100-150)	root	113	0.46	37.1	0.28	25.0	0.2	74.8
Prediction4	shoot	125	0.71	60.7	0.61	13.5	11.8	74.7
(150-200)	root	113	0.53	33.1	0.43	18.1	0.0	81.9
Predicted5	shoot	125	0.71	60.8	0.61	14.5	11.3	74.2
(200-250)	root	113	0.60	28.7	0.57	6.7	0.1	93.2
Predicted6	shoot	125	0.71	**61.3**	**0.60**	15.4	10.9	73.6
(250-300)	root	113	0.61	**27.3**	**0.61**	0.0	0.2	99.7
Predicted7	shoot	125	0.70	61.7	0.59	15.7	10.9	73.4
(300-350)	root	113	0.59	29.6	0.54	6.8	3.6	89.6
Predicted8	shoot	125	0.70	61.9	0.59	15.6	11.2	73.2
(350-400)	root	113	0.60	32.0	0.46	22.3	3.3	74.4
Predicted9	shoot	125	0.70	62.0	0.59	15.3	11.6	73.1
(400-450)	root	113	0.61	35.5	0.34	39.2	1.8	59.0
Predicted10	shoot	125	0.70	62.1	0.59	15.2	11.7	73.1
(450-500)	root	113	0.60	37.7	0.26	44.7	1.6	53.7
Predicted11	shoot	125	0.70	62.0	0.59	15.1	11.8	73.1
(500-550)	root	113	0.59	39.8	0.17	48.3	1.6	50.1
Predicted12	shoot	125	0.70	61.9	0.59	15.0	11.8	73.2
(550-600)	root	113	0.55	42.6	0.05	50.5	2.1	47.3

Appendix 38 Statistical measures of shoot and root biomass for remobilization duration values of fall dormancy 10 (FD10) from a field experiments conducted from 2014 to 2019 at Iversen field, Lincoln University, Canterbury, New Zealand. N = number of simulated and observed data pairs; R^2= coefficient of determination; R_RMSE = relative root mean square error (%); NSE = Nash-Sutcliffe efficiency; SB = Standard bias; NU = Nonunity slope; LC = Lack of correlation.

Regrowth coefficient	Biomass	N	R^2	R_RMSE	NSE	SB	NU	LC
Predicted0	shoot	124	0.67	55.5	0.66	1.4	0.0	98.5
(0)	root	112	0.08	71.8	-0.58	35.3	6.4	58.4
Predicted1	shoot	124	0.70	52.5	0.70	0.1	0.0	99.9
(0-50)	root	112	0.02	83.8	-1.15	45.8	8.9	45.3
Predicted2	shoot	124	0.70	52.6	0.69	0.2	0.0	99.8
(50-100)	root	112	0.04	81.2	-1.02	44.6	8.0	47.4
Predicted3	shoot	124	0.69	52.8	0.69	0.3	0.0	99.6
(100-150)	root	112	0.08	76.8	-0.81	43.1	5.8	51.1
Prediction4	shoot	124	0.69	53.1	0.69	0.5	0.0	99.4
(150-200)	root	112	0.11	72.9	-0.63	41.1	4.5	54.3
Predicted5	shoot	124	0.69	53.1	0.69	0.7	0.0	99.3
(200-250)	root	112	0.20	66.3	-0.35	38.9	2.0	59.1
Predicted6	shoot	124	0.69	53.5	0.68	0.9	0.0	99.1
(250-300)	root	112	0.35	56.2	0.03	31.8	0.6	67.6
Predicted7	shoot	124	0.68	54.6	0.67	1.2	0.0	98.8
(300-350)	root	112	0.47	45.9	0.35	17.2	0.2	82.6
Predicted8	shoot	124	0.68	54.6	0.67	1.2	0.0	98.8
(350-400)	root	112	0.50	41.7	0.47	5.8	1.2	93.0
Predicted9	shoot	124	0.68	54.6	0.67	1.1	0.0	98.9
(400-450)	root	112	0.48	41.9	0.46	0.5	2.2	97.3
Predicted10	shoot	124	0.68	54.5	0.67	1.1	0.0	98.9
(450-500)	root	112	0.50	40.6	0.49	0.3	0.7	99.1
Predicted11	shoot	124	0.68	**54.5**	**0.67**	1.1	0.0	98.9
(500-550)	root	112	0.56	**38.8**	**0.54**	4.2	0.2	95.6
Predicted12	shoot	124	0.68	54.5	0.67	1.1	0.0	98.9
(550-600)	root	112	0.53	41.2	0.48	9.2	0.0	90.8

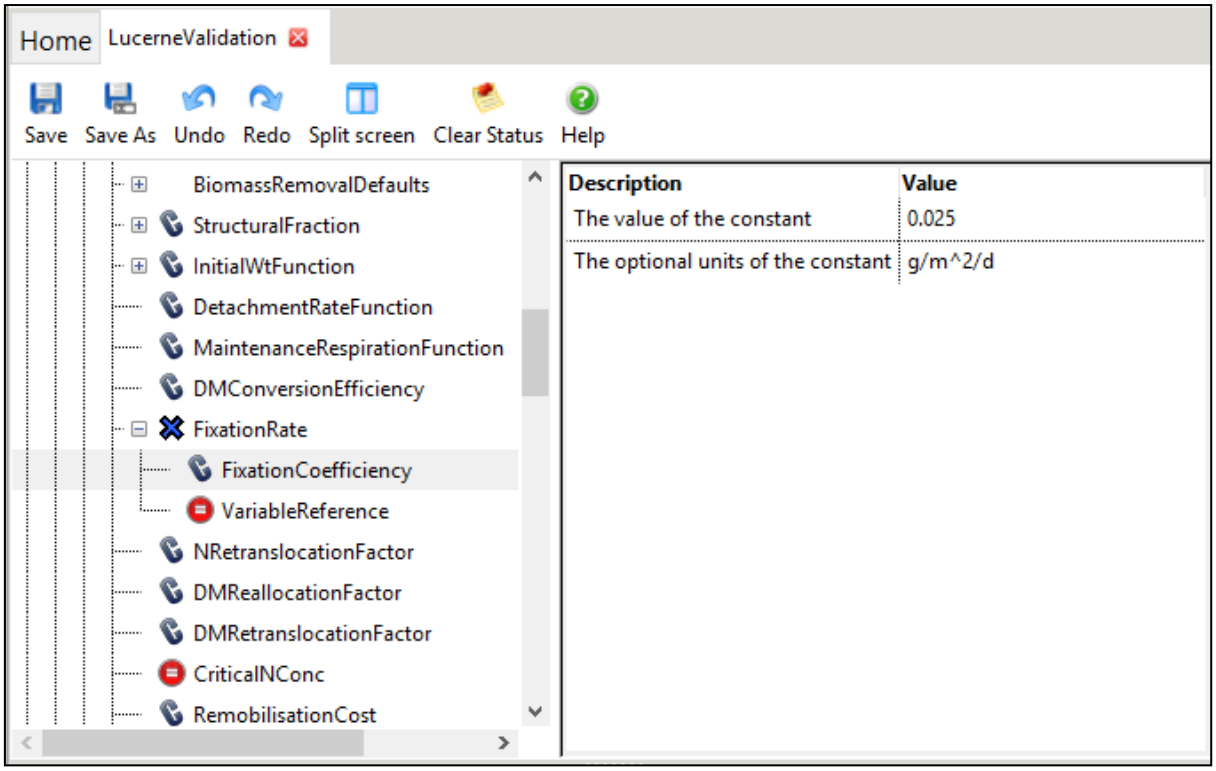

Appendix 39. Model structure for N supply function in APSIM NextGen lucerne model.

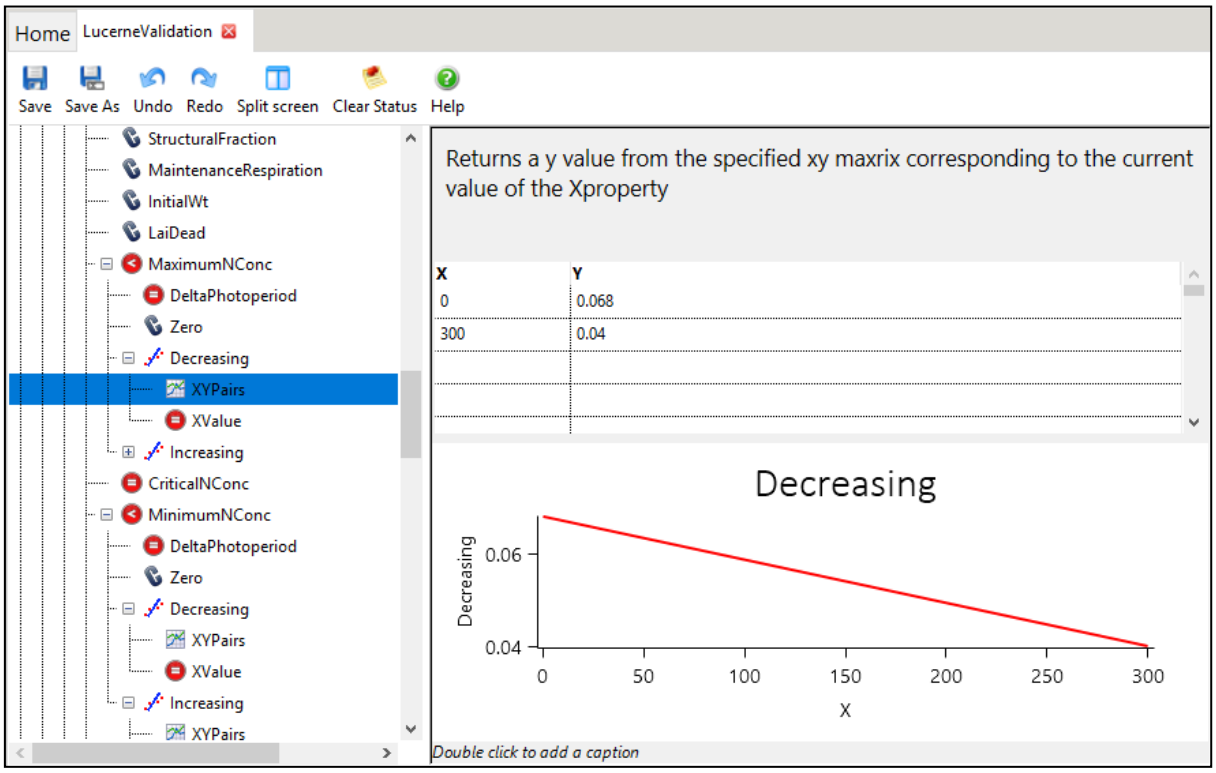

Appendix 40. Model structure for leaf maximal N concentration in APSIM NextGen lucerne model.

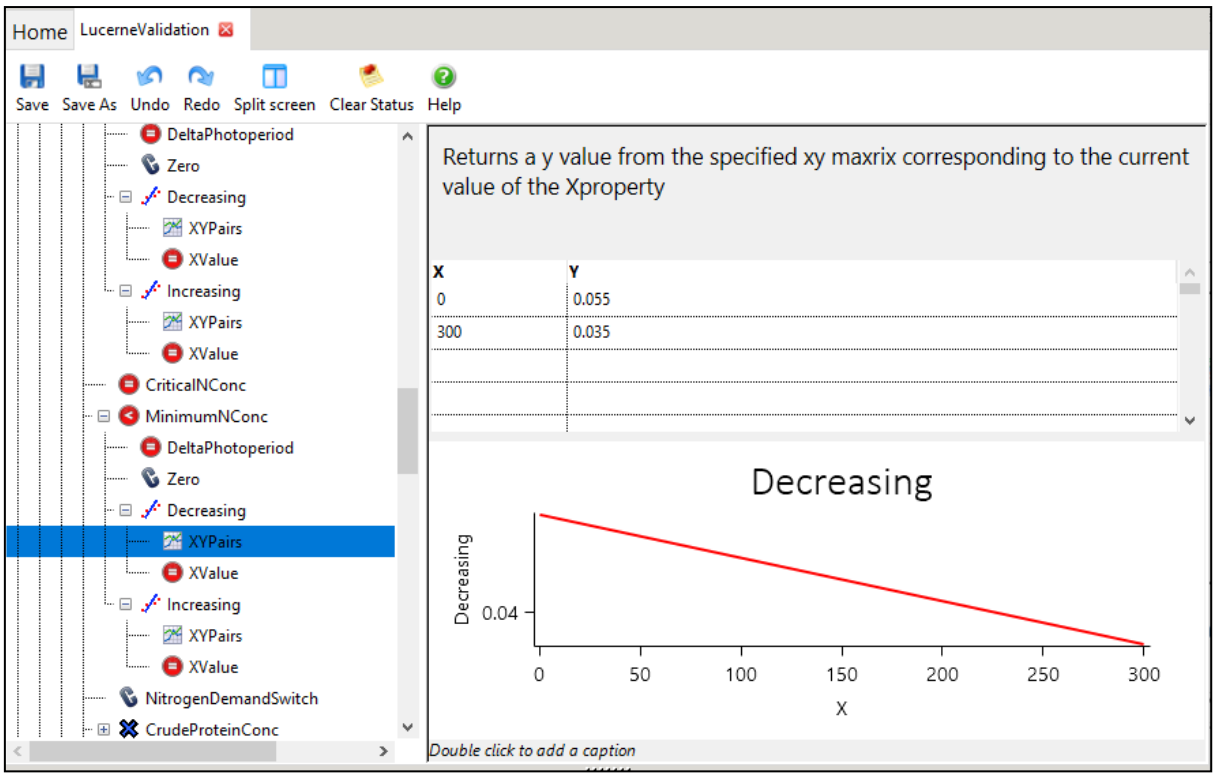

Appendix 41. Model structure for leaf minimal N concentration in APSIM NextGen lucerne model.

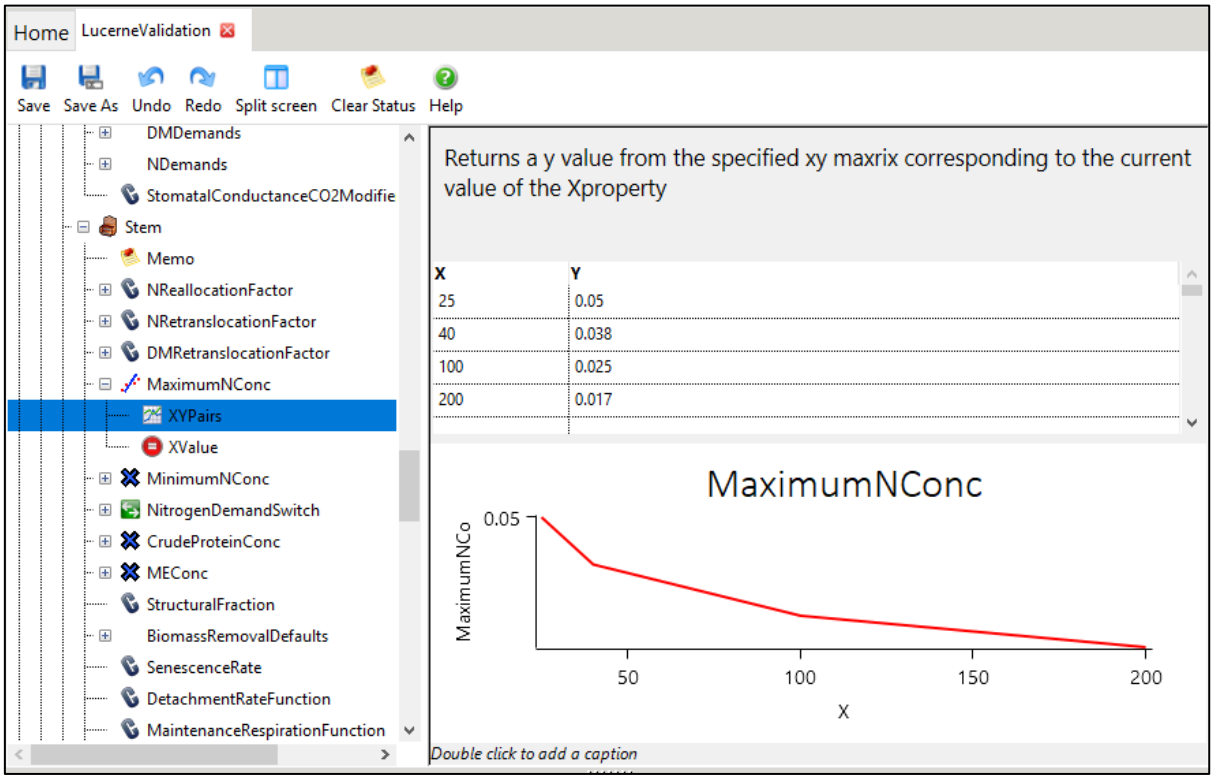

Appendix 42. Model structure for stem maximum N concentration in APSIM NextGen lucerne model.

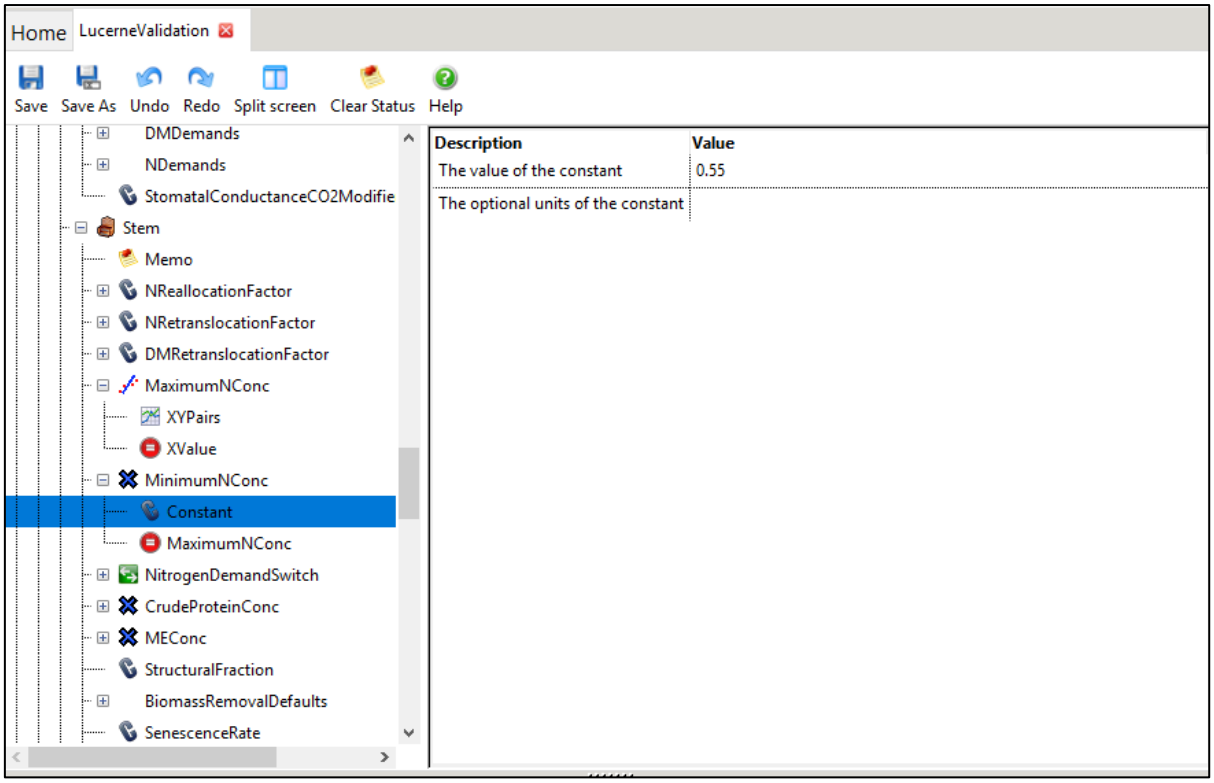

Appendix 43. Model structure for stem minimal N concentration in APSIM NextGen lucerne model.

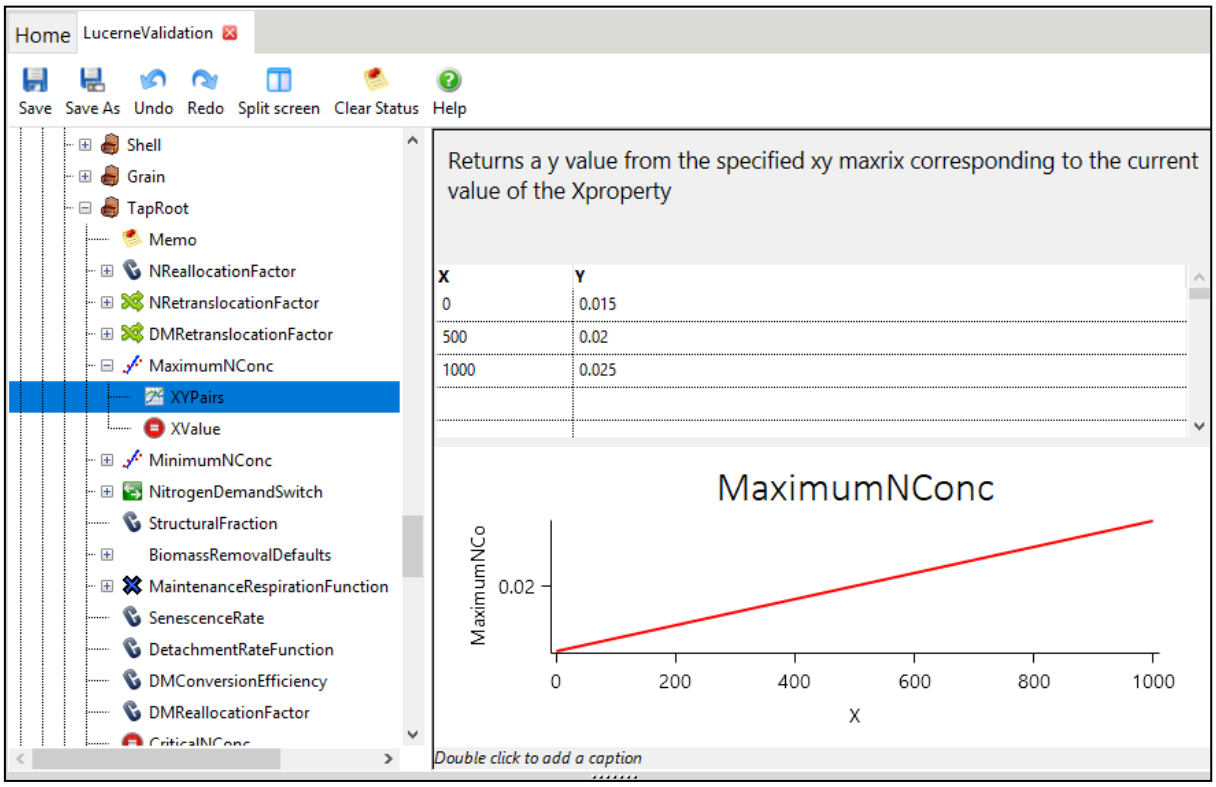

Appendix 44. Model structure for root maximum N concentration in APSIM NextGen lucerne model.

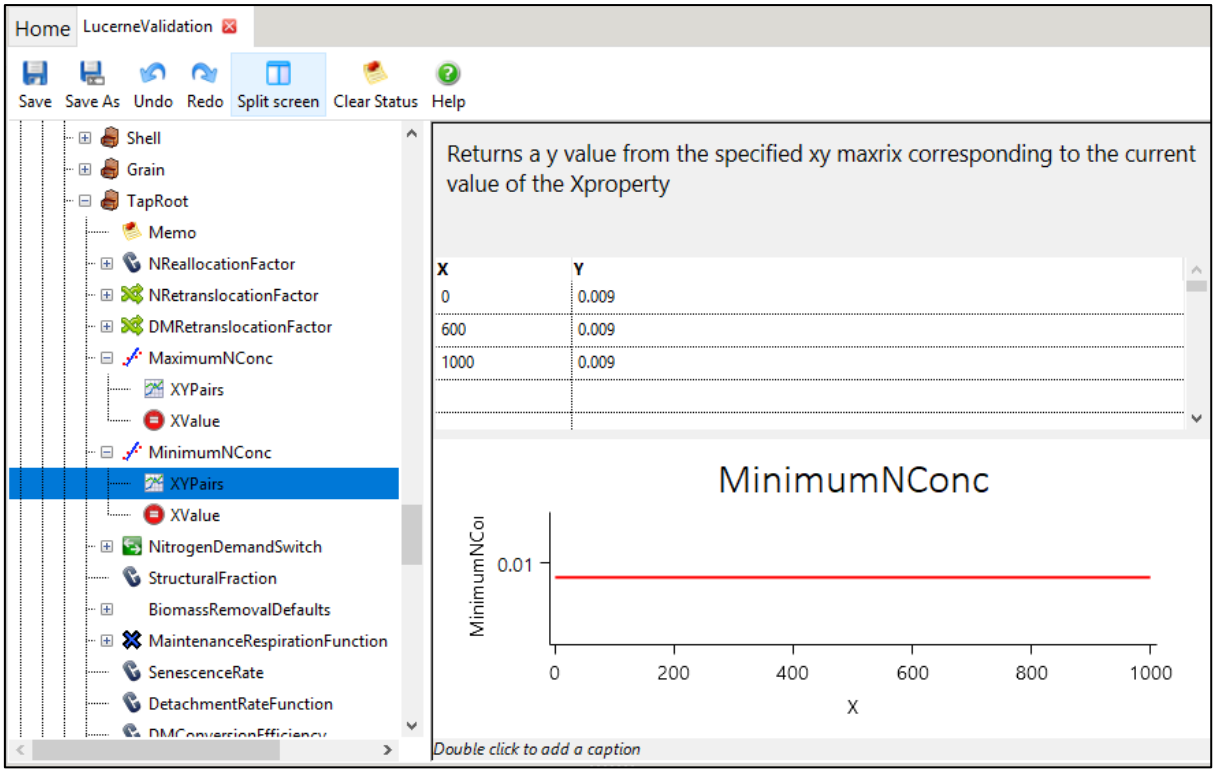

Appendix 45. Model structure for root minimum N concentration in APSIM NextGen lucerne model.

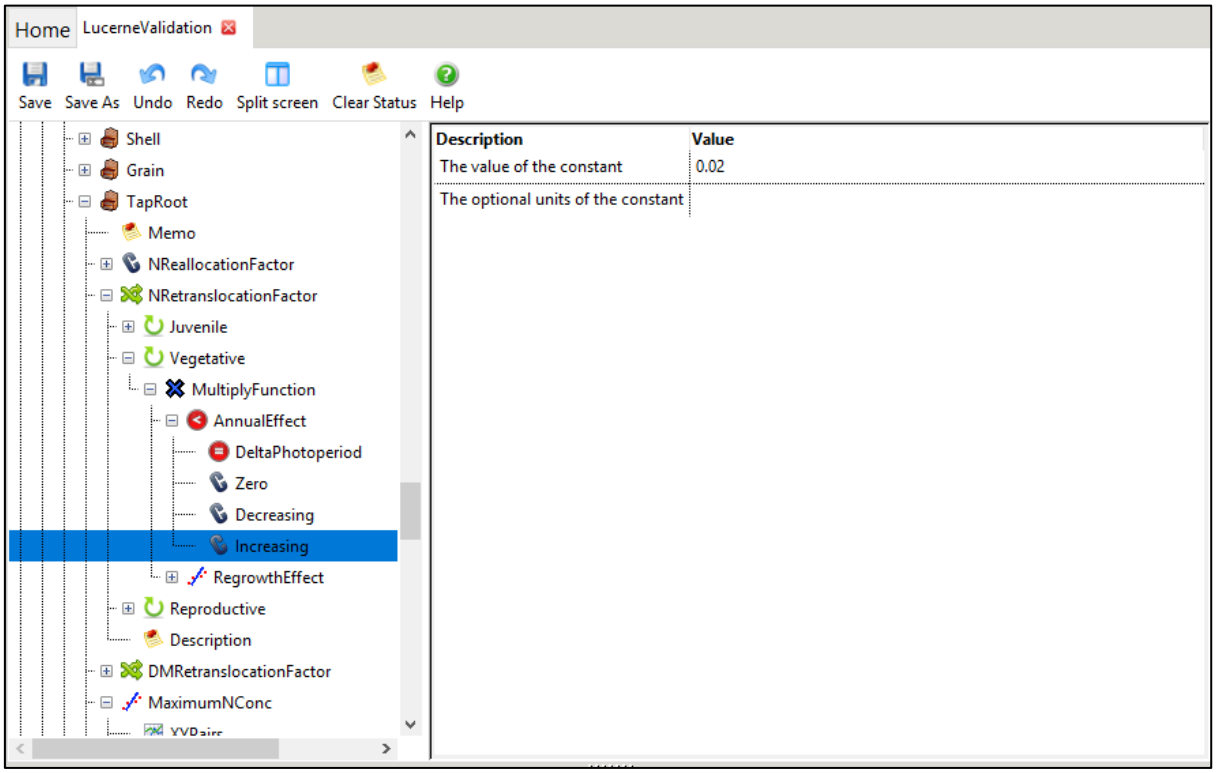

Appendix 46. Model structure for root N remobilization in APSIM NextGen lucerne model.

Appendix 47 Statistical measures of N remobilization coefficient values for fall dormancy 2 (FD2) experiments conducted from 2014 to 2019 at Iversen field, Lincoln University, Canterbury, New Zealand. N = number of simulated and observed data pairs; R^2= coefficient of determination; R_RMSE = relative root mean square error (%); NSE = Nash-Sutcliffe efficiency; SB = Standard bias; NU = Nonunity slope; LC = Lack of correlation.

Prediction	N remobilization coefficient	N	R^2	R_RMSE	NSE	SB	NU	LC
Predicted0	0	54	0	69.4	-8.81	55.3	34.6	10.2
Predicted1	0.005	54	0.44	**20.3**	**0.16**	0.6	33	66.5
Predicted2	0.01	54	0.41	24.7	-0.24	6.1	46.1	47.8
Predicted3	0.015	54	0.39	27.4	-0.53	11.5	48.9	39.7
Predicted4	0.02	54	0.38	29	-0.72	14.3	49.7	36
Predicted5	0.025	54	0.38	30.1	-0.84	16	50.1	33.8
Predicted6	0.03	54	0.38	30.6	-0.91	17	50.3	32.7
Predicted7	0.035	54	0.37	31	-0.95	17.5	50.4	32.1
Predicted8	0.04	54	0.37	31.2	-0.99	18	50.5	31.5

Appendix 48 Statistical measures of N remobilization coefficient values for fall dormancy 10 (FD10) experiments conducted from 2014 to 2019 at Iversen field, Lincoln University, Canterbury, New Zealand. N = number of simulated and observed data pairs; R^2= coefficient of determination; R_RMSE = relative root mean square error (%); NSE = Nash-Sutcliffe efficiency; SB = Standard bias; NU = Nonunity slope; LC = Lack of correlation.

Prediction	N remobilization coefficient	N	R^2	R_RMSE	NSE	SB	NU	LC
Predicted0	0	54	0.08	88.7	-16.99	64	30.9	5.1
Predicted1	0.005	54	0.63	**14.7**	**0.51**	1	22.8	76.1
Predicted2	0.01	54	0.65	17.6	0.29	20.8	29	50.2
Predicted3	0.015	54	0.62	21	0	29.4	32.4	38.3
Predicted4	0.02	54	0.60	22.8	-0.19	32.3	34.3	33.4
Predicted5	0.025	54	0.59	23.9	-0.31	33.3	35.5	31.2
Predicted6	0.03	54	0.58	24.5	-0.37	33.7	36.2	30.1
Predicted7	0.035	54	0.58	24.9	-0.42	33.8	36.8	29.4
Predicted8	0.04	54	0.58	25.2	-0.45	34	37.2	28.8

Appendix 49 Statistical measures of shoot and root biomass from experiments conducted between 1997 to 2019 at Iversen field, Lincoln University, Canterbury, New Zealand. N = number of simulated and observed data pairs; R^2= coefficient of determination; R_RMSE = relative root mean square error (%); NSE = Nash-Sutcliffe efficiency; SB = Standard bias; NU = Nonunity slope; LC = Lack of correlation.

	Biomass	N	R^2	R_RMSE	NSE	SB	NU	LC
E1ILL	shoot	111	0.51	46.4	0.47	5.8	1.6	92.6
E2ILLS1	shoot	45	0.80	30.9	0.73	24.4	0.1	75.5
E2ILLS2	shoot	24	0.70	37.8	0.55	28.8	3.5	67.6
E2ILLS3	shoot	24	0.79	35.5	0.57	47.5	2.9	49.6
E2ILLS4	shoot	23	0.55	57.1	-0.23	55.7	7.7	36.6
E3ILL	shoot	81	0.94	47.9	0.74	41.3	34.2	24.5
	root	65	0.49	13.7	0.4	15	0.3	84.7
E3ILS	shoot	79	0.94	48.5	0.8	32.1	39.4	28.6
	root	63	0.13	20.4	-0.4	22.1	15.6	62.3
E3ISL	shoot	72	0.86	41.2	0.81	15.2	6.8	77.9
	root	58	0.19	18.4	0.02	1	16.3	82.6
E3ISS	shoot	73	0.46	82.1	0.43	1.6	3.8	94.7
	root	59	0.22	23.9	-0.68	0.1	53.7	46.2
E4IHHF2	shoot	25	0.54	44	0.52	4.1	0.6	95.4
	root	25	0.20	26.3	0.11	10.1	0	89.8
E4IHHF5	shoot	45	0.69	63.1	0.67	3.7	2.3	94.1
	root	28	0.45	36.6	0.22	29.3	0	70.7
E4IHHF10	shoot	25	0.43	41.9	0.4	5.3	0.4	94.3
	root	25	0.01	32.8	-0.54	15.5	20	64.5
E4ILLF2	shoot	56	0.76	68.2	0.43	19.3	38.3	42.5
	root	44	0.44	28.7	0.35	4.8	9.2	86
E4ILLF5	shoot	67	0.81	64	0.65	12.4	33.2	54.4
	root	66	0.36	28.3	0.05	22.6	9.4	68
E4ILLF10	shoot	56	0.74	44.5	0.7	0.1	13.2	86.7
	root	44	0.44	46	-0.24	52.3	2.4	45.3
E4ISSF2	shoot	44	0.58	61.1	0.01	10.5	47.2	42.3
	root	44	0.02	35.1	-1.52	45.8	15.2	39
E4ISSF5	shoot	84	0.75	128.5	-0.17	17.8	61	21.2
	root	47	0.38	26.1	0.27	7.5	7.7	84.7
E4ISSF10	shoot	43	0.39	78.8	-0.47	22.6	35.9	41.5
	root	43	0.51	30.4	0.39	15.5	3.2	81.3

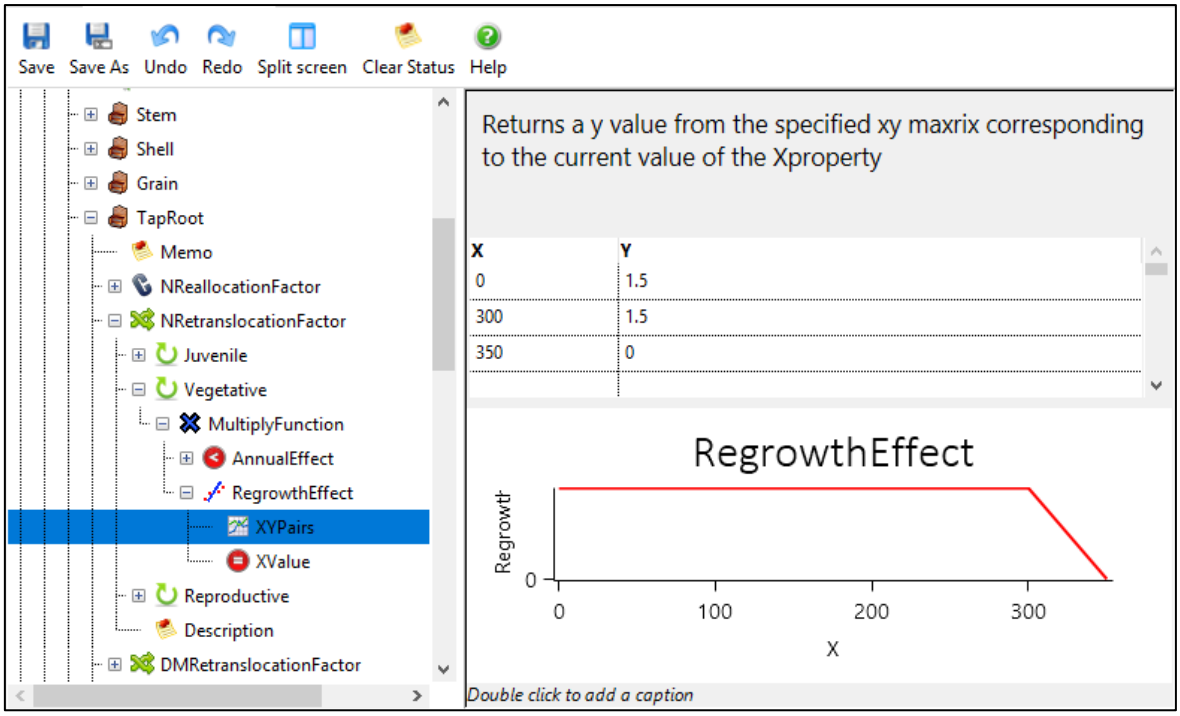

Appendix 50. Model structure for root N demand function in APSIM NextGen lucerne model.

Appendix 51. Statistical measures of linear relationship between height and thermal time (Tt) for four field experiments conducted within 1997 to 2019 at Lincoln University, Canterbury, New Zealand.

Stage	ID	Growth season	Regrowth cycle	R^2	Slope	Intercept	p
Seedling	E2ILLS1	1	1	0.99	0.93	386.74	<0.0001
	E2ILLS1	1	2	1.00	0.68	34.31	<0.0001
	E2ILLS1	1	3	0.98	0.89	23.63	0.001
	E2ILLS1	1	4	0.99	5.22	-213.05	0.04
	E2ILLS2	1	1	0.92	1.16	299.14	0.0001
	E2ILLS2	1	2	0.99	0.80	-6.37	<0.0001
	E2ILLS2	1	3	0.98	6.67	-377.71	0.09
	E2ILLS3	1	1	0.98	1.43	252.48	<0.0001
	E2ILLS3	1	2	0.99	2.02	-275.17	0.0003
	E2ILLS4	1	1	0.98	1.22	327.38	<0.0001
	E2ILLS4	1	2	1.00	1.54	1.35	0.0009
	E4ILLF5	1	1	0.98	1.59	241.65	0.009
	E4ILLF5	1	2	0.99	0.81	37.70	0.0007
	E4ILLF5	1	3	0.95	1.51	40.45	0.0048
	E4ILLF5	1	4	0.99	2.50	102.08	0.0031
Regrowth	E1ILL	2	2	0.99	0.48	112.49	0.0002
	E1ILL	2	3	1.00	0.51	109.12	0.04
	E1ILL	2	4	1.00	0.62	108.46	0.01
	E1ILL	2	5	0.99	0.70	180.67	0.003
	E1ILL	2	6	0.93	1.99	-0.75	0.16
	E1ILL	3	2	1.00	0.30	187.94	NA
	E1ILL	3	4	1.00	0.48	102.34	NA
	E1ILL	3	5	0.99	0.53	110.24	0.004
	E1ILL	5	1	0.99	2.02	150.11	<0.0001
	E1ILL	5	2	0.99	0.64	98.69	0.0002
	E1ILL	5	3	1.00	0.49	96.45	0.0003
	E1ILL	5	4	0.98	0.52	112.93	0.009
	E1ILL	5	5	0.99	0.68	80.86	0.0005
	E1ILL	5	6	0.97	1.42	-143.41	0.018
	E2ILLS1	2	1	0.97	0.78	156.46	0.002
	E2ILLS1	2	2	0.98	0.57	108.75	0.0001
	E2ILLS1	2	3	0.98	0.58	96.01	0.0009
	E2ILLS1	2	4	0.99	0.67	85.00	0.0001

E2ILLS1	2	5	0.96	0.77	-18.61	0.02
E2ILLS1	2	6	0.97	1.68	25.99	0.002
E3ILL	3	1	0.99	0.92	255.04	<0.0001
E3ILL	3	2	0.99	0.49	62.85	<0.0001
E3ILL	3	3	0.99	0.53	68.67	<0.0001
E3ILL	3	4	0.98	0.57	9.43	0.002
E3ILL	3	5	0.99	0.88	-23.14	<0.0001
E3ILL	3	6	0.98	1.24	-13.30	0.0008
E3ILL	3	7	0.97	2.66	1.28	0.0003
E3ILL	4	1	0.97	1.30	241.48	<0.0001
E3ILL	4	2	0.98	0.55	72.66	0.001
E3ILL	4	3	1.00	0.53	71.98	<0.0001
E3ILL	4	4	0.99	0.67	24.20	0.0005
E3ILL	4	5	0.99	0.67	49.49	<0.0001
E3ILL	4	6	1.00	1.34	22.20	<0.0001
E3ILL	4	7	0.99	4.01	1.15	0.005
E3ILL	5	1	0.96	1.19	308.81	0.003
E4ILLF5	2	1	0.99	0.74	81.96	0.0029
E4ILLF5	2	2	1.00	0.69	-3.48	<0.0001
E4ILLF5	2	3	0.99	0.41	86.53	0.005
E4ILLF5	2	4	1.00	0.67	12.02	<0.0001
E4ILLF5	2	5	1.00	0.84	95.94	0.002
E4ILLF5	2	6	1.00	1.80	43.29	0.0001
E4ILLF5	3	1	1.00	0.95	12.40	<0.0001
E4ILLF5	3	2	1.00	0.89	9.51	<0.0001
E4ILLF5	3	3	0.99	0.75	-15.87	<0.0001
E4ILLF5	3	4	0.98	1.01	-24.83	0.0080
E4ILLF5	3	5	1.00	1.11	3.36	0.0001
E4ILLF5	3	6	0.99	3.92	-18.53	0.003
E4ILLF5	3	7	0.99	1.74	-14.48	0.068
E4ILLF5	4	1	0.95	0.35	132.56	0.14
E4ILLF5	4	2	1.00	0.78	32.51	0.002
E4ILLF5	4	3	0.99	0.60	149.89	0.07
E4ILLF5	4	4	1.00	0.59	76.45	0.014
E4ILLF5	4	5	1.00	1.16	-4.75	NA
E4ILLF5	5	2	1.00	1.25	-18.58	0.04
E4ILLF5	5	3	0.94	0.87	24.08	0.006

E4ILLF5	5	4	0.99	0.70	29.08	0.0006
E4ILLF5	5	5	1.00	0.90	-76.49	0.0008
E4ILLF5	5	6	0.91	1.66	-223.43	0.04

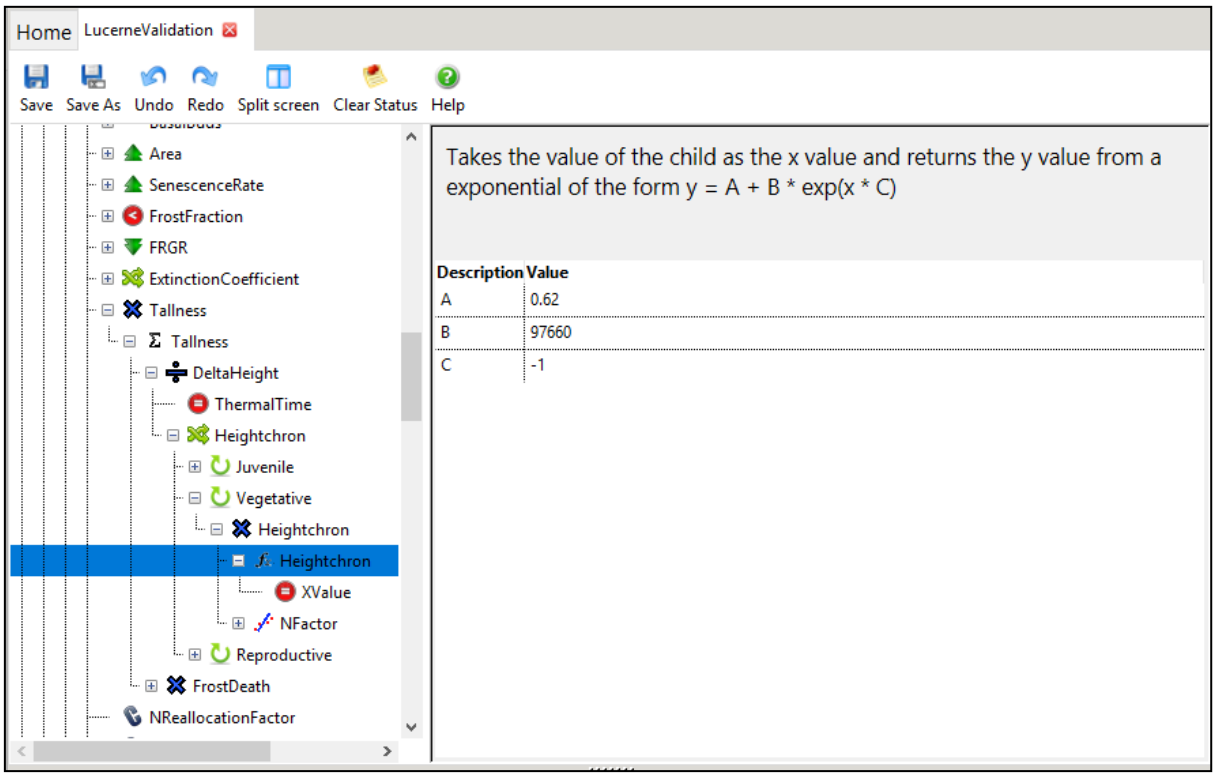

Appendix 52. Model structure of heightchron$_{veg}$ function in APSIM NextGen lucerne model.

Appendix 53. Statistical measures of linear relationship between height and thermal time (Tt) for one field experiments with an 84 day (HH) defoliation treatment conducted within 2014 to 2019 at Lincoln University, Canterbury, New Zealand.

Stage	ID	Growth season	Regrowth cycle	R^2	Slope	Intercept	p
Regrowth	E4IHHF5	1	2	0.998	0.57	47.47	0.03
Vegetative	E4IHHF5	1	3	0.818	4.11	-21.04	0.00
	E4IHHF5	2	1	0.990	1.01	2.20	0.01
	E4IHHF5	2	2	0.965	0.65	41.36	0.02
	E4IHHF5	2	3	0.911	0.87	60.60	0.05
	E4IHHF5	3	1	0.908	0.81	75.37	0.00
	E4IHHF5	3	2	1.000	0.61	6.97	0.00
	E4IHHF5	3	3	1	0.77	14.71	NA
	E4IHHF5	3	4	1.00	2.01	6.93	0.00
	E4IHHF5	4	1	0.96	1.10	41.92	0.00
	E4IHHF5	4	2	0.98	0.56	24.83	0.01
	E4IHHF5	4	3	1.00	0.87	24.00	0.04
	E4IHHF5	5	1	0.97	1.29	29.33	0.00
	E4IHHF5	5	2	0.99	1.44	-52.39	0.01
	E4IHHF5	5	3	1	0.81	-68.54	NA
Reproductive	E4IHHF5	1	2	0.85	3.08	-1403.02	<0.0001
	E4IHHF5	2	2	0.84	3.51	-1915.26	<0.0001
	E4IHHF5	2	3	0.87	2.02	-598.50	<0.0001
	E4IHHF5	3	2	0.83	1.56	-642.78	0.03
	E4IHHF5	4	3	1.00	3.07	-2119.38	NA
	E4IHHF5	5	2	0.99	0.82	174.75	<0.0001

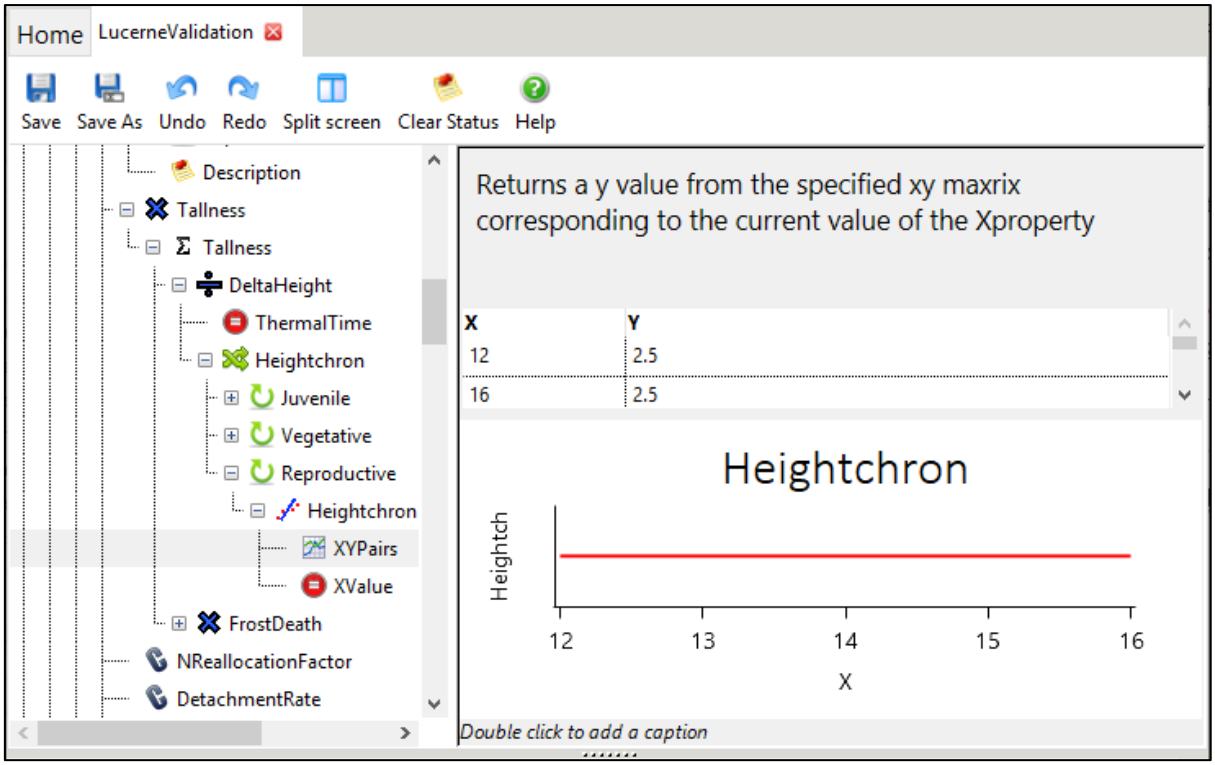

Appendix 54. Model structure of heightchron$_{rep}$ function in APSIM NextGen lucerne model.

Appendix 55 Statistical measures of plant height from four field experiments with multiple defoliation treatments [HH (84 day), LS (42, 28 day), SL (28, 42 day), and SS (28 day)] conducted between 2000 and 2019 at Lincoln University, Canterbury, New Zealand. N = number of simulated and observed data pairs; R^2= coefficient of determination; R_RMSE = relative root mean square error (%); NSE = Nash-Sutcliffe efficiency; SB = Standard bias; NU = Nonunity slope; LC = Lack of correlation. Predicted 1-9 represent the N limitation factor (NLF) ranged from 1 to 1.8 at 0.1 intervals.

Prediction	Treatment	N	R^2	R_RMSE	NSE	SB	NU	LC
Predicted1	HH	162	0.90	32.8	0.8	21.3	27.6	51.2
(1)	LL	456	0.88	41.4	0.7	46.5	13.2	40.2
	SS	284	0.81	93.2	-0.28	71.6	13.4	15.1
Predicted2	HH	162	0.90	32.8	0.8	21.3	27.6	51.2
(1.1)	LL	456	0.88	40.3	0.71	46	12.1	41.9
	SS	284	0.79	88.3	-0.15	70.3	11.7	18
Predicted3	HH	162	0.90	32.8	0.8	21.3	27.6	51.2
(1.2)	LL	456	0.88	39.5	0.72	45	11.3	43.7
	SS	284	0.78	84.6	-0.05	68.1	10.6	21.4
Predicted4	HH	162	0.90	32.8	0.8	21.3	27.6	51.2
(1.3)	LL	456	0.88	39.1	0.73	43.6	10.7	45.6
	SS	284	0.75	82	0.01	65	9.9	25.1
Predicted5	HH	162	0.90	32.8	0.8	21.3	27.6	51.2
(1.4)	LL	456	0.87	38.8	0.73	42.1	10.3	47.5
	SS	284	0.73	80	0.06	61.5	9.5	28.9
Predicted6	HH	162	0.90	32.8	0.8	21.3	27.6	51.2
(1.5)	LL	456	0.87	38.7	0.73	40.5	10.1	49.4
	SS	284	0.70	78.6	0.09	57.8	9.4	32.8
Predicted7	HH	162	0.90	32.8	0.8	21.3	27.6	51.2
(1.6)	LL	456	0.86	38.7	0.73	39	9.9	51.1
	SS	284	0.68	77.7	0.11	53.9	9.5	36.6
Predicted8	HH	162	0.90	32.8	0.8	21.3	27.6	51.2
(1.7)	LL	456	0.86	38.7	0.73	37.4	9.9	52.7
	SS	284	0.65	77.2	0.12	50.1	9.8	40.1
Predicted9	HH	162	0.90	32.8	0.8	21.3	27.6	51.2
(1.8)	LL	456	0.86	38.8	0.73	35.9	9.8	54.2
	SS	284	0.62	76.9	0.13	46.4	10.1	43.4

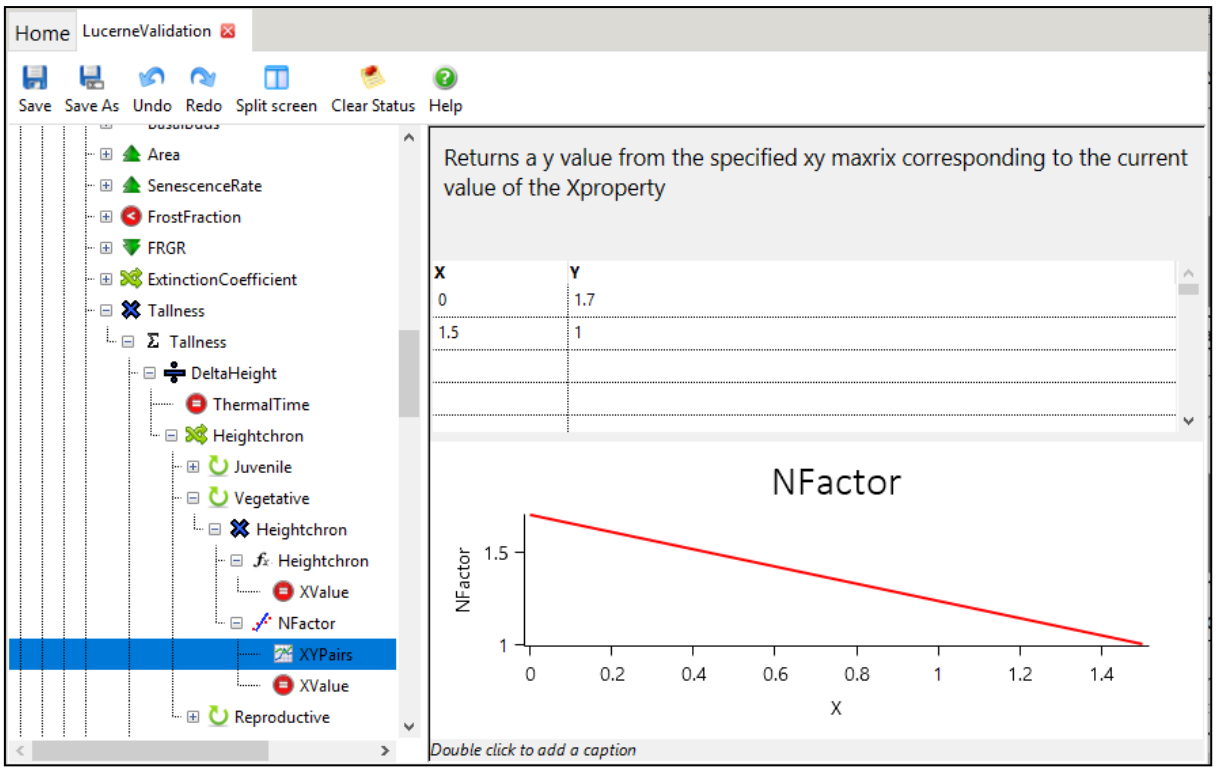

Appendix 56. Model structure of N factor function in height function in APSIM NextGen lucerne model.

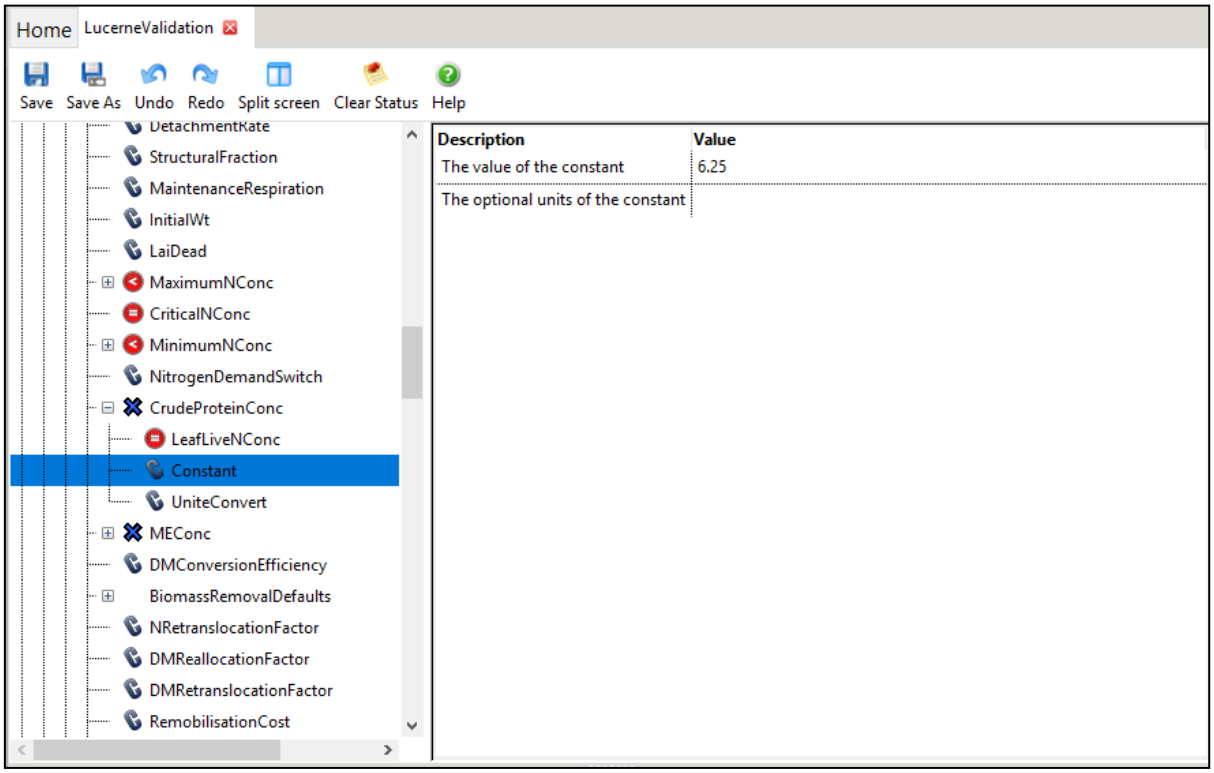

Appendix 57. Model structure of leaf and stem crude protein (CP) in APSIM NextGen lucerne model.

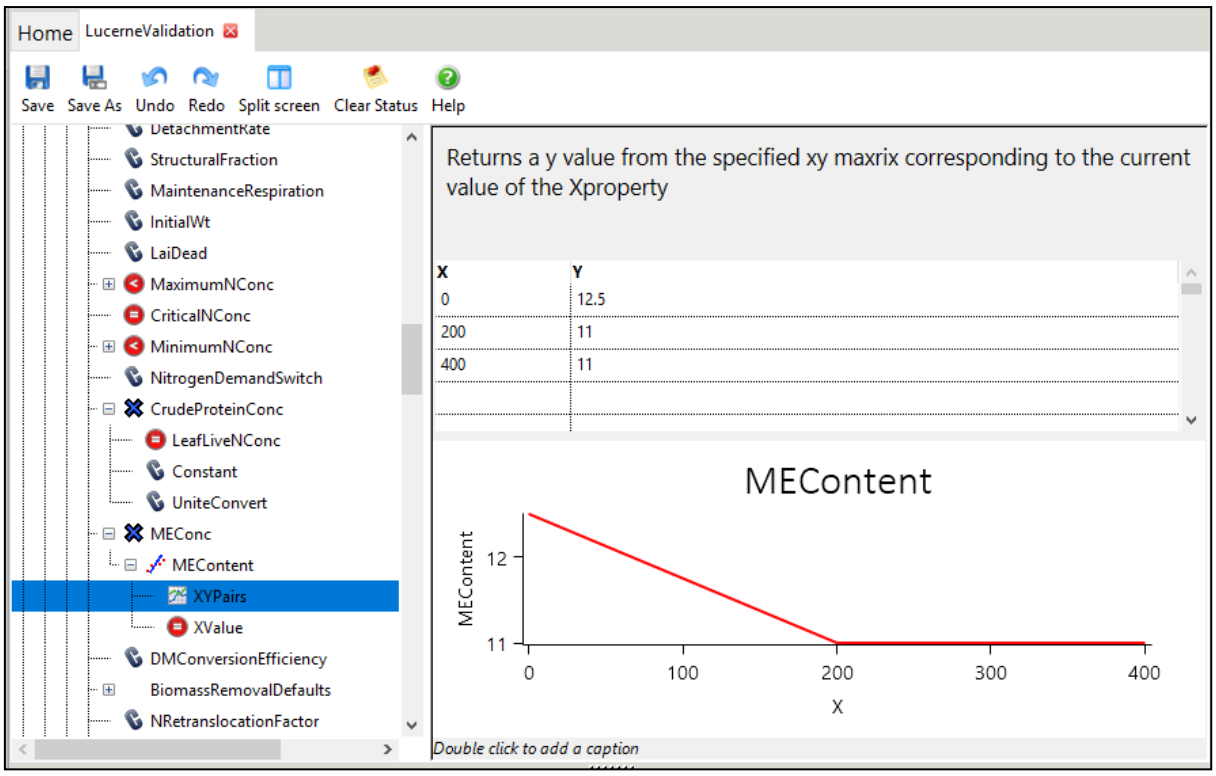

Appendix 58. Model structure of leaf metabolisable energy (ME) in APSIM NextGen lucerne model.

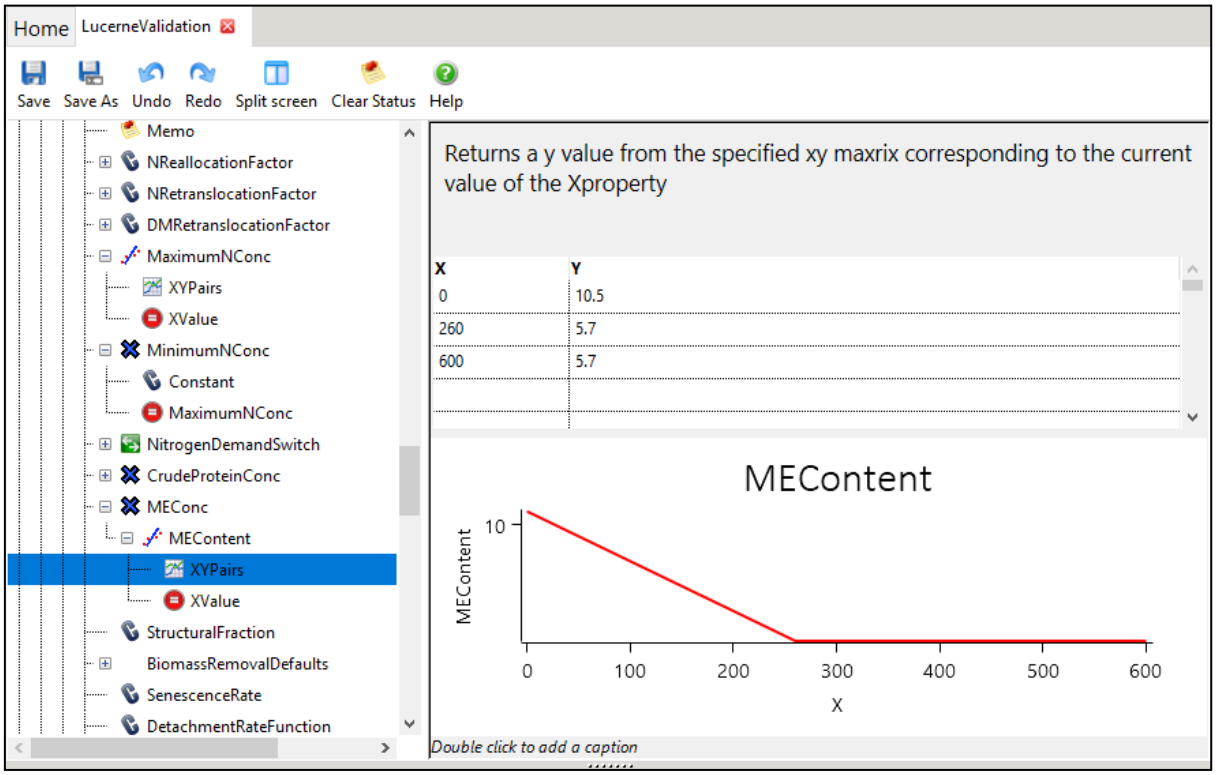

Appendix 59. Model structure of stem metabolisable energy (ME) in APSIM NextGen lucerne model.